Lab-on-Chips for Capture, Detection, and Isolation of Cancerous Extracellular Vesicles

Srinivas Bathini

A Thesis

In the Department

of

Mechanical, Industrial and Aerospace Engineering

Presented in Partial Fulfillment of the Requirements

For the Degree of

Doctor of Philosophy (Mechanical Engineering) at

Concordia University

Montreal, Quebec, Canada

April 2021

CONCORDIA UNIVERSITY

SCHOOL OF GRADUATE STUDIES

This is to certify that the thesis prepared

By: **Srinivas Bathini**

Entitled: **Lab-on-Chips for Capture, Detection, and Isolation of Cancerous Extracellular Vesicles**

and submitted in partial fulfillment of the requirements for the degree of

Doctor of Philosophy (Mechanical Engineering)

Complies with the regulations of the university and meets the accepted standards with respect to the originality and quality.

Signed by the final examination committee:

_____ Chair
Dr. Catherine Mulligan

_____ External Examiner
Dr. Krishnan Venkatakrishnan

_____ External to Program
Dr. Zahangir Kabir

_____ Examiner
Dr. Javad Dargahi

_____ Examiner
Dr. Rama Bhat

_____ Thesis Co-Supervisor
Dr. Anirban Ghosh

_____ Thesis Supervisor
Dr. Muthukumaran Packirisamy

Approved by: _____
Dr. Ivan Contreras, Graduate Program Director

_____
Dr. Mourad Debbabi, Interim-Dean,
Gina Cody School of Engineering & Computer Science

Abstract

Lab-on-Chips for Capture, Detection, and Isolation of Cancerous Extracellular Vesicles

Srinivas Bathini, Ph.D.

Concordia University, 2021

Cancer is a group of diseases involving abnormal growth of cells with a potential to spread to the other parts of the body. It is predicted that one in two will be diagnosed with Cancer by 2030 and one in four would die. The continuous growth and metastasis of cancer cells depend upon cell-to-cell communication. This communication largely involves the secretion of soluble factors by cancer cells within the tumor microenvironment, although these cell types have also shown to export membrane-encapsulated particles containing regulatory molecules that contribute to cell-to-cell communication. These particles are known as extracellular vesicles (EVs) and include exosomes and microvesicles. EVs are a group of extracellular communication organelles enclosed by a phospholipid bilayer secreted by all types of cells throughout the animal kingdom. These vesicles are in the range of 30 to 1000 nm containing a myriad of substances like RNA, DNA, proteins, and lipids from their origin cells, offering a good source of biomarkers. Although their characteristics provide EVs great potential as biomarkers, efficient isolation and detection techniques are still challenging. Currently, the standard method for their isolation and quantification from body fluids is by ultracentrifugation, which is not a practical method to be implemented in a clinical setting. Thus, a versatile and cutting-edge platform is required to detect and isolate exosomes selectively for further analysis at a clinical level.

This dissertation is focused on developing lab-on-chip devices for the capture, detection, and isolation of cancerous extracellular vesicles from MCF7 (breast cancer cell lines) culture media. Here, we have explored three platforms based on gold nanoparticles, namely, in-situ synthesized nanocomposites, gold nano-islands on a substrate, and colloidal platform with suspended gold nanoparticles (AuNPs).

The first step was to identify the suitable platform for the capture and isolation of EVs, based on the sensitivity of the platform. Initially, gold – poly (dimethylsiloxane) (PDMS)

nanocomposites, were created by the *in-situ* synthesis of nanoparticles on the surface of PDMS substrate by reducing gold precursor solution with curing agent of PDMS. The Au-PDMS nanocomposites are a special category of composites, with gold nanoparticles segregated in a sub-surface layer of the polymer. The second platform is the gold nano-island platform, where AuNPs are synthesized using Turkevich's method and then deposited on a glass substrate by thermal convection. Then, the deposited nanoparticles are heat-treated at 560°C for an hour to form gold nano-islands. The refractive index sensitivity of nanocomposite and gold nano-islands is found to be around 50 and 111nm/RIU, respectively. The lower sensitivity in the nanocomposites as the nanoparticles are under the surface covered by a thin PDMS layer, whereas the in case of gold nanoislands, they are above the surface and available to interact directly with the analyte. Considering the sensitivities, the gold nano-island platform was utilized further for the capture and detection of EVs. The gold nano-islands on a substrate platform, where only half of the islands are available for sensing and capture, exhibited a better sensitivity meaning that utilizing the whole surface of nanoparticle would result in even better sensitivity as in the case of the third platform where gold nanoparticles suspended in a colloidal solution.

This dissertation then focuses on the biosensing protocol developed based on localized surface plasmon resonance (LSPR) of gold nano-islands, for the detection of EVs. The protocol involves the adsorption or binding of multiple bio-entities to the gold nano-island and absorption spectrum measurement after each step. The molecular interactions shift the gold plasmon band in the visible spectrum toward longer wavelengths and the shift is proportional to the concentration of the entity. The sensing protocol utilizes the strong affinity between EVs, and polypeptide called Venceremin or Vn96, which is specifically designed to capture EVs by binding the heat shock proteins (HSPs) present on their surface. Physical modeling, based on the characteristics of the gold nano-islands and the bio-entities involved in the sensing, is developed to determine the detection capability of the platform, which is optimized experimentally at each stage of the sensing protocol. The results and modeling present a relationship between the plasmonic shift and the concentration of exosomes. Further, a simple microfluidic device is designed for detecting EVs consists of a glass substrate with gold nano-islands, sealed by a PDMS film that contains a microchannel with a collection chamber in between. The same biosensing protocol has been transferred to a microfluidic environment by infusing biosensing entities into the device and measurement of the spectrum after each step. The capture and detection ability of the device is

validated by Atomic Force Microscopy (AFM) and the measurement of gene copy numbers using droplet digital PCR (ddPCR). The results indicate that the developed device can capture and isolate the EVs from a very low sample volume, in less than 30 minutes, without affecting their size and shape, a major advantage compared to existing methods. Later, to increase the sensitivity, a two-level microfluidic device is fabricated utilizing a double-sided gold nano-island substrate, where AuNPs are deposited on both sides. This technique can be extended to multi-level microfluidics by introducing an intermediate channel in between the nanoisland substrates.

Parallelly, the gold nanoparticles suspended in a colloidal solution were utilized for the capture, detection, and isolation of EVs using the same protocol. Initially, this technique was studied at the cuvette stage by mixing the desired volume and concentrations of bio-entities manually and measuring the absorption spectrum at each stage for LSPR shift. As the nanoparticles are freely suspended in the solution, the binding of EVs on the entire surface area contributes the nanoparticles to sediment at the bottom of the cuvette. Thus, the precipitation method was used to isolate EVs. Then, a liquid biopsy chip is designed and fabricated using soft-lithography consisting of a 3D mixer, a collection chamber, and gravity assisted sedimentation unit. The streptavidin-coated magnetic particles are utilized in the liquid biopsy chip for the isolation of EVs. The device consists of a 3D mixer to ensure capture efficiency and it also consists of a sedimentation unit, which allows EV-captured magnetic particles to settle in it. The sedimented EV-captured magnetic particles are then isolated from the chip for elution of EVs and their validation using Nanoparticle Tracking Analysis (NTA), AFM, and gene amplification. The results clearly show that the proposed liquid biopsy chip can isolate the EVs without affecting their morphology. Thus, this chip can be considered as a potential point-of-care device for diagnostics in a clinical setting and for the isolation of EVs for future therapeutics.

Acknowledgements

I sincerely thank my Ph.D. advisor, Professor Muthukumaran Packirisamy, who believed in me and provided me with this opportunity to pursue my dream. I am very much grateful for his supervision, invaluable guidance, innovative methods, ideas, and encouragement throughout my research work. I am very thankful to Dr. Anirban Ghosh for his suggestions and guidance in the biological aspects during entire course of my research work. I express my sincere thanks to Dr. Simona Badilescu, who always supported and motivated me during my entire stay in the lab. I appreciate her help and support in carrying out my research work in the lab.

It has been my pleasure to be a member of the "Optical Bio-Microsystems Laboratory". In addition to this, I would also thank Dr. Shanmugasundaram Pakkiriswami and Dr. Jayan ozhikandathil for their support and motivation and I extend my thanks to all my colleagues. Special thanks to the administrative staff at the department of Mechanical Engineering, Concordia University, Leslie Hossein, Arlene Zimmerman, Sophie Merineau, and Maureen Thuringer. I also would like to thank Mr. Mazen Samara (Concordia University) for his assistance with SEM imaging, Mr. Zhizhong for his assistance with the NTA analysis, Mr. Mathieu Durand (University of Sherbrooke) for his assistance with the ddPCR measurements.

Words simply cannot express my gratitude to my parents, Rajanarsaiah and Lingamma, for their trust, invaluable love, and endless support. I thank my well-wishers from Laboratory for Electro-Optic Systems (LEOS-ISRO), Mr. Jiju John, Dr. Giridhar MS and Ashwini Jambalikar who always believed in me, and my friends and other family members for their support and motivation throughout my research.

Dedicated

To

My Parents

Table of contents

List of Figures

List of Tables

List of Symbols

t	Time
t_{synth}	Synthesis time
$\Delta\lambda$	Wavelength shift
T	Temperature
Δn	Change in Refractive Index
L	Length
W	Width
$\emptyset$	Diameter
C	Concentration
A	Absorbance units
$f(x)$	Real distribution
$f_1(x)$	No mixing
$f_2(x)$	Full mixing
η	Efficiency of mixing
λ	Wavelength

Nomenclature

3D	Three Dimensional
AFM	Atomic Force Microscopy
Ag	Silver
Au	Gold
AuNPs	Gold Nanoparticles
BCA	Bicinchoninic Acid Assay
BGH	Bovine Growth Hormone
BST	Bovine Somatotropin
CCM	Cell-Conditioned Medium
CT	Computed Tomography
CTC	Circulating Tumor Cells
ctDNA	Circulating Tumor DNA
ddPCR	Droplet Digital PCR
DIW	De-Ionized Water
DLS	Dynamic Light Scattering
DMF	Dimethylformamide
DS-AuNI	Double-Sided Gold Nanoisland
EDC	N-(3-Dimethylaminopropyl)-N′-ethylcarbodiimide hydrochloride
ELISA	Enzyme-Linked Immunosorbent Assay
EM	Electron Microscopy
EVs	Extracellular Vesicles
FBS	Fetal Bovine Serum
FC	Flow Cytometry
FE	Finite Element
GCS	Gold Colloidal Solution
HSP	Heat Shock Proteins
IGF	Insulin-like Growth Factor
ILV	Intraluminal Vesicles
IPA	Isopropyl Alcohol

LC–MS/MS	Liquid Chromatography–Tandem Mass Spectrometry
LOC	Lab-On a Chip
LSPR	Localized Surface Plasmon Resonance
MF	Microfluidic
MRI	Magnetic Resonance Imaging
MVE	Multivesicular Endosomes
NGS	Next-Generation Sequencing
NHS	N-Hydroxy Succinimide
NTA	Nanoparticle Tracking Analysis
PBS	Phosphate Buffered Saline
PCR	Polymerase Chain Reaction
PDMS	Poly (dimethyl siloxane)
PEG	Polyethylene Glycol
PK	Proteinase K
POCT	Point-of-Care Testing
rBST	Recombinant Bovine Somatotropin
RI	Refractive Index
RIA	Radioimmunoassay
SAM	Self-Assembled Monolayer
SEC	Size Exclusion Chromatography
SEM	Scanning Electron Microscopy
SERS	Surface-Enhanced Raman Scattering
SPP	Surface Plasmon Polaritons
SPR	Surface Plasmon Resonance
TRPS	Tunable Resistive Pulse Sensing
UC	Ultracentrifuge
WB	Western Blotting
XPS	X-ray Photoelectron Spectrometry
XRD	X-ray Diffraction

Chapter 1

Literature Review and Scope

1.1 Introduction to Extracellular Vesicles

Cancer has a major impact on society across the world because it is among the leading causes of death worldwide. The progression of cancer to late stages without the appearance of symptoms is one of the main reasons for being the leading cause of death. There were 14.1 million new cases and 8.2 million cancer-related deaths worldwide in 2012, out of which, 57% of new cases and 65% of deaths occurred in less developed regions of the world that include Central America and parts of Africa and Asia; Based on the statistics, it was found that 1.73 million new cases were diagnosed in the United States in 2018 and the estimated number of new cases per year is expected to rise to 23.6 million by 2030. The number of new cases diagnosed in Canada is around 0.22 million in 2020. According to Canadian cancer statistics: 2018 special report, 1 in 2 Canadians is expected to be diagnosed with cancer in their lifetime, whereas 1 in 4 is expected to die. Figure 1.1 shows the common cancers including lung, breast, colorectal, and kidney cancers, and the Canadian cancer statistics. [1, 2].

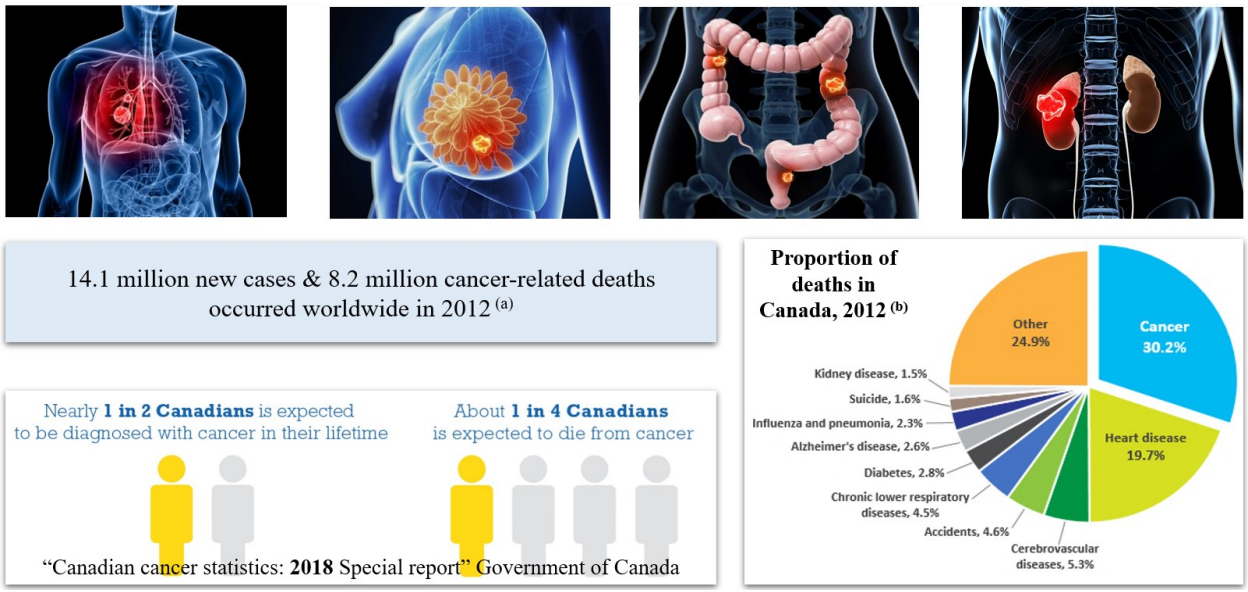

Figure 1.1: Common types of cancers and the Canadian cancer statistics [1, 2]

Cancer is a group of diseases involving abnormal growth of cells with the potential to spread to the other parts of the body. The stages of cancer for each person are determined by

combining the Tumor, Node, Metastasis results and other factors specific to cancer. Most types of cancer have four stages: stages I (1) to IV (4) and some cancers also have a stage 0, which is still located in the place they started and have not yet spread to any nearby tissues. This stage of cancer is often highly curable by removing the entire tumor with surgery. Stage I is usually small cancer or tumor that has not grown deeply into nearby tissues. It also has not spread to the lymph nodes or other parts of the body. It is often called *early-stage cancer*. Stage II and Stage III indicate larger tumors that have grown more deeply into nearby tissue. They may have also spread to lymph nodes but not to other parts of the body. And Stage IV means that cancer has spread to other organs or parts of the body. It may also be called advanced or metastatic cancer [3, 4]. The continuous growth and metastasis of cancer cells depend upon cell-to-cell communication. This communication largely involves the secretion of soluble factors by cancer cells within the tumor microenvironment, although these cell types have also shown to export membrane-encapsulated particles containing regulatory molecules that contribute to cell-to-cell communication. These particles are known as extracellular vesicles (EVs) and include exosomes and microvesicles.

EVs are spherical particles enclosed by a phospholipid bilayer, which are released from Eukaryotic and Prokaryotic cells. These EVs consists of DNA, RNA, mRNA, miRNA, proteins, nucleic acids and equipped with heat shock proteins (HSP70 and HSP90), the tetraspanins such as CD9, CD63, and CD81, RAB proteins that regulate docking and membrane fusion of EVs with recipient cells adhesion molecules (integrins and lactadherin). The cell-derived vesicles or the EVs are present in all biological fluids including blood, urine, saliva, breasts milk, and cultured media [5-7], play a key role in processes such as coagulation, inflammation, cellular homeostasis and survival, intercellular communication, waste management, and transport and delivery of cargo between cells [8, 9]. The typical diameter of exosomes, type of EVs, is between 30 and 100 nm, which is much smaller than that of red blood cells. Consequently, there is a growing interest in the clinical applications of EVs/exosomes. EVs can potentially be used for therapy, prognosis, and as biomarkers for disease diagnosis. Despite increasing scientific and clinical interest, no standard procedures are available for the isolation, detection, and characterization of EVs, because of their size, which is below the reach of conventional detection methods.

EVs/Exosomes are released from the cell when multivesicular bodies fuse with the plasma membrane or they are released directly from the plasma membrane. There are two ways in which exosomes are released as shown in Figure 1.2. First, the “classic pathway” of exosome biogenesis,

which involves the formation of Intraluminal Vesicles (ILVs) within Multivesicular Endosomes (MVEs). In turn, the membrane of MVE fuses with, either lysosome for cargo degradation, or with the plasma membrane, resulting in the release of ILVs. Once secreted, ILVs are called exosomes. The second and much more immediate route of exosomes is the "direct pathway" in which, T cells and erythroleukemia cell lines release exosomes directly from the plasma membrane, both spontaneously and after cross-linking of surface receptors. These vesicles are indistinguishable from exosomes formed by the classic endosomal pathway because they are enriched in classic exosome markers such as CD63 and CD81 and have a similar diameter and density. The extent to which such exosomes are released from other cells or in vivo (e.g., in biological fluids) is unknown.

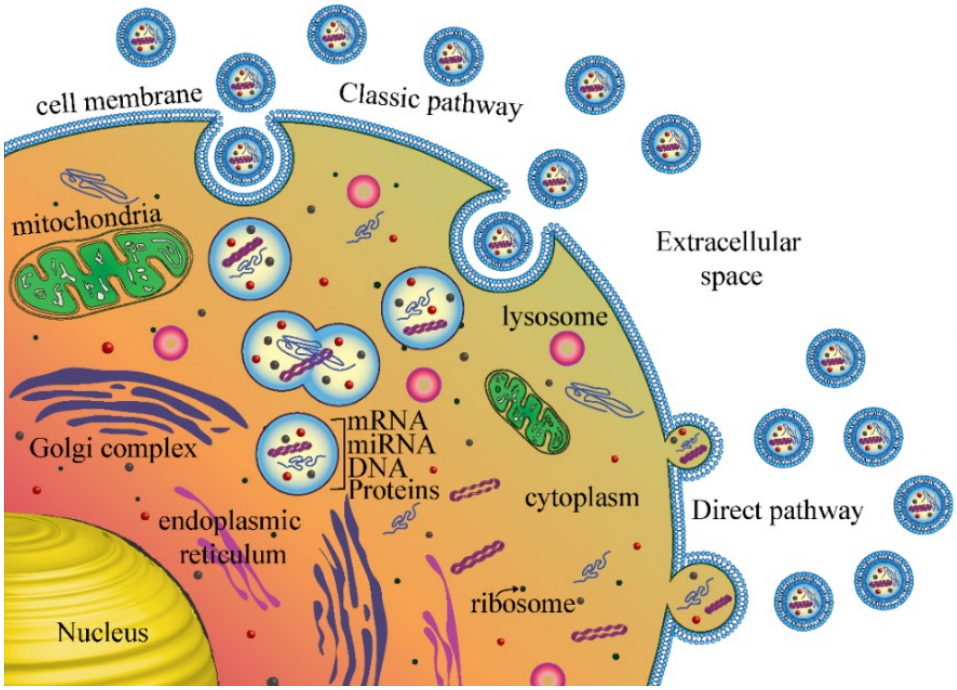

Figure 1.2: Biogenesis of Extracellular Vesicles

1.1.1 History

Cell-derived vesicles were first discovered in 1940, addressing the biological significance of the thromboplastin protein of blood. After centrifugation at different speeds, plasma clotting times were determined and prolonged high-speed centrifugation (150min at 31,000g) was shown to significantly extend the clotting time of supernatant reported by Chargaff and West [10]. Furthermore, when the pellet was added to plasma, the clotting times shortened, indicating that cell-free plasma contains a subcellular factor that promotes the clotting of blood. More than 20

years later, in 1967, this subcellular fraction was identified by electron microscopy and was shown to consist of small vesicles, originating from platelets and termed “platelet dust” by Wolf [11]. These vesicles were reported to have a diameter between 20 and 50 nm and a density of 1.020 to 1.025 g/ml. One decade later, fetal calf serum was also shown to contain “numerous microvesicles” ranging in diameter from 30 to 60 nm.

The term “exosomes” was first used for the membrane vesicles exfoliated from various normal and neoplastic cell lines by Trams et. al. [12]. Then later, the vesicles formed in the multivesicular bodies by endocytosis pathway and released by fusion of multivesicular bodies with plasma membrane as “exosomes” was defined by Johnstone et al. in 1987 [13]. Meanwhile, within a completely different line of research, EVs were isolated from the conditioned culture medium of sheep reticulocytes. These EVs had several characteristic activities in common with the reticulocyte plasma membrane, including the presence of transferrin receptors, whereas cytosolic enzyme activities were not detectable. Therefore, it was concluded that “vesicle externalization could be a mechanism for the shedding of specific membrane functions, which are known to diminish during maturation of reticulocytes to erythrocytes”. Because these exosomes contained the transferrin receptor but expressed no lysosomal activities, it was also suggested that there may be a common mechanism to segregate and externalize specific membrane proteins. The formation of transferrin receptor-containing exosomes proved to be a major route for the removal of plasma membrane proteins. Because not only mammalian but also embryonic chicken reticulocytes were shown to produce transferrin receptor-containing exosomes, this may be a conserved and common pathway. It was then discovered that exosomes are formed within multivesicular endosomes (MVEs), also known as multivesicular bodies, and are being released when membranes of MVEs fuse with the plasma membrane. This pathway of protein sorting turned out to be highly selective, because other major transmembrane proteins, such as the anion transporter, are fully retained within the mature red cells and are absent within exosomes. Taken together, these early studies revealed that exosomes might be essential in a sophisticated and specific mechanism to remove obsolete transmembrane proteins.

In 1996, Raposo et al. [14] discovered that immune cells such as B lymphocytes also secreted exosomes and that these EVs carry membrane-bound molecules essential for the adaptive immune response. Two years later, further research demonstrated yet another exosome-secreting cell type, whose exosomes carried functional immune agents that could promote induction of

antitumor responses in mice [15]. These results prompted explorations into their clinical applications and being tested as a new type of adjuvant therapy for the treatment of non-operable lung cancer.

Over the past few years, the development of large-scale protein analysis techniques allowed researchers to detail the type of cargo transported by exosomes [16]. Different cell types secrete exosomes that carry specific sets of proteins that differ from the proteins contained in the membrane vesicles released by apoptotic cells, suggesting that exosomes are actively secreted by living cells.

Exosomes purified in vitro showed that the EVs can be captured by other cells, thus transferring any information enclosed in/on the exosome. Exosome-bound molecules can induce the inactivation or even the death of the target cell they encounter. In 2007, Jan Lotvall [17] in Sweden discovered messenger RNA and microRNA inside the exosomes. Moreover, in vitro experiments showed that mRNA could be translated into proteins in target cells. This remarkable discovery not only indicates a new form of intercellular communication but suggests that exosomes could perhaps behave like viruses, meaning that they bring genetic material with them that is translated to proteins in the cells they "infect".

1.1.2 Other types of cell-derived vesicles or EVs

The other types of cell-derived vesicles are microvesicles and apoptotic vesicles [18] as shown in Figure 1.3.

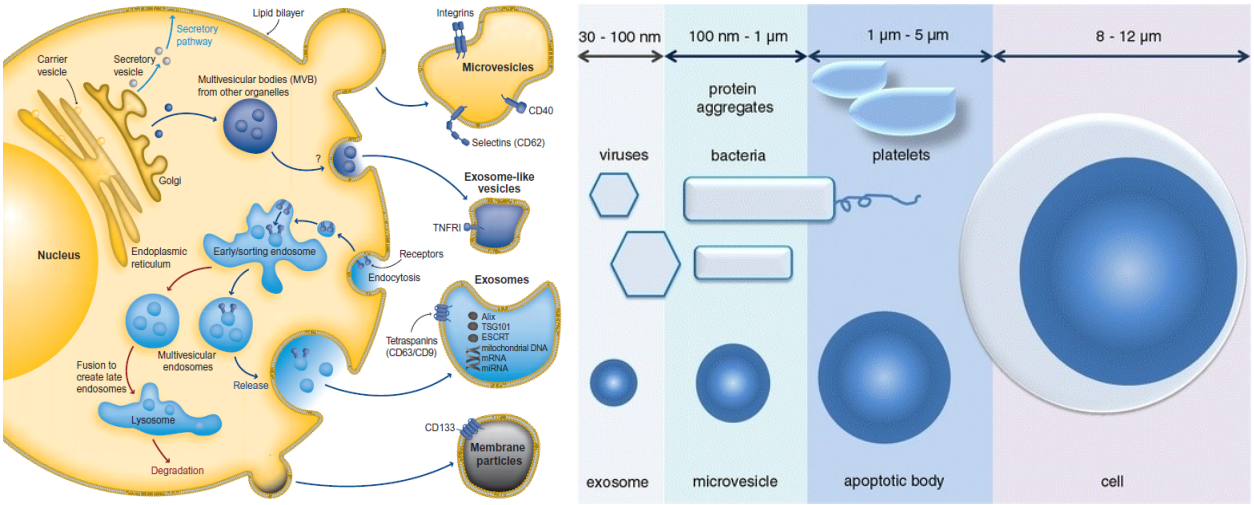

Figure 1.3: Biogenesis of the various types of extracellular vesicles and size comparison with a cell [18]

Microvesicles are released from the plasma membrane during cell stress i.e., by budding and the subsequent fission of the plasma membrane into the extracellular space, due to the dynamic interactions between phospholipid redistribution and cytoskeletal protein contraction (due to the stimulus). These microvesicles, often called microparticles, are present in most if not all biological fluids and cell-conditioned medium (CCM). The typical diameter of these microvesicles is between 100 – 1000 nm and is heterogeneous. Their density is yet to be determined and is generally larger than exosomes. The size ranges of microvesicles and exosomes may overlap, especially when body fluids are used as a source for the isolation of vesicles. Although microvesicles and exosomes are distinct types of EVs, neither size, morphology, nor exposure of phosphatidylserine is a sufficient criterion to distinguish both types of EVs from each other.

Apoptotic bodies or vesicles are released when the cells undergo apoptosis, and they contain cell organelles and nuclear fractions. Their reported diameter ranges between 1 and 5 μm which is the major difference when compared with other cell-derived vesicles. The size of these vesicles is almost in the range of platelets in the human blood. Their density is ranging between 1.16 – 1.28 g/ml, which is partly overlapping with the density of exosomes. When these vesicles are analyzed by electron microscopy, morphology is heterogeneous. Two immunologically distinct types of apoptotic vesicles are released by apoptotic cells. Apoptotic vesicles originating from the plasma membrane contain DNA and histones, whereas apoptotic vesicles originating from the endoplasmic reticulum expose immature glycoepitopes. The main characteristics of different types of cell-derived vesicles are summarized in Table 1.1.

Table 1.1: Main characteristics of different types of cell-derived vesicles

	Diameter (nm)	**Density (g/ml)**	**Morphology (TEM)**	**Cellular origin**	**Composition**
Exosomes	50 – 100	1.13-1.19	Cup-shaped	Most cell types	Known composition, but most proteins and lipids are not unique
Microvesicles	20-1000	Unknown	Cup-shaped	Most cell types	Insufficiently known
Apoptotic vesicles	1000-5000	1.16-1.28	Heterogeneous	All cell types	Histones, DNA

1.1.3 Physiological and pathological functions

It is known that, for cancer progression, the direct interaction between tumor cells and their environment is essentially required. Exosomes induce a pro-tumoral microenvironment for carcinogenesis regulating the immune response to promote tumor progression and survival by cell-to-cell communication, which is an efficient information exchange. To do these tasks, exosomes are released into the extracellular environment to promote angiogenesis, thrombosis, and tumor cell proliferation [19]. Owing to their stability, the specific tissue uptake, and their ability to transfer microRNA and proteins to recipient cells, exosomes may travel to distant sites and promote a pro-tumor environment to harbor metastatic niches [20]. Exosomes may additionally exert an immune suppression profile, thus favoring a tumor escape mechanism to evade the immune attack.

Exosomes can modulate nearby or distant target cells by direct contact of their surface molecules to activate intracellular pathways and also contribute to waste management and protection against stress. They have been associated with the coagulation process in the presence of calcium ions. They are also responsible for the vascular function and integrity for the pathological functions such as the transmission of viruses, prions, and β-amyloid in Alzheimer's disease as well as in tumor pathogenesis.

1.1.4 Clinical applications

EVs are the membrane vesicles that are secreted by many cell types into the extracellular environment under normal and pathological conditions. Exosomes are recognized as a potential source of disease biomarkers as they are found in cell culture supernatants and different biological fluids. Hence, exosomes are being explored for their clinical applications.

Immune properties of different types of EVs suggest that they could be used as vaccines for infectious diseases [21]. EVs derived from dendritic cells, tumor cells, and malignant effusions demonstrate immunomodulatory functions and can present antigens to T-cells and stimulate antigen-specific T-cell responses. They are also involved in the stimulation of the immune system and increased levels of antigen. Thus, EVs are now potential sources for anticancer vaccines and the elimination of infections [22]. EVs have also been examined for their clinical applications in the treatment of infections such as toxoplasmosis, diphtheria, tuberculosis, and a typical severe acute respiratory syndrome as well as autoimmune diseases. As EVs play a vital role in the drug

delivery system, researchers are trying to find applications in the treatment of cancers, autoimmune/inflammatory diseases [23]. Phase 1 clinical trials in human cancer evaluated the effectiveness of patient-specific exosomes released by dendritic cells and loaded with tumor antigen-derived peptides for melanoma and non-small lung cancer and showed that immunotherapy was feasible, safe, and led to the induction of both natural and adaptive immune responses, disease stabilization and patient's long-term survival [24]. Also, ascites-derived exosomes from colorectal cancer patients were shown to be safe, non-toxic, and tolerable when used as a cancer vaccine [25].

1.1.5 Sample collection protocols

Extracellular Vesicles are the critical components of intercellular communication and are capable of inducing local and systemic changes by promoting disease progression. The problem impeding the advancement of EV research is the standardization of sample collection protocols such as sample collection, sample processing, and sample analysis for translating EVs to suitable clinical biomarkers.

EVs can be detected in a wide range of body fluids, but the discussion here is limited to the analysis of blood. Low-speed centrifugation is used to remove cells and large vesicles and high-speed ultra-centrifugation is used to pellet EVs is the current "gold standard" for the purification of EVs [26]. It has also been suggested that repeated ultracentrifugation steps can damage the EVs and reduce yield, thereby potentially impacting the proteomic and RNA analysis of their content [27]. Therefore, both the International Society for Thrombosis and Haemostasis (ISTH) and the International Society for Extracellular Vesicles (ISEV) have recently described the guidelines and recommendations regarding the standardization of sample collection and handling protocols [28] as shown in Figure 1.4.

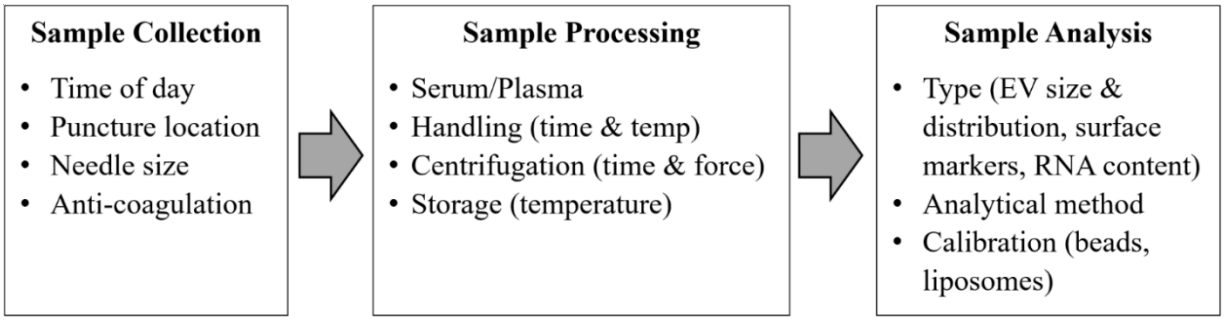

Figure 1.4: Critical standardization issues for EV analysis from blood samples [28]

During the collection of blood, the time of the day can influence the EV concentration in the collected sample. Physical forces can activate platelets and cause the release of platelet-derived EVs. Therefore, it is recommended to use the same puncture location and needle size (≥21-gauge) to collect blood and discard the first few milliliters of blood collected [29, 30]. A study by Gyorgy et al. [31] concluded that acid-citrate-dextrose (ACD) tubes are recommended for the assessment of plasma EVs as ACD does not interfere with protein or RNA analysis. Furthermore, the amount of times tubes inverted for mixing of the blood sample with anticoagulant, should be limited.

The collected sample should be handled with care to avoid agitation. Depending on detection purpose, both plasma and serum can be used for measurements. Plasma is recommended for most purposes. Centrifugation is the predominant step that influences EV analysis [32]. Blood samples were centrifuged for 15 minutes at 2500g to obtain plasma, and by repeating, platelet-free plasma can be obtained and stored at -80°C. Then depending on the type of EVs, samples are analyzed using different types of beads such as polystyrene and silica beads by using synthetic lipid vesicles as calibration strategies. These may be more suitable due to the comparable refractive index with EVs [33].

1.2 Motivation

To detect cancer, screening tests are performed, when they are most likely to be curable. The screening tests include imaging techniques, biopsy, and cytology tests. Imaging techniques are used for screening cancer in order to find the location of the tumors. Techniques such as Computed Tomography (CT) scan, X-rays, Magnetic Resonance Imaging (MRI), and ultrasound scan are currently used. Imaging techniques are useful only when the tumor is already too large. Tumors that can be imaged may contain already a few million cells and, at this stage, the disease would be too advanced for treatment. To have a better idea about the stage of the disease, a biopsy has to be performed. For this purpose, a small piece of tissue, skin, organ, or suspected tumor is surgically taken out and sent to a lab for testing. A biopsy is the only way to diagnose most cancers whereas imaging tests identify only the areas of concern as they cannot differentiate cancerous and non-cancerous cells. A biopsy is performed based on the symptoms associated with cancer [34]. The main drawback with these methods includes time consuming, painful, and can detect only very late. As cancer covers up the major percentage of the death rate and the early diagnosis of it

is challenging, any techniques for its early diagnosis non-invasively will have a major impact on the social and economic status.

Despite the increasing scientific and clinical interests, no standard procedures are available for the isolation, detection, and characterization of exosomes, because of their size, which is below the reach of conventional detection methods. Given the growing evidence that exosomes may be a clinically-relevant biomarker source, there is a great demand for their simple and efficient detection from bio-fluids. Most affinity-based methods rely on antibodies directed against exosome surface markers [35]. Therefore, considering the potential and scope of EVs/exosomes, the whole motivation was to develop label-free methods or techniques to capture, isolation, detection, and characterization of EVs for early diagnosis of cancer. The isolation of EVs is by using a synthetic peptide called Vn96 [36], detection by localized surface plasmon resonance (LSPR), and the characterization using polymerase chain reaction (PCR). The platforms are developed by exploiting the properties of gold nanoparticles at the substrate and microfluidic level, nanocomposites, and in colloidal suspensions. Considering the developed platforms and protocols, multiple microfluidic devices and a liquid biopsy chip will be designed and fabricated which could potentially be used for point-of-care testing (POCT) applications.

1.3 Thesis Objectives

The purpose of this research is to capture, isolate, detect, and characterize the extracellular vesicles by designing and fabricating a microfluidic device. This device will use either gold nano-islands on a glass substrate or colloidal platform with gold nanoparticles (AuNPs) or magnetic particles through the integration of a polypeptide-based affinity capture of EVs. The device could be potentially used as a point-of-care testing application. The scope and objectives of this research work can be outlined as follows:

i. Designing and developing biosensing protocols to test on the substrates and microfluidic platforms.
ii. Optimization of biosensing protocol with various concentrations of the entities involved in the protocol by utilizing LSPR.
iii. Theoretical studies involving the design, modeling using COMSOL software, and analysis of a liquid biopsy chip for the capture, isolation, and detection of EVs.
iv. Characterization of EVs from MCF7 cancer cell line through imaging (SEM and AFM).

v. Molecular analysis of isolated EVs by PCR-based amplification and sequencing for diagnostic purposes such as a point of care testing device.

vi. Fabrication and testing of a liquid biopsy chip for the capture, detection, and isolation of EVs.

1.4 Why EVs and why is it important to isolate them?

Extracellular vesicles are spherical particles enclosed by a phospholipid bilayer [37, 38], present in all biological fluids [39]. EVs play a key role in intercellular communication by transport and delivery of cargo between cells promoting disease progression. Not only EVs, but also circulating tumor cells (CTC), and circulating tumor DNA (ctDNA) have attracted much attention in the past decades as biomarkers for early diagnosis of cancer. The major challenge in the isolation of CTCs and ctDNA is that the isolation and analysis of CTCs which are very difficult as they are extremely rare and heterogeneous [40] while the ctDNA is not stable in the blood or the other body fluids and highly fragmented [41, 42]. Because of these intrinsic limitations of CTCs and ctDNA, the definite isolation and precise detection of them remain challenging even though there are lot of advancements in the technology. Compared to CTCs and ctDNA, exosomes have a lot of advantages in terms of stability, quantity, and accessibility. Exosomes are released by cancerous and non-cancerous cells, but the concentration of exosomes increases tremendously (by many folds) as the tumor progresses when compared with the other biomarkers such as tumor antigen, CTC, and ctDNA. For example, in the case of a glioblastoma (GBM) patient's plasma study [43], the concentration of exosomes was found to be approximately 50 times higher than that of a healthy patient. As mentioned, Figure 1.5 shows that the expression level of exosomes is relatively higher than that of CTCs and tumor antigens in stage I, which is *early-stage cancer* [44]. Exosomes are highly stable and are capable of protecting nucleic acids and proteins that are closely related to cancer development. Many studies have shown that the cancer cell-derived EVs contain specific nucleic acids and proteins that reflect the origin of cancer cells, with which the type of cancer can be identified [45, 46]. Therefore, considering these merits, EVs/exosomes can potentially be used for therapy, prognosis, and as promising biomarkers for early diagnosis of cancer.

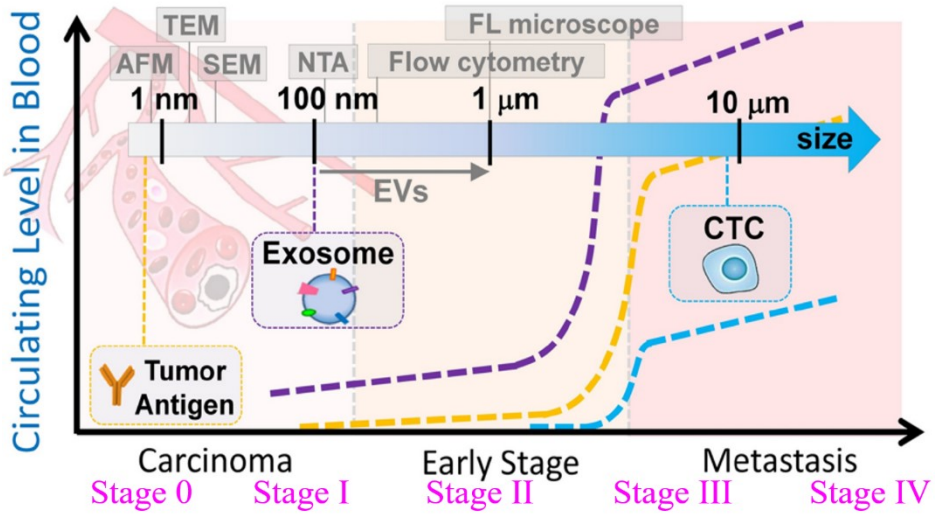

Figure 1.5: The circulating levels of Tumor antigens, CTCs, and exosomes in blood during the cancer progression [44]

1.5 Isolation and detection techniques currently available

The traditional methods for physical characterization and molecular analysis of EVs is presented in Figure 1.6(a). The techniques used to measure the physical properties such as morphology, size, and zeta potential or concentration of EVs are electron microscopy (EM), atomic force microscopy (AFM), nanoparticle tracking analysis (NTA), dynamic light scattering (DLS), tunable resistive pulse sensing (TRPS), or flow cytometry (FC). The biomolecular properties of EVs can be analyzed by conventional bioanalytical methods including bicinchoninic acid (BCA) assay, western blotting (WB), enzyme-linked immunosorbent assay (ELISA), liquid chromatography–tandem mass spectrometry (LC–MS/MS), nucleic acid extraction, polymerase chain reaction (PCR) amplification, and sequencing techniques. While the isolation methods are majorly classified into four types, namely density-based, size-based, surface component-based, and precipitation methods as shown in Figure 1.6(b). The methods that come under the density-based separation of EVs are differential ultracentrifugation and density gradient centrifugation. These were developed during the very early research on EVs. In differential ultracentrifugation, the large cell debris and cells are removed at low speed around 20000xg, and further, the EVs are removed by precipitating them at higher speeds more than 100000xg [26] while in density gradient centrifugation, series of solutions with different densities are preloaded into a centrifugal tube before the addition of the sample. EVs can then be isolated due to differences in the densities once

the balance is achieved between centrifugal force and buoyancy via ultracentrifugation. The gold standard and the frequently used technique is the ultracentrifugation for the isolation of EVs. However, these techniques include multiple proceeding steps and take around 5 to 6 hours. To improve the purity, more centrifugation cycles need to perform, which might cause the loss of EVs [47]. Expensive equipment and larger duration limit the use of ultracentrifugation in a real clinical setting for early diagnosis of cancer.

The isolation techniques based on size include membrane filtration, size exclusion chromatography (SEC), and other isolation methods in microfluidic chips. In filtration, the EVs are isolated based on the size differences of the bioparticles in the sample. It is a simple and high-throughput method. Size exclusion chromatography (SEC) enables separation of polymer or proteins based on their size or hydrodynamic volume, where a porous matrix is usually packaged into a column as a stationary phase. When a sample passes, the components with a size smaller than the pore diameter can enter porous material, which takes a longer time to pass through the column, while the larger size components than the pore diameter will be excluded from the pores. Thus, different elution times can be used to separate the components. This method is extensively used for the isolation of EVs/exosomes [48, 49]. However, there is a high chance for EVs or the other contaminant aggregates to get trapped in the pores. Throughput can be greatly reduced with this unavoidable issue and consequently can damage the EVs because of the higher pressure that forces the sample through the filter.

The polymer precipitation method for isolation EVs ensures high yield by simplifying the process and reducing the handling time. These polymer-based precipitation methods have been commercialized by some companies (ExoQuick, Total exosome isolation, and Exospin) because of their simple protocols and fast isolation. In this method, polymers are dissolved in the sample to reduce the solubility, because of which, low-speed centrifugation can precipitate EVs for isolation. Polyethylene glycol (PEG) has been used for the isolation of EVs as a precipitation agent [51]. Though this method is simple, fast, and with a high yield, it lacks purity as the protein aggregates and other contaminants may be coprecipitated by the added polymers. Besides, it may change the structure and cover the surface characteristics of the EVs [52]. These drawbacks can severely affect the further analysis of EVs.

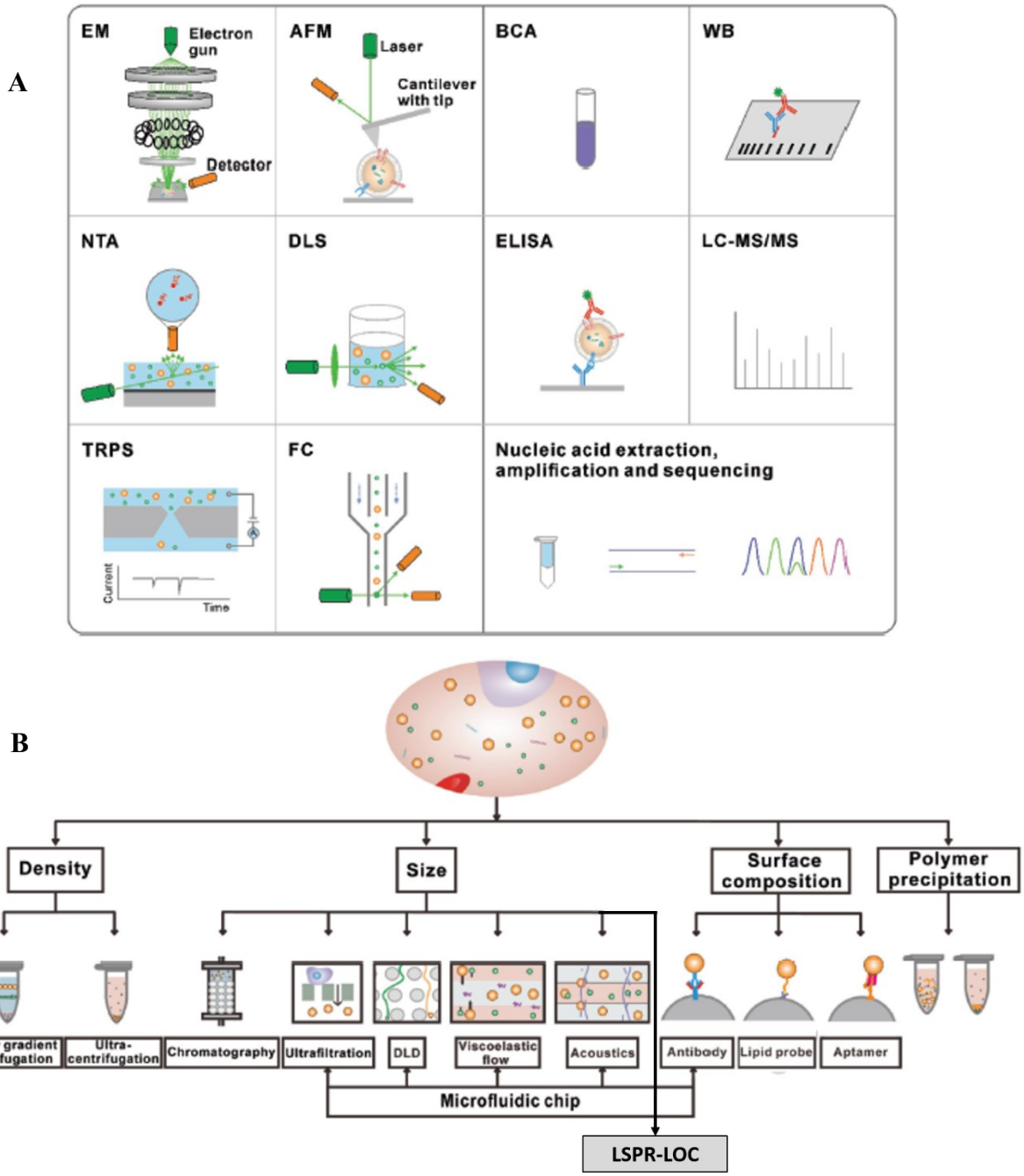

Figure 1.6: Traditional methods for the characterization of EVs (A) Characterization techniques to measure physical properties (morphology, size, and zeta potential), concentration, and biomolecular properties (B) Classification of EV isolation strategies [50]

The presence of a large number of proteins on the surface of EVs and lipid bilayer make the immunoaffinity-based methods highly suitable for their isolation. For specific capture and isolation of EVs, the frequently used method is affinity-based isolation. These methods are based

on the binding of antibodies and aptamers or by a lipid probe as shown in Figure 1.7. An antibody with affinity to EV proteins is usually modified on a solid surface such as magnetic beads and microfluidic chips to separate EVs from a culture media or nonspecific vesicles and other contaminants [53]. In addition to beads or microfluidic chips, nanoparticles or nanomaterials may provide more suitable substrates to capture EVs because of increased binding sites on the surface. Peptides can also be used as affinity agents similar to antibodies for the isolation of EVs. The aptamer is a screened nucleic acid fragment with a specific sequence and has a high affinity towards the specific proteins on the surface of EVs with which it can bind to the target protein for the isolation of EVs. The usage of aptamers for the isolation of EVs has advantages such as low cost, high stability, and easy production [54]. Though aptamers have these advantages over antibodies, the major drawback is the availability of aptamers with specific affinity to EVs is still rare. To avoid this drawback, the other alternative approach for the isolation is to bind with the lipid bilayer by designing the lipophilic isolation probe. The capture efficiency can be improved, and full-scale extraction can be obtained by a lipid probe isolation method. Wan et al. [55] reported using the lipid probe for the isolation of EVs by using magnetic extraction and the purity of the EVs is higher than that of ultracentrifugation. This method of isolation can capture EVs regardless of size and their surface antigen avoiding the loss brought by the surface marker.

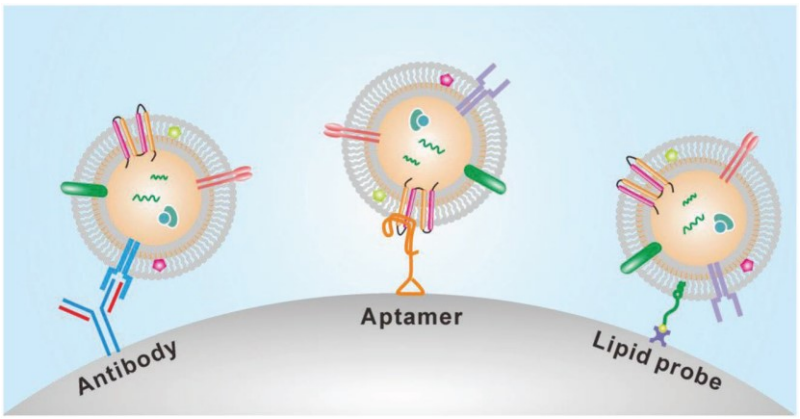

Figure 1.7: Immunoaffinity-based isolation of EVs [50]

An alternating current electrokinetic method was recently employed for the isolation of EVs. This method was fast but has less purity. To improve performance in EV isolation, several researchers have taken the advantage of combining different isolation methods, such as combining filtration with ultracentrifugation while some of them were integrating isolation methods into

microfluidic devices. Various microfluidic-based isolation techniques are tabulated in terms of their yield, sample capacity, and efficiency in Table 1.2. This table clearly shows that the developments in the microfluidic/LOC technology have enhanced the isolation of EVs in terms of their speed and efficiency compared to the gold standard ultracentrifugation.

Table 1.2: Performance of various microfluidic techniques in the isolation of EVs [44]

Techniques	Sample & capacity	Isolation speed	Yield	Advantages	Disadvantages
Microfluidic/LOC Technology					
Anti-CD63 functionalized surface with herringbone groves by Chen et al. [43]	Serum, 400µl	16µl/min in 25 min	42 – 94%	High specificity, Isolation time(~1h)	Specific for CD63
Array of surface-functionalized circular microchambers by Kanwar et al. [56]	Serum, 400µl	8µl/min in 60 min	15 –18 µg of total proteins	Easy scale up, On-chip quantification	Low capture capacity
Online mixing in serpentine channel with immunomagnetic beads by Zhao et al. [57], He et al. [35]	Plasma, Continuous flow, 10ml	10µl/min in 100 min	42– 97.3%	Isolation time(~1.5h), 30µl of sample, higher capture efficiency	Specific for CA125, EpCAM, and CD24
Precaptured polystyrene beads with inertial solution exchange by Dudanie et al. [58]	CCM, Continuous flow	140µl/min	n/a	High throughput and processing volume (~70µl/min)	Bead incubation (~4h), Not suitable for acute care
Array of porous silicon nanowire-on-micropillar by Wang et al. [59]	Standard liposome Sol., 100µl	10µl/min in 10 min	45 – 60%	Trapping is relatively fast (~10min), High purity exosomes	Recovery time (~1 day)
Filtration with photopolymerized nanoporous membranes by Davies et al. [60]	Blood, Saturation 100µl	1µl/min	3%	Shorter separation time, Performed directly on whole blood	Low recovery, Saturation point (3-4 µl)
Acoustic nanofilter chip by Lee at al. [61]	CCM, Continuous flow, 50µl	n/a	>80%	90% separation yield, In-situ control of size	Specific MV targets
Obstacle arrays in deterministic lateral displacement by Santana et al. [62]	CCM, 170µl	n/a	39%	High purity - 98.5%	Low recovery efficiency (39%)
Ultracentrifugation					
Bobrie, A et al [63], Tauro et al [64]	Plasma, 12ml	≥600 min	5–25%		

Various research groups have used immunological approaches combined with different techniques in the past few years, permitting for enhanced isolation, or detection, or both. The sensing capability along with their sensitivity of the developed microfluidic devices are

summarized in Table 1.3. This table clearly shows that the microfluidic platforms showed a better performance when compared to conventional methods. Thus, these developments will certainly give solutions to the present hurdles in liquid biopsy of cancers.

Table 1.3: Performance of exosomes detection – sensing technologies [44]

Approaches	**Detection sensitivity**	**Detection Multiplexity**	**Markers detected**
ExoChip by Kanwar et al. [56]	0.5 pM	Doi dye staining, No multiplexity	CD63 capture exosomes and extract total RNA
ExoSearch chip by Zhao, Z.et al. [57]	750 particles/µl	Simultaneous detection of 3 markers	CA125, EpCAM, and CD24
nPLEX chip by Im et al. [65]	1000 particles/µl	Parallel detection of 12 potential exosomal markers	EpCAM, CD24, CA125, CA19-9, HER2, MUC18, EGFR, CLDN3, CD45, CD41, D2-40
GO/PDA nano-IMEX by Zhang, P et al. [66]	50 particles/µl (80 aM)	Single-plex sandwich ELISA	D9, CD63, CD81, EpCAM
iMEX chip by Zhu et al [67]	10^4 particles/µl	8 channels for simultaneous detection of 4 markers	EpCAM, CD24, CA125, CD63, HER2, MUC18, EGFR
µNMR chip by Shao, H et al. [68]	2×10^6 particles/µl	Magnetic nanoparticle labeling	EGFR, PDGFR-α, PDPN, EphA2, EGFRvIII6, IDH1, R132H, HSP90, CD41, MHCII
ExoScreen plate by Yoshioka et al [69]	ELISA grade	96-well plate	CD9, CD63, CD147, CEA, CA19-9
Nanoshearing microfluidic Approach by Vaidyanathan et al [70]	2760 particles/µl	Simultaneous detection of 3 markers	HER2, PSA, CD9
EV array by Jorgensen et al. [71, 72]	5000 particles/µl	Simultaneous detection of 21 markers	CD9, CD63, CD81, TNF RI, TNF RII, HSAP90, HLA-ABC, GRP78, Mucin16, PLAP, SPA, P53, EGFR, HER2, CD276, Osteopontin, SFTPD, Coilin, NYESO-1, EpCAM, PAX-8
SPR approach by Zhu et al [67]	4.87×10^4 particles/µl, or low pM	No multiplexity	CD63, CD9, CD24, CD44, EpCAM, HER2
FLOWER/laser dark-field Imaging by Akagi, T et al. [73]	Single exosome	No multiplexity	N/A

1.6 Why Lab-on a Chip (LOC)/Microfluidics?

For an improved treatment and outcome, and to control the progression of the disease, a rapid and early diagnosis is required. Traditional biomarker detection methods such as polymerase chain reaction (PCR), enzyme-linked immunosorbent assay (ELISA) heavily depend on bulky, expensive, and sophisticated equipment. Therefore, quantification of specific proteins and genetic

biomarkers in blood or other fluids such as saliva or urine is needed. Thus, researchers have been driven to develop new diagnostic tools, suitable for rapid point-of-care (POC) applications. In the past two decades, Lab-on-a-chip (LoC) technology has drawn significant interest from the researchers and industries for biomedical applications. The lab-on a chip (LOC) or microfluidics integrates the conventional isolation methods or applies the principles of fluid dynamics. This is how LOC plays a very crucial role in advancing EV isolation technology. The development of LOC/microfluidics, nanomaterials, biomolecular probes, and the idea of using EVs as biomarkers for the detection of cancer, have greatly boosted the development of novel EV isolation technologies. The advantages of LOC include high throughput, low sample, and reagent consumption, short assay time, and multiplexed detection [74, 75]. The technology has shown the potential to improve molecular biomarker detection by offering sensitive and wide-ranging measurements in a compact format. Microfluidics-based platforms have been developed for the isolation and quantification of biomolecules and more complex entities that show potential for early cancer detection.

1.7 Importance of liquid biopsy

Tumor biopsy provides critical information on the diagnosis of cancer, its prognosis, and prediction of response to treatment. Biopsy has been and continues to be the standard procedure for decades. Moreover, tissue biopsy has been the only option to determine the origin and stage of cancer. Although surgical biopsies typically provide the highest amount of intact tumor tissue for analysis, the procedure is invasive, costly, and time-consuming. As the number of tests required for the diagnosis and genetic evaluation has grown, it needs more tumor tissue for additional testing. Current biopsy procedures are invasive and, often produce too few cells or tissue sections for broad analysis. So, multiple biopsies are not practical for many patients, such as the elderly and those with multiple diseases. The major limitation to any biopsy technique is that analysis of a single tumor may not capture all the mutations that are present. Cancer grows genetically over time, causing the tumors to metastasize and develop resistance to treatments that are initially effective. Therefore, improved biopsy methods that produce sufficient sample amounts that are reflective of the overall tumor and are flexible to frequent testing are undoubtedly needed.

A liquid biopsy refers to the analysis of any tumor-derived material circulating in the blood or any other body fluid with a possibility of multiple analyses as shown in Figure 1.8 [76, 77].

Liquid biopsies are performed on body fluid samples – blood being of most interest, other body fluids such as saliva, urine, spinal fluid, etc. are used, to look for a wide range of cancer biomarkers, starting from DNA and RNA fragments, to 'vesicles' containing tumor material, to whole cancer cells. Liquid biopsies can detect any targetable genomic modification and guide corresponding targeted therapy. Due to the non-invasive nature of the technique, liquid biopsy has the potential for frequent testing of multiple tumor sites and provides complete genetic signature with less risk to the patient while a single tumor biopsy may provide limited information invasively.

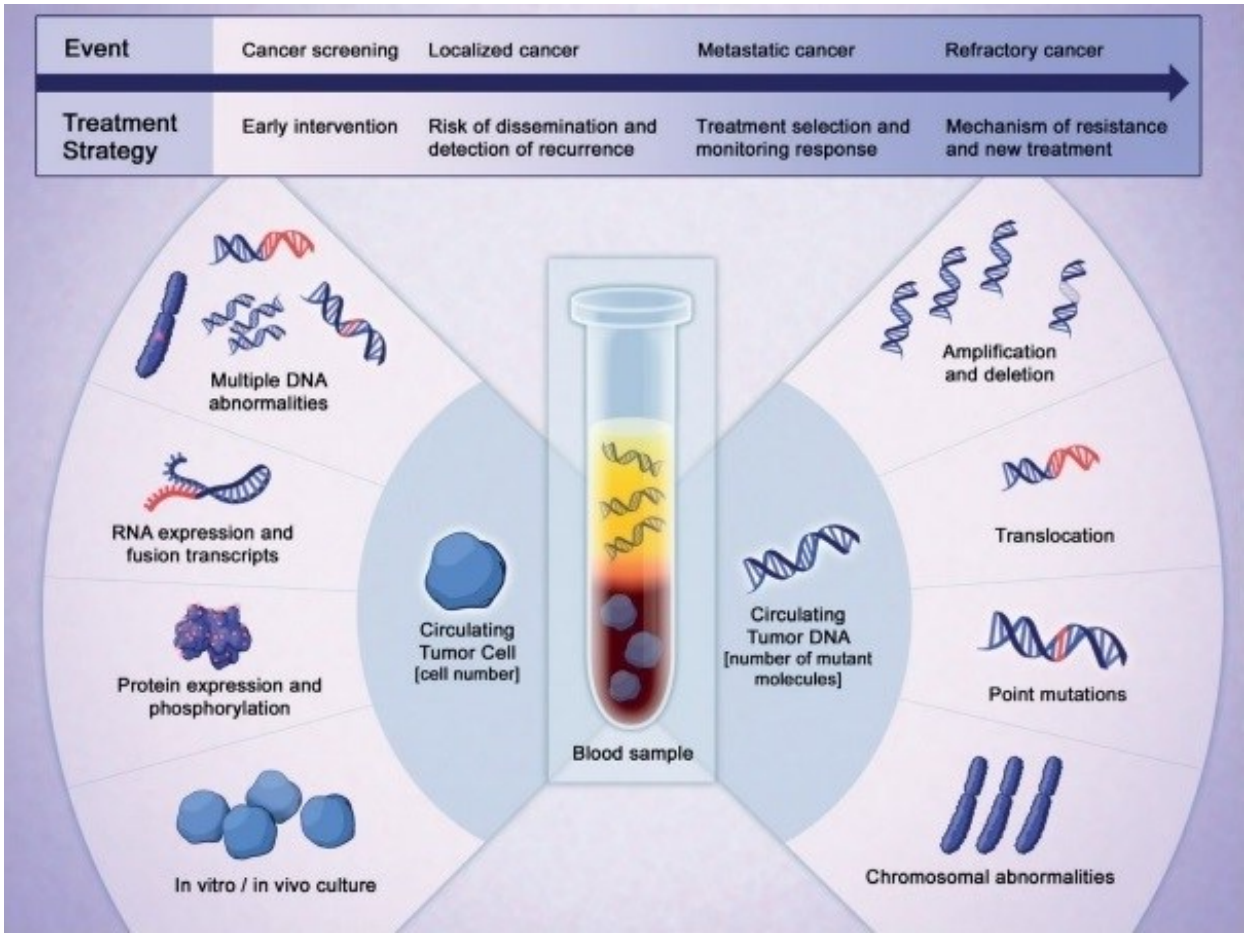

Figure 1.8: Clinical applications of CTCs and ctDNA in liquid biopsy [77]

Liquid biopsy techniques are based on either PCR amplification or next-generation sequencing (NGS) technology to maximize the sensitivity. Liquid biopsies use circulating tumor cells (CTCs) or EVs/exosomes as the source for tumor DNA along with circulating free DNA (cfDNA). CTCs are intact tumor cells released into the bloodstream that can provide a source of

tumor DNA. Many patients with early-stage cancer may not possess CTCs in their blood, making these cells a less reliable sample source for identifying genetic variations or assessing prognosis. But as seen in Figure 1.5, the expression level of exosomes at an early stage of cancer is quite high compared to CTCs, making the exosomes a reliable source for the early diagnosis of cancer. Liquid biopsy has the potential to help throughout all stages of cancer in general: screening, minimal residual disease detection to guide treatment, early detection of relapse, systemic treatment initiation and monitoring of response, and resistance genotyping [78, 79].

1.8 Why gold nanoparticles and LSPR?

Gold is one of the first metals to have been discovered. The gold that was first obtained by Chinese, Arabian, and Indian scientists as early as in the V-IV centuries B.C, has been used for medicinal purposes. Colloidal gold was used in alchemist laboratories during the middle ages in Europe. The first book on colloidal gold was published by the philosopher and Doctor of Medicine Francisco Antonii in the year 1618 [80]. Earlier, colloidal gold was obtained by reducing the gold chloride by vegetable extracts in alcohols or oils. Later, Turkevich *et al.* [158] developed a method for the preparation of gold nanoparticles (AuNPs) by treating the hydrogen tetrachloroaurate ($HAuCl_4$) with citrate acid in boiling water. Citrate acts as a reducing and stabilizing agent. Gold nanoparticles have unique properties and multiple surface functionalities. Due to these properties, they have been widely employed in bio-nanotechnology for diagnostics and are also used in the area of therapeutics. The versatility of AuNPs made them important components for biomedical applications. Functionalized AuNPs with controlled geometrical and optical properties are the current intensive studies and the subject of biomedical applications. These applications include biosensors, immunoassays, clinical chemistry, laser phototherapy of cancer cells and tumors, the targeted delivery of drugs, DNA, and antigens, optical bioimaging, and the monitoring of cells and tissues.

In the last two decades, surface plasmon resonance (SPR) technology has revolutionized the biosensing field with the start of nanotechnology, especially in the field of plasmonics. A highly sensitive transducing mechanism is the primary for the major importance of SPR. Transducing mechanism is where surface plasmon polaritons (SPPs), which are the surface propagating EM waves show an extraordinary sensitivity to the refractive index interfacial changes. However, the activation of this mechanism in SPR requires complex supporting optics,

due to the inability of SPP excitation by freely propagating light [81]. The propagating nature of SPPs limits the miniaturization. To overcome this miniaturization and device bulkiness, metallic nanoparticles supporting localized surface plasmon resonance (LSPR) have been primarily identified as the next generation of optical label-free biosensors. The main reason behind this consideration is the extreme sensor miniaturization capability, to the scale of a single nanoparticle [82, 83].

The sensitivity of the LSPR property of metallic nanoparticles such as silver and gold nanoparticles (AuNPs) to any change in their surrounding medium forms the basis for a label-free bio-sensing application [84-86]. Binding biomolecules to AuNPs or nano-islands immobilized on substrate results in a redshift of the LSPR bands or/and an increase in the absorbance of the band. The optical properties of AuNPs have been thoroughly studied and optimized for sensing applications, in terms of size and shape [87, 88]. LSPR sensors, based on plasmonic nanostructures, are now widely used to interrogate biomolecular interactions in real-time. Despite the increasing interest in the LSPR phenomenon and its applications, there is still little research going on with the integration of LSPR biosensing with a microfluidic platform, thereby, contributing to the emerging field of plasmofluidics [89]. In the past, for the detection of bovine growth hormone (bGH), also known as bovine somatotropin (bST), the label-free LSPR technique has been used and proved to be effective. It can be understood that the LSPR technique is best suited, because of its detection limit which is in the range of 1-5 ng/ml among the various LOC methods [90]. Vn96 is a synthetic polypeptide, specifically designed to captures exosomes by binding to the heat shock proteins (HSPs) present on their surface and the exosomes are complex vesicular cargo of proteins and other biomolecules, so, it seemed logical to use the nanoplasmonic platforms based on LSPR generated by metal nanoparticles, typically gold nanoparticles in the current studies.

1.9 Organization and layout of the thesis

This thesis has been organized as follows:

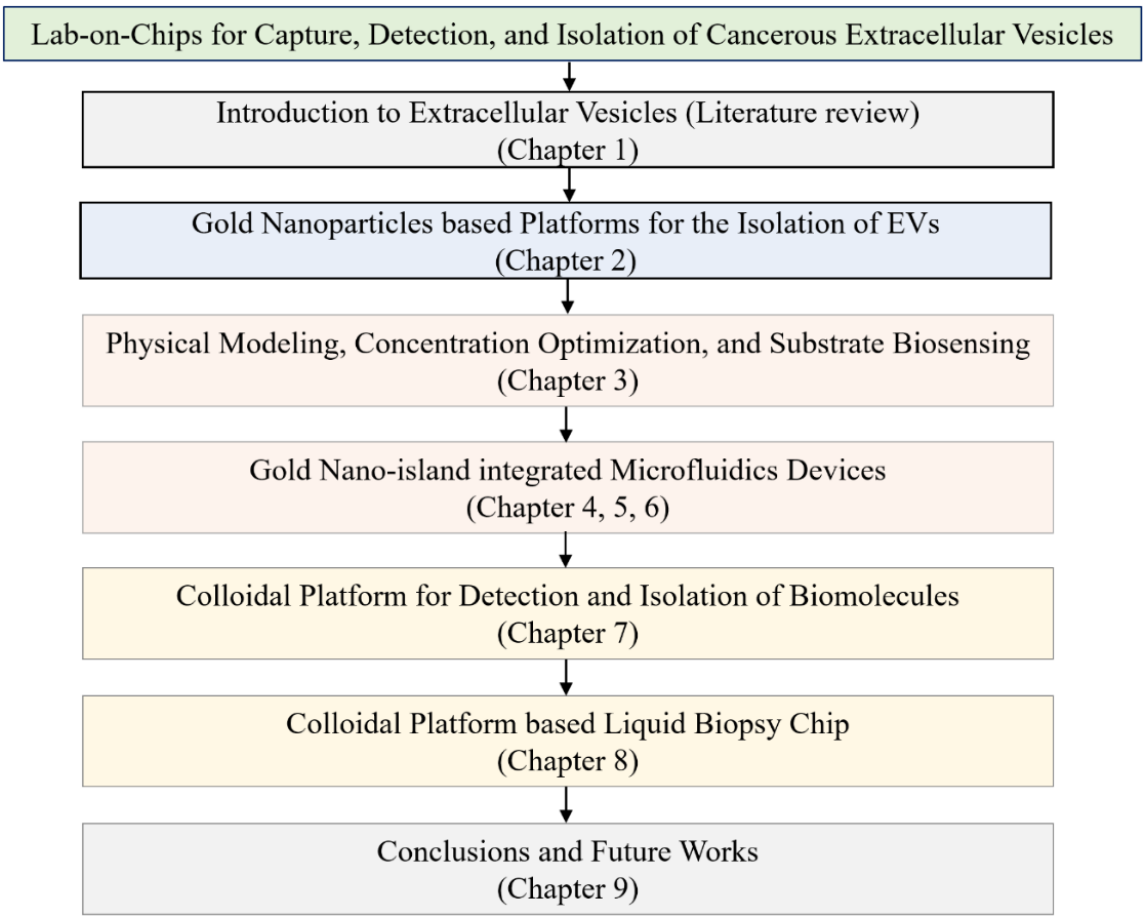

Chapter 2: Platforms for Capture, Detection, Isolation, and Characterization of Extracellular Vesicles: This chapter presents the detection sensitivities of the gold nanoparticles based on the refractive index of the solvents. The platforms discussed in this chapter are gold nanocomposites, gold nano-islands on a glass substrate, and the gold nanoparticles suspended in a colloidal solution. The part of the gold nanocomposites is duplicated from the paper published in the Journal of Nanoparticle Research. This paper discusses the gold-PDMS nanocomposites that were created by the in-situ synthesis of gold by using the gold precursor solution. The *in-situ* reduction and the subsequent diffusion of AuNPs into the PDMS matrix through heat treatment. The interplay between the reduction of gold ions and the continuous diffusion of the cross-linking agent toward the surface is also discussed in detail. Further, the effect of sub-surface segregation of AuNPs and their subsequent spatial distribution on the sensing capability of the nanocomposite are presented. Also, the ex-situ synthesis of gold nanoparticles using the Turkevich method and their deposition on a glass substrate to form gold nano-islands is discussed. Finally, the chapter

concludes with the identification of platforms based on their refractive index sensitivity for capture, isolation, and detection of EVs from MCF7 CCM.

Chapter 3: Nano-Bio interactions of Extracellular Vesicles with Gold Nano-islands for Early Cancer Diagnosis: This is chapter is duplicated from the paper published in the Journal Research which presents the physical modeling based on the characteristics of the gold nano-islands and the bio-entities to determine the detection capability of the platform, which is optimized experimentally at each stage. Preliminary results and modeling present a relationship between the plasmonic shift and the concentration of exosomes, and essentially indicate possibilities for label-free early diagnosis.

Chapter 4: Plasmonic Detection of Extracellular Vesicles using a Gold Nano-island Integrated Microfluidic Platform: This chapter is duplicated from the paper published in the Journal of Biomedical and Biological Engineering from (WASET), which presents a microfluidic device, designed for sensing of exosomes on a glass substrate sealed by a PDMS layer that contains the channel and a collection chamber. When the biochemical entities were introduced, an Ocean Optics spectrometer was used to measure the position of the Au plasmon band at each step of the sensing. The experiments have shown that the LSPR shift is proportional to the concentration of exosomes and, thereby, exosomes can be accurately quantified.

Chapter 5: Microfluidic Isolation of Extracellular Vesicles and Validation through AFM and DNA Amplification: This chapter is duplicated from the paper published in the European Journal of Extracellular Vesicles, which presents a microfluidic device containing multiple channels and a collection chamber to capture EVs. The capture and detection ability of the device is validated by AFM measurements and the measurement of gene copy numbers using droplet digital PCR (ddPCR). The results indicate that the developed device can be considered as a prospective point-of-care apparatus for diagnostics in a clinical setting.

Chapter 6: Sensitivity Amplification by Multi-level Microfluidic Device for the Detection of Extracellular Vesicles: This chapter is duplicated from the manuscript prepared for the Journal of Advanced NanoBioMed Research, which presents a gold nano-islands integrated

multilevel microfluidic device for the amplification of detection sensitivity. This device contains consists of a glass substrate deposited with gold nano-islands on both sides, PDMS films containing microchannels one above the other in different levels, and a collection chamber on each level to capture, detect, and isolate EVs.

Chapter 7: Methods for Detecting, Isolation, and Quantifying an Analyte in a Sample Based on Colloidal Suspension of Plasmonic Metal Nanoparticles: This chapter presents the details of the invention submitted, which discusses a colloidal platform for detection and isolation of biomolecules utilizing the gold or metal nanoparticles suspended in a colloidal solution. The precipitation method was used to isolate biomolecules by binding them to the metal nanoparticles in the colloidal solution and the usage of the supernatant as a biosensor for the diagnosis of cancer at an early stage is also proposed.

Chapter 8: Liquid Biopsy Chip for Isolation of Extracellular Vesicles using Magnetic Particles by Gravity Assisted Sedimentation and Characterization by Gene Amplification: This chapter is duplicated from the manuscript prepared for the Journal of Biosensors and Bioelectronics, which presents a liquid biopsy chip for the capture and isolation of EVs from the MCF7 CCM using magnetic particles based on the colloidal platform. To ensure the capture efficiency by proper binding of the magnetic particles and the EVs, a split and recombination 3D mixer is integrated into the chip design and it also consists of a sedimentation unit, which allows EV-captured magnetic particles to settle in it. The captured EVs are then isolated from the chip based on gravity-assisted sedimentation technique for elution of EVs and their validation. The isolated EVs are characterized by the SEM measurements and the ability to capture and isolation of EVs is validated by the NTA and AFM measurements. Finally, the absolute quantification of RNase P gene copies from the isolated EVs are characterized using droplet digital PCR (ddPCR)

Chapter 9: Conclusions and Future Works: This chapter presents the summary of the platforms discussed in the thesis for the capture, detection, and isolation of EVs from MCF7 conditioned media, concluding remarks, and recommendations for future works.

To comply with the Concordia thesis regulations, figures, tables, and equation numbers may have been modified from the original submitted or published article. As such, the references of all the articles are combined and presented at the end of the thesis.

1.10 The outcome from the thesis

1.10.1. Patent

1. **S. Bathini**, M. Packirisamy, "Methods for Detecting, Isolation and Quantifying an Analyte in a Sample Based on Colloidal Suspension of Plasmonic Metal Nanoparticles" (US provisional (63,084,960) filed in September 2020)

1.10.2. Published/to be submitted/prepared journals

1. **S. Bathini**, M. Packirisamy, "Synthesis of Gold Nanoparticles and the relation between Concentration and absorbance", 2021 (To be prepared from Patent)
2. **S. Bathini**, M. Packirisamy, "Detection of biotin tagged biomolecules using Free Suspended Gold Nanoparticles in a Colloidal Solution", 2021 (To be prepared from Patent)
3. **S. Bathini**, M. Packirisamy, "Detection of Bovine Growth Hormone using Gold Nanoparticles Suspended in Colloidal Solution", 2021 (To be prepared from Patent)
4. **S. Bathini**, M. Packirisamy, "Capture, Detection of Extracellular Vesicles using Gold Nanoparticles Suspended in Colloidal Solution", 2021 (To be prepared from Patent)
5. **S. Bathini**, A. Ghosh, M. Packirisamy, "Liquid Biopsy Chip for Isolation of Extracellular Vesicles using Magnetic Particles by Gravity Assisted Sedimentation", 2021 (to be submitted to *Journal of Biosensors and Bioelectronics*)
6. **S. Bathini**, A. Ghosh, M. Packirisamy, "Sensitivity Amplification by Multi-level Microfluidic Device for the Detection of Extracellular Vesicles", 2021 (to be submitted to *Journal of Advanced NanoBioMed Research*)
7. **S. Bathini**, D. Raju, S. Badilescu, S. Pakkiriswami, A. Ghosh, R. J. Ouellette, M. Packirisamy, "Microfluidic Isolation of Extracellular Vesicles and Validation through AFM and DNA Amplification", *Euro J. of Extracell. Ves.*, Vol.1, 3-10, 2020
8. **S. Bathini**, D. Raju, S. Badilescu, M. Packirisamy, "Effect of Cross-Linking and Thermal Budget on Plasmonic Sensing and Sub-Surface Segregation of *In-Situ* Synthesized Gold in Polymer-Nano Composite", *J. Nanopart Res*, 23, Article 21, 2021

9. **S. Bathini**, D. Raju, S. Badilescu, A. Kumar, R. J. Ouellette, A. Ghosh, M. Packirisamy, "Nano-Bio Interactions of Extracellular Vesicles with Gold Nanoislands for Early Cancer Diagnosis," *Research*, vol. 2018, Article ID 3917986, 10 pages, 2018
10. **S. Bathini**, D. Raju, S. Badilescu, M. Packirisamy, "Microfluidic Plasmonic Bio-Sensing of Exosomes by Using a Gold Nano-Island Platform", *Intl. J. of Biomed. Biol. Engg (WASET).*, Vol. 12, No. 5, 226 – 229, 2018
11. S. Badilescu, D. Raju, **S. Bathini**, M. Packirisamy, "Gold Nano-Island Platforms for Localized Surface Plasmon Resonance Sensing: A Short Review", *Molecules*, 25(20), 4661, 2020
12. D. Raju, **S. Bathini**, S. Badilescu, R.J. Ouellette, A. Ghosh, M. Packirisamy, "LSPR Detection of Extracellular vesicles using a silver-PDMS nano-composite platform suitable for sensor networks", *Enterprise Information System (EIS)*, 14(4), 532-541, 2020
13. D. Raju, **S. Bathini**, S. Badilescu, R.J. Ouellette, A. Ghosh, M. Packirisamy, "Study of Detection and Capture of Exosomes by Using the Morphologies of Ex Situ and In Situ Nanostructures", *J. Electrochem. Soc.*, 166(9) B3001-B3006, 2019
14. D. Raju, **S. Bathini**, S. Badilescu, R.J. Ouellette, A. Ghosh, M. Packirisamy, "Comparison of Ex-Situ and *In-situ* Nano Plasmonic Platforms for Capture and Detection of Exosomes", *ECS Trans.*, Vol. 85, Issue 13, 1407-1414, 2018
15. D. Raju, **S. Bathini**, S. Badilescu, R.J. Ouellette, A. Ghosh, M. Packirisamy, "Exosomes Detection by a Label-free Localized Surface Plasmonic Resonance Method", *ECS Trans.*, Vol. 75, Issue 17, 11-17, 2016

1.10.3. Conference publications

1. **S. Bathini**, D. Raju, S. Badilescu, S. Pakkiriswami, A. Ghosh, R. J. Ouellette, M. Packirisamy, "Genetic Validation of Physical Modeling of Nano-Bio Interactions between Extracellular Vesicles and Different Morphologies of Gold Nano Particles", *MRS-ISEV Conference on Extracellular Vesicles in Cancer*, August 2019, Nashville, USA
2. D. Raju, **S. Bathini**, S. Badilescu, S. Pakkiriswami, A. Ghosh, R. J. Ouellette, M. Packirisamy, "Plasmonic biosensing of exosomes using a microfluidic device (lab-on-a-chip) and its validation using droplet digital PCR", *MRS-ISEV Conference on Extracellular Vesicles in Cancer*, August 2019, Nashville, USA

3. **S. Bathini**, D. Raju, S. Badilescu, R.J. Ouellette, A. Ghosh, M. Packirisamy, "Comparison of Extracellular vesicles detection by microfluidic plasmonics of gold nano-island and nanocomposite platforms", *International Society for Extracellular Vesicles (ISEV)*, April 2019, Kyoto, Japan
4. **S. Bathini**; R Duraichelvan; S Badilescu; A Ghosh; M Packirisamy, "Gold nano-island platform for the microfluidic plasmonic detection of exosomes", *International Conference of Theoretical and Applied Nanoscience and Nanotechnology* (*TANN'18),* June 2018, Niagara Falls, Canada
5. **S. Bathini**; R Duraichelvan; S Badilescu; M Packirisamy, "Microfluidic Plasmonic Bio-Sensing of Exosomes by Using a Gold Nano-Island Platform", *20th International Conference on Mechanical Engineering* (*ICME),* May 2018, Montreal, Canada
6. R. Duraichelvan, **B. Srinivas**, S. Badilescu, A. Ghosh, M Packirisamy, "Comparison of Ex-Situ and In-Situ Nano Plasmonic Platforms for Capture and Detection of Exosomes", *233rd ECS Meeting, May 2018, Seattle, USA*
7. D. Raju, **S. Bathini**, S. Badilescu, A. Ghosh, RJ. Ouellette, M. Packirisamy, "Gold Nanoparticle Ring and Hole Structures-Based Platforms for Capture and Label-free Detection of Exosomes", *International Society for Extracellular Vesicles (ISEV2018) Annual Meeting,* May 2018, Barcelona, Spain
8. A. Ghosh, **S. Bathini**, D. Raju, S. Badilescu, A. Kumar, R. J. Ouellette, M. Packirisamy, "Capture and label-free detection of extracellular vesicles on gold-nano-island based microfluidic Lab-on-a-CHIP device using synthetic-peptide Vn96", *ISEV2018 Annual Meeting, May 2018, Barcelona, Spain*
9. **S. Bathini;** R Duraichelvan; S Badilescu; M Packirisamy, "Plasmonic detection of Extracellular vesicles in a microfluidic environment using synthetic-peptide (Vn96) based affinity capture", *International Society for Extracellular Vesicles* (*ISEV2017), May 2017, Toronto, Canada*
10. R Duraichelvan; **S. Bathini;** S Badilescu; M Packirisamy**,** "Label-free Detection of Extracellular Vesicles Using Plasmonic Platforms", *TEXPO 2016 Conference, October 2016, Montreal, Canada*

11. R Duraichelvan; **S. Bathini;** S Badilescu; M Packirisamy**,** "Exosomes Detection by a Label-free Localized Surface Plasmonic Resonance Method", *ECS Conference, October 2016, Hawaii, USA*
12. R Duraichelvan; **S. Bathini;** S Badilescu; M Packirisamy**,** "Label-free Detection of Extracellular Vesicles Using Nanocomposite Platform", *Keystone Symposia Conference, June 2016, Colorado, USA*

1.10.4. Author contribution

The works which are contributed by the author were only included in the thesis. Amongst the co-authors in the journals; Dr. Muthukumaran Packirisamy (M.P) and Dr. Anirban Ghosh (A.G) have conceived and supervised all the study and investigations presented in the thesis. Dr. Simona Badilescu (S.B) has supervised the works. Duraichelvan Raju (D.R) has helped with the measurements and Dr. Rodney J. Ouellette (R.O) has provided the materials.

Chapter 2

Platforms for Capture, Detection, Isolation, and Characterization of Extracellular Vesicles

The main objective of this dissertation is to develop lab-on-chip devices for the capture, detection, and isolation of cancerous extracellular vesicles from MCF7 culture media, which is the breast cancer cell line. To do this, three platforms have been explored using plasmonic of gold nanoparticles, namely, in-situ synthesized gold nanocomposites, gold nano-islands on a glass substrate, and the colloidal solution with suspended gold nanoparticles (AuNPs). The first step was to identify a sensitive platform which is suitable for the capture and isolation of EVs. Therefore, the sensitivity of the above-mentioned platforms is studied and discussed below.

The nanocomposite part of this chapter is reproduced from the article published in *Journal of Nanoparticle Research*, 23, Article 21, 2021

Surface gold – Poly (dimethyl siloxane) nanocomposites are a special category of composites, with gold nanoparticles segregated in a sub-surface layer of the polymer. In this work, sub-surface nanocomposites were created by in-situ synthesis of gold by using the solution of a gold precursor. The *in-situ* reduction of gold ions by the polymer's cross-linking agent (a vinyl silicon compound) and the subsequent diffusion of gold nanoparticles into the PDMS matrix through heat treatment are investigated, principally, by UV-Vis spectroscopy, Scanning Electron Microscopy (SEM), Atomic Force Microscopy (AFM), X-ray diffraction (XRD) and X-ray photoelectron spectrometry (XPS). It is shown that the freshly formed gold nanoparticles are stabilized by the diffusion into sub-surface layer, where they form into small aggregates. The kinetics of the *in-situ* reduction reaction at the solution-film interface is studied. The interplay between the reduction of gold ions and the continuous diffusion of the cross-linking agent toward the surface are also discussed in detail. Further, the effect of sub-surface segregation of gold nanoparticles and their subsequent spatial distribution on the sensing capability of the nanocomposite are presented as well.

2.1. Introduction to nanocomposites

Nanoparticle-polymer composites are advanced functional materials, with nanoparticles integrated into a polymer matrix. In addition to the characteristics of polymers such as transparency and processability, nanocomposites may acquire outstanding electrical, optical, and magnetic properties of their metal components. Optical nonlinearities and/or infra-low/ultra-high refractive indices suitable for ultrathin color filters, UV absorbers, tunable optical filters [91], optical sensors, waveguides, optical strain detectors, thermo-chromic materials, are only some of the potential applications of nanocomposites that originate from the properties of nano-sized noble metals [92-99]. The design, fabrication, and characterization of conducting polydimethylsiloxane (PDMS) with metallic powder for microheaters and temperature sensors have also been reported [100]. Stretchable PDMS structures, doped with gold nanoparticles have been prepared and suggested for strain sensors [101]. Gold (Au) and silver (Ag) nanocomposites have also been used for water purification, targeted drug release, antimicrobial coatings, and analysis of environmental pollutants [102-105].

Because of the strong Localized Surface Plasmon Resonance (LSPR) bands of gold and silver nanoparticles in the visible spectrum, stemming from the excitation of plasmons by the incident light and giving rise to characteristic absorption, some gold-nanocomposites are appropriate for sensing applications. In general, the biosensing properties of nanocomposites depend on parameters related to the conditions of their preparation that are pivotal for the distribution of metal particles in the polymer matrix. Since the spatial distribution of the (AuNPs) determines the biosensing properties, it is important to develop mechanisms and methods to control it [106].

Nanocomposites can be synthesized either by *in-situ* method in which polymer reacts with precursor to create nanoparticles or by *ex-situ* method in which prefabricated nanoparticles are embedded. In addition, physical methods such as chemical vapor deposition, ion implantation and thermolysis have been successfully used to prepare nanocomposites having gold on the surface of the polymer [107, 108].

In some cases, depending on the softening temperature of the polymer, nanoparticles can be embedded just below the surface of the polymer, where they reach a metastable state with minimum Gibbs free energy [109]. The limited movement of nanoparticles (from the surface to the sub-surface layer) is accounted by the tendency to reduce their high surface energy. Despite

the efforts to prepare nanocomposites with appropriate morphologies and enhanced surface properties, the control of nanoparticles spatial distribution remains still at an emerging stage [110].

Generally, when nanoparticles are well-dispersed in the polymer matrix, in the absence of nanoparticle-nanoparticle interactions, the nanocomposite will have only the additive properties of the individual components. But, if the polymer is structured, entirely new properties would emerge. For example, in the case of PDMS that has a segregated layer, nanoparticles are formed and concentrated in the segregated layer(s) and the new properties originate from their closeness [111]. These special categories of nanocomposites, called surface nanocomposites, have a three-dimensional distribution of the AuNPs and they were found suitable, especially, for Surface-Enhanced Raman Scattering (SERS) applications [112-115].

An ordered structural design such as the segregated layer, in the case of PDMS, can be used to control the degree of nanoparticle aggregation within the polymer. PDMS is a polymer used for the fabrication of microfluidic devices. It has received utmost attention due to its ease of preparation, low cost, good transparency, and non-toxicity to biomolecules.

The cross-linking of PDMS is obtained by hydrosilylation, where vinyl groups of one component (the pre-polymer) react with hydrosilane groups of the second component (the curing agent, a vinyl silicon compound) in a Pt-catalyzed reaction [116, 117] as shown in Eq. (1).

$$(Cross-linker)-Si-H\ +\ CH_2\ =\ HC-Si-(polymer)\ \underset{heat}{\overset{Pt\ catalyst}{\rightarrow}}\ -Si-CH_2-CH_2-Si-(3D\ network) \quad (1)$$

Many authors [118, 119] have studied the kinetics of the hydrosilylation reaction catalyzed by a platinum complex but only for the case of bulk reaction between vinyl-terminated PDMS and silane cross-linkers. For thin films or coatings, the kinetics of the cross-linking reactions is different from the bulk behavior because of segregation, either at the interface with the atmosphere or at the substrate. In this way, the migration towards the surface decreases the concentration of the cross-linker and Pt catalyst in the bulk.

Zhang et al., and Goyal et al., [120, 121] have suggested that, in the case of *in-situ* synthesis of gold, the excess of curing agent may act as a reducing agent of gold ions. Zhang [120] investigated the effect of changing the curing (cross-linking) agent to monomer ratio (η), that is, the curing agent concentration. The poor sensing performance was explained by the local deformation of the polymer surface due to nanoparticles growth and their partial embedding into the polymer. The optical and thermoplasmonic response of the *in-situ* reduced AuNPs have been

measured [122] and various applications of the *in-situ* prepared Au-PDMS nanocomposite have been reported [123, 124].

Our group has systematically studied the *in-situ* synthesis of gold and silver nanocomposites of PDMS, especially for microfluidic sensing applications [125-128]. In order to develop *in-situ* nanocomposite for various applications it is important to undertake a systematic investigation of the *in-situ* surface nanocomposites, prepared by the reduction of gold ions by the excess of cross-linking agent in thin self-standing PDMS films. We are especially interested in how (i) cross linking agent concentration influence the distribution and the *in-situ* synthesis of gold nanoparticles after a specific synthesis time as shown in the schematic of Figure 2.1(A), and (ii) how the thermal budget drives the sub-surface layers of the polymer deeper as shown in the schematic of Figure 2.1(B). In the case of free-standing films, the diffusion of the precursor molecules occurs simultaneously through all the six sides of the sample. Because the focus of the work is on sensing applications, we were interested in both the agglomeration state of AuNPs in the surface segregated layers due to cross linking agent and their diffusion into PDMS during the annealing process. This work represents an attempt to establish how the distribution of AuNPs affects the sensing capability of the nanocomposite. The work is also pertinent to the general topic of the diffusion of nanoparticles in polymer films (coatings) and its effect on the properties of nanocomposites.

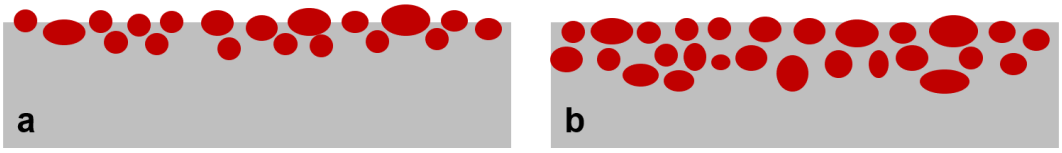

Figure 2.1: Illustration of diffusion of gold nanoparticles and effect of heat-treatment on a nanocomposite sample; (A) Schematic showing AuNPs in as-prepared sample. (B) Heat-treated sample (only the upper portion of the sample is shown for simplicity)

2.2. Materials

Gold (III) chloride trihydrate ($HAuCl_4.3H_2O$), isopropyl alcohol, dimethylformamide, chloroform, toluene, and anisole were purchased from Sigma-Aldrich. The Sylgard® 184 elastomer kit for the PDMS fabrication was purchased from Dow Corning. De-ionized (DI) water with a resistivity of 18MΩ, used in all the experiments, was obtained from the NANO pure ultrapure water system (Barnstead). Ethanol was purchased from Fisher Chemicals.

2.3. In-situ synthesis of gold-PDMS nanocomposites

The gold precursor solution is prepared by dissolving gold (III) chloride trihydrate ($HAuCl_4.3H_2O$) in ethanol. The concentration of the precursor solution was 0.6% (wt/v). The PDMS samples were prepared with two concentrations of base to cross linking agent namely 4:1 and 10:1. For the synthesis of Au-PDMS nanocomposites, the prepared PDMS films were immersed vertically in the gold precursor solution and incubated for around 48hrs. Figure 2.2(A) illustrates the immersed film in the precursor solution and Figure 2.2(B) shows the nanocomposite, after the completion of the reaction, (the PDMS film is shown slightly slanted for clarity). In the following sections, this nanocomposite will be referred as "as-prepared sample", (meaning the sample was taken out after a synthesis time of 48hrs at room temperature and was not heat-treated (t_{synth}= 48hrs, no heat-treatment). After the in-*situ* synthesis, the morphology of formed gold nanoparticles aggregates in the as-prepared sample is altered by heat treating the Au-PDMS nanocomposite samples at 200°C for 30 minutes. These samples will be referred as "heat-treated samples" (t_{synth}= 48hrs, Temp = 200°C, 30min heat-treatment).

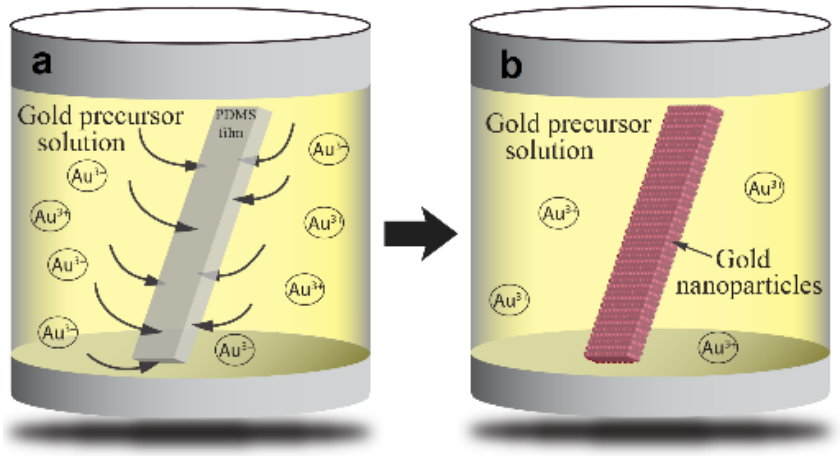

Figure 2.2: *In-situ* synthesis and slicing of the sample: (A) Schematic of *in-situ* synthesis; the PDMS film, immersed in the gold precursor solution (B) Au-PDMS nanocomposite (red), after 48 hrs.

2.3.1. Sensitivity measurements of the platforms

The sensitivity of the synthesized nanocomposite for sensing was measured, using solvents with different refractive indices. The measurements were performed by measuring the

absorption spectra, after immersing the nanocomposite sample in a quartz cuvette, filled with the solvent, for 1 hour. The refractive index sensitivity of 1mm thick 10:1 and 4:1 nanocomposite sample for as-prepared treated and heat-treated at 200°C, measured using various solvents as mentioned in the experimental section. Figure 2.3 shows the corresponding sensitivity plots. From the plots, it can be clearly seen that the sensitivity of all the nanocomposite platforms is quite low.

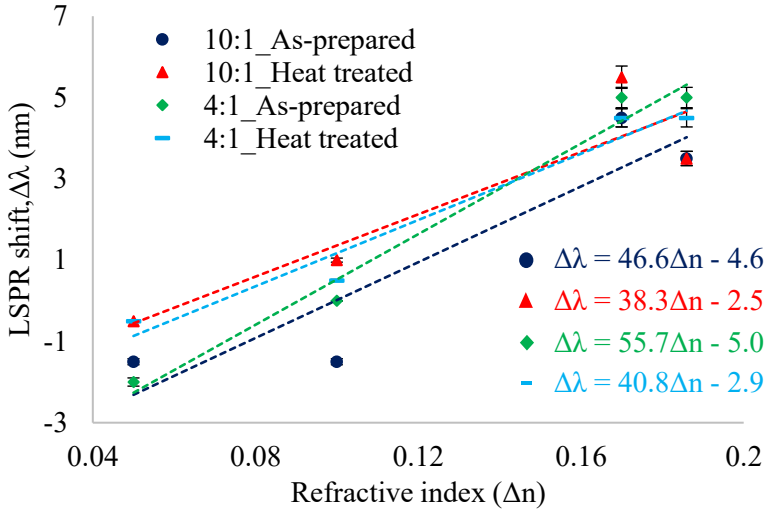

Figure 2.3: Sensitivity measurements of a 1mm thick 10:1 and 4:1 nanocomposite sample, as-prepared (t_{synth}= 48hrs, no heat-treatment) and heat-treated (t_{synth}= 48hrs, T = 200°C, 30min heat-treatment), (n=6)

The low refractive index sensitivity found for the Au-PDMS nanocomposite samples confirms the presence of most nanoparticles under the surface, covered by a thin polymer layer, that is, not available for sensing. Gold nanoparticles, prepared by *ex-situ* synthesis, or physical deposition methods such as chemical vapor deposition, ion implantation and thermolysis are located on the surface of the film [107, 108], while, in the case of *in-situ* synthesis, the Au nanoparticles are submerged under the surface, surrounded by the polymer chains and, therefore, are not in direct contact with the analyte. Even after heat-treatment, when more nanoparticles diffuse into the polymer, there are not particles on the surface. This would explain the low sensitivity of the platform in the case of *in-situ* synthesized Au NP.

2.4. Ex-situ synthesis of gold nanoparticles

Spherical gold nanoparticles were synthesized by reduction of Gold (III) Chloride trihydrate ($HAuCl_4.3H_2O$) by sodium citrate, following Turkevich's method. Briefly, 15mg of Gold (III) Chloride trihydrate ($HAuCl_4.3H_2O$) are added to 95 mL of DI water in a beaker and heated till it

reaches its boiling point. Then, 5ml of sodium citrate solution (2%), are added to the boiling solution. After the addition of sodium citrate, a change in color from the original yellow to a transparent purple can be clearly observed, showing the presence of gold nanoparticles. Parallelly, glass substrates of desired dimensions (37mmx12mm in this case) were cleaned with soap solution, DI water, and then rinsed with acetone, dried with 2-proponol (IPA) and air. Then the substrates were heated in an oven at 100°C for 1 hour to remove any moisture before the deposition process.

2.4.1. Fabrication of gold nano-islands

Fabrication of gold nano-islands on glass substrates includes the synthesis of gold nanoparticle (AuNPs) and, subsequently, their deposition on glass substrates by using the thermal convection method. The glass substrates were immersed at an angle of approximately 30° in a beaker containing the gold colloidal solution and kept in the oven at temperatures between 50 and 55 °C until the whole amount of the colloidal solution is evaporated, depositing the multilayers of gold nanoparticles on the glass substrate as shown in Figure 2.4. The glass substrate with gold multilayers was heat-treated at 560°C to form nano-islands.

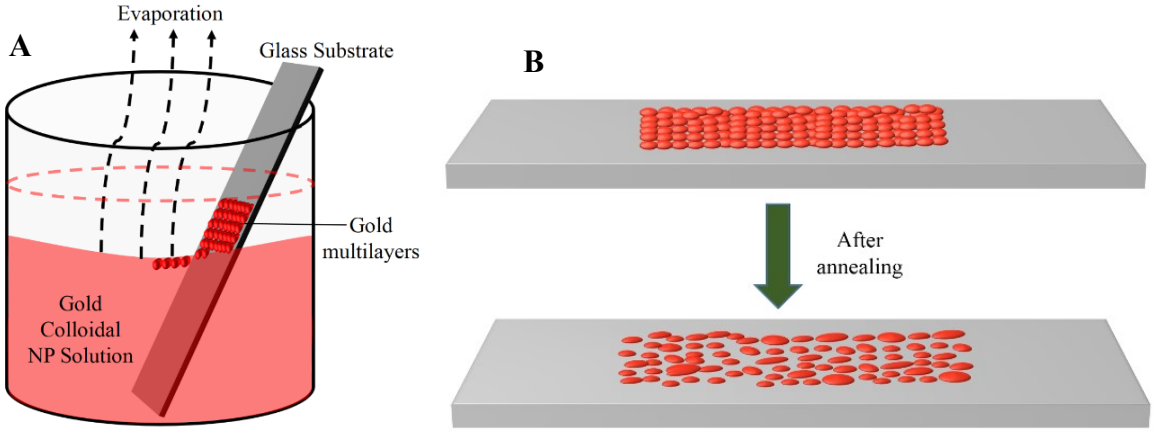

Figure 2.4: (A) Schematic of the convective assembly process (B) schematic of the morphological tuning of gold multilayers to gold islands by heat treatment

2.4.2. Sensitivity of gold nano-islands on glass substrate platform

The spectral sensitivity of the sensor can be calculated by using various solvents with different refractive indices. The spectral density denoted by S, for any sensor is defined as $S = \Delta\lambda/\Delta n$ where $\Delta\lambda$ is the shift of sensor resonance in nm, and Δn is the change of refractive index of the solution. In our experiments, we measured the sensitivity of the platform as a function of

refractive index of various solvents. The measurements were achieved by immersing glass substrate with gold nano-islands in a quartz cuvette filled with a solvent and measuring the absorption spectrum of the sample using the standard spectrophotometer from PerkinElmer (Lambda650). The shift of the resonance of the glass substrate with nano-islands as a function of the solvent filled allows us to determine the sensitivity of the substrate. The results of these measurements for all the solvents are as shown in Figure 2.5. The highest sensitivity was found to be 111.61 nm/RIU with a very good reproducibility (differences in the order of 5%) for the glass substrate with gold nano-islands. Table 2.1 below shows the solvents used for the sensitivity measurements.

Table 2.1: Solvents used in the sensitivity measurements and their refractive indices

Solvent	**RI (Refractive index)**
DI Water	1.33
Ethanol	1.36
IPA	1.8
Dimethylformamide (DMF)	1.43
Toluene	1.5
Anisole	1.516

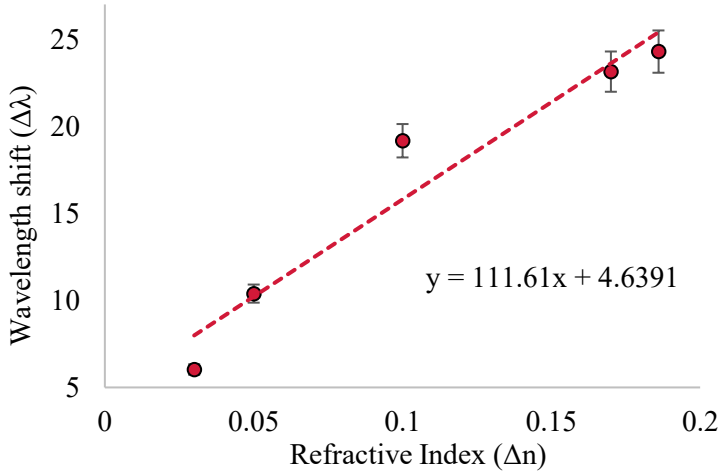

Figure 2.5: Sensitivity of gold nano-islands on glass substrate as a function of the variation of refractive index (Δn) (n=3)

2.5. Conclusions

The distribution of *in-situ* prepared AuNPs on the surface of PDMS self-standing films has been investigated by UV-Visible spectroscopy. It was found that nanoparticles are formed by *in-situ* reduction of gold ions on the surface of the film by the curing (crosslinking) agent and, right after formation, they are segregated in the sub-surface layer of PDMS, and only a few nanoparticles in the depth. The pattern of distribution at room temperature and after heat-treatment at 200°C was studied in relation to the amount of the curing agent in the PDMS composition. It is inferred that in thin self-standing PDMS films, the excess of curing agent migrates toward the interfaces with the atmosphere and reduces the incoming gold ions. The influence of the amount and distribution of AuNPs in PDMS on the refractive index sensitivity of the nanocomposite platform is discussed. The results show that the sensing capability of Au-PDMS surface nanocomposite film is low due to the polymer layer covering the AuNPs. The formation of the sub-surface structure in a thin self-standing nanocomposite film is accounted for by the weak Au-PDMS interfacial interactions, permitting the gold to sink under the surface and embed in the polymer. Because of which the sensitivity is found to be around 50nm/RIU. The gold nano-islands on a glass substrate platform, where synthesized AuNPs are deposited on a glass substrate by thermal convection and then heat-treated at 560°C for an hour to form gold nano-islands. The refractive index sensitivity of gold nano-islands is found to be around 111nm/RIU. The sensitivity is higher in case of gold nano-islands as the gold nano-islands are above the surface and are available to interact directly with the analyte. Considering the individual sensitivity of nanocomposite and nano-islands platforms, the gold nano-island platform was utilized further for the capture, detection, and isolation of EVs. The gold nano-islands on a glass substrate, where only half of the islands are available for sensing and capture, exhibited a better sensitivity meaning that utilizing the whole surface of nanoparticle would result in even better sensitivity as in the case of the third platform where gold nanoparticles suspended in a colloidal solution.

Hence, the gold nano-island platform and the colloidal platform are utilized further for the capture, detection, and isolation of EVs from the MCF7 culture media. To optimize the bio-nano interactions, it is important to understand the limitations of binding between gold nanoparticles and EVs or exosomes. So, the next chapter (Chapter 3) will discuss the physical modeling that defines maximum numbers of EVs or exosomes that can be accommodated on any kind of nanoparticle or a nanoisland based on their surface area.

Chapter 3

Nano-Bio Interactions of Extracellular Vesicles with Gold Nano-Islands for Early Cancer Diagnosis

This chapter is reproduced from the article published in *Research*, vol. 2018, Article ID 3917986, 2018.

Extracellular vesicles or Exosomes are membrane encapsulated biological nanometric particles secreted virtually by all types of cells throughout the animal kingdom. They carry a cargo of active molecules to proximal and distal cells of the body as mechanism of physiological communication, to maintain natural homeostasis as well as pathological responses. Exosomes carry a tremendous potential for liquid biopsy and therapeutic applications. Thus, there is a global demand for simple and robust exosome isolation methods amenable to point-of-care diagnosis and quality control of therapeutic exosome manufacturing. This can be achieved by molecular profiling of the exosomes for use with specific sets of molecular-markers for diagnosis and quality control. Liquid biopsy is undoubtedly the most promising diagnosis process to advance 'personalized medicine'. Currently, liquid biopsy is based on circulating cancer cells, cell free-DNA or exosomes. Exosomes potentially provide promise for early-stage diagnostic possibility; In order to facilitate superior diagnosis and isolation of exosomes, a novel platform is developed to detect and capture them, based on localized surface plasmon resonance (LSPR) of gold nano-islands, through strong affinity between exosomes and peptide called Venceremin or Vn96. Physical modeling, based on the characteristics of the gold nano-islands and the bio-entities involved in the sensing is also developed to determine the detection capability of the platform, which is optimized experimentally at each stage. Preliminary results and modeling present a relationship between the plasmonic shift and the concentration of exosomes; and essentially, indicate possibilities for label-free early diagnosis.

3.1. Introduction

Exosomes or Extracellular vesicles are vital sources of biomarkers for cancer and other pathological conditions such as inflammatory and neurodegenerative diseases, and also for clinical

diagnostics. They are membrane bounded nano-scale extracellular communication organelles that are released from almost all cell types to the extracellular space, transporting a cargo of active molecules (DNA, RNA, proteins/enzymes, lipid, and metabolites) to neighboring and distal parts of the body and represent real-time snapshots of the physiological/pathological status of the source cells. They are present in all body fluids, including urine, blood, ascites, and cerebrospinal fluid and semen. When cells are cultured in laboratory or bioreactor settings, the cells discharge their exosomes in the culture-media used, called conditioned media. Exosomes are mostly spherical and their diameter ranges from 30 - 100 nm, which is about hundred times smaller than the smallest cell [5-7, 37-39]. Exosomes are formed by inward budding of luminal membrane of multivesicular bodies and are constitutively released by fusion with the cytoplasmic membrane. Amongst the active molecules in the cargo, heat shock proteins (such as HSP70) are shown to be exosome membrane bound as well as inside [129-135]. It is evident in many cancers (for example breast and ovarian) that the concentration of the total cancer-cells and their exosome-bound HSPs are elevated [136] and implicated in various aspects of cancer biology.

The detection, isolation and characterization of exosomes are still challenging due to the natural complexity of body fluids. For this reason, a versatile platform and an easy-to-use technique is required to detect adequately and selectively, isolate, quantify and characterize exosomes for clinical applications. Given the growing evidence that exosomes may be the best liquid biopsy source materials for biomarker identification and discovery, there is a great demand for their simple, robust, and efficient isolation/detection from bio-fluids. However, currently available exosome isolation methods are precipitation based (ultracentrifugation and using polyethylene glycol) which are not suitable for point-of-care (POC) clinical-diagnosis. Ultrafiltration yields relatively pure exosomes but is technically challenging. For the development of routine exosome-based POC diagnostics, affinity-based exosome capture is technologically desirable. Most affinity-based exosome capture methods rely on monoclonal antibodies, directed against exosomes surface markers [35, 43, 56, 57], driving higher the cost of production and inconsistency in assays such as batch-to-batch variations of antibodies. Antibody-based affinity-capture and all the other precipitation-based exosome isolation facilitate capturing all the exosomes present in the given fluid, without differentiating healthy and diseased (cancer) exosomes. Quite sophisticated micro- and nano systems have gained attention in recent years for their high sensitivity to detect exosomes. Among them are the electrochemistry-based approaches,

using electroactive molecules tagged with a detection antibody and the captured exosomes are detected by electrochemical sensing [137-139]. Nanoplasmonic sensors and microfluidic exosome analysis platforms having an antibody functionalized channel have also been reported [140, 141]. In spite of the advances in the exosome detection techniques, because of the complexity and heterogeneity of exosomes' composition, none of the existing techniques can be considered as a general method to be used for the detection of exosomes for both clinical purposes and research. The challenges are both technical and biological and any step toward solving them is useful. The development of exosome detection methods is a continuous process and there is still a lot of room for improvement.

We used a synthetic peptide (Venceremin or Vn96), having a high affinity for canonical HSPs [36, 142] as tool to capture exosomes for the platform described in this work. The rational to use Vn96 based affinity-capture of exosomes for POC diagnostic platform is that cancer cells and their exosomes over express HSPs in their lumen as well as on their surface [143], but only at a minimum level in healthy cells or their exosomes. It is also evident that cancerous cells release a higher number of exosomes, compared to normal cells implicated in tumor progression [43, 144, 145]. Thus, Vn96 provide stronger affinity capture of canonical HSP-overexpressed (from cancer cells) exosomes from a given body fluid on Vn96 grafted nano-platforms and thus may provide superior diagnostic value for early cancer diagnosis [36].

While it is important to characterize exosomes by their molecular composition, there is presently a growing demand for an accurate method to detect the absolute concentration of exosomes in body fluids for potential POC diagnosis. For this purpose, surface-based detection methods such as Surface Plasmon Resonance (SPR) and more recently, Localized Surface Plasmon Resonance (LSPR), have emerged, in addition to flow cytometry [146], Tunable Resistive Pulse Sensing (TRPS), and Nanoparticle Tracking Analysis (NTA).

LSPR is one of the most important optical properties of gold and silver nanostructures. It occurs, when the oscillation of free conduction electrons of nanoparticles is resonant with the incident light. Both the position and intensity of LSPR band are dependent on the size and shape of nanoparticles and they are highly sensitive to dielectric properties of the surrounding medium.

Platforms based on gold nano-islands and silver nano-islands were used for numerous sensing applications [91, 128, 147-151]. In this work, we have used a thermal convection method for the fabrication of nano-islands on glass substrates [128, 149]. We used a specific chemistry to

covalently attach streptavidin to nano-islands, followed by grafting of the biotinylated Vn96 peptide to create a plasmonic surface where the exosomes will be captured.

The objective of the present study is to determine the detection capability of the Vn 96-gold nano-islands platform by physical modeling. The density of Vn96- peptide molecules that can be accommodated on this platform has been evaluated and the concentrations of streptavidin, biotin-Vn96, and exosomes, have been estimated accordingly. At the same time, the different steps of the sensing protocol are discussed from the point of view of the successive binding events and their effect on the entire detection process. To the best of our knowledge, this is a new approach to evaluate the effectiveness of a nano-island sensing platform, designed for the multistep, exosome capture and detection. In an attempt to find new information that would be helpful for the exosome-based POC diagnosis, we tried to find a correlation between the experimental values of the Au-LSPR band shift and the amount of exosomes in the conditioned media of a breast cancer cell line. This modeling work is very useful in evaluating the morphology of new structures for a given size and concentration of exosomes or any other biomolecules.

3.2. Materials and Methods

3.2.1. Materials

The substrates used in this experiment are the microscope glass slides purchased from Technologist Choice, Bio Nuclear diagnostics Inc., with a glass transition temperature, $T_g = 820°C$. Substrates are cut to the size of 37mm x 12.5mm x 1mm. Gold (III) chloride trihydrate ($HAuCl_4.3H_2O$) and sodium citrate were purchased from Sigma Aldrich. De-ionized (DI) water with a resistivity of 18MΩ, used in all the experiments was obtained from the NANO pure ultrapure water system (Barnstead). 11-mercaptoundecanoic acid in ethanol (Nano Thinks Acid 11), N-(3-Dimethylaminopropyl)-N′-ethylcarbodiimide hydrochloride (EDC) and N-Hydroxy succinimide (NHS), phosphate buffered saline (PBS) were obtained from Sigma Aldrich, Canada. PBS tablets were dissolved in DI water at 0.1M concentration (pH = 7.2). Streptavidin was purchased from IBA GmBH. Biotin-PEG-Vn96 was purchased from New England Peptide. MCF7 exosomes were purified from MCF7 cells conditioned media in a bioreactor, using ultracentrifugation (and re-suspended in fetal bovine serum free cell-culture media and the exosome concentration was determined by using NTA [36].

3.2.2. Fabrication of the gold nano-island platform

Three-dimensional (3D) gold (Au) nano-island structures on glass substrates were fabricated from gold colloidal solution that, subsequently, was deposited on glass substrates by the thermal convection method. The gold colloidal solution was prepared by the reduction of Gold (III) Chloride trihydrate ($HAuCl_4.3H_2O$) (chloroauric acid) by sodium citrate, following Turkevich's method [158]. Briefly, 15mg of $HAuCl_4.3H_2O$ were dissolved in 90 mL of DI water and heated until the solution reached its boiling point. Then, 5mL of 2% sodium citrate solution is added to the boiling solution. After the addition of sodium citrate, a change in color from the original yellow to a transparent purple (wine red) can be clearly observed, showing the presence of gold nanoparticles. Meanwhile, the glass substrates were cleaned with soap solution and DI water, then rinsed with acetone, 2-propanol (IPA) and dried. Further, the substrates were heated at 100°C in an oven for 1 hour in order to remove the moisture and possible contaminants. The glass substrates were immersed in the beaker containing the gold colloidal solution at an angle of approximately 30° and kept at a temperature between 50 and 55°C. The Au nanoparticles from the colloidal suspension will slowly evaporate and deposit multilayers of Au particles on the substrate as shown in Figure 2.1 (A, B). Au nano-islands were fabricated by annealing the samples at 560°C for one hour and 10 hours.

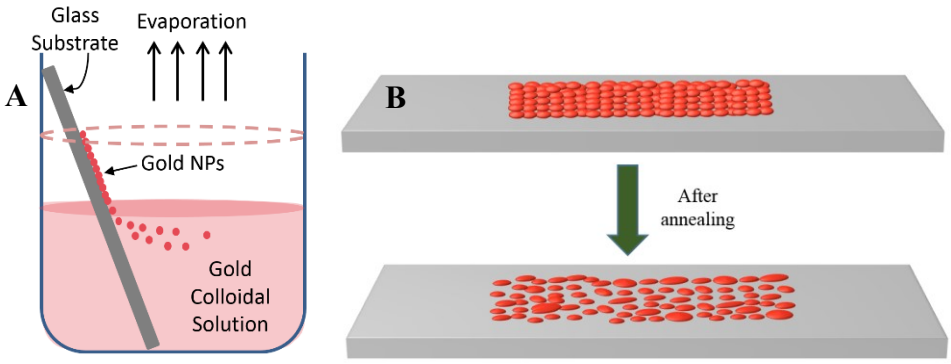

Figure 3.1: Fabrication of gold nano-island platforms (A) schematic of the convective assembly process (B) schematic of the morphological tuning of gold multilayers to gold islands by annealing

3.2.3. Biosensing protocol

The different steps involved in the biosensing protocol and their corresponding LSPR shifts are shown in Figure 3.1 (A, B). The first step consists of the functionalization of the Au nanoparticles by immersing the sample into the solution of 11-mercaptoundecanoic acid

(Nanothink) (5mM) for 3 hours and then allowing to dry. After this step, the absorption spectrum is measured using the Perkin Elmer spectrophotometer (Lambda650). The shift of the Au plasmon band towards longer wavelengths confirms the presence of the self-assembled monolayer of linker molecules on the surface of nano-islands. In the next step, the monolayer formed on the surface of Au nano-islands is activated by adding 200 µL of cross-linker, which is a mixture (1:1) of 0.1M N-(3-dimethylaminopropyl)-N'-ethylcarbodiimide hydrochloride (EDC) and then incubated for 2 hours. After drying, the spectrum is measured again. The next step is the immobilization of streptavidin to the activated linker layer. 200 µL of a 0.19 nM solution of streptavidin in PBS is added to the activated linker layer and incubated for an hour, left to dry before taking a spectral measurement. In the next step, 200 µL of a 0.87 nM of biotin-PEG-Vn96 solution is deposited on top of the streptavidin layer and incubated for 4 hours, dried and the spectral measurement is taken again. The final step of the biosensing protocol includes in the deposition of 200 µL of the MCF 7 (breast cancer cell line) cell culture conditioned media, containing EVs/exosomes for their relative immobilization.

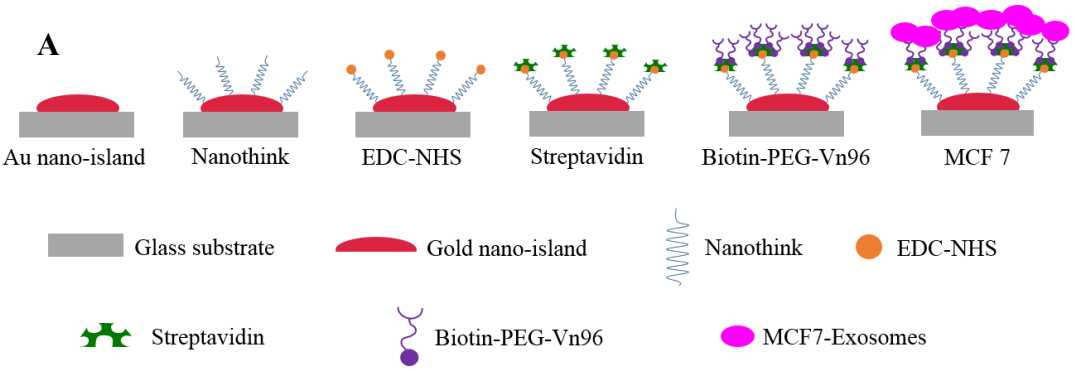

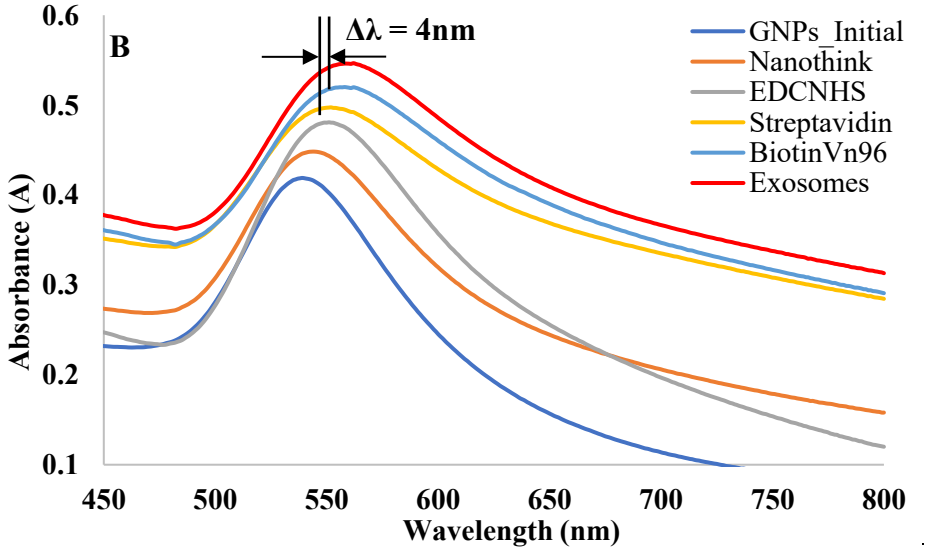

Figure 3.2: Biosensing protocol and their corresponding absorbance bands (A) Schematic of the bio-sensing protocol (B) Au nano-island plasmon band corresponding to the different steps of the protocol

3.3. Results and discussions

3.3.1. SEM characterization of gold nano-islands

The gold nano-islands on glass substrates, formed after annealing, were characterized by Scanning Electron Microscopy (SEM) and Transmission Electron Microscopy (TEM) images. Figure 3.3 (A, B) shows the SEM images of the gold aggregates, before annealing, and that of the nano-islands obtained after annealing, respectively. From the images, it can be seen that the annealing at 560°C for 1 hour, tunes the morphology from aggregates of gold nanoparticles into nano-islands. The TEM image shows that most of the islands have an ellipsoid shape and there is a wide size distribution.

3.3.2. Image analysis of gold nano-islands

The SEM image of nano-islands is analyzed using the ImageJ analysis software (Wayne Rasband, NIH, USA) to determine the dimensions of the islands and their surface density. An area of 3.2 μm x 2.4 μm with 20 nano-islands is considered for the analysis. The nano-islands were analyzed, and the average length and width were measured and also the average inter-island distances were calculated using the center-to-center distance between the nearest neighbor islands. The maximum and minimum lengths of nano-islands were found to be 450 nm and 60 nm, and the widths 200 nm and 60 nm. Figure 3.3 (C, D) show the image used for the analysis and Table 3.1 summarizes the average values of major and minor axes of gold nano-islands, aspect ratios, inter-island distances and calculated surface density.

Table 3.1: Average physical characteristics of the gold nano-islands prepared by thermal convection

Length	198.89 nm
Width	146.67 nm
Aspect ratio (Length/width)	1.37
Inter-island distance	342.5 nm
Surface density	3 nano-islands/μm^2

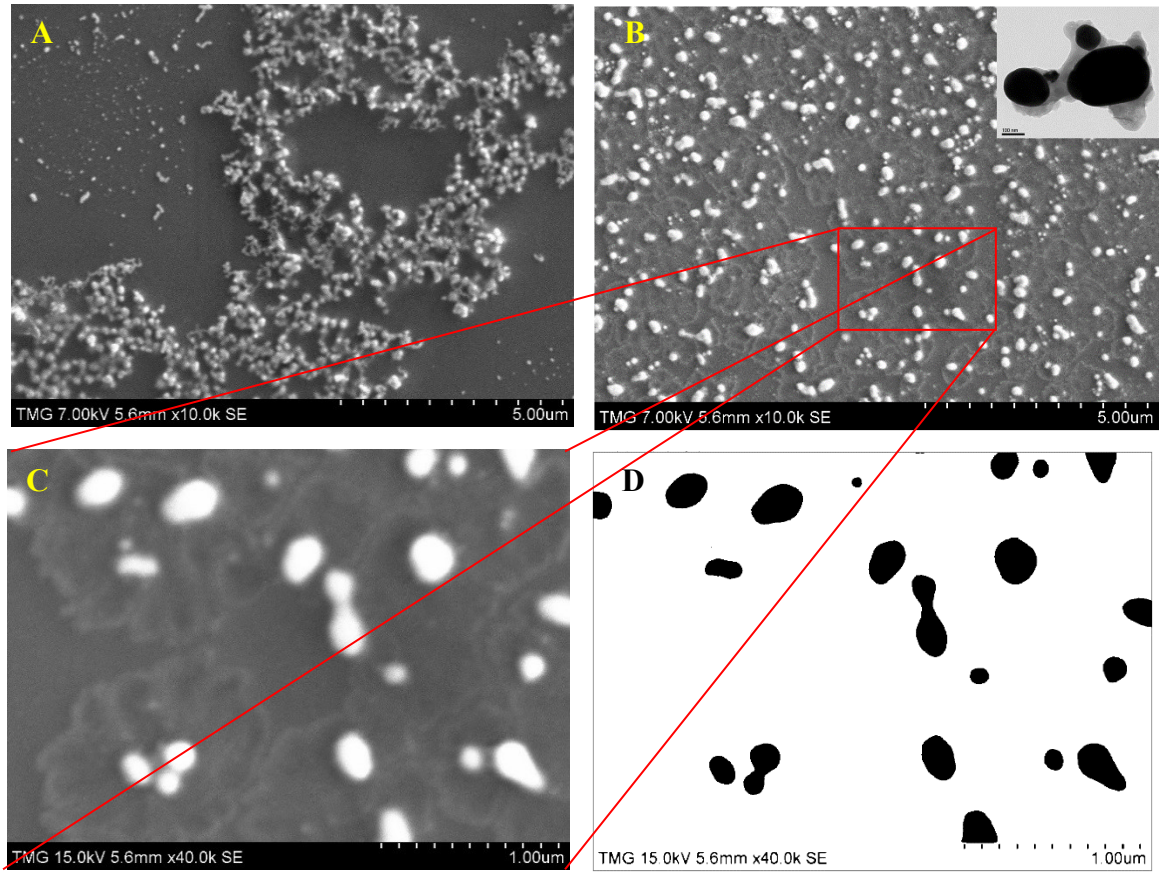

Figure 3.3: Morphological tuning of gold aggregates to nano-islands shown by SEM images (A) SEM image of the large gold aggregates (B) nano-islands (after annealing at 560°C) (Inset: TEM image of nano-islands) (C) selected SEM image used for particle analysis (D) its binary image

Table 3.1 shows that the nano-islands are quite large, far from one to the other and their surface density is low. The size distribution of the gold nano-islands was also calculated. These calculations were based on the lower magnification SEM image shown in Figure 3.4(A). To calculate the island size distribution, an area of 12.7µm x 9.52µm is considered as shown in the rectangle in the Figure 3.4(B). The histogram in Figure 3.4(C) clearly shows a wide size distribution (20 nm to approximately 350 nm diameter), all of the sizes having almost an equal contribution. The size distribution of nano-islands could be improved by annealing the deposited nanoparticles at the same temperature (560^0C) but for a much longer time (10 h). The SEM image and the corresponding histogram are shown in Figure 3.4(D, F).

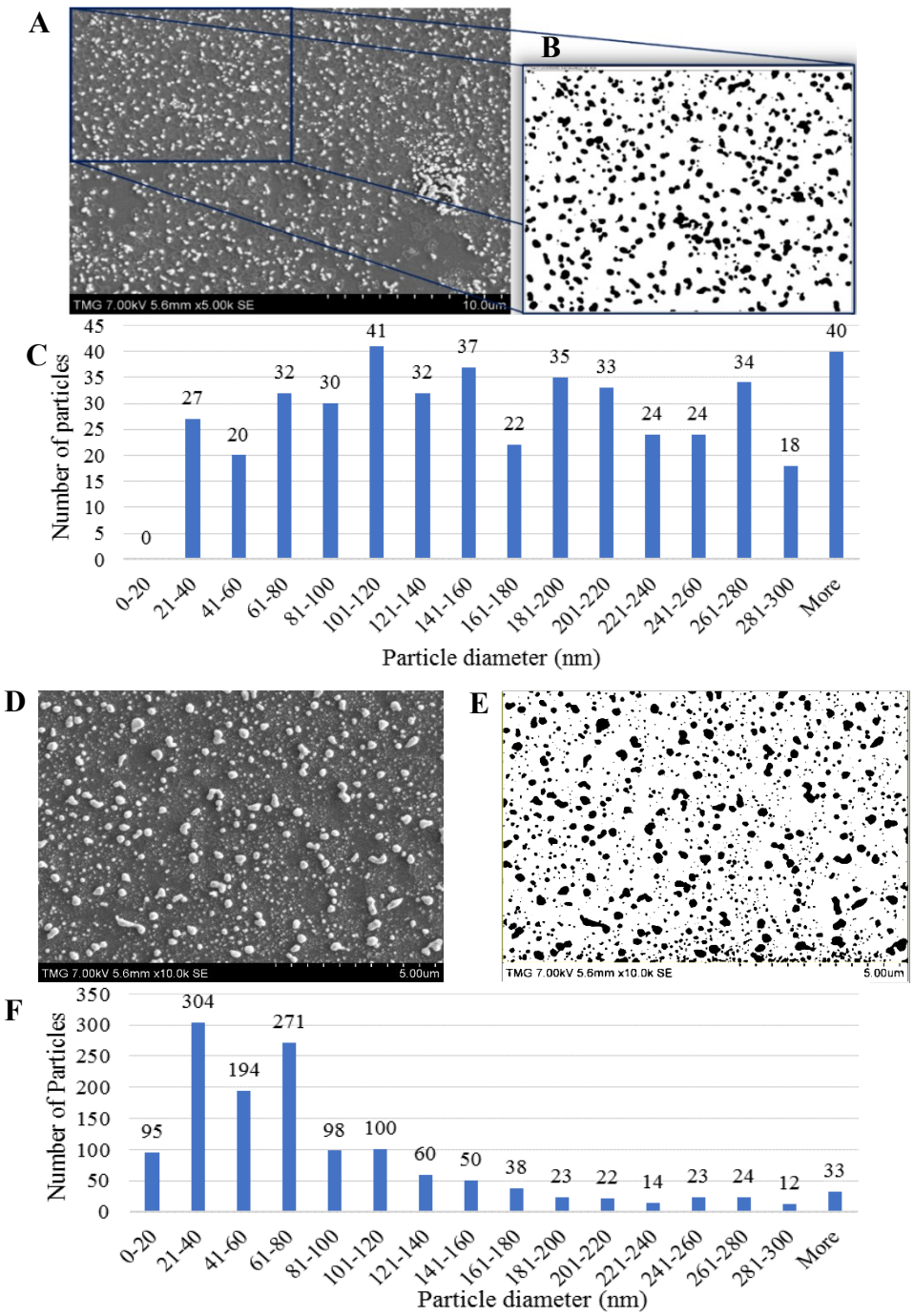

Figure 3.4: Size distributions of gold nano-islands under two different annealing times (A) Large area SEM image of gold nano-islands after 1-hour annealing (B) its binary image (C) and the histogram corresponding to their size distribution; (D) after 10 hours annealing (E) binary image (F) and the histogram corresponding to their size distribution

As the histogram shows, the sizes of the majority of islands are concentrated in the range of 20 nm to 80 nm. In spite of a better distribution, we opted for a shorter annealing time, because the size of nano-islands under these conditions is larger. Taking into account the complex multi-step sensing protocol, having large nano-islands with a large penetration depth of the plasmon field would be more suitable and advantageous for higher sensitivity in the case of exosomes which are generally large in size.

3.3.3. Physical modeling of a gold nano-island

In this section, we have built up a model based on the quantitative analysis of the nano-islands shown in the previous section. Taking into account the average size and the surface density of nano-islands as found from the SEM data, we have calculated the number of the different entities involved in the bio-sensing process that can be immobilized on the surface of nano-islands. When immobilizing the successive layers on the surface of a nano-island, we have considered their dimensional sizes as known from the literature [37, 38]. A typical gold nano-island has the shape of an ellipsoid as shown in Figure 3.5(A) with average dimensions of 200 nm (L), 150 nm (W) and 50nm (T) obtained from the particle analysis. The maximum area available for immobilization with these ellipsoidal nano-islands is approximated as

$$A \approx 4\pi \left(\frac{(LW)^{1.6} + (LT)^{1.6} + (WT)^{1.6}}{3} \right)^{\frac{1}{1.6}} \qquad (2)$$

The surface area of nano-island limits the number of different ligands that can be immobilized on its surface. The surface area calculated using Eq. (2) was used for further evaluations. Figure 3.5(B) shows that, in spite of the larger size of the bio entities involved in the sensing process, the decaying plasmon field of a large nano-island reaches the exosomes that are the target of the detection process. Figure 3.5(C) shows the cross-section of one nano-island, carrying the successive layers of compounds involved in the detection of exosomes. As shown in the model (Figure 3.5(C)), the ligands consist of a linker and the streptavidin bound to biotin-Vn96. The shape of the linker-streptavidin-biotin complex is assumed to be a rectangular body with the dimensions of 4.2 nm x 4.2 nm x 9 nm [152, 153]. The next layer consists of Vn96, a polypeptide specifically designed to capture exosomes, having a predictive spherical shape with a diameter of 2 nm and the exosomes are modeled as spheres with a diameter of 100 nm. Taking into account the available surface area, the numbers of Vn96 and exosomes that can be

accommodated per nano-island were estimated based on their physical dimensions and constraints and shown in Table 3.2.

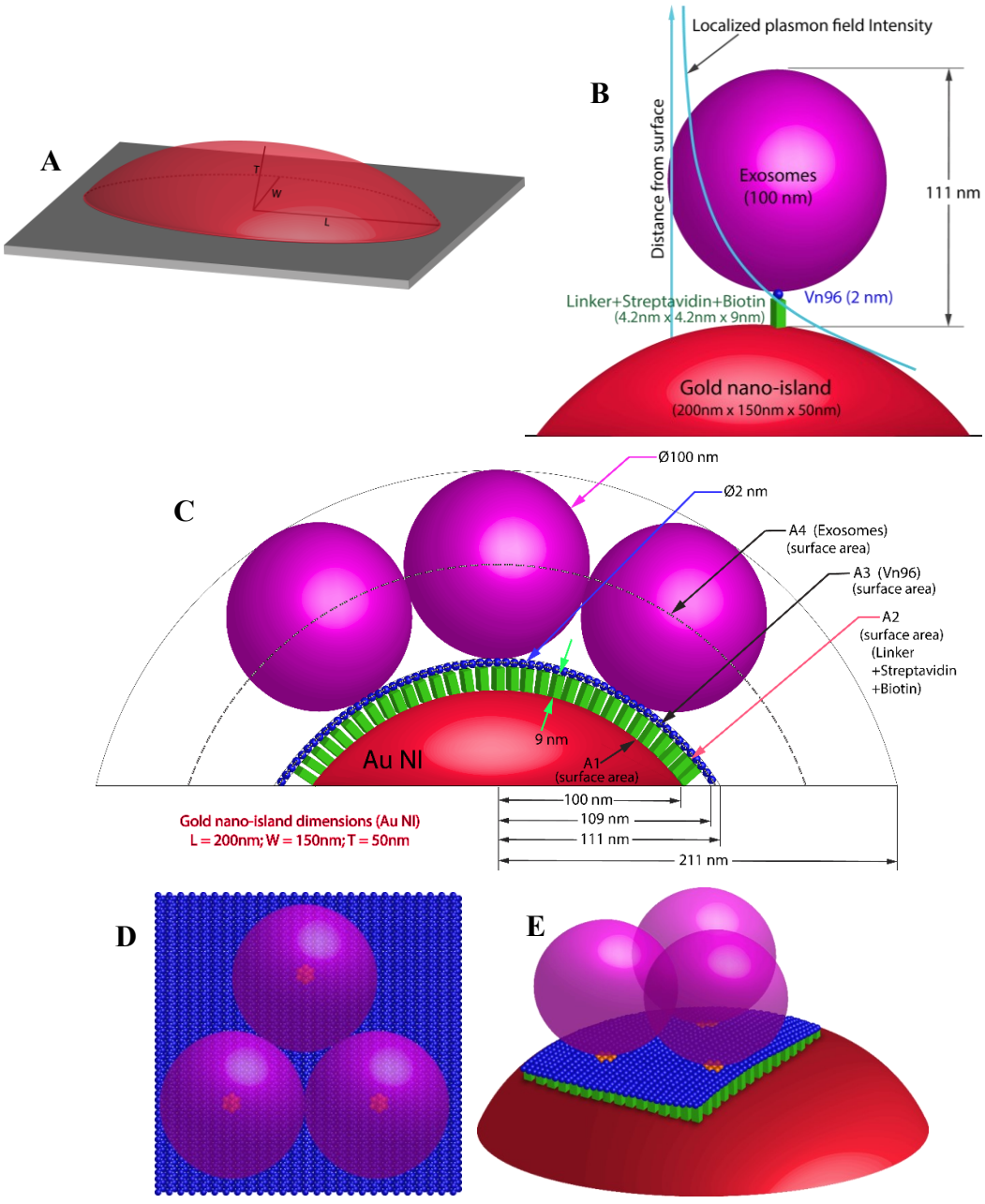

Figure 3.5: Physical modeling of interactions (A) Gold nano-island in the shape of a half-ellipsoid (B) decay of the plasmon field of a large nano-island (C) Cross-section of one nano-island immobilized with the successive layers of bio-entities involved in the detection of exosomes; Exosomes captured by Vn96 molecules ((D) top view and (E) isometric view). The spheres in pink and blue represent the exosomes and the Vn96 molecules, respectively

Table 3.2: Surface area of a single nano-island and the maximal number of ligands that can be accommodated

Streptavidin		**Biotin-PEG-Vn96**		**Exosomes**	
Surface area of nano-island (A1)	*No. of ligands*	*Surface area for Vn96 (A3)*	*No. of Vn96*	*Surface area for exosomes (A4)*	*No. of exosomes*
3.486 x10^4 nm^2	1976	4.49 x10^4 nm^2	12810	1.16 x10^5 nm^2	9

It can be seen from the Table 2 that each nano-island can accommodate a maximum of 1976 ligand of streptavidin, 12810 Vn96 molecules and only 9 exosomes. In our experiments, each Vn96 molecule is linked with a biotin through a PEG linker; therefore, the number of Vn96 a nano-island can accommodate is equal to the number of biotin complexes, that is, 12810 on each nano-island. As streptavidin can bind to 4 biotin molecules, while only 7904 biotin-PEG-Vn96 molecules can be bound to the maximum available streptavidin and the rest of the molecules will be washed away.

Theoretically, each Vn96 molecule can latch onto the exosome by binding to one heat shock protein contained on the surface of the exosomes. From the physical modeling, it is clear that the number of Vn96 molecules available to capture the exosomes is much higher than the exosomes that each nano-island can accommodate. Hexagonal orientation of exosomes is considered, in order to understand how many Vn96 molecules could actually contribute to capture the exosomes. The percentage of Vn96 molecules involved in bonding of exosomes is very low, only around 5%. Figure 3.5(D, E) show the orientation of exosomes, while Figure 3.5(D) shows the top view and Figure 3.5(E), the isometric view of the exosomes captured by the Vn96 molecules. The Vn96 molecules which actually contribute to the capture of exosomes are shown in orange as seen in Figure 3.5(D, E).

The biosensing protocol, tailored to detect the exosomes, consists of immobilization of different compounds on gold nano-islands, by binding or by adsorption of layers with varying thicknesses. For the approach used here, it is important to optimize the two steps - the streptavidin-biotin binding and the capture of exosomes, while the concentrations of Nanothink and EDC-NHS used here are similar to those used for biosensing of other biomolecules [126]. For this purpose, the concentration and the amount of the entities involved in biosensing protocol were varied, to maximize the shift of the Au plasmon band, at each of the important steps. As the main step in

deciding the outcome of the sensing process is the Vn96-exosome interaction, it seemed reasonable to optimize the formation of the streptavidin - biotin complex, in the specific case of biotin, connected to Vn96, through a PEG moiety. Because of the high affinity and the stability, the streptavidin-biotin model system and its structure and mechanism of formation have been thoroughly investigated [154-156]. This is not the case for the biotin-PEG-Vn96 complex, synthesized quite recently, with the only objective of binding the exosomes.

First, only the concentration of streptavidin solution was varied to find the concentration that will result in the maximal shift of the Au LSPR band. The dependency of $\Delta\lambda$ on the concentrations of streptavidin is shown in Figure 3.6(A). The highest shift (4.5 nm) is seen when the concentration of streptavidin is around 0.04 nM. From the experimental results, it has been observed that at lower concentrations of streptavidin, the LSPR shift values are more stable, compared to those corresponding to higher concentrations. Therefore, instead of considering concentrations with the highest LSPR shift, the concentration with a more stable LSPR shift is considered for further optimization of the biosensing protocol. The streptavidin concentration of 0.19 nM is considered and the concentration of Biotin-PEG-Vn96 is varied to study the effect of the ratio of streptavidin to Biotin-PEG-Vn96. Figure 3.6(B) shows the dependency of the average LSPR shift when different ratios of biotin-PEG-Vn96 to streptavidin are used, keeping streptavidin concentration constant at 0.19 nM.

It is well-known that one streptavidin molecule can bind to four biotin molecules and the LSPR shift corresponding to this ratio is maximal [154, 157]. Hence, if the ratio of biotin to streptavidin is maintained around four, the LSPR shift of Au has to be the largest. It is noticeable from Figure 3.6(B) that, as expected, the maximum shift is obtained when the ratio of biotin to streptavidin is maintained around four. This corresponds to 5.23×10^{14} biotin-PEG-Vn96 complexes containing 1.14×10^{14} molecules of streptavidin. Further, the LSPR shift decreases with the increase in ratio of the complex. The results have shown that, working with lower concentrations of biotin-PEG-Vn96 to streptavidin, the LSPR shift values show a poor repeatability. This might be because of less available biotin-PEG-Vn96 molecules, compared to those that may be accommodated by the streptavidin molecules and, in this situation, the binding is random. Comparing this number with the one calculated theoretically, it can be seen that, under the conditions of the experiment, a considerably higher number of complexes were formed. However, if we consider the removal of the non-bound complexes through the washing process,

the number of molecules from the experimental results matches those from the physical modeling, validating the model.

The results show that the surface density of nano-islands, fabricated through the thermal convection method, is high enough to accommodate the biotin-PEG-Vn96 complex molecules, involved in the experiment. The optimized concentrations of all the entities used in the biosensing protocol and the corresponding LSPR shifts are summarized in Table 3.3. The amount (volume) of each entity in the biosensing protocol is chosen to cover the whole sensing area.

Table 3.3: Concentrations and volume of the entities used in the biosensing protocol with their corresponding average LSPR shift

Entity	**Optimized concentration**	**Avg. Δλ (nm)**
11-MUA*	5mM	6
EDC + NHS	0.1M+0.05M	4.8
Streptavidin	0.19 nM	3.1
Biotin-PEG-Vn96	0.87 nM	5.7
Exosomes (MCF7)	2%, 4%, 10%, 20%, 100%	-

*11- Mercaptoundecanoic acid (the samples are immersed in the solution)

The dependency curve, showing the shift of the Au LSPR band for different concentrations of exosomes, namely, corresponding to dilution factors of 50x, 25x, 10x, 5x, 1x is shown in Figure 3.6(C). The Figure 3.6(D), represents the size distribution and counts of exosomes corresponding to different dilutions of MCF7 exosomes, quantified using the Tunable Resistive Pulse Sensing (TRPS) (qNano from iZON science) instrument. The dependency curve (Figure 3.6(C)) is built by using the concentration of MCF-7 exosomes, containing 1.33 X 10^{10} particles/ml. From this plot, it can be seen that the average shift increases as the dilution factor decreases and reaches the highest shift for the undiluted sample. It has to be noted that the equation of the curve reflects a non-linear trend in the form of Lx^M where x corresponds to the number of exosomes-Vn96 interactions. It can be observed from the experimental results that the LSPR shift has a non-linear dependency on binding to the Vn96 and that the curve is not saturated, which clearly shows that the capacity of the nano-island platform is still high enough to capture more exosomes than the actual number of exosomes in the culture media used in this experiment.

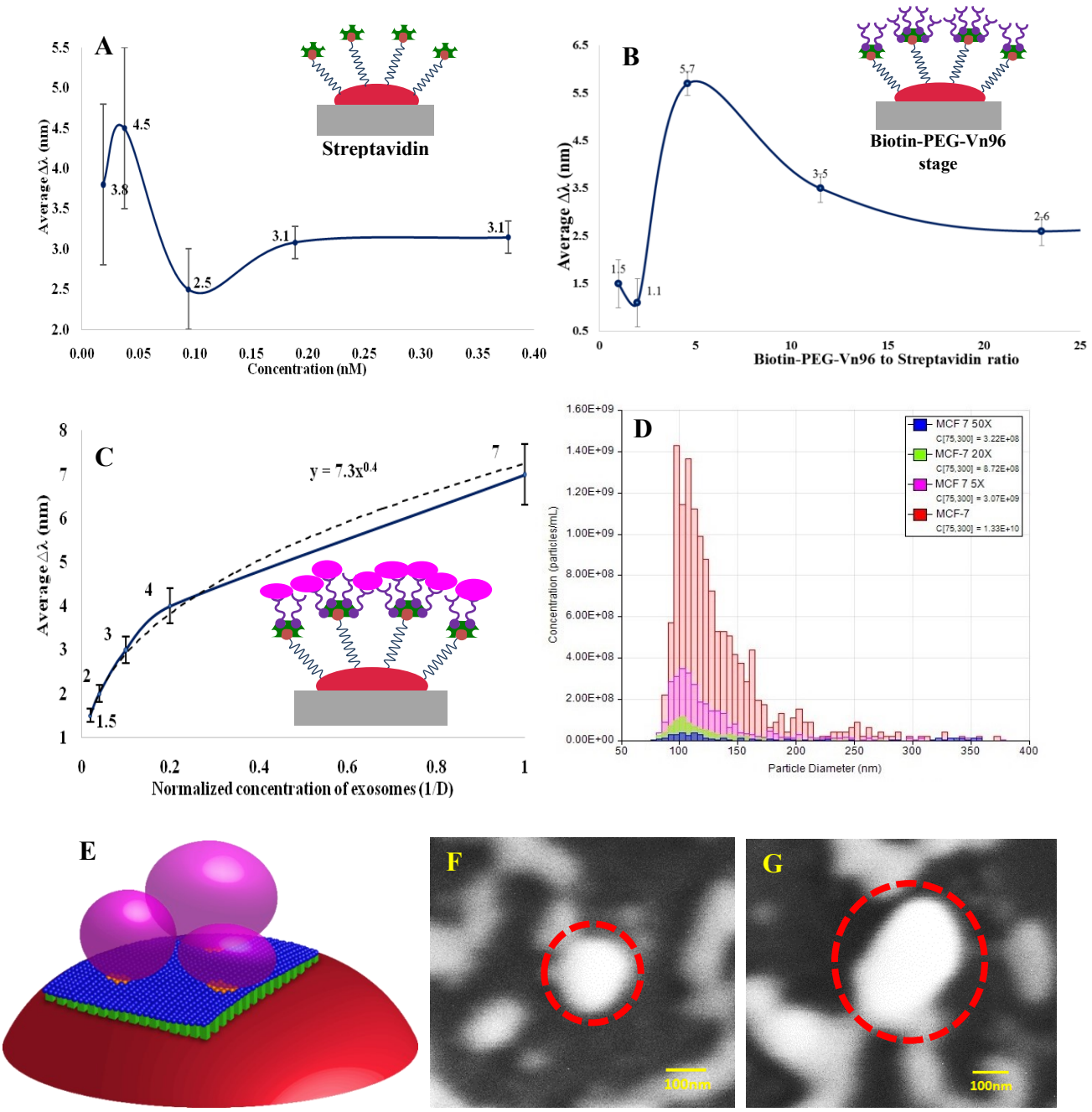

Figure 3.6: Plasmonic shift due to streptavidin and Biotin-PEG-Vn96 interactions (A) Dependency of Δλ on the concentration of streptavidin only (B) Ratio of Biotin-PEG-Vn96 to Streptavidin (C) Dependency of the shift of Au LSPR band on the concentration of MCF-7 exosomes; (D) Size distribution of MCF7 exosomes as obtained by Tunable Resistive Pulse Sensing (TRPS) measurements. (E) Exosomes with different sizes and shapes captured by Vn96

molecules (F, G) SEM images of exosomes captured by gold nano-islands during the last step of the biosensing (exosomes are marked in circles)

For modeling purposes, exosomes were considered spherical and having a uniform size (100 nm) but, actually, their size varies from 30 - 100 nm and the shape may not be exactly spherical as shown in Figure 3.6(E). An exosome, captured by a gold nano-island is shown in Figure 3.6(F), whereas Figure 3.6(G) shows a cluster of exosomes, captured by a larger gold nano-island as depicted in the modeling. This can be clearly seen in the in Figure 3.7(A, B). The number of available HSP on the surface of exosomes varies depending on the size of exosomes and the stage of the disease. When exosomes are captured by Vn96, the interactions could result in a deformation due their elastic nature. Hence, the binding of HSP to the Vn96 molecules (protein – protein binding) will result in a non-linear behavior. The dependency curve allows the estimation of the concentration in terms of the number of exosomes in the sample.

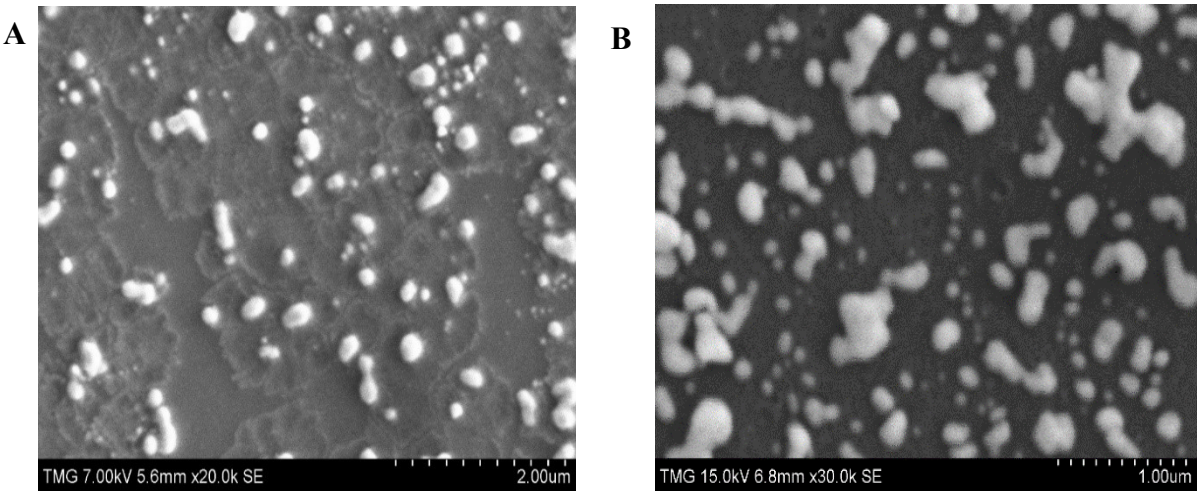

Figure 3.7: SEM image of gold nano-islands with and without exosomes (A) SEM image of the gold nano-islands without exosomes (B) SEM image of the gold nano-islands with exosomes

Particle analysis has shown that the density of nano-islands is around 3 nano-islands/μm^2. As found by modeling, each of them can accommodate 9 exosomes, that is, a total of 27 exosomes on an area of 1μm^2 of the developed platform. A Previous study has indicated that the average number of exosomes that can be captured from a glioblastoma patient's plasma on anti-CD63 monoclonal-antibody grafted 2D planner surface of the chip, is 9 microvesicles/μm^2 [43], whereas our platform is able to accommodate a much higher number of exosomes. As the sample used in this work corresponds to the cell culture of a breast cancer cell-line, the concentration of exosomes

in the undiluted sample may be attributed to a cancerous condition as shown in Figure 3.8(C), where the total number of exosomes in the unit volume of plasma is noticeably higher than in the normal plasma [43]. Alternatively, the concentration of exosomes corresponding to a 50x dilution would mean a non-cancerous situation or a very-early stage of the disease. Hence, the tested range of concentrations covers a wide range, starting with concentrations of exosome present in a given body-fluid, simulating a non-cancerous, early-stage disease, to a fully developed cancerous condition. Thus, one can infer that the nano-island platform developed in this work, based on LSPR, can effectively detect from early stage to advanced stages of cancer.

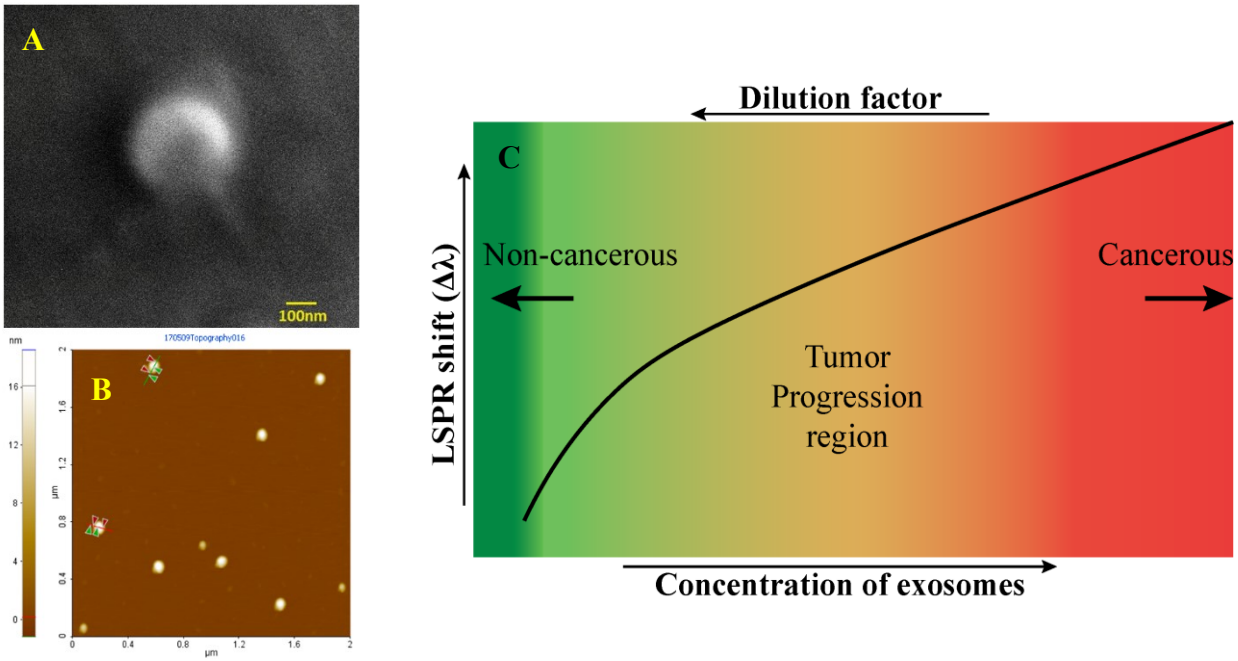

Figure 3.8: SEM, AFM images of exosomes and the relationship between the plasmonic shift and concentration (A) SEM image of the MCF7 exosomes (B) AFM image of the MCF7 exosomes (C) The relationship between plasmonic shift and concentration of exosomes during cancer progression

SEM and AFM images of exosomes from the breast cancer cells (MCF7) are shown in Figure 3.8(A, B) respectively. The relationship between the LSPR shift and the concentration of exosomes during cancer progression is schematically shown in Figure 3.8(C). It is known that the concentration of exosomes present in the body fluids increases tremendously (by many folds) in a cancer patient, compared to a healthy patient. For example, in the case of a glioblastoma patient's plasma study mentioned above [43], the concentration of exosomes was found to be approximately

50 times higher than that corresponding to a healthy patient. Hence, we could envisage that the concentration of exosomes, detected by measuring the LSPR plasmonic shift, will reflect the progression of cancer as shown in Figure 3.8(C).

3.3.4. Physical modeling for colloidal platform in Liquid biopsy

The physical modeling approach that is discussed previously can be applied to any situation where molecular quantification is required. For instance, if we consider the spherical gold nanoparticles suspended in a colloidal solution, the diameter of nanoparticles can be modified based on the Turkevich's method of gold nanoparticles synthesis. In the biosensing protocol, the number of EVs that can be accommodated on each nanoparticle depends on the surface area of that nanoparticle. Therefore, the number of EVs accommodated by each nanoparticle can be determined by calculating the surface area of a nanoparticle when attached with the ligands, streptavidin and Vn96 molecules as shown Figure 3.9(A). Hence, it clearly shows that the number of EVs that could be accommodated on a nanoparticle is highly dependent on the diameter of a nanoparticle. This approach is not just limited to gold nanoparticles, as it could be applied to any metallic nano/microparticles or magnetic particles by evaluating their surface area.

With this approach, for a given number of EVs/Exosomes, the concentration of gold required to capture all the EVs can be calculated by evaluating the mass of each nanoparticle. The mass of each nanoparticle can be calculated by knowing its diameter and the density of gold, which is 19.32 g/cc. The concentration of MCF7 culture media was measured to be around 1.33×10^{10} particles/mL, as shown previously, corresponds to a cancerous condition. As mentioned, dilution of this sample by 50x would correspond to a non-cancerous situation. Therefore, with a known number of EVs corresponding to cancerous and non-cancerous condition, a relation can be plotted between the diameter of gold nanoparticle and the concentration of gold required to capture all the EVs present in the culture media for liquid biopsy as shown in Figure 3.9(B) and the calculation of mass of each nanoparticle and the concentration of gold required to capture EVs in cancerous and non-cancerous condition are tabulated in Table 3.4. In Table 3.4, the number of EVs per nanoparticle are evaluated in a similar way as mentioned earlier, by calculating the surface area of the nanoparticle to find the number of ligands and then number of EVs subsequently. From the plot in Figure 3.9(B), it can be interpreted that the area between the cancerous and the non-cancerous condition can be used for the early diagnosis of cancer.

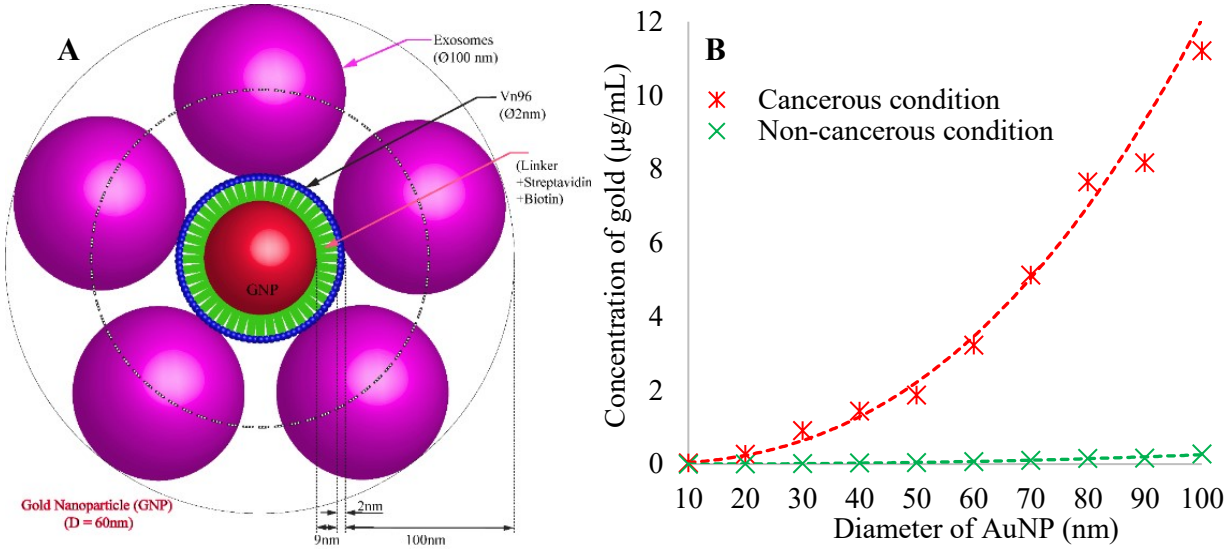

Figure 3.9: Physical modelling of a spherical particle (A) Cross-section of one nanoparticle immobilized with the successive layers of bio-entities in the protocol (B) Relation between diameter of a AuNP and the concentration of gold required to capture EVs in a cancerous and non-cancerous condition

Table 3.4: Calculation of mass of each nanoparticle and the concentration of gold required to capture EVs in cancerous and non-cancerous condition

Diameter (nm)	Mass of one AuNP (µg)	No. of EVs each NP can accommodate	Total no. of NPs req. in cancerous	Gold conc. correspond to cancerous (µg/mL)	Total no. of NPs req. in non-cancerous	Gold conc. correspond to non-cancerous (µg/mL)
D	**M=Vol*Density**	**N**	**T_1= 1.33E10/N**	**=M*T_1**	**T_2= 2.66E8/N**	**=M*T_2**
10	1.01E-11	4	3.33E+09	0.0336	6.75E+07	0.0007
20	8.09E-11	4	3.33E+09	0.2691	6.75E+07	0.0055
30	2.73E-10	4	3.33E+09	0.9082	6.75E+07	0.0184
40	6.47E-10	6	2.22E+09	1.4351	4.50E+07	0.0291
50	1.26E-09	9	1.48E+09	1.8686	3.00E+07	0.0379
60	2.19E-09	9	1.48E+09	3.2290	3.00E+07	0.0656
70	3.47E-09	9	1.48E+09	5.1275	3.00E+07	0.1041
80	5.18E-09	9	1.48E+09	7.6539	3.00E+07	0.1554
90	7.37E-09	12	1.11E+09	8.1734	2.25E+07	0.1659
100	1.01E-08	12	1.11E+09	11.2120	2.25E+07	0.2761

3.4. Conclusion

In this work, the sensing protocol for the LSPR detection of extracellular vesicles, based on their high affinity to the Vn96 polypeptide was optimized. A simple physical model was developed by analyzing the characteristics of gold nano-islands, calculating their surface area and the number of the different species that can be successively immobilized on the surface of a nano-island. It is estimated that the most important step in the protocol, deciding the outcome of the overall sensing process, is the formation of the streptavidin-biotin-PEG-Vn96 complex. Therefore, the concentrations of streptavidin and biotin-PEG-Vn96 complex were optimized experimentally and the maximum LSPR shift was found for the ratio of 1 to 4 in agreement with the physical modelling. Particle analysis performed on SEM images has shown that the density of nano-islands is about around 3 nano-islands/μm^2. By modelling, it was found that each of the nano-islands can accommodate 9 exosomes, that is, a total of 27 exosomes per μm^2. Practically, it means that the developed Au nano-island platform can capture a much higher number of extracellular vesicles than that present in the MCF7 sample used for this study, providing a very broad detection range covering from early stages to advanced stages. Based on our preliminary results, the novel LSPR detection method of extracellular vesicles could be used as a tool to diagnose cancer at an early stage of the disease.

The concept of physical modeling has been developed for gold nano-island or nanoparticle platforms for quantification of number of particles or concentration required to capture all or most of the EVs from the conditioned media. Based on the fabrication limitations, one can select different platform based on application, which could be used for various types of microfluidic devices. So, the next chapter (Chapter 4) discusses a gold nano-island integrated microfluidic chip based on the optimized concentrations of biosensing entities for the capture, isolation and plasmonic detection of EVs from the MCF7 CCM.

Chapter 4

Plasmonic Detection of Exosomes using a Gold Nano-Island Integrated Microfluidic Platform

This chapter is reproduced from the article published in *International Journal of Biomedical and Biological Engineering (WASET).*, 12(5), 226 – 229, 2018

A bio-sensing method, based on the plasmonic property of gold nano-islands, has been developed for detection of exosomes in a clinical setting. The position of the gold plasmon band in the UV-Visible spectrum depends on the size and shape of gold nanoparticles as well as on the surrounding environment. By adsorbing various chemical entities, or binding them, the gold plasmon band will shift toward longer wavelengths and the shift is proportional to the concentration. Exosomes transport cargoes of molecules and genetic materials to proximal and distal cells. Presently, the standard method for their isolation and quantification from body fluids is by ultracentrifugation, not a practical method to be implemented in a clinical setting. Thus, a versatile and cutting-edge platform is required to selectively detect and isolate exosomes for further analysis at clinical level. The new sensing protocol, instead of antibodies, makes use of a specially synthesized polypeptide (Vn96), to capture and quantify the exosomes from different media, by binding the heat shock proteins from exosomes. The protocol has been established and optimized by using a glass substrate, in order to facilitate the next stage, namely the transfer of the protocol to a microfluidic environment. After each step of the protocol, the UV-Vis spectrum was recorded, and the position of gold Localized Surface Plasmon Resonance (LSPR) band was measured. The sensing process was modelled, considering the characteristics of the nano-island structure, prepared by thermal convection, and annealing. The optimal molar ratios of the most important chemical entities involved in the detection of exosomes were calculated as well. Indeed, it was found that the results of the sensing process depend on the two major steps: the molar ratios of streptavidin to biotin-PEG-Vn96 and, the final step, the capture of exosomes by the biotin-PEG-Vn96 complex. The microfluidic device designed for sensing of exosomes consists of a glass substrate, sealed by a PDMS layer that contains the channel and a collecting chamber. In the device, the solutions of linker, cross-linker, etc., are pumped over the gold nano-islands and an

Ocean Optics spectrometer is used to measure the position of the Au plasmon band at each step of the sensing. The experiments have shown that the shift of the Au LSPR band is proportional to the concentration of exosomes and, thereby, exosomes can be accurately quantified. An important advantage of the method is the ability to discriminate between exosomes having different origins.

4.1. Introduction

Exosomes are a group of nano-scale extracellular communication organelles released by all cells, which transports cargoes of molecules and genetic materials to proximal and distal cells and are enclosed by a phospholipid bilayer. They are in the size range of 50 nm to 120 nm and are homogenous in nature. Exosomes are found abundant in all biological fluids, including urine, blood, ascites, and cerebrospinal fluid fractions of body fluids such as serum and plasma, as well as in the cultured medium of cells [22, 26, 39]. They are the intercellular communicators, which transport cargos between cells as shown in Figure 4.1 and spread proteins, lipids, mRNA, DNA, and are involved in the progression of diseases. Thus, they have the potential to be used for minimal-invasive molecular diagnostics.

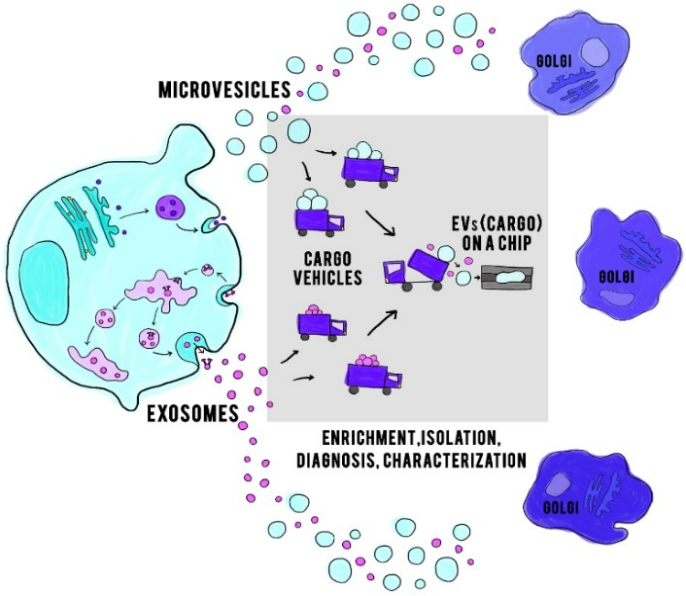

Figure 4.1: Schematic of intercellular communication and transportation of cargo between cells

Presently, very few methods are available for the isolation and detection of exosomes. The golden standard method that is widely used for their isolation and quantification is ultracentrifugation. This method is time consuming, laborious, infrastructure intensive, may lack specificity so it may not be a practical method to be implemented in a clinical setting. Hence, an

adaptable platform is required to selectively detect and isolate exosomes for further analysis at clinical level.

To capture EVs, a synthetic polypeptide called Vn96, specifically designed and validated to capture exosomes, is used [36]. The detection methods were initially carried out on a self-standing substrate level, by performing the sensing protocol in a discontinuous manner. Further, to enhance the sensitivity of the detection and to accomplish the molecular profiling of the captured exosomes, microfluidic devices were designed, developed, and tested. The concentrations of the chemical and biological entities at each stage of biosensing were optimized to facilitate the transfer to the microfluidic stage.

The optical properties of noble metal nanostructures are extensively adapted for biological detection. Predominantly, the localized surface plasmon resonance (LSPR) property of noble metal nanoparticles is widely used as a highly sensitive label-free technique for the detection of chemical and biomolecular binding events [159, 160]. The sensing mechanism consists of monitoring the change in the position of the LSPR band, change due to the binding of chemical entities and bio-molecules immobilized onto the nanoparticles. The shift of the band towards longer wavelengths is due to the change of the refractive index of the surrounding media. [147, 161-165]. The aim of the present work is the detection of exosomes, based on the change in the position of Au-LSPR band corresponding to different binding events.

4.2. Materials and methods

The substrates used in this experiment are microscope glass slides from Technologist Choice, Bio Nuclear diagnostics Inc. with a glass transition temperature, T_g = 820°C. Gold (III) chloride trihydrate ($HAuCl_4.3H_2O$), sodium citrate was purchased from Sigma Aldrich. Polydimethylsiloxane (PDMS) is from Dow Corning. De-ionized (DI) water with a resistivity of 18MΩ, used in all the experiments was obtained from the NANO pure ultrapure water system (Barnstead). 11-mercaptoundecanoic acid in ethanol (NanoThinks Acid 11), N-(3-Dimethylaminopropyl)-N′-ethylcarbodiimide hydrochloride (EDC) and N-Hydroxysuccinimide (NHS), phosphate buffered saline (PBS) were obtained from Sigma Aldrich, Canada. PBS tablets were dissolved in DI water at 0.1M concentration with a pH of 7.2. Streptavidin was purchased from IBA GmBH and biotin-PEG-Vn96 and MCF7 CCM EVs were supplied by the Atlantic Cancer Research Institute (ACRI) in Moncton, New Brunswick, Canada.

4.2.1. Cell culture and Sample preparation (EVs from Bioreactor and UCF isolated EVs)

Breast cancer cell line (MCF7) was purchased from the American Tissue and Culture Collection (ATCC) and adapted for continuous long-term conditioned cell culture media harvest in Two-Compartment Bioreactor (CELLine, AD 1000 bioreactor) as shown in Figure 4.2.

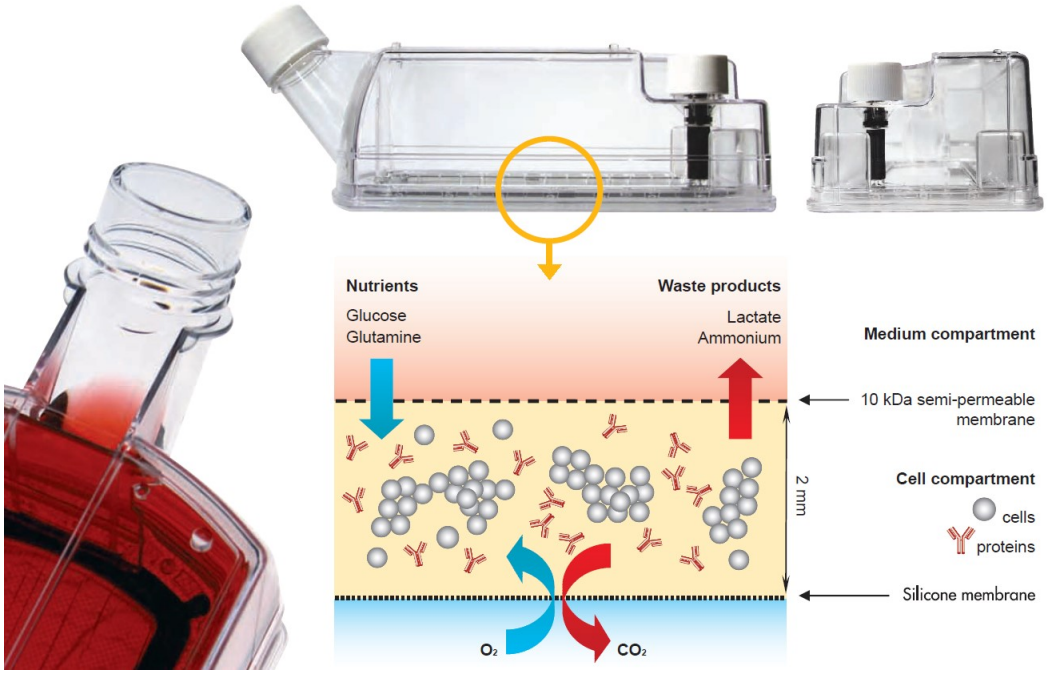

Figure 4.2: Schematic and mechanism of medium and cell compartments in the Bioreactor [166]

The efficient cultivation of cells relies on maintaining an optimal supply of nutrients and oxygen, along with the effective removal of inhibiting metabolic waste products. These are the primary factors that limit achieving a high expression levels of proteins. The Bioreactor from CELLine is designed with two compartments to overcome such limitations. These compartments separate the bioreactor into a medium and cell compartment using a 10 kDa cutoff dialysis membrane, which allows a continuous diffusion of nutrients into the cell compartment with a simultaneous removal of any inhibitory waste product. The compartment separation and individual accessibility allows to supply cells with fresh medium without interfering with the culture. There is a silicone membrane placed at the bottom of cell compartment to ensure efficient gas transfer by providing optimal oxygen and control of carbon dioxide levels. Altogether, the compartmental cultivation conditions in the CELLine bioreactor leads to a high density of cells.

The cell culture media prepared with exosome free (Exo-Free) Fetal Bovine Serum (FBS) were added to the cell growth chamber. The Exo-free FBS was prepared by centrifugation of FBS (100,000xg, 2h, 4°C) prior to use in the bioreactor. The conditioned media were harvested once a week from the cell-growth chamber only. The harvested cell culture media were centrifuged at 1,800 x g for 5 minutes to remove the floating cells, followed by 17,000 x g for 15 minutes to remove cellular debris, followed by syringe filtration through a 0.22 μm membrane. The filtered solution was then immediately added with preservatives such as 5 ml of protease inhibitor cocktail-III (EDM-Millipore) and 0.1% (v/v) ProClin300 (Sigma) and then stored at 4°C [167].

The CCM of 10 ml which was precleared for cellular debris at 17000 x g was loaded into UCF tube and 0.1μ filtered sucrose (30%) of around 600-700μl was added to the bottom of the same tube. Then, the tubes were placed in the UCF rotor and spin at 130,000 x g for 2hrs at 4°C. After the first round of spinning, around 650ul of sucrose was collected and transferred to a new UCF tube and 10ml of 0.1μ filtered 1X PBS was added to the same tube. Then, spinning was repeated at 130,000 x g for another 1.5 hours at 4°C. After the second spin, the supernatant was removed by aspiration, and 1X PBS was added to the UCF pellet to re-suspend the EVs by gently vortexing.

4.3. Experimental results and discussion

This section discusses the simulation of microfluidic structures, fabrication of microfluidic device and it is testing using an Ocean Optics spectrometer for detection of exosomes. A scheme of the microfluidic devices designed and simulated in COMSOL Multiphysics 5.2 is shown in Figure 4.3. The design shows the inlet and outlet, connected to a microfluidic channel, containing a collection chamber. The designs are mainly analyzed for the streamline contours of fluid flow. The rhombic and triangular designs have some unused portions of space in the collection chamber, where the velocity of the fluid is so low that it might not cover that region. The fluid covers the entire region in the collection chamber of the circular design. Therefore, the circular design is selected for the fabrication of the device. The channel is 500 μm wide, its depth is 200 μm, and the collection chamber has a diameter of 5 mm. This diameter is considered relatively large, so that the fluid covers the entire region with considerably low velocity, enabling the binding of the compounds flowing in the channel to the gold nano-islands.

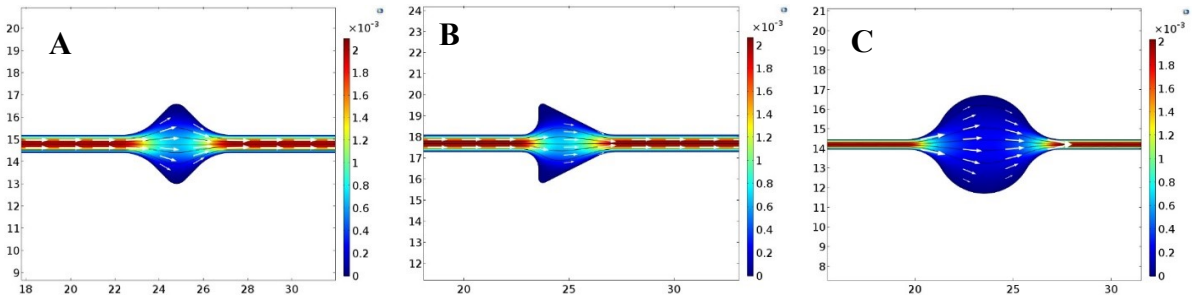

Figure 4.3: Designed microchannel and predicted streamline contours (A) Rhombic design (B) Triangular design (C) Circular design

The device contains a wide opening around the middle of the channel which is a collection chamber where the chemical and biochemical entities will be collected during the biosensing protocol. The exosomes will be captured and isolated in this chamber. A mold for this design is fabricated on a silicon wafer, using a standard fabrication process [126] with a negative photoresist. The same concept can be used to create more designs for a better flow pattern in the channel.

The PDMS base (pre-polymer) and curing agent are mixed in the ratio of 10:1 by weight. The PDMS mixture was placed in a vacuum desiccator and degassed to remove the air bubbles. Then, the PDMS was casted onto a mold on a silicon wafer made with a standard fabrication process to make the PDMS microfluidic channel. Prior to PDMS casting, the mold was silanized by using few drops of the trichlorosilane at 60°C for 1 hour on a hot plate and covering it with a Petri dish. Then, the mold was placed in a Petri dish and the PDMS mixture was poured on the wafer to a thickness of ~2mm and baked at 60°C for 10 hours. On the wafer containing the microfluidic channel, the PDMS layer was then cut into individual samples of predefined size.

The microfluidic device is illuminated with a UV/visible light source through a 600µm optical fiber. The transmitted light from the device is collected through another 600µm optical fiber, which is linked to an Ocean Optics USB2000 spectrometer. This spectrometer is connected to a computer using Spectrasuite software to measure the absorption spectra. The schematic of the microfluidic device used with the Ocean Optics spectrometer setup for absorbance measurement is shown in Figure 4.4.

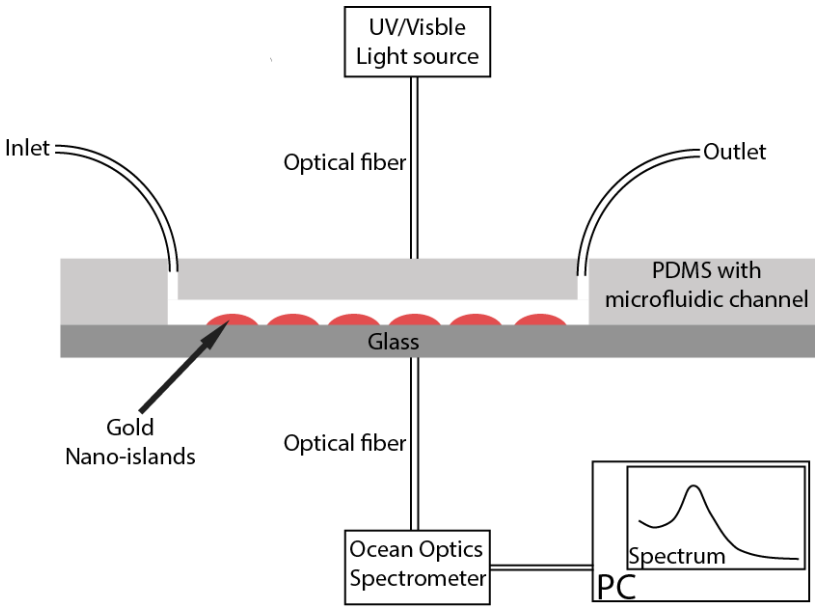

Figure 4.4: Schematic of microfluidic device used in the Ocean Optics spectrometer setup for absorbance measurement

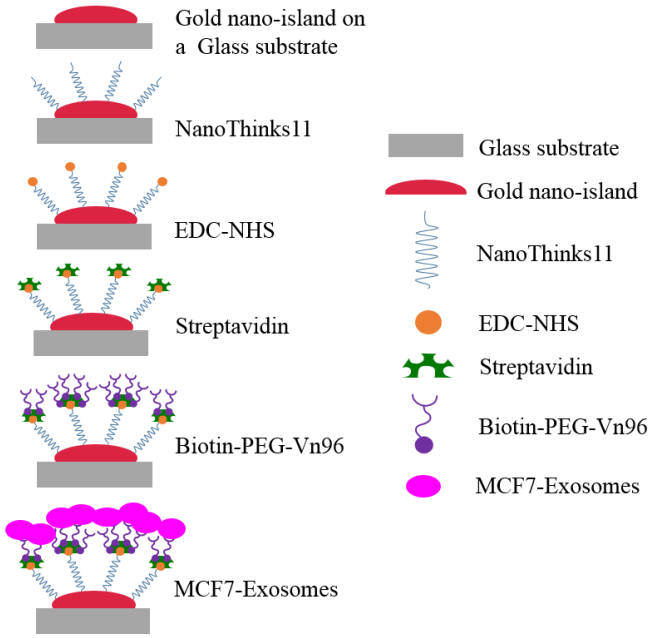

Figure 4.5: Schematic of biosensing protocol used for detection of exosomes

4.3.1. Biosensing protocol

The biosensing protocol shown in Figure 4.5 used to capture the exosomes is an affinity-based approach [151] developed in our laboratory. The chemical compounds were first

immobilized on a glass substrate with gold nano-islands to optimize the molar concentrations at each stage. They were optimized based on the stability of the LSPR shift. The optimal concentrations of streptavidin and the biotin-PEG-Vn96 complex were found to be 0.19nM and 0.87nM, respectively. After all the parameters were optimized, the whole protocol was transferred to a microfluidic environment.

In a typical experiment, initially, the absorption spectrum of the gold nano-islands in the collection chamber are measured. Then, a Nano Thinks 11 solution is passed through the microfluidic channel at the flow rate of 10 µl/min continuously for 30 minutes and next incubated for 3 hours for the formation of hydroxyl bonds. Then the spectrum is measured, and EDC-NHS mixture is infused at same flow rate and the device is incubated again for 4 hours for the amidation. The same procedure is repeated with the streptavidin, biotin-PEG-Vn96 and the exosomes. With the adopted procedure, a shift in the peak of the Au LSPR in each spectrum is observed at every stage, confirming the binding of each compound.

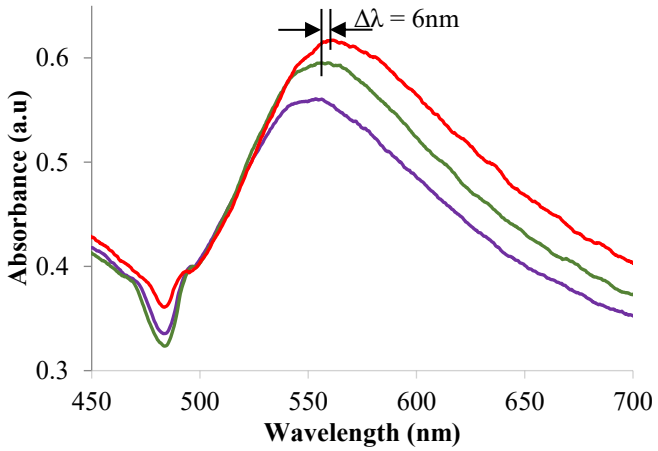

Figure 4.6: Absorption spectra measured from Ocean optics spectrometer for last three stages

The Au-LSPR band is recorded at each stage of the biosensing protocol using an Ocean optics 2000 USB series spectrometer, with a fiber of 600µm diameter. The Au-LSPR band is recorded after the functionalization of the nano-islands with the linker, followed by binding of the cross linker, the streptavidin, Vn96-linker-biotin and MCF7 exosomes. The observed spectra showed a shift towards longer wavelength of Au LSPR band. The shift upon the interaction of biotin-PEG-Vn96 and exosomes is found to be around 6 nm as shown in Figure 4.6. For detection purposes, only the shift due to the final capture step is considered.

4.4. Conclusion

In this work, a microfluidic method for the isolation and detection of exosomes has been developed. The detection is based on the sensitivity of the LSPR property of gold nano-islands to any change in the surrounding environment. The biosensing protocol is carried out in a microfluidic device, specially designed for the collection and detection of exosomes. The detection of exosomes in this work is possible because of the high affinity of Vn96 toward the proteins located at the periphery of exosomes. This results in a red shift of the Au LSPR band and allows the quantification of exosomes. The results indicate that label-free technique, based on the sensitivity of the Au-LSPR band to the surrounding environment is promising for the detection of MCF-7 exosomes by the immune-affinity approach using the Vn96 polypeptide. This approach seems to be better than the previous approaches. Thus, this technique may lead to the miniaturization of device for point of care application.

Using the optimized protocols and the concentrations of the entities, the capture and isolation of EVs from MCF7 CCM using gold nano-island enabled microfluidic chip has been proved using plasmonic technique, localized surface plasmon resonance (LSPR). Therefore, now it is important to characterize the isolated EVs using mechanical and biological techniques. So, the next chapter (Chapter 5) discusses another gold nano-island enabled microfluidic device utilized to capture and isolate the EVs from MCF7 CCM and validating the measured plasmonic shift with the AFM and DNA amplification.

Chapter 5

Microfluidic Isolation of Extracellular Vesicles and Validation through AFM and DNA Amplification

This chapter is reproduced from the article published in *European Journal of Extracellular Vesicles (EJEV).* 2020, Vol.1, 1-10.

Extracellular vesicles (EVs) or exosomes are nano-sized particles containing lipids, proteins, mRNAs, and microRNAs from their origin cells, playing thus a critical role in cell-to-cell communication. The currently existing detection methods are expensive, time consuming and lack in yield and purity. Here, we present a simple microfluidics-based method to capture EVs by a novel affinity-based approach, using, instead of antibodies, a synthetic polypeptide, Vn96, that binds to the heat shock proteins (HSPs) present on the surface of EVs/exosomes. The captured EVs are detected by using the high sensitivity of the Localized Surface Plasmon Resonance (LSPR) property of gold nano-islands to any changes in their local environment. The microfluidic devices developed for the isolation of exosomes, contain multiple channels and a collection chamber to capture EVs. The capture and detection ability of the device is validated by AFM measurements of isolated EVs from the device and the measurement of gene copy number using droplet digital PCR (ddPCR). The results indicate that the developed device can capture and isolate the EVs from a very low sample volume, in less than 30 minutes, without affecting their size and shape, a major advantage compared to existing methods. Thus, the device can be considered as a prospective point of care apparatus for diagnostics in a clinical setting.

5.1. Introduction

Cancer has a major impact on societies across the world because it is among the leading causes of death. There were 14.1 million new cases and 8.2 million cancer-related deaths worldwide in 2012, out of which, 57% of new cases. 65% of deaths occurred in less developed regions of the world that include Central America and parts of Africa and Asia. Based on the statistics, it is estimated that 1.73 million new cases were diagnosed in United States in 2018 and the number of new cases per year is expected to rise by 23.6 million by 2030 [1].

With the increasing need of improved disease treatment and to control the progression of the disease, rapid and early diagnosis is required. Thus, researchers have been driven to develop new diagnostic tools, suitable for rapid point-of-care (POC) applications. In the past two decades, Lab-on-a-chip (LoC) technology has drawn significant interest from the researchers and industries for biomedical applications. The advantages of LOC include high throughput, low sample and reagent consumption, short assay time, and multiplexed detection [74, 75]. The technology has shown potential to improve molecular biomarker detection by offering sensitive and wide-ranging measurements in a compact format.

Microfluidics-based platforms have been developed for the isolation and quantification of biomolecules and more complex entities that show potential for early cancer detection. Among them are the EVs shed from cells, carrying invaluable information about the parent tumor, especially, and its state of malignancy. Therefore, EVs are a potential source of cancer biomarkers as they carry proteins and nuclei acids from the host cell. Current protocols, commonly used for isolation and quantification of EVs involve filtration, ultra-centrifugation steps, followed by NTA, DLS and AFM analysis etc. The procedure is time consuming and the recovery of EVs through these techniques, is relatively low.

The sensitivity of the LSPR property of silver and gold nanoparticles (AuNPs) to any change in their surrounding medium forms the basis for label-free bio-sensing applications [84-86]. Binding biomolecules to AuNPs or nano-islands immobilized on a substrate, results in a red shift of the LSPR bands or/and an increase in the absorbance of the band. The optical properties of AuNPs have been thoroughly studied and optimized for sensing applications, in terms of size and shape [87, 88]. LSPR sensors, based on plasmonic nanostructures, are now widely used to interrogate biomolecular interactions in real time. Despite the increasing interest in the LSPR phenomenon and its applications, there is still little research going on regarding the integration of LSPR biosensing with a microfluidic platform. Work to this purpose has been reported by our group [126, 168] and others [147, 169] thereby, contributing to the emerging field of plasmofluidics [89].

Extracellular vesicles (EVs), known also as shedding vesicles ranging from 30 to 1000nm, are potential sources of biomarkers for the diagnosis of cancer and other pathological conditions such as inflammatory and neurodegenerative diseases. They are membrane bounded nano-scale

extracellular communication organelles that are released from all cells [170] to the extra cellular space, transporting the identity of their mother cells.

For the capture, quantification, and characterization of EVs, several LSPR-based microfluidic approaches have been developed [65, 171, 172]. These approaches are attractive for clinical applications because of the requirement of low amounts of sample and reagents, and shorter reaction times. From small volumes of serum and cell culture medium, using anti-CD63 capture antibody coated on the surface of micro channels serum vesicles were captured and from them RNA was extracted [43]. A similar immune-affinity approach was used for the capture of exosomes [56]. The microfluidic platform, ExoChip, developed by the authors, enables the isolation and, at the same time, visualization, and molecular profiling of the captured exosomes. Visualization and quantification of exosomes is done by using an on-chip fluorescent assay. On-chip molecular profiling of the isolated exosomes, especially, the isolation of total RNA was also demonstrated. Further advancing of microfluidic technology for the detection and molecular profiling of exosomes was done [65] who designed a SPR-based nano-plasmonic exosomes sensor (nPLEX) for quantitative analysis of exosomes. To improve the sensitivity and enable portable operation, the authors used periodic nanohole arrays, patterned in a gold film, functionalized with antibodies for sensing the surface proteins of exosomes from ovarian cancer cell lines.

Recently, our group developed a LSPR method to capture EVs, by using a small synthetic polypeptide called Vn96 [36] instead of antibodies, on a gold (Au) nano-island sensing platform that has a high affinity toward exosomes [151, 173].The method was first validated at the macro level, by using gold nano-islands on glass substrates and carrying out the sensing protocol in a discontinuous manner. At each step, the spectral shift of the Au LSPR was measured and the one corresponding to the binding of exosomes to the biotin-Vn96 was used for calibration purposes. In order to enhance the sensitivity of the detection and to accomplish the molecular profiling of the captured EVs, a novel microfluidic device was designed. In this paper, we report on the design and fabrication of the microfluidic device, isolation of EVs captured using the synthetic polypeptide Vn96, in the device and the validation of the isolated EVs through droplet digital PCR gene amplification.

5.2. Materials and Methods

This section describes the fabrication of the three-dimensional (3D) gold nano-islands on a glass substrate by the thermal convection method. The self-assembly of gold nanoparticles to form the 3D nanostructure is based on the flow of colloidal solution, induced by evaporation at the interface of the substrate and solution.

5.2.1. Materials

Gold (III) chloride trihydrate ($HAuCl_4.3H_2O$) and sodium citrate were purchased from Sigma Aldrich. The Sylgard® 184 elastomer kit for the PDMS fabrication was purchased from Dow Corning. De-ionized (DI) water with a resistivity of 18MΩ, used in all the experiments was obtained by using the NANO pure ultrapure water system (Barnstead). 11-mercaptoundecanoic acid in ethanol (Nano Thinks Acid 11), N-(3-Dimethylaminopropyl)-N′-ethylcarbodiimide hydrochloride (EDC) and N-Hydroxysuccinimide (NHS), phosphate buffered saline (PBS) were obtained from Sigma Aldrich, Canada. PBS tablets were dissolved in DI water at 0.1M concentration with a pH of 7.2. Streptavidin was purchased from IBA GmBH and biotin-PEG-Vn96 and MCF7-CCM EVs were supplied by the Atlantic Cancer Research Institute (ACRI), Moncton, N.B., Canada.

5.2.2. Fabrication of gold nano-islands

Fabrication of gold nano-islands on glass substrates includes the synthesis of gold colloidal solution (AuNPs) and, subsequently, the deposition of Au multilayers on glass substrates by using the thermal convection method. Spherical gold nanoparticles were prepared by reduction of Gold (III) Chloride trihydrate ($HAuCl_4.3H_2O$) (chloroauric acid) by sodium citrate, following Turkevich's method. Briefly, 15mg of Gold (III) Chloride trihydrate ($HAuCl_4.3H_2O$) are added to 95ml of DI water in a beaker and heated till it reaches its boiling point. Then, 5ml of sodium citrate solution (2%) are added to the boiling solution, reducing ions to nanoparticles. Then, the reduced gold nanoparticles are deposited on a glass substrate and the morphology was tuned to form gold nano-islands [174].

5.2.3. Design, simulation, and fabrication of microfluidic device

Microfluidic channel architectures were designed and simulated in COMSOL Multiphysics 5.2. The architecture scheme shows an inlet and outlet connected with a microfluidic channel,

containing a collection chamber. The designs were analyzed for the streamline contours of fluid flow in the channel. The architecture of the channel is designed in such a way that the fluid covers the entire region of the collection chamber where the absorption spectra corresponding to the molecular interactions will be measured. The channel is 500µm wide with a depth of 150µm. The EVs collection chamber in the device is designed with a diameter of 5mm and a thickness of approximately 150µm and can hold a maximum of 3µl of sample. The predicted streamline contours of the design are shown in Figure 5.1(A).

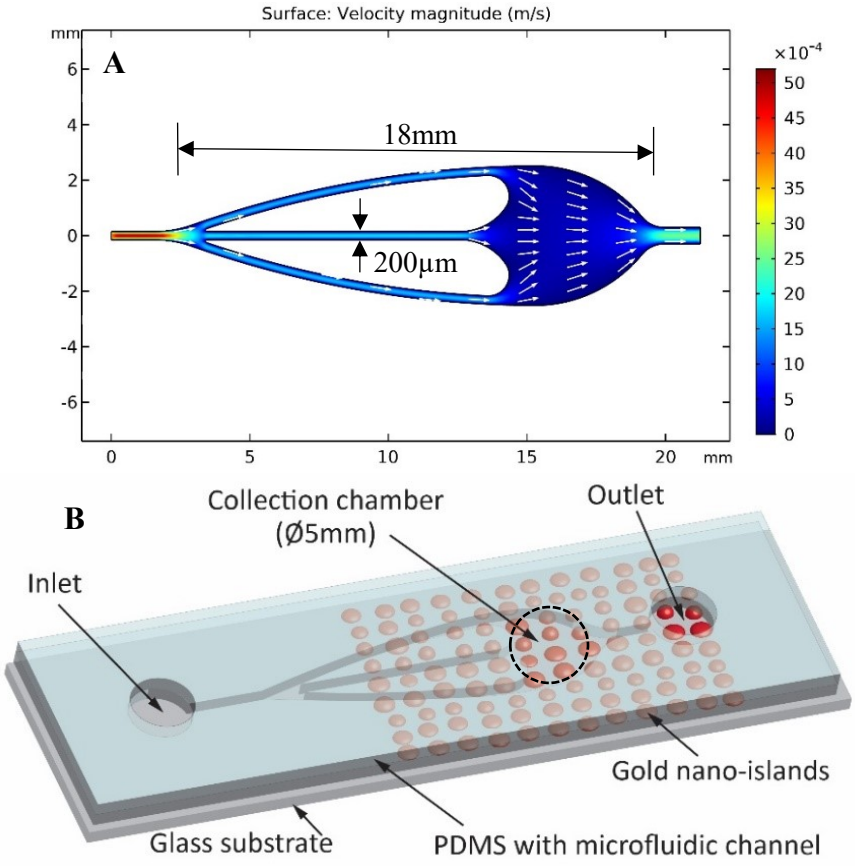

Figure 5.1: Predicted streamline contours in the designed microfluidic channels (A) streamline contours showing the magnitude of fluid velocity in the microfluidic channels (B**)** Schematic of the fabricated microfluidic device

The microfluidic device with the channel of 200µm wide and 200µm depth consists of an inlet and outlet connected to a collection chamber of 5mm diameter where the EVs captured by Vn96 are collected. A mold for this design fabricated on a silicon wafer, using the standard fabrication process with a negative photoresist.

The PDMS base (pre-polymer) and curing agent are mixed in the ratio of 10:1 by weight. The PDMS mixture was placed in a vacuum desiccator and degassed to remove the air bubbles. Then, to make the PDMS microfluidic channel, PDMS was casted onto a mold on a silicon wafer made with a standard fabrication process. Prior to PDMS casting, the mold was silanized by using 100µl of trichlorosilane at 60°C for 1hr on a hot plate, by covering it with a petri dish. Then, the mold was placed in a petri dish and the PDMS mixture was poured on the wafer to a thickness of ~2mm and baked at 60°C for 10hr. On the wafer containing the microfluidic channel, the PDMS layer was then cut into individual samples of predefined size. To form a microfluidic device, a PDMS slice cut from the mold is bonded with the glass substrate containing the gold nano-islands, using plasma bonding. Figure 5.1(B) shows the schematic of the microfluidic device.

5.2.4. Microfluidic setup for spectral measurements

The microfluidic device is illuminated with a UV/visible light source through a 600µm optical fiber. The transmitted light from the device is collected through another 600µm optical fiber, which is connected to the Ocean Optics USB4000 spectrometer. This spectrometer is linked to a computer through Spectrasuite software to measure the absorption spectra at each stage of the biosensing protocol. This spectrometer is custom built, and the arrangement can be modified as per requirement. In this setup, the optical fibers are placed vertically in such a way that the microfluidic device is placed in-between the optical fibers aligned with the collection chamber. The light from the optical fiber is shined on the device through a collimator to cover the entire area of the collection chamber. Then, the transmitted light is collected through another collimator, connected to the optical fiber that leads to the spectrometer. An attenuator was used in the setup to adjust the intensity of the light received from the device.

The biosensing protocol used to capture the EVs, an affinity-based approach developed in our laboratory, was published recently [173]. The EVs from the MCF7 CCM were used for microfluidic isolation and their size distribution was measured by nanoparticle tracking analysis (NTA) using NanoSight LM20 Nanoparticle Analysis System. The CCM was diluted by 100x for the measurement purposes and the size is around 100nm as shown in Figure 5.2. The schemtaic of the biosensing protocol and the schematic of the experimental setup including the Ocean Optics spectormeter, showing the flow of compounds using a syringe pump involved in the detection through the microfluidic device is shown in Figure 5.3(A, B).

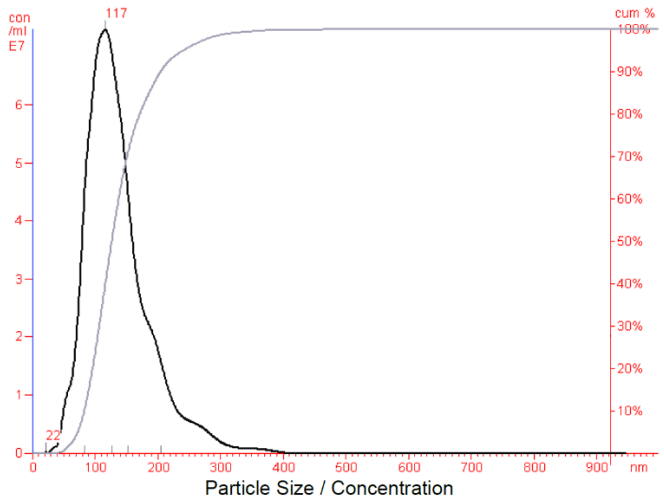

Figure 5.2: Representative figure that displays the size distribution of 100x diluted MCF7 CCM measured by NTA (NanoSight LM20 Nanoparticle Analysis System) with identical settings. The measurements were done in triplicate and the mean was calculated.

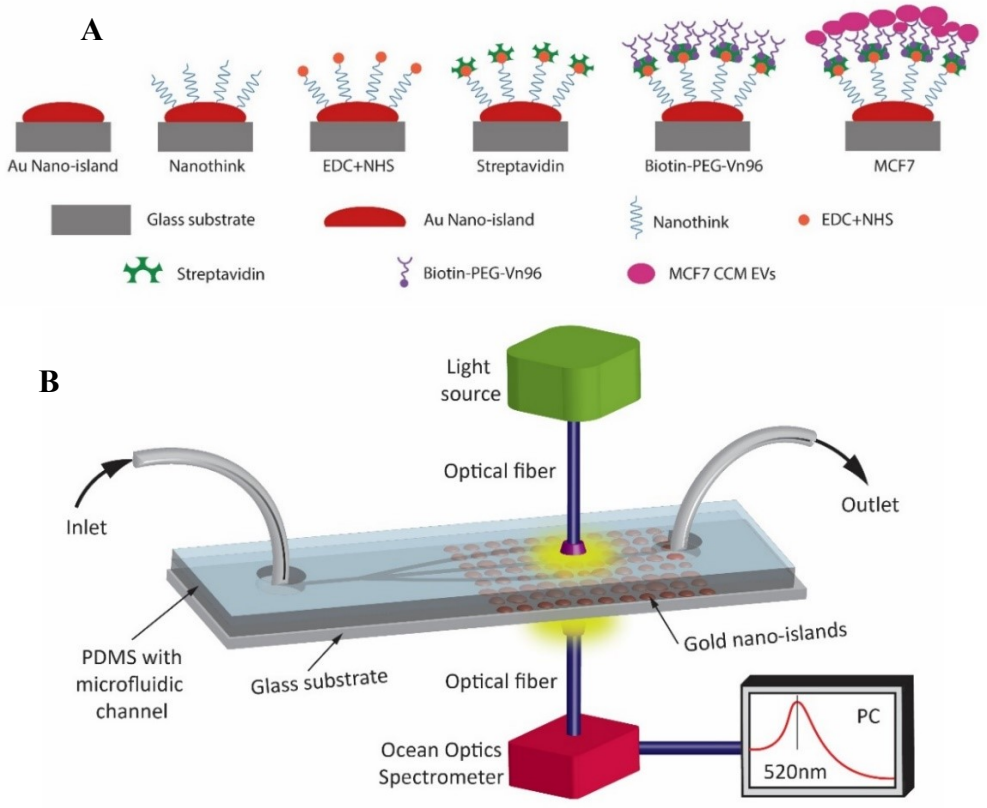

Figure 5.3: Microfluidic setup for the measurement of LSPR spectra. (A) Schematic of the biosensing protocol used for the capture and isolation of EVs using Vn96 peptide, (B) Schematic of microfluidic device used in an Ocean Optics spectrometer setup for the detection of isolated EVs using LSPR

5.2.5. Elution and characterization of EVs

The microfluidic devices were washed with PBS at a flow rate of 10µl/min to remove any unbound EVs from the collection chamber and the channel. Proteinase K (PK), which is a robust protein/peptide digesting enzyme, was prepared using PBS with a concentration of 20µg/ml and 12µl of proteinase K was used to elute EVs from the chip. PK was infused into the device to digest the protein/peptides bridging gold nano-islands and EVs so that the liquid flown out of the device will contain the EVs captured on the sensing platform. Proteinase K was flown to fill the entire channel and collection chamber and then the device was incubated at 37°C for 1hr. After incubation, ~15µl of PK was eluted from the device, called eluent. The eluent, containing EVs, was characterized by Atomic Force Microscopy (AFM), and by gene copy number estimation amplification using ddPCR.

The size of the EVs from the eluent measured using a Park Systems XE-100 atomic force microscope by scanning in a non-contact mode, equipped with a silicon cantilever (f0~300 kHz, Park Systems). Topographic and phase images were recorded simultaneously at a scan rate of 1Hz and then processed using the Park Systems XEI software.

The ddPCR analysis has been recently developed as an accurate way for absolute quantification of nucleic acids present in a very few numbers in the target samples. It has been used for absolute copy number quantitation and was shown to be more reliable than other digital PCR methods or any other conventional copy number determination methods. A droplet digital PCR was performed, according to manufacturer's instructions using the QX200™ Droplet Digital™ PCR System (Bio-Rad Laboratories) to determine the number of copies of RNAseP gene present in the EV-samples that is eluted from the microfluidic chips. For the ddPCR reactions 2µl of collected eluent from the chips was used as template. The ddPCR reaction mixture consists of 10µl of Taqman probe assay (no dUTP) (Bio-Rad Laboratories) for a gene amplification, in the total volume to 20µl reaction mix. Then, this 20µl volume of mixture is further mixed with 70µl of droplet generation oil and loaded onto a disposable plastic cartridge, covered with a specific gasket, and placed in the droplet generator. For control, the eluent was replaced with PBS buffer. After droplet generation, samples were transferred to a 96-well PCR plate and then, sealed, using the PX1 PCR plate sealer. Then, the PCR amplification was carried out in C1000 Touch™ Thermal Cycler (Bio-Rad laboratories) as per the protocol provided by the manufacturer. After PCR

amplification, the plate was shifted to the QX200™ Droplet Reader (Bio-Rad Laboratories), and the droplets from each well were automatically read for fluorescent signal detection. The Quanta Soft™ analysis software (Bio-Rad Laboratories) was used to analyze the data and quantify the copy numbers. A threshold signal value was set based on the resolution of positive and negative droplets to eliminate background noise.

5.2.6. AFM and ddPCR techniques for characterization

Atomic Force Microscopy (AFM) consists of a cantilever with sharp tip at its end that scans a sample surface. By using the movement of tip, a three-dimensional image is created by software. AFM was developed in 1986 by Binnig et al. [175] provides lateral resolution of 3 nm and vertical resolution <0.1 nm. Yuana et al. [176] showed that AFM can be used to measure the relative size of microvesicles in their physiologic state. To have a high resolution, EVs or microvesicles must be bound to an extremely flat surface.

PCR is Polymerase Chain Reaction, or it can be simply called as "molecular photocopying". It is one of the most important scientific advances in the molecular biology for which its creator, Kary B. Mullis was awarded the Nobel Prize for Chemistry in 1993. It has revolutionized the study of DNA as studying isolated pieces of DNA for molecular and genetic analyses are next to impossible without PCR. It is a fast and inexpensive technique used to "amplify" small segments of DNA. Once the DNA is amplified, it can be used in different laboratory and clinical techniques such as detection of bacteria or viruses, DNA fingerprinting, and diagnosis of genetic disorders.

PCR technique is based on the natural processes a cell uses to replicate a new DNA strand. To perform a PCR, few biological ingredients are required such as template DNA, primers, DNA polymerase, and nucleotides. The template DNA is the integral part that contains the region to be amplified. Even a single DNA molecule can serve as a template. To initiate the copying, two DNA primers that are complementary to the 3’ (three prime) ends of each of the template are required. They bind, or anneal, to the template at their complementary sites and serve as the starting point for copying. Then, the DNA polymerase, an enzyme that does the building of the new DNA strand by sequentially adding on free nucleotides (subunits of DNA), according to the instructions of the template. DNA synthesis at one primer is directed toward the other, resulting in replication of the desired sequence. The common DNA polymerase is the heat resistant Taq polymerase.

It majorly involves three steps for amplification of DNA fragments, i.e., denaturation, annealing, and synthesizing as shown in Figure 5.4, which are carried out in repeated cycles. To amplify a DNA target, first, the sample is heated around 95°C so the DNA denatures or separates into two pieces of single-stranded DNA by breaking the hydrogen bonds between the complementary bases. Next, the temperature is lowered to about 55°C so that the primers can anneal to each of the single-stranded DNA templates. Then in the last step, the temperature is raised about 72°C, and an enzyme called Taq polymerase begins to synthesize the new strands of DNA by adding nucleotides onto the ends of the annealed primers, using original strands as template. With this process, the original DNA has been duplicated with each of the new molecules including one old and one new strand of DNA. Similarly, each of these new molecules can be used to create two new copies, and so on, and so on. The whole cycle is repeated around 40 to 45 times, resulting in more than a billion exact copies of the original DNA fragment. This whole cycle is directed by thermocycler, which is programmed to change the temperature of the reaction after a set time to allow denaturing and synthesis of new DNA strands. This entire process is automated and can be completed in just a few hours.

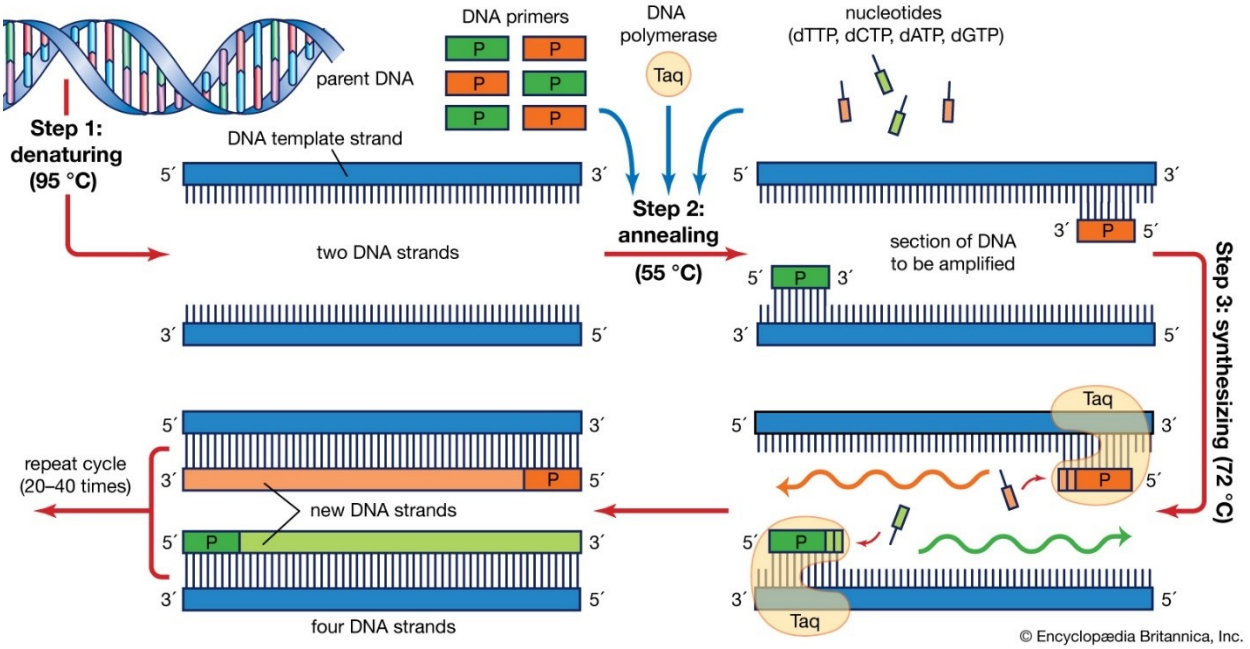

Figure 5.4: The three steps involved in the DNA amplification process by PCR [177]

Droplet Digital PCR (ddPCR) is a digital PCR technique that is used for the absolute quantification of DNA molecules based on water-oil emulsion droplet technology. Unlike regular

PCR, as discussed earlier, a sample is fractionated into 20,000 droplets, and the amplification of the template DNA molecule occurs within each individual droplet that is generated. The reagents and workflows used in the ddPCR technology are similar to those used for most standard TaqMan probe-based assays. The droplet generation is a crucial aspect of the ddPCR technique as each of the droplet serves basically the same function as the individual test tubes. The partition means that a single sample can generate tens of thousands of measurements rather than a single result. This technique requires a smaller sample volume around few microliters compared to other digital PCR commercially available, reducing the cost while maintaining the sensitivity and precision, and the preserving the precious sample.

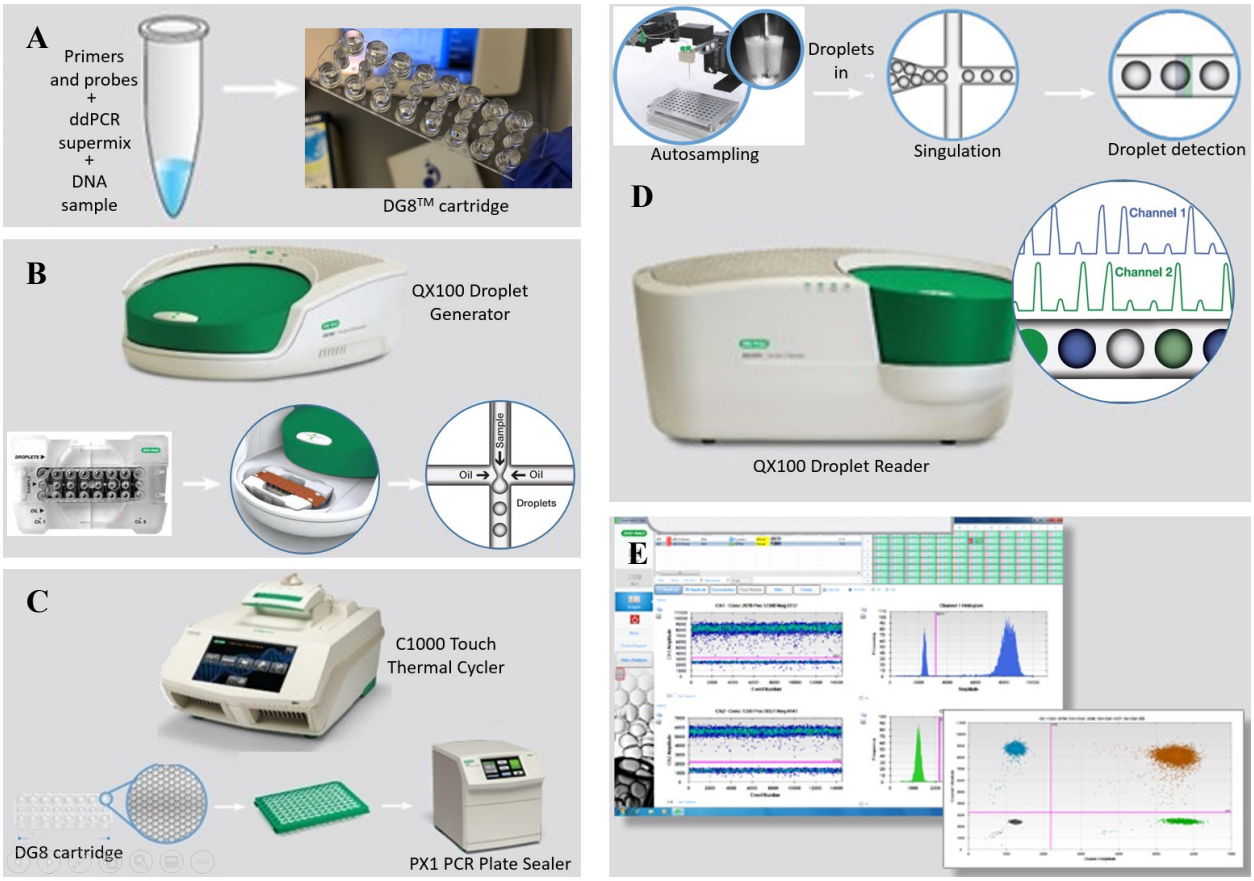

Figure 5.5: Steps involved in the absolute quantification of gene using ddPCR (A) Preparation of PCR ready sample (B) Droplet generation using QX100 Droplet Generator (C) PCR amplification in C1000 Thermal cycler (D) Reading and analyzing each droplet individually to determine the concentration of target DNA in the sample (E) Visualization of the analyzed data and determining concentration in copies/µl

The workflow of ddPCR is quite simple as shown in Figure 5.5. First, the sample is prepared by mixing the DNA sample with the primers, fluorescent probes, and proprietary ddPCR supermix developed specifically for droplet generation. The prepared sample is loaded into QX200 Droplet Generator to partition the sample into 20,000 monodispersed nanoliter-sized droplets. The generated droplets are then transferred to a 96-well plate and the plate is sealed using a PX1 PCR plate sealer before the DNA amplification in each droplet using C1000 thermal cycler for about 40 to 45 cycles. Once the PCR amplification of the DNA target in the droplets has be done, the samples are placed in the QX200 Droplet Reader to analyze each droplet individually using a two-color detection system. Then the QuantaSoft™ software is used to count the positive and negative reactions in the droplets. The number of positive reactions determines the absolute quantification or the concentration of target DNA in the sample and the software allows to visualize the analyzed results in several ways and determine the concentration in copies/µl.

5.3. Results and Discussion

The absorption spectra were measured at each stage of the biosensing protocol using the Ocean Optics USB4000 spectrometer. As per the biosensing protocol, the volume, and concentrations of all the entities remain the same, except the concentration of MCF7 EVs. The LSPR shift corresponds to the molecular interactions, i.e., it quantitatively represents the number of EVs captured by the Vn96 in the microfluidic device. The LSPR shift ($\Delta\lambda$) has been measured at each stage of the protocol and the shift corresponding to various concentrations of extracellular vesicles is plotted in Figure 5.6. As expected, the shift is increasing as the concentration of EVs is increasing.

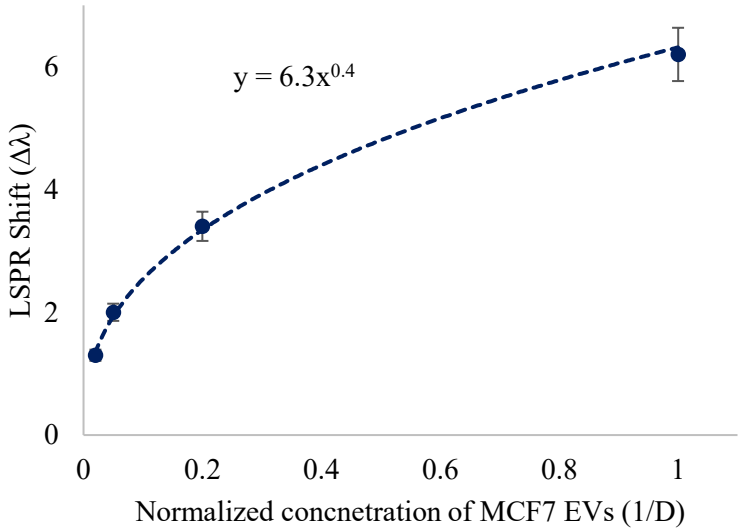

Figure 5.6: LSPR shift measured from the microfluidic device using the adopted biosensing protocol corresponding to various dilutions of MCF7 CCM EVs (D is dilution factor: 50x, 20x, 5x, and undiluted). Each data point can be tagged to identify the corresponding dilution of the sample (n=6)

5.3.1. AFM-analysis of the eluted EVs

To validate the shifts in the LSPR spectral measurements of the microfluidic device, the eluent from the device was further analyzed by AFM. The samples were diluted to 1:100 with de-ionized water and adsorbed onto freshly cleaved mica sheets to perform AFM scanning. The topographic and phase images and line profiles of the EVs and control eluent are shown in Figure 5.7. It is noticeable from the image and line profile of the MCF7-CCM EVs eluent that the spherical particles are in the height and width of around 15nm and 60 – 80nm respectively (Figure 5.7(A)). This size is within the size range of EVs published in the literature [178, 179]. The control eluent did not show any spherical particles, but mostly irregular shapes of heights around 1-2 nm, without any phase contrast (Figure 5.7(B)). The morphology of isolated EVs can be seen as spherical in shape from the line profiles with a diameter of around 80nm while the control shows irregular shapes of around 2nm. The size of isolated EVs is almost in agreement with the size shown by the NTA measurements. Therefore, the AFM measurements confirm that the proposed microfluidic devices have successfully captured and isolated the EVs from the CCM, validating the shift in the LSPR spectral measurements.

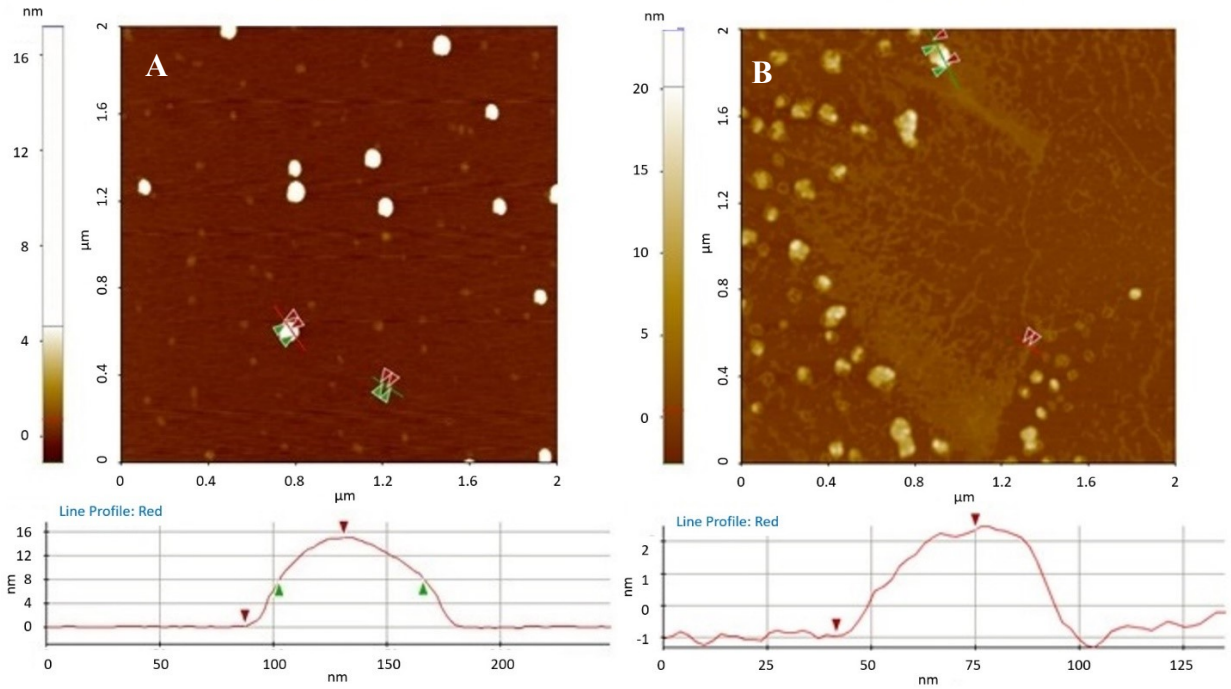

Figure 5.7: Morphology of isolated EVs by AFM phase images and line profiles. (A) Phase image of the Vn96 peptide-precipitated (Proteinase K digested) EVs and its line profile, (B) Phase image of the control sample, which is EV-free media, that was used for culturing MCF7 cells and its line profile. A differential size distribution pattern is observed between EVs. The marked spots in the image are used to measure the width and thickness of two individual EVs

5.3.2. RNase P gene copy number quantification by ddPCR

To further validate and find out whether the gold-LSPR red shift observed is due to the high affinity binding of EVs to Vn96, droplet digital PCR (ddPCR) analysis was performed on the eluted fraction of EVs collected from the chips to quantitate the RNAseP DNA copy numbers as a reference gene. It has been shown that RNase P DNA sequence is present in the EVs and can be used as a reference gene in ddPCR reactions [180]. In this work, undiluted and 5x times diluted MCF7-CCM was used to run through the chips to capture EVs. Initially, the concentration of undiluted MCF7-CCM EVs was measured by NTA and found to be $6x10^9$ particles/ml and as per the designed protocol, only 100µl was used to run through the device. The number of RNase P gene copies from the eluent of undiluted and 5x diluted CCM infused microfluidic devices were found to be 3.66 and 1.08 copies/µl, respectively. As expected, the eluent collected from the microfluidic devices (MF-isolated EVs) showed an appreciable number of RNAseP gene copies

amplified by ddPCR reactions as shown in Figure 5.8(A). This data validates that the red shift seen in the LSPR spectra is primarily due to the binding of EVs to the Vn96 in the devices.

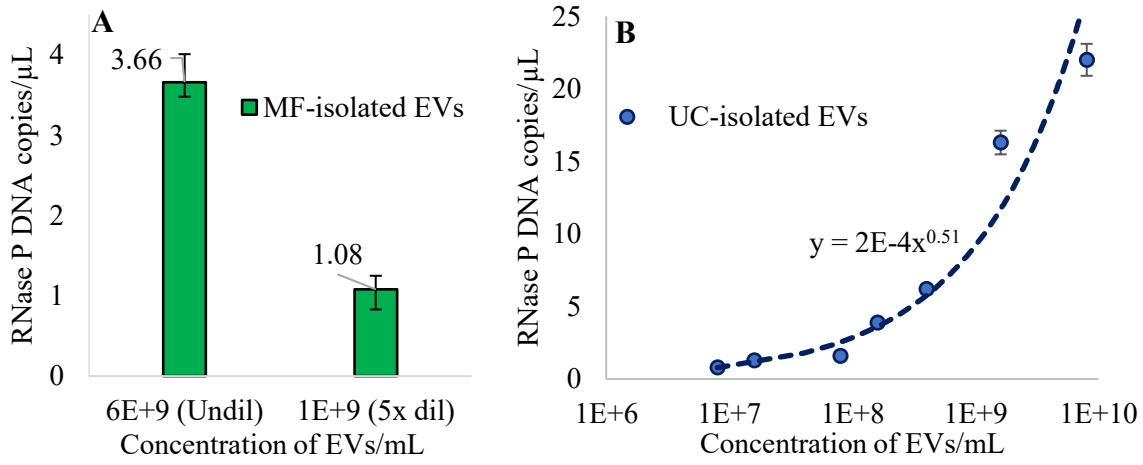

Figure 5.8: Quantification of isolated EVs by using droplet digital PCR (A) Number of gene copies amplified from microfluidic device eluent corresponding to undiluted and 5x diluted infused CCM (B) Number of RNase P gene copies amplified from various dilutions of UC-isolated EVs (n=3)

In parallel, for comparison and as a positive control, EVs isolated through gold standard ultracentrifugation (UC-isolated EVs), whose concentration was $8x10^9$ EVs/ml, was used for RNAseP gene amplification in ddPCR. Figure 5.8(B) shows the number of RNase P gene copies amplified with various dilutions of UC-isolated EVs. For negative controls, PBS buffer or EV-free CCM was used, and no amplification of RNase P DNA fragment was observed. By keeping the UC-isolated gene copies data as a reference, the 3.6 copies/µl determined through MF-isolated EVs corresponds to a concentration of $1.6x10^8$ EVs/ml approximately. It means such a number of EVs should be captured in the collection chamber of the chip. On the other hand, in our recent work [181], the physical modelling of Vn96-chip of the nano-island-EV interaction has shown that the collection chamber of 5mm diameter in a microfluidic device can accommodate up to a maximum of $5.3x10^8$ EVs. As per the protocol, only 100µl of undiluted CCM, which corresponds to almost $6x10^8$ particles, was infused into the microfluidic device. However, the chip was able to capture only ~$1.6x10^8$ EVs by Vn96 present in the collection chamber. Similarly, with the 5x diluted CCM, only ~$1x10^8$ EVs, got captured out of $1.2x10^8$ particles that were infused. It is

interesting to note that capture capacity of Vn96 chip is better with diluted (5x) CCM compared to undiluted CCM. In 5x diluted CCM infused into the device, around 83% of the EVs infused were captured while in undiluted CCM, only 25% of the infused EVs got captured. This difference in the EVs captured and isolated, and the number of gene copies amplified from the eluent of microfluidic devices can be attributed to (1) the efficiency of the Vn96 capture in the collection chamber and their specific binding with the HSP heavy EVs; (2) the loss of EVs that could have occurred during the Proteinase K mediated elution of EVs from the chip; (3) the presence of RNase P gene in the EVs as the this DNA fragment of the genome may not be present in all the EVs; (4) the number of gold nanoislands formed in the collection chamber; and (5) aggregated EVs in highly concentrated CCM could prevent its binding with Vn96. Therefore, this data clearly shows the capability of the microfluidic device for the isolation of extracellular vesicles from a very low sample volume in less than 30 minutes. In this study, we have demonstrated the capability of Vn96 enabled gold nanoisland-based microfluidic platform for capture and isolation of EVs originating from cancer cells and their DNA analysis through ddPCR reactions after eluting from the device.

5.4. Conclusions

In the present study, the capture and detection ability of the developed microfluidic device were examined using the EVs from the breast cancer cell-line (MCF7) conditioned media, grown in a small bioreactor. To evaluate the performance of the device, two different concentrations of EVs, the undiluted and 5x diluted MCF7-CCM were flown through the Vn96 functionalized microfluidic devices at a flow rate of 10µl/min. The LSPR measurements at each stage were performed after the incubation as per our developed biosensing protocol. To validate the measured Au-LSPR shift, the CCM was eluted from the device and then analyzed for size and shape by AFM and their RNase P gene amplification by ddPCR. The RNase P gene amplified from the undiluted and 5x diluted CCM infused microfluidic devices were in the order of 3.66 and 1.08 copies/µl respectively. The gene amplification from the device and AFM data further validate that the developed microfluidic devices have the ability to bind, capture and isolate EVs from the CCM, resulting in higher efficiency, without affecting their size or shape. The major advantages of this label-free microfluidic technique include isolation of EVs from a very low sample volume starting from 3µl, in less than 30 minutes using a simple device, when compared with the traditional techniques. In addition, as the standard protocol for the detection and isolation was optimized, the

inconsistencies caused by the procedure can be reduced and the detection reproducibility improved. Isolation and analysis of EVs are the cornerstones of any technique for EV-based diagnosis and therapeutic applications. The microfluidic technology empowers the capture, isolation, and analysis of EVs. In conclusion, the gold nanoisland-based microfluidic technique, with vn96-peptide functionalization can be a reliable tool in the EV-based diagnosis in a real-life clinical setting.

With the proposed the gold nano-island enabled microfluidic device, the EVs from the MCF7 CCM have been isolated. The measured plasmonic shift has been compared and validated using the morphology of isolated EVs by AFM measurements and the absolute quantification of RNase P DNA from the isolated EVs using ddPCR. So, now it is important to improve the sensitivity of detection in the microfluidic environment. So, the next chapter (Chapter 6) discusses more sensitive gold nano-island integrated microfluidic device, which is a multi-level microfluidic device for the amplification of the sensitivity of detection.

Chapter 6

Sensitivity Amplification by Multi-level Microfluidic Device for the Detection of Extracellular Vesicles

This chapter is reproduced from the manuscript prepared for the *Journal of Advanced NanoBioMed Research*.

Extracellular Vesicles (EVs) are nano-sized particles containing lipids, proteins, mRNAs, and microRNAs from their origin cells, playing a critical role in cell communication. Although their characteristics provide EVs great potential as biomarkers, efficient isolation and detection techniques are still challenging. In this work, we present a two-level microfluidic technique to capture EVs by an immuno-affinity-based approach, using a synthetic polypeptide, Vn96, that binds to the heat shock proteins (HSPs) present on the surface of EVs. The captured EVs are detected using the high sensitivity of the Localized Surface Plasmon Resonance (LSPR) property of gold nano-islands to any changes in their local environment. The microfluidic devices developed for exosomes' isolation contain multiple channels and collection chambers to capture EVs. In order to increase the sensitivity, the gold nanoparticles are immobilized by thermal convection on both sides of a thin glass substrate, contrary to our earlier work, where the nanoparticles were deposited only on one side. A two-level device is fabricated for the isolation and detection of EV, utilizing this double-sided gold nano-island substrate; the detection sensitivity of the platform has been increased due to the increased molecular interactions in the collection chambers. This technique can be extended to multi-level microfluidics by introducing an intermediate channel in between the nanoisland substrates. The preliminary results suggest that the multi-level microfluidic device can be used for a high sensitivity detection of EVs.

6.1. Introduction

Extracellular Vesicles (EVs) are the vital sources of biomarkers for cancer, other pathological conditions such as inflammatory and neurodegenerative diseases, and for clinical diagnostics. EVs are the shedding vesicles with sizes ranging from 30 to 1000nm. They are membrane-bounded nano-scale extracellular communication organelles that are released from all

cell types to the extra cellular space, transporting the identity of their mother cells. Therefore, for an early diagnosis of cancer and improved treatment, the isolation, and detection of EVs is of utmost important [5, 37].

In recent years, microfluidics has boomed as an emerging technology due to its benefits such as miniaturization, smooth integration with optical components, and the ability to perform fast detection [182]. Microfluidics has been addressing applications in a wide range of fields [183, 184]. Especially, it has shown considerable potential in the biomedical field [185, 186]. Several researchers have reported hybrid microfluidic devices by incorporating integrated structures to enable complex lab-on-a-chip (LOC) research platforms and point-of-care testing (POCT) devices. Those structures are electrode arrays, permeable membranes, and other functional structures [187]. To realize these complex microfluidic devices, various fabrication techniques have been reported [188-191]. Polydimethylsiloxane (PDMS) is the most extensively used material for the fabrication of microfluidic devices due to its inherent biocompatibility with the samples, low cost, favorable chemical, and mechanical properties, and optically transparency in the frequencies range from 240 nm to 1100 nm [192].

The microfabrication techniques reported in the literature to realize the above-mentioned complex microfluidics can be primarily categorized into three types. The first type depends on sequential traditional 2D microfabrication to achieve multi-layer structures [193]. This approach has been the foundation for a decade to realize complex microfluidic structures, however, as the complexity in the microfluidic devices kept on increasing, this technique has not evolved much [194]. The layering of 2D microfabricated structures is interesting as, due to its maturity, complex systems often require multiple manual alignments and bonding processes. The second type of fabrication is the casting of PDMS around a 3D sacrificial structure, which will be removed or dissolved later [195]. The layering approaches, including the alignment and bonding issues, are eliminated with this type of fabrication; however, this fabrication method often requires removal of the sacrificial structure, which can limit the geometry, impact yield, or again, require skilled manual processing because of the complex protocols mentioned. The third type of fabrication is the mold based ‘membrane sandwich’ approach, which has shown great potential [196]. As the PDMS pre-polymer is sandwiched between a patterned wafer-based mold and a passivated PDMS mold, the efforts in the fabrication of layered channel structures are reduced.

The most important parameter for the label-free biosensing applications is the sensitivity of the LSPR property of silver and gold nanoparticles (AuNPs) to any change in their surrounding medium [84]. The molecular interactions with the immobilized nanoparticles result in a redshift of the LSPR bands or/and an increase in the absorbance. The optical properties of AuNPs for sensing applications in terms of size and shape have been meticulously studied and reported in the past [88]. Presently, the plasmonic nanostructures based LSPR sensors are widely used to interrogate biomolecular interactions in real-time. Despite the increasing interest in the LSPR phenomenon and its applications, there is still little research on the integration of LSPR biosensing with a microfluidic platform [89]. In this paper, we report on the design and fabrication of a multi-level microfluidic device, isolation of EVs captured, using the synthetic polypeptide Vn96 [36], in the two-level microfluidic device, and the validation of the isolated EVs through LSPR detection technique.

6.2. Materials

The Sylgard® 184 elastomer kit for the PDMS fabrication was purchased from Dow Corning. Cover glasses of size 18mm x 18mm with a thickness of 150µm were purchased from VWR International company. Gold (III) chloride trihydrate ($HAuCl_4.3H_2O$) and sodium citrate were purchased from Sigma Aldrich. De-ionized (DI) water with a resistivity of 18MΩ was obtained by using the NANOpure ultrapure water system (Barnstead). 11-mercaptoundecanoic acid in ethanol (NanoThinks Acid 11), N-(3-Dimethylaminopropyl)-N′-ethylcarbodiimide hydrochloride (EDC) and N-Hydroxysuccinimide (NHS), phosphate-buffered saline (PBS) was obtained from Sigma Aldrich, Canada. PBS tablets were dissolved in DI water at 0.1M concentration, with a pH of 7.2. Streptavidin was purchased from IBA GmBH, and biotin-PEG-Vn96 was purchased from New England Peptide, USA and MCF7 EVs were collected from a conditioned media.

6.3. Experimental procedures

6.3.1. Deposition of AuNPs on both sides of a glass substrate

A gold colloidal solution is prepared as per Turkevich's method by dissolving 16mg of gold chloride trihydrate in 95ml of DI water and this solution is called the precursor solution. Then, the precursor solution is boiled until it reaches the boiling point and then 5ml of 2% sodium citrate

solution is added to the boiling solution. The glass substrate is 150µm thick, with a length and width of 18mm each. These thin glass substrates are habitually used as a micro cover glass under the microscope. The advantage of using thin glass substrates for the deposition of gold nanoparticles is that multiple substrates can be used in a single device, without making it bulky. The gold nanoparticles are deposited by the thermal convection method, based on the evaporation of gold colloidal solution at the interface of the substrate and solution. After this first deposition, the substrate was heat-treated at 560°C for an hour for morphology tuning, where the deposited gold nanoparticles turn into gold nano-islands. Once the substrate reaches room temperature, the same substrate was reversed and placed again in a beaker containing a gold colloidal solution for a second deposition on the other side of the substrate by the same method. After the second deposition, the substrate was heat-treated again at 560°C for an hour and allowed to cool to room temperature. The heat-treated glass substrate with gold nanoislands on both sides is further called double-sided gold nanoisland substrate (DS-AuNI substrate), and its absorption spectrum is shown in Figure 6.1. The spectrum indicates a high number of gold nano-islands available for interaction with the biochemical entities.

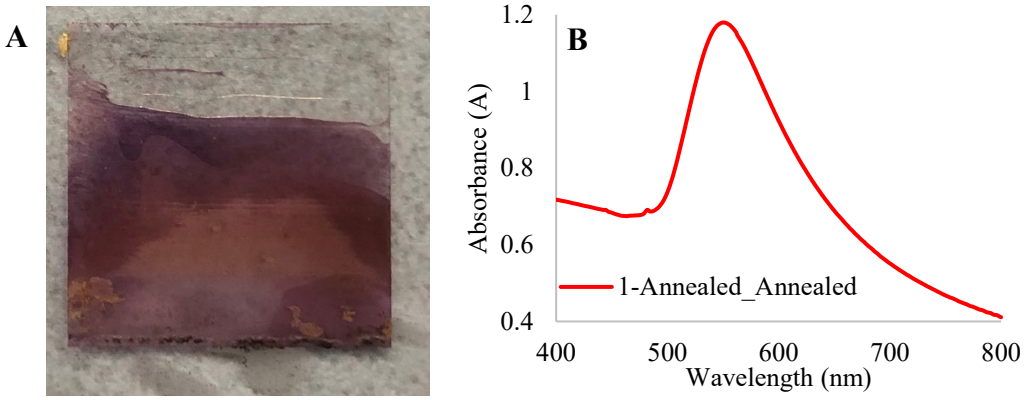

Figure 6.1: DS-AuNI substrate with its absorption spectrum (a) Picture of an 18mm x 18mm glass substrate with AuNIs on both sides (b) Absorption spectrum of DS-AuNI substrate

6.3.2. COMSOL simulation of microfluidic channels

A symmetric structure of the microfluidic channel is designed so that the same channel can be utilized as a top and bottom channel just by reversing it. The microfluidic channel's scheme is designed and simulated in COMSOL Multiphysics 5.5, as shown in Figure 6.2. The design shows the inlet and outlet connected to a channel, containing an extensive collection chamber. The designs are analyzed for the streamline contours to observe the magnitude of the fluid velocity

inside the channels, considering the water as a solvent with a flow velocity of 10µL/min. The channel's width is 300 µm, with a depth of 150 µm, and the collection chamber has a diameter of 7 mm. This collection chamber is larger than the one in our previous microfluidic devices, enabling much higher interactions/binding of the entities to the AuNIs.

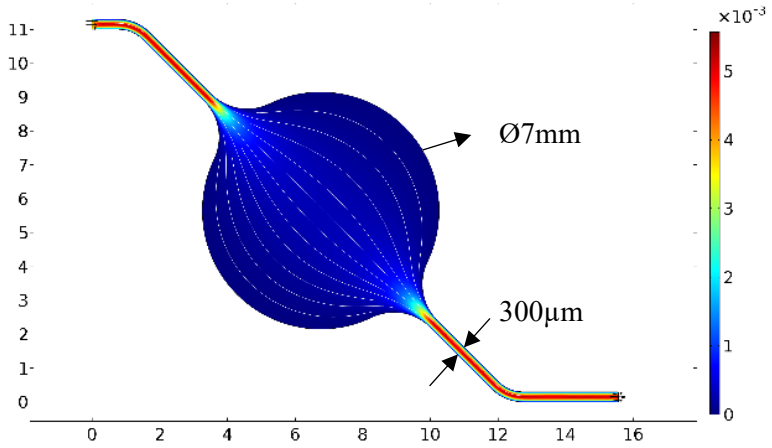

Figure 6.2: COMSOL simulation for fluid flow pattern of top/bottom channel

6.3.3. Fabrication of the device

Unlike the other microfluidic devices [173, 197], a thick glass substrate is not used in these devices. Instead, a 150 µm thin glass substrate was utilized for the deposition of gold nanoparticles. Because of the very thin glass, the utmost care has to be taken while bonding and handling the devices. There are three layers for a two-level device microfluidic device. Therefore, there are individual masks for the fabrication of the mold for each layer. The schematic of the fabrication steps of the device is shown in Figure 6.3. The SU8 molds and their corresponding PDMS layers include top, spacer, and bottom layers. The top and bottom layers being symmetrical, only one mask or one mold is enough to make both the layers. The spacer layer is a mandatory thin layer to cover up space or the gap created due to the DS-AuNI glass substrate between the top and bottom PDMS layers. Standard patterning of SU8-2075 photoresist was used for the fabrication of these molds and the soft-lithography parameters are tabulated in Table 6.1. All the molds have been silanized for 2 hours after the fabrication to be used for PDMS fabrication.

The proposed device was fabricated using poly (dimethylsiloxane) (PDMS) from Sylgard® 184 elastomer kit from Dow Corning Corporation. The base polymer (pre-polymer) and the curing agent (crosslinking agent) from the kit are mixed in the ratio of 10:1 by weight for the fabrication. As shown in Figure 6.3(a), the proposed device includes two thick layers (top and bottom) having

200 µm microchannels and a thin spacer layer with a thickness of 150 µm. The fabrication process of the thin spacer layer is schematically shown in Figure 6.3(b). For the fabrication of this layer, PDMS was poured onto the mold, and then a large glass slide was placed on PDMS and pushed gently to remove the excess of PDMS from the mold. While maintaining the same pressure on the glass slide with a hook, the PDMS was cured at 80°C for 2 hours. After curing, the PDMS spacer layer can be easily peeled off from the mold as the mold was already silanized [198]. The cross-sectional and the exploded view of the two-level microfluidic device is shown in Figure 6.3 (c, d).

Table 6.1: Soft lithography parameters for the fabrication of molds for the top/bottom, spacer, and the intermediate layers

	Spin-coating	**Pre-bake**	**UV Exposure**	**Post-bake**
Top/bottom layer	500rpm for 10sec 1600rpm for 40sec	65°C for 10 min 95°C for 40 min	90 sec	65°C for 5 min 95°C for 10 min
Spacer layer	500rpm for 10sec 800rpm for 40sec	65°C for 10 min 95°C for 40 min	80 sec	65°C for 5 min 95°C for 10 min

The bonding strength of PDMS to glass is relatively stronger than that of PDMS to silicon. Therefore, when the spacer layer is peeled off the mold, it comes along with the supporting glass slide. As the spacer layer is very thin, of around 150 µm, leaving it on the supporting glass slide helps in keeping the structures intact. Then, the AuNI glass substrate was placed in the center of the spacer layer, as shown in Figure 6.3(d), and bonded with the bottom PDMS layer, using the oxygen plasma. Then, the top PDMS layer was bonded on the other side of the spacer layer with the nano-island substrate to seal the channels. The alignment of the three layers must be taken care of to match the outlet and the microchannels. The fabricated two-level microfluidic device is then used for biosensing experiments. An intermediate channel can be introduced multiple times to obtain a multi-level microfluidic device.

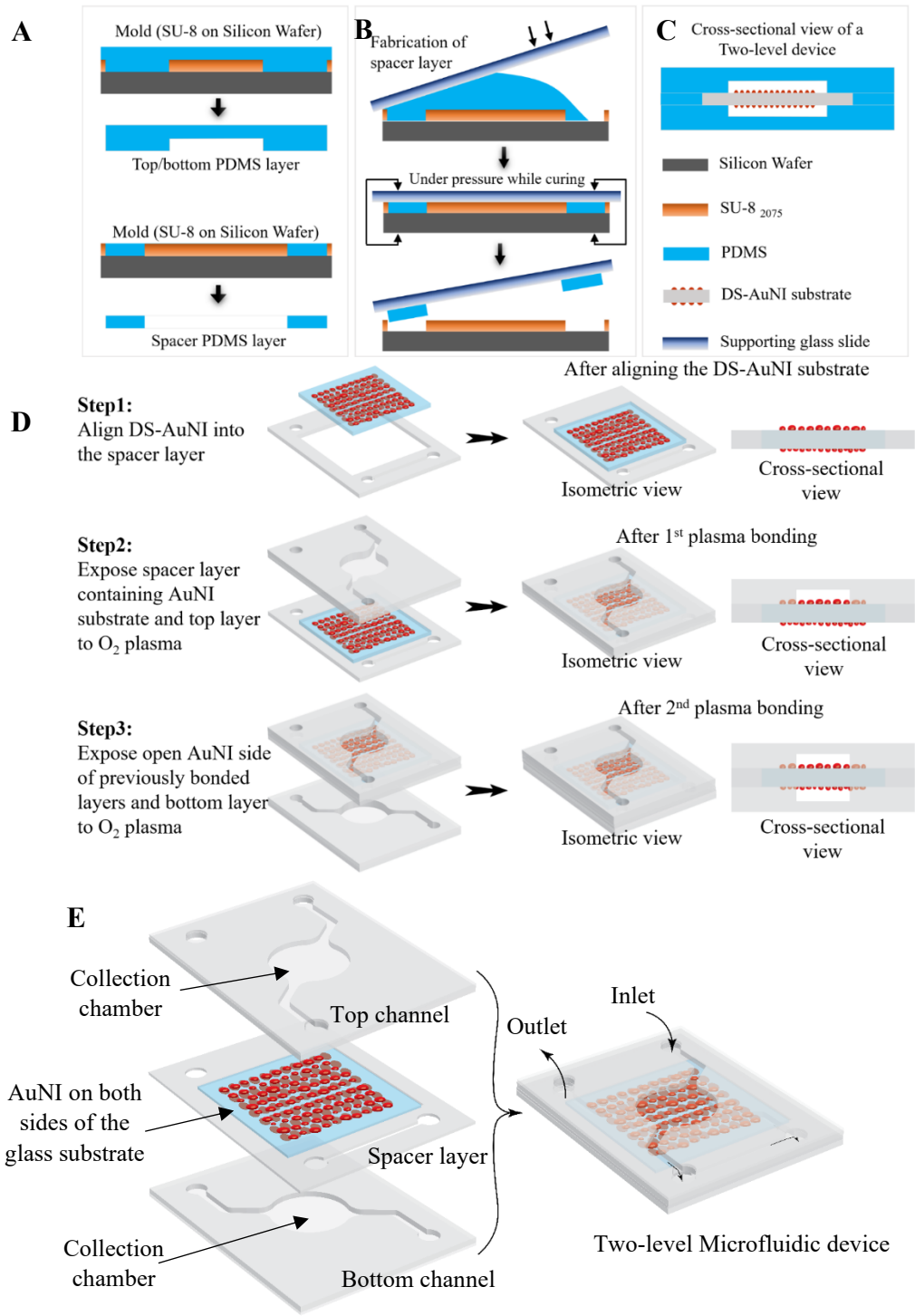

Figure 6.3: Fabrication process of the two-level microfluidic device; (a) SU8 molds used for fabrication of top/bottom and spacer layer (b) PDMS fabrication process to make the spacer layer (150 µm thick) (c) Schematic of the two-level microfluidic device (cross-section view) showing how the PDMS layers are aligned to form the device (d) Steps involved in fabrication (e) Exploded view of the two-level microfluidic device

6.4. Results and Discussion

As discussed in the experimental section, the substrate with the gold nanoislands undergoes the process of heat treatment twice. The substrate is first heat-treated at 560°C for an hour when the nanoparticles are deposited on one side and it is heat-treated again at 560°C for another one hour when the nanoparticles are deposited on the other side. So, the morphology and the physical characteristics of the nanoislands deposited first are expected to be slightly different from that of the second deposition because of the two hours of heat treatment. Therefore, the gold nanoislands heat-treated for two hours were characterized by SEM as shown in Figure 6.4(a).

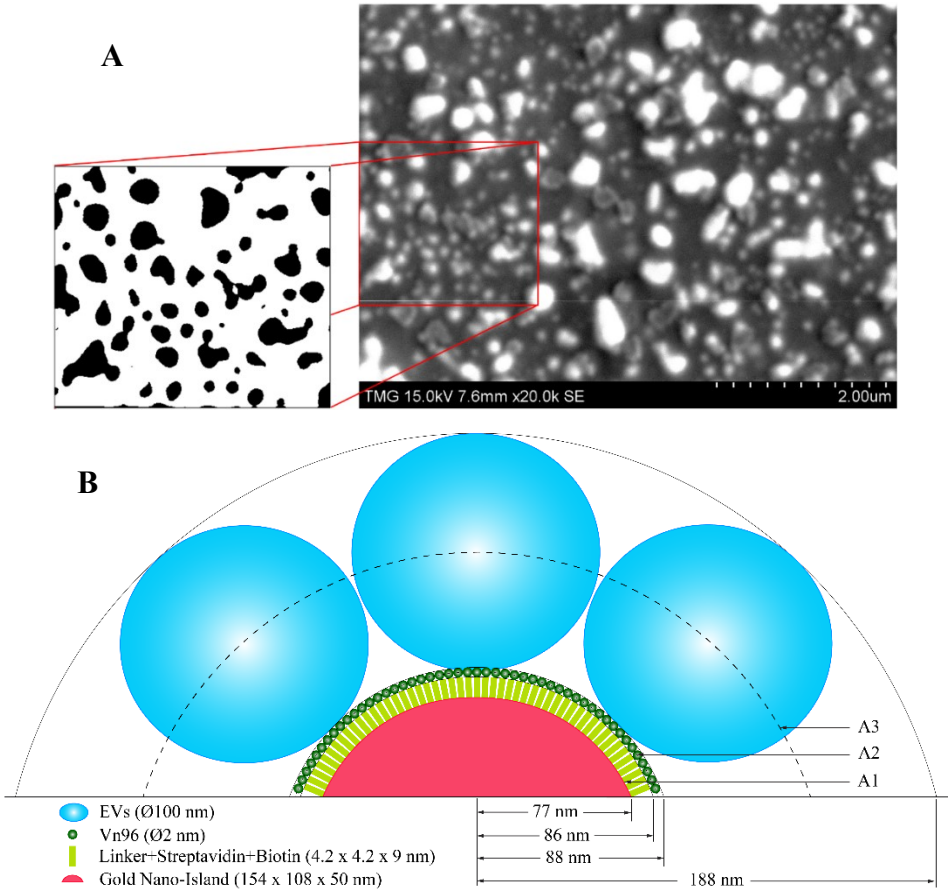

Figure 6.4: Morphology of heat-treated gold nanoislands and its physical modeling (a) SEM image of the gold nanoislands (heat-treated at 560°C for 2 hours) and its binary image (b) Schematic of a cross-section view of a nanoisland immobilized with bio-entity layers involved in the detection of EVs captured by Vn96 molecules

As presented in our earlier paper [181], to determine the dimensions and the surface density of the nanoislands, the SEM image is analyzed using the ImageJ analysis software (Wayne Rasband, NIH, USA). An area of 2.1 µm x 1.8 µm with 35 nano-islands is considered for the analysis. The nano-islands were analyzed, and the average length and width were measured, and the average inter-island distances were calculated using the center-to-center distance between the nearest neighbor islands. Table 6.2 summarizes the average values of major and minor axes of gold nanoislands, aspect ratios, inter-island distances, and surface density.

Table 6.2: Average physical characteristics of the gold nanoislands deposited by thermal convection and whose morphology was tuned by heat treatment for an hour and 2 hours

	1-hr heat treatment [181]	**2-hrs heat treatment**
Length (nm)	198.89	153.64
Width (nm)	146.67	107.59
Aspect ratio	1.37	1.42
Inter-particle distance (nm)	342.5	258.6
Surface density (nanoislands/µm^2)	3	9

Table 6.3: Surface area of a single nano-island and the maximal number of ligands it can accommodate when the morphology was tuned by heat treatment for 1 hour and 2 hours

	Streptavidin		**Biotin-PEG-Vn96**		**EVs**	
	Surface area of nano-island (A1)	No. of ligands	Surface area for Vn96 (A2)	No. of Vn96	Surface area for EVs (A3)	No. of EVs
1-hr heat treatment [181]	3.48 x10^4 nm^2	1976	4.49 x10^4 nm^2	12810	1.16 x10^5 nm^2	9
2-hrs heat treatment	2.26 x10^4 nm^2	1283	3.08 x10^4 nm^2	8787	9.23 x10^4 nm^2	6

The results obtained from the particle analysis of two-hour heat-treated gold nanoislands clearly shows that the size and inter-particle distance of the nanoislands have been reduced due to the increase in the time of heat treatment, resulting in increase in the surface density from 3 to 9 nanoislands/µm^2. In order to obtain the number of bio-entities each nano-island can accommodate, a similar physical model presented in [181], as shown in Figure 6.4(b), is built based on the quantitative analysis of the nanoisland with their average size and the surface density. Table 6.3

summarizes the surface area of a single nanoisland and the ligands it can accommodate and also the subsequent surface area when functionalized with different bio-entities and the number of bio-entities it can accommodate. When the average size of EVs is considered as 100nm, the analysis shows that the nanoislands heat-treated for 1 hour can accommodate 9 EVs/nanoisland whereas the 2 hours heat treated can accommodate 6 EVs. But because of their surface densities, it can be clearly understood that the 1-hour heat treated can accommodate only 27 EVs whereas the 2-hours heat-treated platform can accommodate 54 EVs/μm^2. As mentioned earlier, in this device, the nanoislands deposited on the substrate were heat-treated for 2 hours on the first deposited side while the second side for an hour. With this analysis, it is clear that the number of EVs that can be accommodated per μm^2 have been doubled on 2-hour heat-treated side of the substrate. Therefore, the number of molecular interactions on the 2-hour heat-treated gold nano-islands are expected to increase, resulting in the amplification of the overall detection sensitivity.

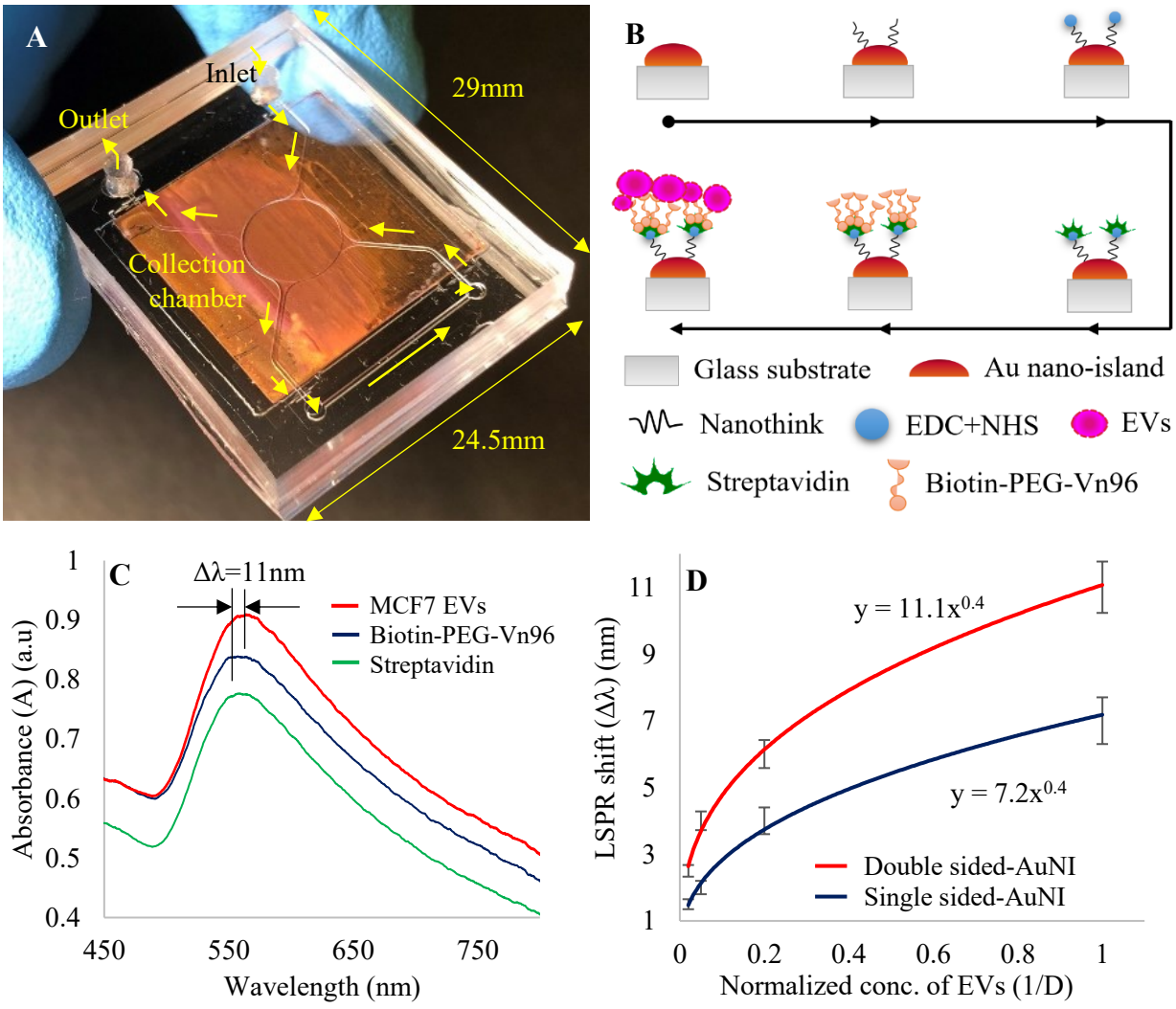

Figure 6.5: The biosensing protocol using the fabricated device and spectral measurements (a) Fabricated two-level microfluidic device (b) Schematic of biosensing protocol (c) the LSPR spectra corresponding to the last three stages of the protocol where the concentration of EVs is undiluted (d) Comparison of LSPR shifts corresponding to various concentrations of EVs from the microfluidic devices, having gold nano-islands on one side and both the sides (D is the dilution factor: 50x, 20x, 5x and undiluted) (n=5)

A biosensing protocol, where various biochemical entities are flown into the fabricated device, to functionalize the gold nanoislands to bind Vn96 to capture EVs. Specifically, the first step in any LSPR experiment is to measure the absorption spectrum of gold nano-islands in the collection chamber. Then, a NanoThinks11 solution is infused into the device at a flow rate of 10 µl/min continuously for 10 minutes, and the spectrum is measured after incubation of 30 minutes to observe the shift ($\Delta\lambda$) in the LSPR peak. A positive shift in the spectrum confirms the molecular binding with the gold nano-islands. Then, the EDC+NHS mixture is passed at the same flow rate, and the spectrum is measured after incubation. The same procedure is repeated with the streptavidin, biotin-PEG-Vn96, and then EVs. With the adopted procedure, a shift in the peak of the Au LSPR is observed at every stage, confirming the molecular binding of each compound. The fabricated two-stage microfluidic device and the schematic of the biosensing protocol are shown in Figure 6.5(a, b).

The concentration of all the entities in the biosensing protocol were maintained same for all the experiments, except for the EVs. The MCF7 EVs were diluted using PBS into various dilutions such as 50x, 20x, 5x, and undiluted were infused into the device and the LSPR shift was measured. The absorption spectrum was measured at all the stages and the Au LSPR spectra corresponding to streptavidin, biotin-PEG-Vn96, and undiluted EVs are shown in Figure 6.5(c). Only the shift due to the final capture step is considered for detection purposes. This spectrum clearly shows that the shift ($\Delta\lambda$) corresponding to the interaction of biotin-PEG-Vn96 and undiluted EVs is around 11nm, which is quite high compared to the single-sided gold nanoisland based microfluidic device. Similarly, other dilutions of EVs were flown through the microfluidic devices and the absorption spectrum was measured for each case to measure the LSPR shift. The LSPR shifts corresponding to various concentrations of EVs from the microfluidic devices having gold nano-islands on one side and both the sides of the substrate are shown in Figure 6.5(d). From

the plot, it can be clearly seen that the detection sensitivity of the double-sided gold nanoisland based microfluidic device has been increased by 1.54 times compared with that of a single-sided gold nanoisland based microfluidic device. This increase in the sensitivity of detection can be attributed to the two-hour heat treatment of gold nanoparticles on one side of the substrate utilized in the device. Thus, the physical modeling of the two-hour heat-treated gold nanoislands validates the increase in the sensitivity of detection.

6.5. Conclusions

A multi-level microfluidic device for the detection of Extracellular Vesicles is presented. The detection is based on the sensitivity of the LSPR property of gold nano-islands to any change in the surrounding environment. The optimized biosensing protocol is carried out in the microfluidic device, specifically designed for the isolation and detection of EVs. The detection of EVs is possible because of the presence of Vn96 functionalized gold nano-islands in the collection chamber. Vn96 has a high affinity towards the heat shock proteins present on the surface of EVs. This label-free technique is promising for the detection of EVs by the immuno-affinity approach using the Vn96 polypeptide. The absorption spectra shows that the EVs have been enriched and isolated in the collection chamber. The results indicate that the detection sensitivity of the two-level microfluidic device has increased by 1.54 times when compared with the microfluidic device having a single-sided gold nano-island substrate as a sensing element. Thus, this technique can be used to build a multi-level microfluidic device by integrating the intermediate channel for the isolation and sensitive detection of EVs for point of care application.

The proposed two-level microfluidic device has shown that the sensitivity of the detection can be increased by integrating double sided gold nano-island substrate in the device and a possibility to build a multi-level microfluidic device. In order to further improve the sensitivity, instead of gold nano-islands, the gold nanoparticles suspended in a colloidal solution can directly be used, by which the entire surface area of the particle can be utilized to capture and isolate EVs or any other biomolecules. So, the next chapter (Chapter 7) discusses methods for capture, isolation, detection, and quantification of biomolecules based on metal nanoparticles suspended in a colloidal solution.

Chapter 7

Methods for Detecting, Isolation and Quantifying an Analyte in a Sample Based on Colloidal Suspension of Plasmonic Metal Nanoparticles

This chapter is reproduced from the patent filed in September 2020 - US provisional (63,084,960)

7.1. Introduction

The colloidal gold was first obtained by Chinese, Arabian and Indian scientists as early as in the V-IV centuries B.C. This first data can be found in their writings, where they used it for medicinal purposes. During the middle ages, colloidal gold was used in alchemist laboratories in Europe. The first book on colloidal gold was published by the philosopher and Doctor of Medicine Francisco Antonii in the year of 1618 [80]. Earlier, colloidal gold was obtained by reducing the gold chloride by vegetable extracts in alcohols or oils. Later, Turkevich *et al.* developed a method for preparation of gold nanoparticles (AuNPs) by treating the hydrogen tetrachloroaurate ($HAuCl_4$) with citrate acid in boiling water [158]. Citrate acts as reducing and stabilizing agent. Gold nanoparticles have unique properties and multiple surface functionalities. Due to these properties, they have been widely employed in bio-nanotechnology for diagnostics and are used in the area of therapeutics. The versatility of gold nanoparticles made them important components for biomedical applications. The functionalized AuNPs with controlled geometrical and optical properties are the current intensive studies and the subject of biomedical applications. These applications include biosensors, immunoassays, clinical chemistry, laser phototherapy of cancer cells and tumors, the targeted delivery of drugs, DNA, and antigens, optical bioimaging and the monitoring of cells and tissues.

Extracellular vesicles (EVs), known also as shedding vesicles or oncosomes, are vital sources of biomarkers for cancer, other pathological conditions such as inflammatory and neurodegenerative diseases, and for clinical diagnostics. They are membrane bounded nano-scale extracellular communication organelles that are released from almost all cell types to the extra cellular space, transporting the identity of their mother cells. These vesicles transport cargoes of

proteins and genetic information, from the parent cells to the recipient ones. They are present in all biological fluids, including urine, blood, ascites, and cerebrospinal fluid fractions of body fluids such as serum and plasma, as well as in cultured medium of cells. Exosomes are type EVs, which are cup-shaped and their diameter ranges from 30 nm to 100 nm, which is about hundred times smaller than the smallest cell [5, 6, 37-39]. Generally, they are released by inward budding of endosome membranes, followed by splitting of plasma membrane through the endocytic pathway. Exosomes carry membrane proteins and heat shock proteins such as HSP70. Thus, EVs are potential sources for liquid biopsy, a remote and minimally invasive technique for early-stage diagnosis of cancer and other diseases. Given the growing evidence that exosomes may be a clinically relevant biomarker source, there is a great demand for their simple and efficient detection in bio-fluids. Most affinity-based methods rely on antibodies directed against EV surface marker(s) [35, 56, 57].

EVs are first discovered by Wolf in 1967 and referred to them as “platelet dust” in plasma as small lipid rich vesicles. From then on, different subtypes of EVs such exosomes and microvesicles have been reported and their biological functions and clinical values have been recognized gradually. Due to their loading capability of some specific proteins and nucleic acids that are closely associated with cancer states, EVs/exosomes have gained a lot of attention and emerged as promising biomarkers of cancer. When compared with circulating tumor cells (CTCs) and cell-free circulating tumor DNA (ctDNA), EVs/exosomes have lot of advantages in terms of stability, quantity and most importantly accessibility. That is, EVs/exosomes are abundantly released from cancer cells and are capable of protecting proteins and nucleic acids that are related to cancer development. In addition, they are very accessible because of their broad distribution in body fluids. Because of these merits, EVs/exosomes have gained much more attention in recent years as biomarkers of cancer. Therefore, detection, isolation and characterization of EVs/exosomes and their contents leads to the diagnosis of cancer at an early stage.

Bovine Growth Hormone (BGH) is a natural growth hormone produced by the anterior pituitary glands in mammals, which is also known as *bovine somatotropin* (BST). Recombinant Bovine Somatotropin (rBST) is a synthetic hormone, which is used to increase the milk production in cows. Both the natural and recombinant hormones increase the levels of another hormone known as insulin-like growth factor (IGF-1) which stimulates the cow’s milk production. The biological

effects of rbST are associated with growth development and reproductive functions. The use of rbST is controversial because of its potential effects on animal and human health [126, 199].

The most widely used methods to separate EVs/exosomes were ultracentrifugation, density gradient centrifugation, size exclusion chromatography, and immune based separation and the characterization techniques were electron microscopy, nanoparticle tracking analysis, flow cytometry and western blotting. In recent years, researchers have developed novel isolation and detection methods by taking the advantages of nanomaterials, biomolecule probes, microfluidics, optics, surface plasmon resonance and so on. While the methods for estimation of bST concentration were either radioimmunoassay (RIA) or enzyme-linked immunosorbent assay (ELISA) or bioassay. Recently, a method based on liquid chromatography-mass spectrometry combined with electrospray ionization has been developed, which allows the discrimination of recombinant from the endogenous forms of somatotropin. Later on, a surface plasmon resonance (SPR) biosensing method has been suggested.

Presently, the standard method for isolation of EVs from the body fluids is differential ultracentrifugation, based on their physical characteristics. This is usually followed by ELISA (enzyme-linked immunosorbent assay) or western blot. However, both the techniques are time consuming, thus requires large number of exosomes and results in low yield and therefore, not suitable for clinical applications. Thus, due to the natural complexity of body fluids, EVs/exosomes detection, isolation, and characterization is still challenging. For this reason, a versatile platform and an easy-to-use technique is required to detect adequately and selectively, isolate, quantify and characterize EVs/exosomes for clinical applications, which our proposed colloidal platform is capable of doing. And for the detection of bST, the principal drawbacks of liquid chromatography-mass spectrometry combined with electrospray ionization is the complex methodology with very expensive instrumentation, makes it difficult for a rapid detection. And the suggested surface plasmon resonance (SPR) measurement was carried out in Biocore 3000, which is an expensive plasmonic instrument. Therefore, it is extremely important that, a highly sensitive method that allows rapid and precise detection of growth hormones in milk are required to provide meaningful information about the rBST-treated animals to the consumers.

Considering the facts of the EVs/exosomes as biomarkers of cancer and the effects of rbST in the milk, the colloidal platform developed by utilizing the gold nanoparticles, is capable of carrying out multiple sensing mechanisms such as detection and isolation of biomolecules. First

of all, it can selectively and specifically detect and isolate EVs/exosomes from media. And the protocol in this platform can be very well adapted for the detection and isolation of biomolecules such as proteins or hormones. Specifically, the biosensing protocols are developed in such a way that the biomolecules tagged to biotin can be detected by the streptavidin-biotin interactions and the hormones such as bovine growth hormone (BGH) can be detected by the antigen-antibody interactions by binding to the AuNPs in the colloidal solution.

7.2. Materials and Methods

The materials and chemicals used in this invention are Gold (III) chloride trihydrate ($HAuCl_4.3H2O$) and sodium citrate were purchased from Sigma Aldrich. De-ionized (DI) water with a resistivity of 18MΩ, used in all the experiments was obtained by using the NANOpure ultrapure water system (Barnstead). Quartz cuvette purchased from Sigma Aldrich, 11-mercaptoundecanoic acid in ethanol (NanoThinks Acid 11), N-(3-Dimethylaminopropyl)-N′-ethylcarbodiimide hydrochloride (EDC) and N-Hydroxysuccinimide (NHS), Streptavidin was purchased from IBA GmBH and biotin-PEG-Alexa647 purchased from NANOCS. Antibody BGH and the BGH antigen were purchased from Cedarlane labs. Vn96-linker-biotin and MCF7 exosomes were supplied by the Atlantic Cancer Research Institute (ACRI), Moncton, New Brunswick, Canada.

7.2.1. Preparation of gold colloidal solution

Gold (III) Chloride trihydrate ($HAuCl_4.3H_2O$) of 18 to 30mg is added to 95ml of DI water in a beaker and boiled till it reaches its boiling point (around 10minutes). Once the gold precursor solution reaches its boiling point, 5ml of 2% sodium citrate is added, to reduce the gold ions to gold nanoparticles, and the solution is further boiled for about 5 to 8 minutes and the change in color to transparent purple can be clearly observed. When the color is changed, the solution is taken out from hotplate and allowed it to reach room temperature. There will be reduction in the volume due to its boiling time. Therefore, add DI water to make it 100ml as final volume.

7.3. Results and discussion

The colloidal platform is a multi-functional sensing platform which is aimed to enhance the sensitivity of the plasmonic detection of biological entities by utilizing gold nanoparticles in a

colloidal solution. First part of this platform talks about detection of biotin by binding to the streptavidin. The intention of this part is to prove that, any biomolecule that is tagged to biotin can be detected and isolated using the streptavidin-biotin interaction by binding to the gold nanoparticles. The second part deals with the detection hormones by using antigen-antibody interactions by binding to the gold nanoparticles, specifically Bovine Growth Hormone (BGH) was detected, and the last part of the platform is the detection and isolation of exosomes by using Vn96 tagged with biotin. In the process of sensing protocol, when the colloidal solution gets precipitated, the how the isolated supernatant can be used as a biosensor for the early diagnosis of cancer is also discussed.

7.3.1. Detection of biotin using streptavidin-biotin binding

The main aim of this study is to detect and isolate any biomolecules tagged to biotin by utilizing AuNPs from the gold colloidal solution. Here, in this case, Alexa647 fluorophore tagged to biotin using polyethylene glycol (PEG) is used. The following colloidal solution preparation and the biosensing protocol are used to detect biotin.

7.3.1.1. Biosensing protocol

The biosensing protocol is a multilayer deposition on AuNPs by adding different chemical and bio-entities directly into the gold colloidal solution. Here in this case, the gold colloidal solution (GCS) is further diluted with DI water in a quartz cuvette to obtain 0.6A absorbance units measured using Perkin-Elmer UV-Vis spectrometer, which approximately corresponds to a gold concentration of 35µg/mL. First the absorption spectrum of colloidal solution is measured and then the linker (Nanothinks11) is added to the solution, which forms a self-assembled monolayer (SAMs) on the surface of the AuNPs and then after 30 minutes of linker addition, cross-linker (EDC+NHS compound) is added for amidification. Then after cross-linker, streptavidin is added to bind the biotin in the next stage. Absorption spectrum is measured at each stage of the biosensing protocol. A shift in the peak of Localized Surface Plasmon Resonance (LSPR) band is recorded after every stage and the red shift after addition of biotin-PEG-Alexa647 confirms the binding of biotin to the AuNPs in the colloidal solution. Typical absorption spectra of whole biosensing protocol are shown in Figure 7.1(A). When the bio-chemical entities are added to the colloidal

solution, there is a change in the color of the colloidal solution in the cuvettes as shown in Figure 7.1(B-F).

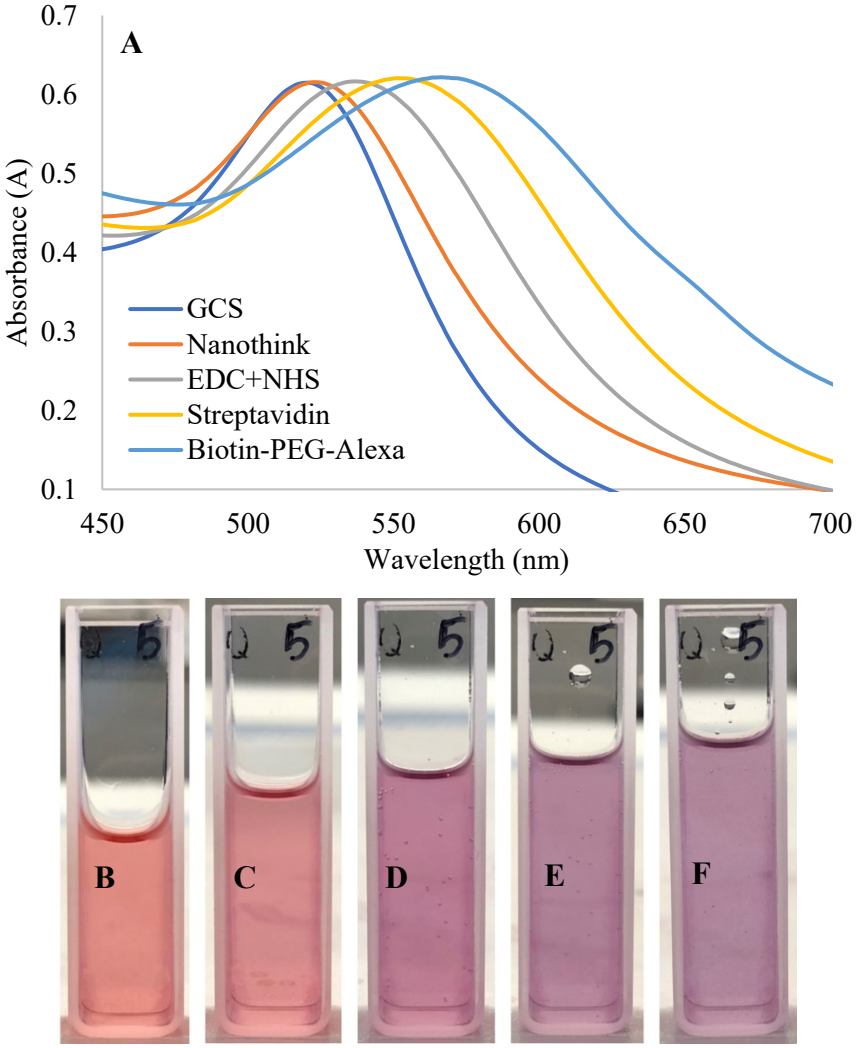

Figure 7.1: Spectral measurements at different stages; (A) Typical absorbance spectra of entities of the protocol; Color of the colloidal solution at various stages; (B) GCS (C) +Nanothink11 (D) +EDC+NHS (E) +Streptavidin (F) +Biotin-PEG-Alexa647

After the whole sensing protocol, shift in LSPR band is calculated at every stage. Table 7.1 shows the concentration of the entities used and the average spectral shift at each step found experimentally by using colloidal platform. The volume of colloidal gold is around 2ml while all the other entities in the sensing protocol are of 0.2ml and incubated for 30 minutes after each stage.

Table 7.1: Shift of the Au plasmon bands corresponding to the different steps of the protocol

Entity	**Concentration**	**LSPR shift (Δλ) (nm)**
Nanothink11	5mM	3.25
EDC+NHS	0.1M+0.05M	12.5
Streptavidin	10 µg/ml	16.25
Biotin-PEG-Alexa647	20 µg/ml	14.25

7.3.1.2. Discussion

Here, colloidal platform for the detection of biotin is proposed by utilizing the AuNPs with the streptavidin-biotin binding. In this case, biotin was detected by the LSPR, and the fluorophore was tagged to the detected biotin through polyethylene glycol (PEG). With the results obtained using the colloidal platform, it can be proposed that any biomolecules tagged biotin can be detected using LSPR and also when biomolecules are tagged with fluorophores, the detected biomolecules can be viewed by a fluorescence microscope.

7.3.2. Detection of Bovine Growth Hormones (BGH)

The main aim of this study is to detect and isolate the bovine growth hormone (BGH) or recombinant bovine growth hormone (rBGH) by antigen-antibody interactions by utilizing AuNPs from the gold colloidal solution. The following biosensing protocol is used to detect and isolate BGH or rBGH.

7.3.2.1. Biosensing protocol

The biosensing protocol is similar to the protocol used in detection of biotin, except the streptavidin-biotin interactions is replaced with the antigen-antibody interactions. The colloidal solution is diluted as mentioned previously and the absorption spectrum is measured at each stage of the protocol. After EDC+NHS stage, instead of streptavidin, the antibody BGH is added to the colloidal solution and the spectrum is measured after incubation. The incubation time required for antibody to react with amine needs to be optimized separately. With the red shift after antibody binding, various concentrations of BGH antigen are added to the colloidal solution and absorption spectrum is measured at different times to see the shift in the spectra. A red shift in the LSPR band of gold after antibody stage confirms the BGH antigen binding to the AuNPs through antibody.

Typical absorption spectra of whole biosensing protocol are shown in Figure 7.2(A). and the color change of the colloidal solution in the cuvette when the biosensing entities are added is shown in Figure 7.2(B-F).

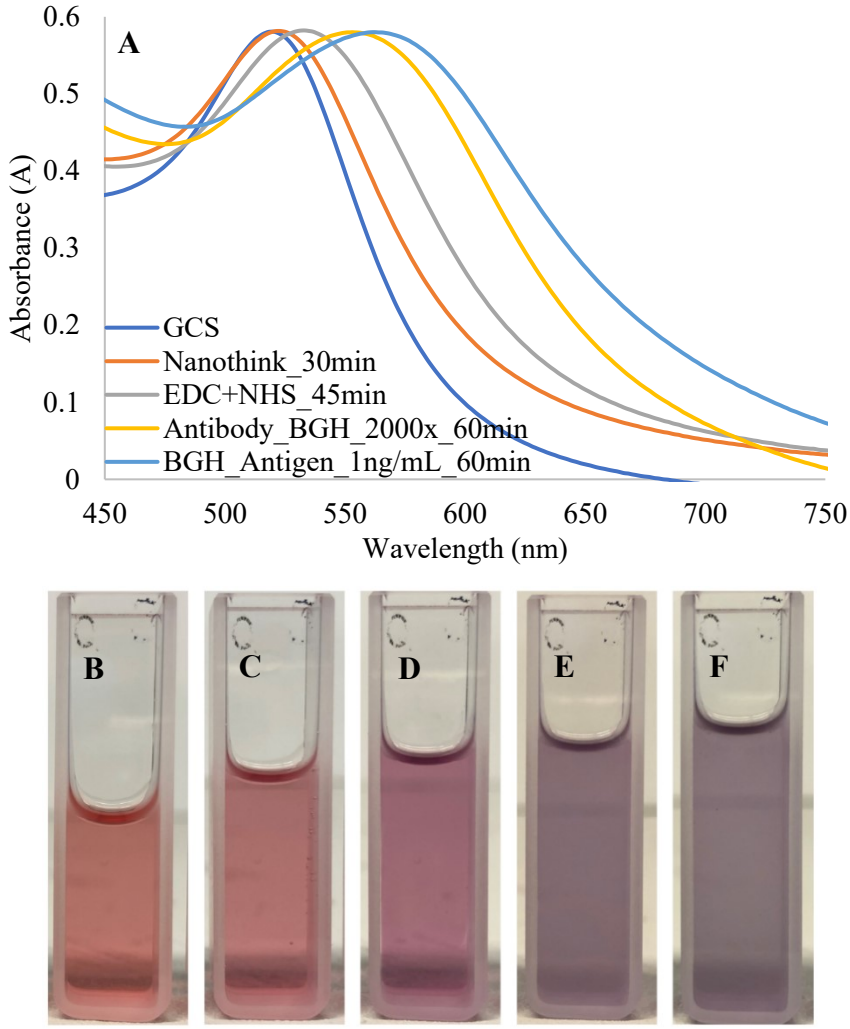

Figure 7.2: Spectral measurements at different stages; (A) Typical absorbance spectra of entities of the protocol; Color of the colloidal solution at various stages; (B) GCS (C) +Nanothink11 (D) +EDC+NHS (E) +Antibody BGH (F) +BGH Antigen (1hr)

After the whole sensing protocol, shift in LSPR band is calculated at every stage. Table 7.2 shows the concentration of the entities used and the average spectral shift at each step found experimentally by using colloidal platform.

Table 7.2: Shift of the Au plasmon bands corresponding to the different steps of the protocol

Entity	Concentration	LSPR shift (Δλ) (nm)
Nanothink_30min	5mM	3
EDC+NHS_45min	0.1M+0.05M	11
Antibody_60min	2000x (dilution)	19.5
Antigen_60min	1 ng/ml	9

7.3.2.2. Optimization of binding time in the protocol

As mentioned in the above section, the incubation time of EDC+NHS and the antibody BGH needs to be optimized such a way that all or maximum molecules are bound to the preceding layer on AuNPs suspended in the colloidal solution. Formation of self-assembled monolayers on AuNPs using 11-mercaptoundecanoic acid (Nanothinks11) with a concentration of 5mM has standard LSPR shift around 4nm within 30 minutes. Therefore, the steps after nanothinks11 need to be optimized. EDC and NHS are added to the colloidal solution to form amine groups by reacting with carboxyl groups on the AuNPs. As the EDC+NHS compound bind to Nanothink, there will be a shift in the gold plasmon band. The absorption spectra were measured at different intervals of incubation time until the LSPR shift saturates, which means the active binding of molecules has stopped. The same procedure is repeated for antibody BGH with the optimized incubation time of EDC+NHS. Figure 7.3 (A, B) shows the change in LSPR shift with respect to incubation time of EDC+NHS and antibody BGH. From the plots it can observed that the binding of EDC+NHS compound is almost saturated after 45 minutes while the antibody BGH is after an hour.

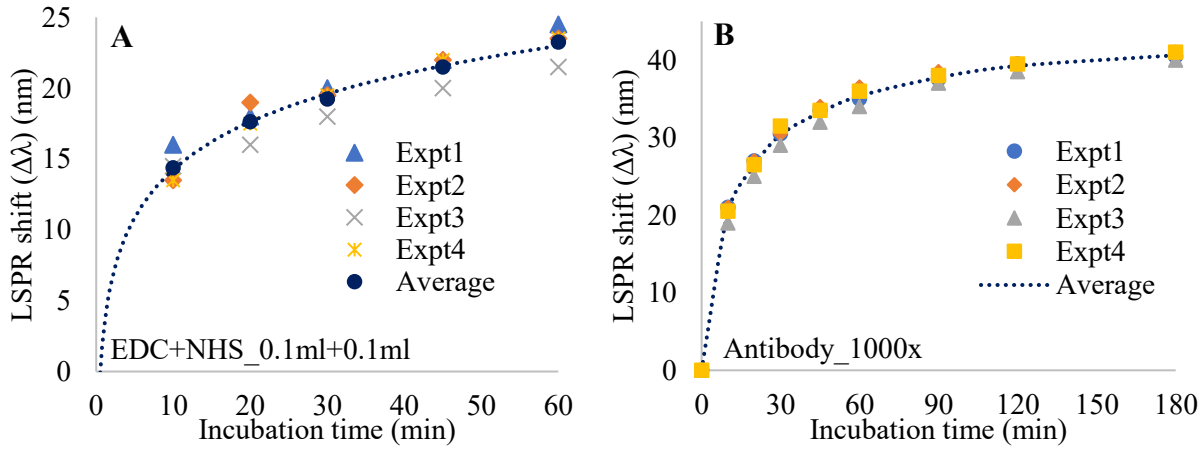

Figure 7.3: Plot of LSPR shift with respect to incubation time in case of (A) EDC+NHS compound and (B) Antibody BGH

7.3.2.3. Discussion

Here, the colloidal platform for the detection of bovine growth hormone is proposed by utilizing the AuNPs with the antigen-antibody interactions. With the optimized concentration and incubation time of EDC+NHS and the antibody BGH, a sensitivity of <0.1ng/mL has been achieved. With above mentioned protocol and results, this platform could be used as a rbST detection kit.

7.3.3. Isolation and detection of EVs

The main aim of this study is to detect and isolate the EVs/exosomes from the MCF7 breast cancer cell line media using a polypeptide, Vn96. This peptide is specifically designed to capture EVs by binding to the heat shock proteins (HSPs) present on surface of them. The biosensing entities required and schematic of the sensing protocol are shown in Figure 7.4.

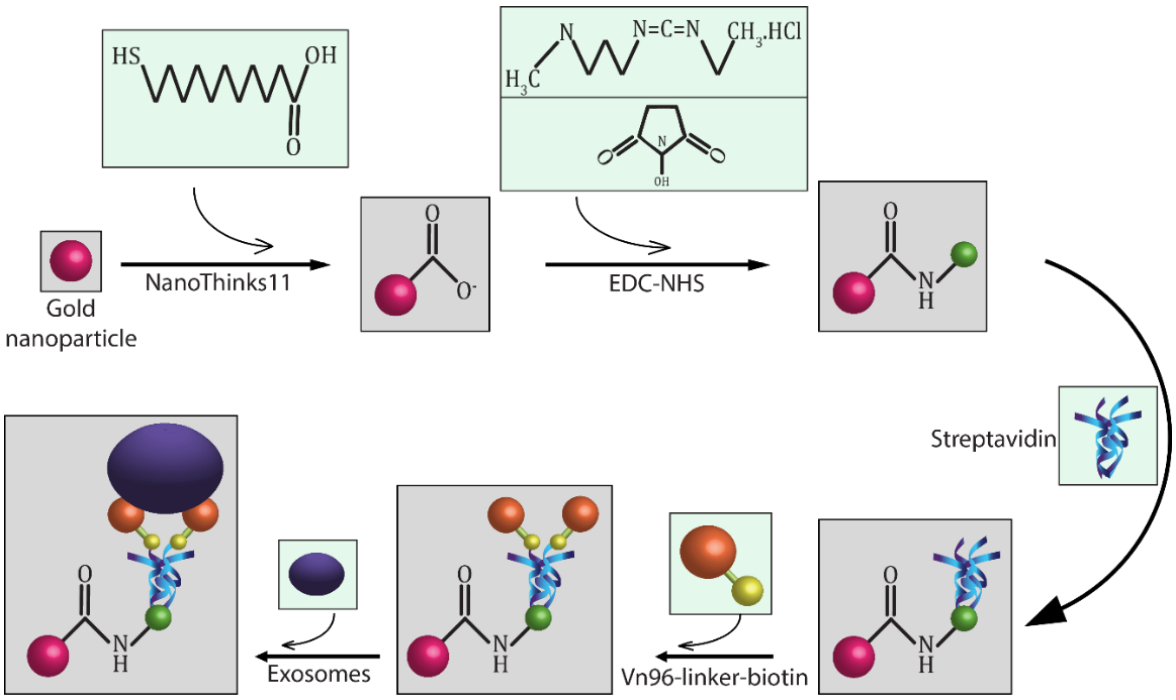

Figure 7.4: Schematic of biosensing protocol for the plasmonic detection of exosomes

7.3.3.1. Biosensing Protocol

In a typical experiment, first, the absorption spectrum of gold nanoparticles in the colloidal solution is measured. Then subsequently, the spectrum is measured after each stage in the protocol

and the exact peak position of the LSPR band is recorded. The shift in the spectra band confirms the binding event. The absorption spectra of whole biosensing protocol are shown in Figure 7.5(A) and Table 7.3 shows the spectral shifts at each stage found experimentally by using colloidal platform along with the spectral shifts observed in case of gold immobilized on a glass substrate [181]. The data show that the extent of the shift of Au LSPR band is almost five times larger for each step when working with the proposed method than the shift found in case of the immobilized gold. As the biosensing protocol involves the addition of a chemical or bio-entities at each stage, the color of the colloidal solution changes at each stage as shown in Figure 7.5(B-G).

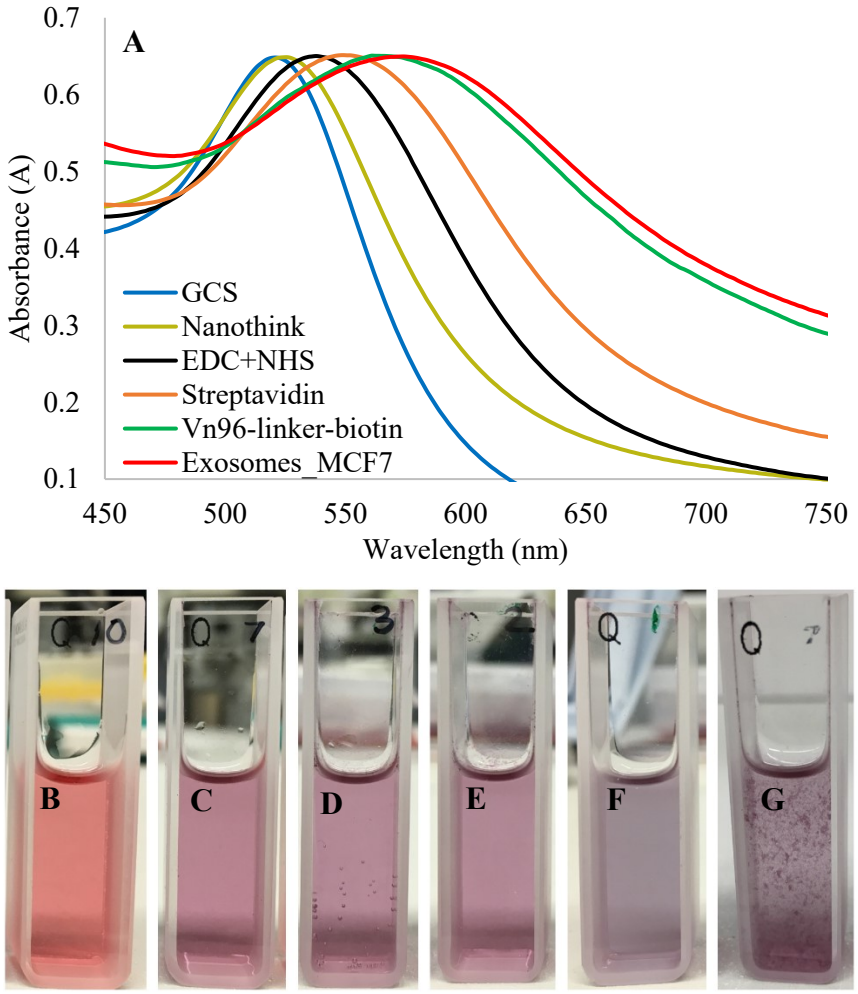

Figure 7.5: Spectral measurements at different stages; (A) Typical absorbance spectra of entities of the protocol; Color of the colloidal solution at various stages; (B) GCS (C) +Nanothink11 (D) +EDC+NHS (E) +Streptavidin (F) +Vn96-linker-biotin (G) +MCF7 EVs (contains the precipitate formed after addition of EVs)

Table 7.3. Shift of the Au plasmon bands corresponding to the different steps of the protocol

Entity	Original Concentration	Optimized Concentration	Δλ (nm) (Gold on Glass)	Δλ (nm) (Colloidal Platform)
11-MUA*		5mM	5 ± 0.5	4.62 ± 0.3
EDC + NHS		0.1M + 0.05M	4.82 ± 0.3	12.43 ± 1.5
Streptavidin	1mg/mL	10µg/mL	3.08 ± 1	17.82 ± 4
Vn96-linker-biotin	1.3mg/mL	13 µg/mL	5.67 ± 1.5	17.6 ± 3
MCF7 EVs	$1.19x10^{12}$/mL	$2.38x10^{11}$/mL	4 ± 1	7.25 ± 2

*11-Mercaptoundecanoic acid

7.3.3.2. Role of gold nanoparticles

To understand the role of gold nanoparticles, two experiments were performed using the same biosensing protocol discussed above. First one is the same with gold colloidal solution while the other experiment where gold colloidal solution is replaced with the DI water (DIW) and rest of the protocol remains same. After finishing the biosensing protocol, sedimentation of MCF7 EVs was observed in both the cases. When the precipitant got settled down, the supernatant was isolated, and absorption spectrum was measured. The measured spectra showed a peak around 263 nm, which is essentially a peak of a protein and also a peak around 560nm in the spectrum of supernatant from GCS. The absorption spectra of supernatant collected from gold colloidal solution and DI water are shown in Figure 7.6(A). After the isolation of supernatant, the precipitate was collected using a pipette and spread on a glass slide as shown in Figure 7.6(B, C) to measure their absorption spectrum. Figure 7.6(D) shows the absorption spectrum of the precipitate from GCS and DI water. The spectra show two peaks, one around 232nm, a protein peak and the other one is around 560nm, a gold peak.

From the experiments carried out using the gold colloidal solution and the DI water, it has been understood that the role of gold nanoparticles is very critical, and the results show that the presence of gold nanoparticles is mandatory. The major advantages of having the gold nanoparticles can be listed out as the concentration or the amount of gold required to capture the biomolecules can be tuned, the captured biomolecules can be completely isolated from the nanoparticles, and the isolation of exosomes/biomolecules is faster.

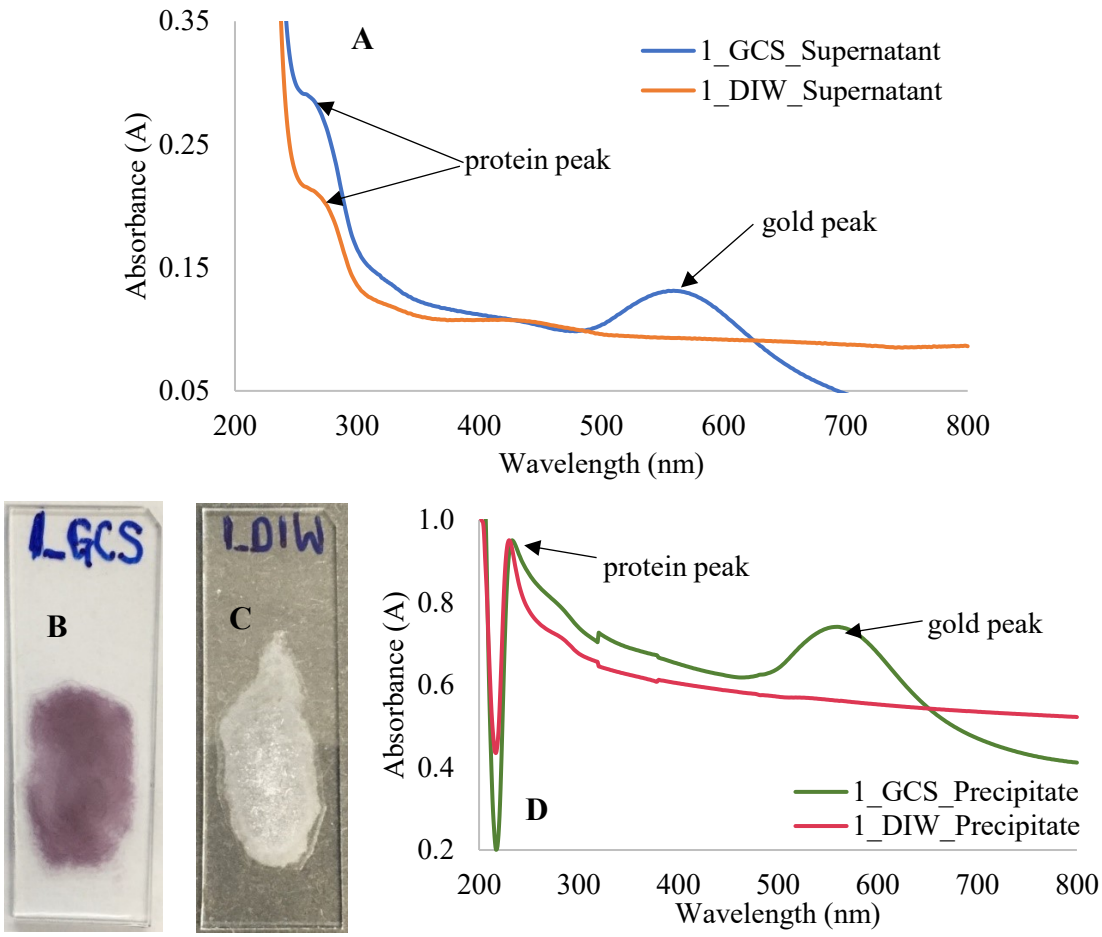

Figure 7.6: Spectra measurements; (A) Absorption spectra of supernatant collected from GCS and DI Water; Precipitate and their absorption spectra (B) Precipitate from GCS dried on a glass slide (C) Precipitate from DI Water dried on a glass slide (D) Absorption spectrum of precipitate from GCS and DIW

7.3.3.3. Concentration of gold can be tuned as required

Gold (III) Chloride trihydrate ($HAuCl_4.3H_2O$) is a gold precursor used to prepare the gold colloidal solution. The nanoparticles in the colloidal solution will be the most important component of the biosensing protocol. The concentration of gold in the colloidal solution can be tuned depending on requirement of sensing. The gold precursor of 18mg, 23mg, and 30mg are used to prepare the gold colloidal solution with sodium citrate of 2% concentration. By varying the concentration of gold, the number of interactions between the gold nanoparticles and the biomolecules can be controlled. Figure 7.7(A) shows the absorption spectra corresponding to the colloidal solution prepared using 18mg, 23mg and 30mg of gold precursor.

A relation has been established between the absorbance units and the concentration of gold present in the colloidal solution using the initial amount of gold precursor, its molecular weight, and the atomic mass of gold is as shown in Figure 7.7(B). The following formulae was used to find the concentration of gold present in the colloidal solution.

$$\text{Concentration of gold} = \frac{\text{atomic mass of gold alone}}{\text{molecular weight}} \times \frac{\text{amount of precursor}}{\text{final volume of colloidal solution}} \quad (3)$$

As the amount of gold is varied in the preparation of colloidal solution, the absorbance value of gold in colloidal solution have changed accordingly. The as-prepared colloidal solution in each case is diluted with DI water to get the equal absorbance value. The plot shows that when the absorbance is maintained at almost same value, the amount of gold present in the solution is almost same. So, depending on the number of biomolecules to be isolated and detected, the concentration of gold in the colloidal solution can be tuned.

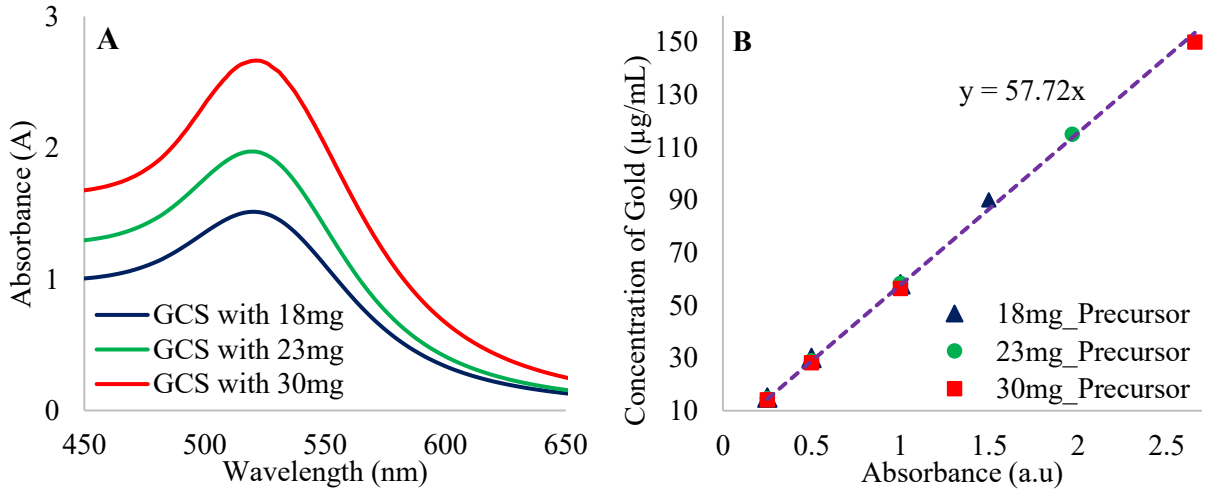

Figure 7.7: Gold colloidal solution and absorption spectra (A) Absorption spectra corresponding to 18mg, 23mg and 30mg of gold precursor; (E) Relation between the absorbance units and the concentration of gold in the colloidal solution

The colloidal solution prepared using 23mg is diluted to have the absorbance values of 1.0, 0.5 and 0.25. The adapted biosensing protocol was carried out using these each colloidal solution with an absorbance value of around 1.0, 0.5 and 0.25 for the capture and isolation of MCF7 EVs. When the whole sensing protocol is completed, the solutions in the cuvettes were untouched until the entire precipitate got settled down, which took 4 hrs approximately. As the concentration of EVs is maintained same while the concentration of gold is different, the excess gold that is not bound with any EVs in each of the case is expected to stay in the supernatant. To check the

presence of gold, the supernatant was isolated from the cuvette when the precipitate got settled down and its absorption spectrum was measured. The measured absorption spectra are shown in Figure 7.8(A) and it show peaks around 265nm and 570nm in each case. The first one corresponds to a protein peak which may belong to any unbound exosomes or to any other protein or molecule having a similar absorption peak and the later one corresponds to the gold nanoparticles. It can be observed from the spectra that the peak of gold has decreased compared to their initial absorbance value meaning, the excess AuNPs or nanoparticles that did not bind with EVs are still suspended in the supernatant. Also, the peak in the spectrum corresponding to 0.25A is almost flat compared to that of 1.0A spectrum meaning, for the concentration of EVs used, the amount of gold in the colloidal solution that is required to isolate all or most of EVs corresponds to an absorbance of less than 0.25A.

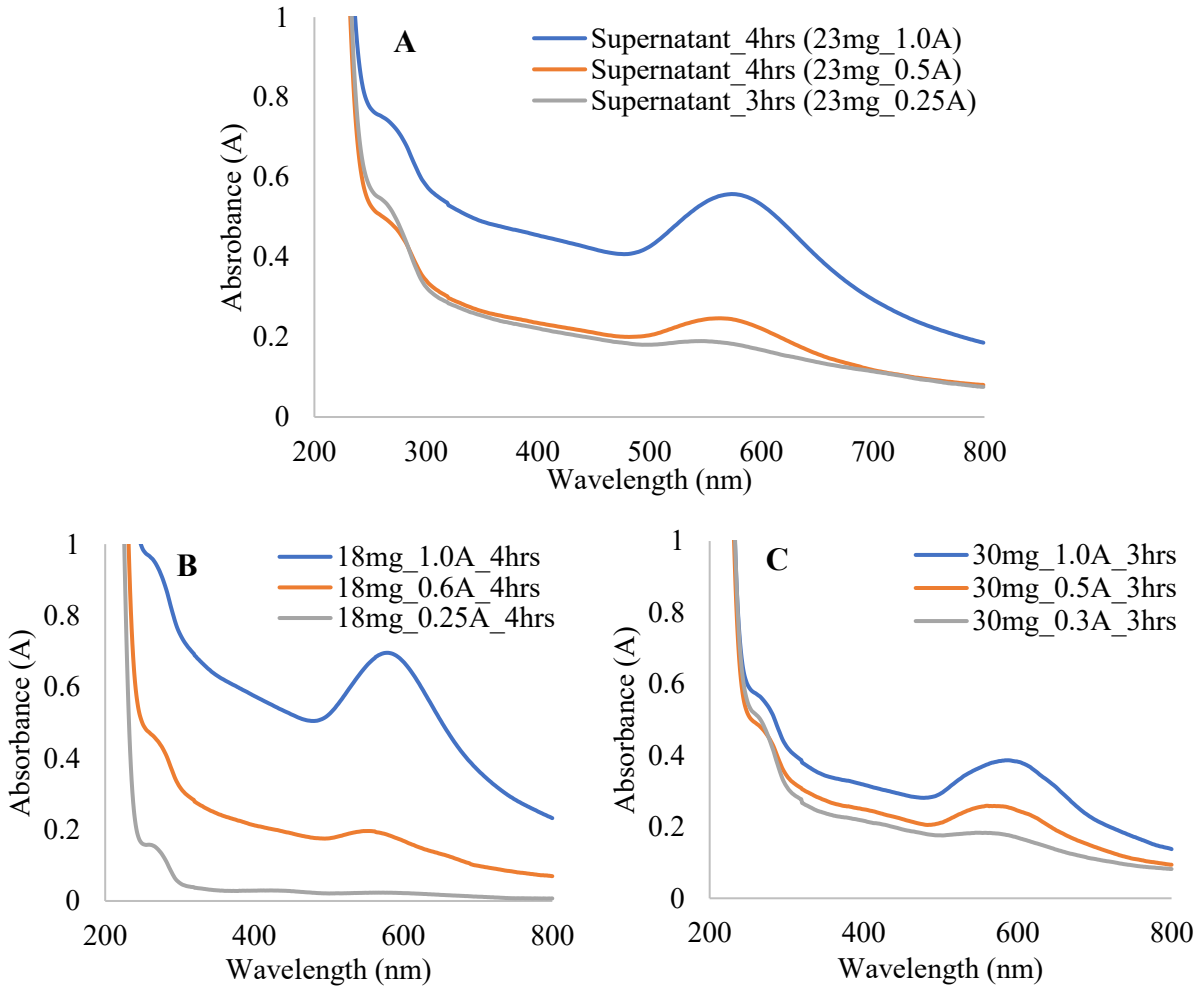

Figure 7.8: Absorption spectra of supernatant from colloidal solution prepared using; (A) 23mg of gold precursor (B) 18mg of gold precursor (C) 30mg of gold precursor

To validate and to see the repeatability, same experiments were carried out using the gold colloidal solution prepared using 18mg and 30mg with the absorbance values around 1.0, 0.5, and 0.25A. The experiments have confirmed that the capture and isolation of EVs can be altered by tuning the concentration of gold nanoparticles suspended in the colloidal solution as shown spectra in Figure 7.8(B, C). From these results, it can be realized that, depending on the condition of the tumor, the concentration of gold required for the isolation and detection of EVs can be adjusted.

7.3.3.4. Complete isolation of EVs/biomolecules

The number of molecular interactions depends on the concentration of gold present in the solution and the number of EVs available. In an ideal situation, if the number of molecular interactions takes place in such a way that all the gold and the EVs are bound to one another and settled down as a precipitate, then there will not be any EVs or gold left in the supernatant giving an absorption spectrum equivalent to that of water. Previously, when the supernatant was measured for its absorption spectrum, two peaks have been noticed which may belong to proteins and to gold. The intensity of the gold peak can be adjusted or reduced by considering the right the amount of gold in the precursor solution or by dilution, to bind to the available EVs. But, when the supernatant consisting of protein and gold was centrifuged at 10,000g for 2 minutes, the gold peak disappeared leaving the protein peak almost unchanged. Absorption spectra of the supernatant before and after the centrifugation is shown in Figure 7.9. From the spectra after the centrifugation, it can be concluded that the peak around 265nm may not be due to EVs but of some other protein from the MCF7 CCM. Therefore, when the right concentration of gold is considered, all the exosomes can be isolated.

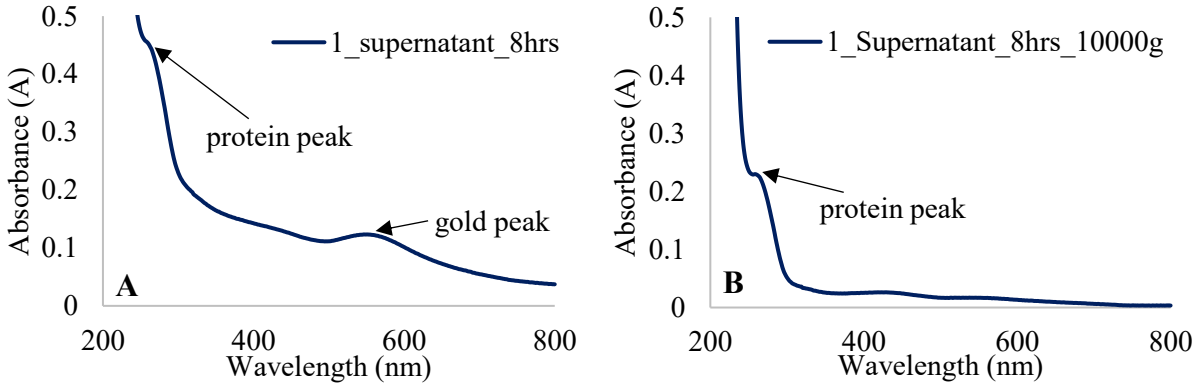

Figure 7.9: Absorption spectra of supernatant (A) after 8 hours of complete biosensing protocol (B) after centrifugation at 10000g for 2 minutes

7.3.3.5. Faster isolation of EVs

As mentioned, the adapted biosensing protocol was carried out using gold colloidal solution and DI water. The sedimentation in case of GCS and DIW at various intervals of time is shown in Figure 7.10(A, B) when the MCF7 EVs were added. The Figure clearly shows that the precipitate in GCS got settled in 2 hrs whereas in DI water, its floating even after 6 hrs of protocol. Therefore, the key advantage of using gold nanoparticles is that when the EVs are added, the gold result in a faster sedimentation compared to DI water.

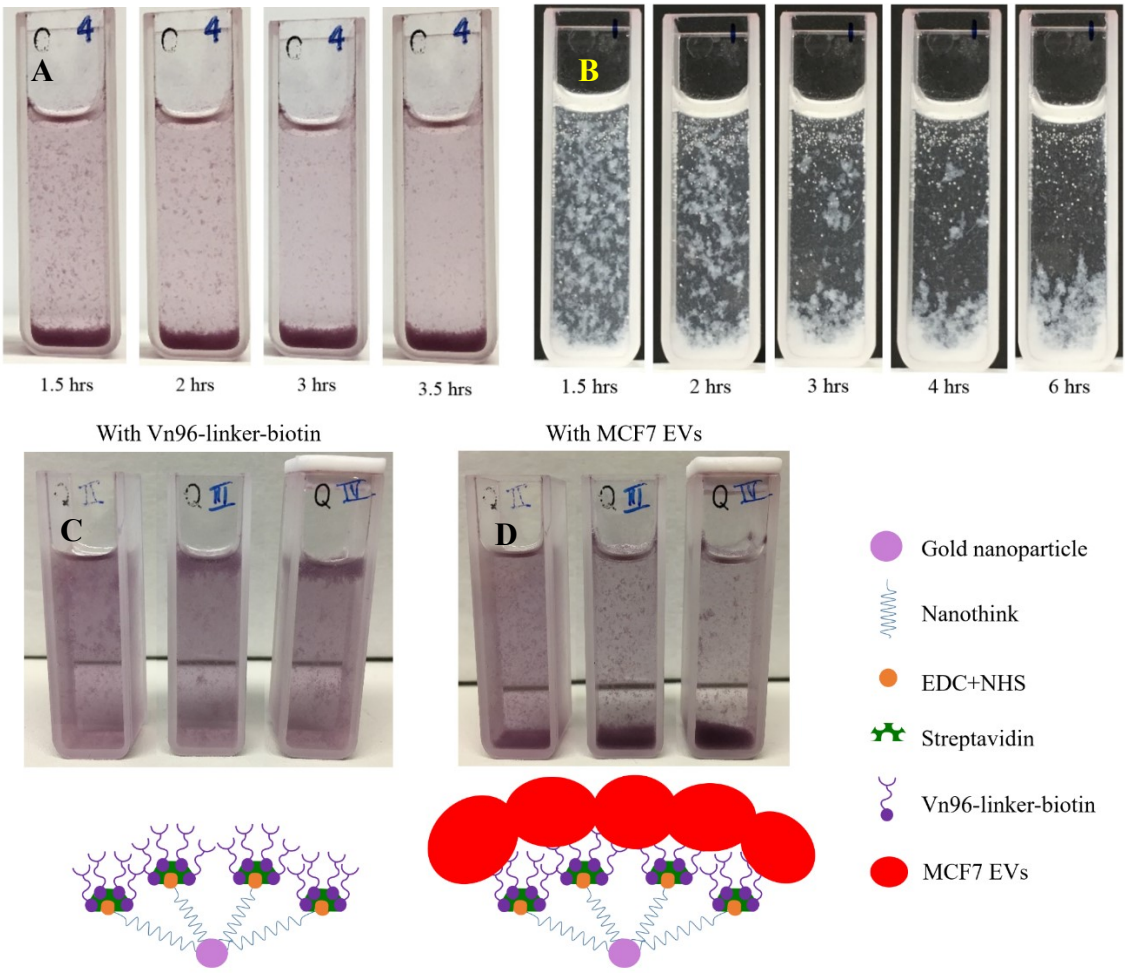

Figure 7.10: Sedimentation of MCF7 EVs (A) In GCS (B) In DI water (C) Colloidal solution after addition of Vn96 and corresponding schematic below (D) Colloidal solution after addition of EVs and corresponding schematic below

Sedimentation is the process of allowing particles suspended in a liquid to settle under the effect of gravity. There are two different types of sedimentation processes: Discrete settling and flocculent settling. Discrete settling happens with inert particles such as sand grains when the flocculation process is finished. The shape, size and weight of particles do not change anymore. In flocculent settling, particles clog together during the settling process, forming bigger flocs that settle faster. This process can be stimulated by a coagulant. With increasing time and depth, the frequency distribution of the settling velocities will change with flocculant settling. Flocculation is the process in which colloids come out of suspension in the form of floc or flakes, either spontaneously, or due to the addition of a clarifying agent. Colloidal solution is a mixture in which one substance of microscopically dispersed insoluble particles are suspended throughout another substance. Sometimes the dispersed substance alone is called the colloid.

Here, the gold nanoparticles are suspended in the colloidal solution and when Vn96-linker-biotin was added as per the biosensing protocol after the streptavidin stage, flocculation was observed, but floating on top of the liquid. This can be due to the low self-weight when Vn96 molecules bound to the streptavidin through the biotin. The size of EVs range from 30nm to 1000nm which are huge compared to gold nanoparticles. So, when EVs were added to the solution, there was a noticeable circular movement of colloids in the solution and the flacons gradually settling at the bottom of the liquid. Pictures of solutions at Vn96 stage and after addition of MCF7 EVs illustrated with the schematics are shown in Figure 7.10(C, D).

7.3.3.6. Supernatant as a biosensor

The diameter of gold nanoparticles can be modified based on the citrate method of synthesis of gold nanoparticles. As discussed in section 3.3.4 of physical modeling, the number of EVs that can be captured or accommodated on each nanoparticle depends on the surface area of that nanoparticle. Considering the same relation between the diameter of gold nanoparticle and the concentration of gold as shown in Figure 7.11, how supernatant could be used as a biosensor is shown below. As discussed earlier, the area between the cancerous (EVs-undiluted) and the non-cancerous condition (EVs-50x diluted) [43] could be used for the early diagnosis of cancer.

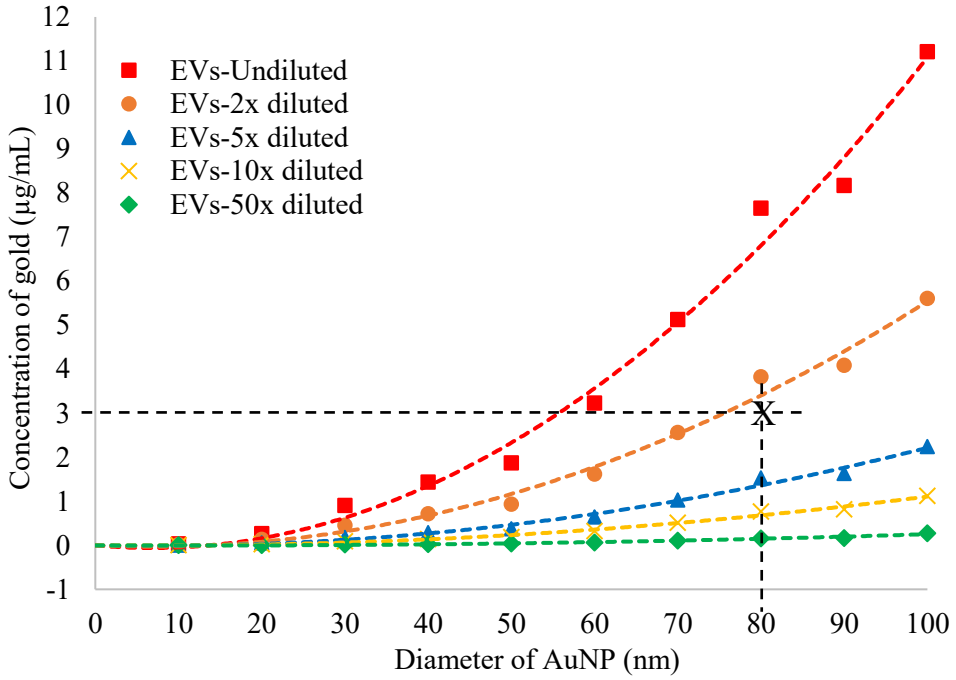

Figure 7.11: Relation between diameter of an AuNP and the concentration of gold required to capture EVs in cancerous (undiluted EVs) and non-cancerous condition (EVs diluted by 50x)

For instance, consider the gold colloidal solution with nanoparticles of 80nm diameter with gold concentration of 3µg/mL (point 'X' marked in the plot) for the isolation and detection of EVs with the adopted protocol using the proposed bio-entities. Once the precipitate gets settle down after addition of EVs, the supernatant could be isolated and measured for its absorption spectrum. The cancer condition could be determined by analyzing the presence of gold peak or a strong protein peak in the measured spectrum of supernatant. If it is a gold peak, which means all the EVs got captured and settled down along with the precipitate showing a non-cancerous condition or if it is a strong protein peak without any gold peak, the EVs are much higher than the number of gold nanoparticles can capture showing a cancerous condition. Therefore, the supernatant from the proposed colloidal platform could be used as a biosensor for the early diagnosis of cancer.

7.4. Conclusions

The colloidal platform for detection and isolation of biomolecules such as EVs, proteins, and/or growth hormones utilizing the gold nanoparticles in a colloidal solution. More significantly, a biosensing protocol is developed and further optimized to detect biomolecules

by using Localized Surface Plasmon Resonance (LSPR) detection technique. In this platform, the sedimentation method is used to isolate EVs/exosomes/biomolecules by binding them to the gold nanoparticles in the colloidal solution. The usage of supernatant from the colloidal solution as a biosensor for the diagnosis of cancer at an early stage is also proposed.

This platform could be used as a point-of-care testing device in several ways, such as an rBST detection kit, for the early diagnosis of cancer, etc. All the experiments discussed in this platform were performed in the laboratory using the 1cm path length standard quartz cuvettes. This mechanism could be converted to a microfluidic device for better sensing and the prototype device can be depicted as shown in Figure 7.12. This device consists of two inlets, two outlets, a 3D mixing chamber, and a gravity assisted sedimentation unit. First, the gold colloidal solution is treated with the entities of optimized concentration from the biosensing protocol until Vn96, and then that solution could be infused through one inlet and the EVs/biomolecules through another inlet. Both the solutions are directed through a 3D mixing chamber, where both the solutions get mixed, and the biomolecules could be captured by the gold nanoparticles. The number of turns in the serpentine microfluidic channel will be decided by the flowrate and the time required to form precipitate. Therefore, as the solution pass through the serpentine microfluidic channel, the biomolecules bound gold nanoparticles form precipitate depending on the concentration of the entities used in the protocol. The formed precipitate settles in the sedimentation chamber due to gravity leaving the supernatant in the serpentine channel. The supernatant can be collected from the outlet when the whole precipitate gets settled in the chamber. The precipitate can also be collected by detaching the device or by connecting to another outlet for further measurements. Also, a collection chamber could be included in the design for the LSPR measurements. The immediate uses of the proposed invention can be seen in the early diagnosis of Cancer, non-invasive treatment, treatment monitoring, point-of-care testing device, rBST detection kit.

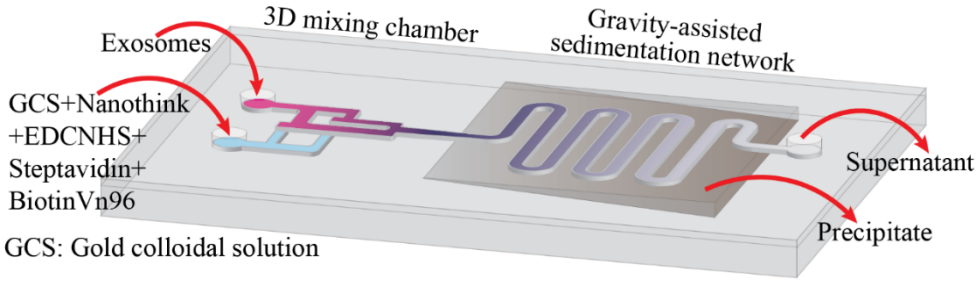

Figure 7.12: Schematic of a microfluidic device for the colloidal platform to isolate and detect the biomolecules

The colloidal platform has been developed for the isolation, plasmonic detection, and encapsulation of biomolecules such as extracellular vesicles from the MCF7 CCM, bovine growth hormone (BGH), or any entity that is attached to biotin. The platform is developed using the gold nanoparticles at cuvette level. The EVs sedimented along with the gold nanoparticles could be isolated by addition of proteinase K to the precipitate and a simple centrifugation will allow nanoparticles to settle at the bottom leaving the EVs in the supernatant. In order transform this colloidal platform from cuvette level to a microfluidic environment and to make the isolation easier, magnetic nanoparticles could be used for the isolation. So, the next chapter (Chapter 8) discusses about a liquid biopsy chip based on colloidal platform for the isolation of MCF7 EVs using magnetic particles and validation of the isolated EVs using mechanical and biological characterizations.

Chapter 8

Liquid Biopsy Chip for Isolation of Extracellular Vesicles using Magnetic Particles by Gravity Assisted Sedimentation and characterization by gene amplification

This chapter is reproduced from the manuscript prepared for the *Journal of Biosensors and Bioelectronics*.

Extracellular vesicles (EVs) are the cell-derived vesicles which play a critical role in cell-to-cell communication, normal homeostasis, and disease progression. These vesicles are the nano-sized particles which contain a myriad of substances like RNA, DNA, proteins, lipids, and multiple metabolites from their origin cells, offering a good source of biomarkers. The existing methods for the isolation of EVs from cell culture medium (CCM) or the body fluids are time-consuming, lack yield and purity, and expensive. In this work, we present a magnetic particle based liquid biopsy chip for the capture and isolation of EVs. The EVs are captured by an immuno-affinity-based approach, using Vn96. Vn96 is a synthetic polypeptide specifically designed to capture EVs by binding to the heat shock proteins (HSPs) present on the surface of EVs. To ensure capture efficiency by proper binding of the magnetic particles and the EVs, a split and recombination 3D mixer is integrated in the chip design and it also consists of a sedimentation unit, which allows EV-captured magnetic particles to settle in it. The captured EVs are then isolated from the chip based on gravity assisted sedimentation technique for elution of EVs and their validation. The EVs captured by the magnetic particles are characterized by the scanning electron microscopy (SEM) measurements and the ability of capture and isolation of EVs is validated by the nanoparticle tracking analysis (NTA) and atomic force microscopy (AFM) measurements of eluted EVs from the chip. The DNA content of the EVs isolated from the chip are further characterized by the absolute quantification of a housekeeping gene (RNase P) copies using droplet digital PCR (ddPCR). The results clearly show that the liquid biopsy chip can capture and isolate the EVs from the CCM, without affecting the morphology of the EVs. Thus, the liquid biopsy chip can be considered as a potential point of care device for diagnostics in a clinical setting.

8.1. Introduction

In modern science, the human health is always considered as one of the more complex topics. So, the vital information regarding the human health represented by DNA, RNA, and cells have become the major focus for the researchers in the field of bioscience. Specifically, for the detection and diagnosis of cancer-causing mutation(s), the biomolecules like DNA and other physiological markers like proteins have proved helpful [200-202]. The biomarkers out of these biomolecules are believed to be a quantifiable entity which reveals some biological states of human health. So, the identification and quantification of these biomarkers has a great potential for the early diagnosis and personalized therapy [203, 204]. As the biomarkers also offer information about the underlying medical conditions, the analysis results between the samples of a normal person and diseased person will provide illness, sub-clinical status, and the other necessary biological information quickly. Therefore, for an early diagnosis and the disease monitoring, the detection and quantification of biomarkers is utmost important, and is of great significance to human health.

Extracellular vesicles (EVs) are the membrane enclosed structures in the range of 30 to 1000 nm, that are released from almost all cells in the body [205]. The EVs are also known as shedding vesicles, which are vital sources of biomarkers for cancer, other pathological conditions such as inflammatory and neurodegenerative diseases, and for clinical diagnostics. The EVs are mainly subcategorized as exosomes, microvesicles and apoptotic bodies, which vary in size, biogenesis, membrane composition, cargo, and function [7, 206]. These are the nano-scale communication organelles containing biomolecules such as RNA, DNA, proteins, and lipids, transports the identity of their mother cells to the other cells. Therefore, the isolation and analysis of the EVs has a huge potential in the early diagnosis and prognosis of cancer.

A rapid and early diagnostic method is required for an improved treatment, and to control the progression of the disease. The conventional methods for the isolation and quantification of EVs are high-speed centrifugation and filtration steps, followed by ultracentrifugation. As the procedure of these methods is time consuming and resulting in low yield, researchers have been motivated to develop new diagnostic methods, suitable for rapid point-of-care (POC) applications. The new methods are required for the quantitative analysis of specific proteins and genetic biomarkers in blood or other fluids such as saliva or urine. For such analyses, Lab-on-a-chip (LoC) or microfluidic technology has drawn considerable attention in the past two decades, from the

researchers and industries for biomedical applications [74, 75]. The major benefits of using LOC devices are low sample volume, short assay time, high throughput, and multiplexed detection.

There are several microfluidic-based platforms have been developed for the isolation and quantification of biomolecules, specifically for EVs. Most of the microfluidics platforms are based on the techniques such as immunoaffinity capture by modifying the inner surface or by using the beads to capture EVs or based on specific size and density of the EVs. Several researchers have developed variety of methods for the capture and isolation of EVs, for example, employing a surface-modified microfluidic channel with "herringbone grooves" [43], designed an antibody-coated mica surface [207], "ExoChip" platform [56] etc. Moreover, the sensitivity and specificity of microfluidic devices has been substantially improved with continual advances in nanotechnology [66, 70]. The microfluidics based on capture beads consist of binding EVs and capture beads in the device and then washing and separating the beads to isolate EVs for the analysis [57, 58, 208]. The primary advantage of microfluidics based on capture beads compared with inner surface modification is its relative convenience for follow-up analysis.

The nanoparticles and various nanomaterials have attracted a growing attention with the rise of the LoC device and microfluidics technology in the scientific world. Particularly, the class of magnetic particles that consists of ferromagnetic particles of diameter in nanoscale range embedded in non-magnetic matrix such as polymer or quartz. The micro-sized particles created this way having superparamagnetic properties are normally in spherical shape, hence the beads or called as magnetic beads. Unless otherwise exposed to magnetizing field, these superparamagnetic particles show a non-magnetic behavior. The magnetic particles can be immobilized with a constant field while the field gradient effects the actuation or transportation. The distinctive characteristics of the magnetic particles is that the samples bound to these particles can be exploited by means of magnetic forces, independently of microfluidic, biological, or chemical processes [209, 210].

The large surface-to-volume ratio of the magnetic particles provides the chemical bonding of target molecules by a specific surface modification, which can be achieved by surface functionalization with the necessary ligands. Several methods have been developed so far for the functionalization comprising the modification of their surface by changing the characteristics such as biocompatibility, reactivity, roughness, hydrophilicity, or surface charge. The magnetic beads or the surface modified magnetic particles have proven to be a standard tool for the detection,

analysis, and quantification of targeted biomolecules [211, 212]. Due to the versatile properties of the magnetic particles, several researchers have reported using them in their platforms for the isolation of EVs [213-215].

Recently, our group developed a method for the capture and isolation of EVs from the MCF7 culture media, by using a small synthetic polypeptide called Vn96 [36] instead of antibodies, on a gold (Au) nano-island sensing platform that has a high affinity toward exosomes [151, 173]. To enhance the isolation and to accomplish the molecular profiling of the captured EVs, a novel magnetic bead based liquid biopsy chip integrated with a 3D mixer, collection chamber, and a sedimentation unit was designed. In this paper, we report on the simulation and design of split and recombine 3D mixer and fabrication of liquid biopsy chip, isolation of EVs captured on the surface of magnetic particles using the synthetic polypeptide Vn96, in the device and the validation of the isolated EVs through NTA, AFM and droplet digital PCR gene amplification.

8.2. Materials and methods

The Sylgard® 184 elastomer kit for the PDMS fabrication was purchased from Dow Corning. De-ionized (DI) water with a resistivity of 18MΩ was obtained by using the NANOpure ultrapure water system (Barnstead). Phosphate-buffered saline (PBS) was obtained from Sigma Aldrich, Canada. PBS tablets were dissolved in DI water at 0.1M concentration, with a pH of 7.2. Streptavidin coated magnetic particles of size 4.0-4.5µm and 8.0-9.9µm were purchased from Spherotech Inc. The Biotin-PEG-Vn96 was purchased from New England Peptide, USA and MCF7 EVs were collected from a conditioned media.

8.2.1. Design and simulation of 3D mixer

The proposed 3D mixer is designed to increase the surface contact between two fluids of interest based on the split and recombination of flow. The layered configuration of microchannels in the mixer is designed in such a way that they guide the fluids infused into the inlets to generate alternate layers at the outlet to maximize the diffusion. In the design, two simple T-type mixers are combined, where each inlet is dispensed into two sub-streams which will further be reunified in such a way that it maximizes the surface contact between the fluids to achieve complete mixing. To increase the diffusion of the fluids further, two mixing units are placed parallelly in the CAD

design. The dimensions of the mixer are optimized to have a better distribution of fluid in the channels and the design was simulated for the finite element (FE) analysis using COMSOL Multiphysics 5.5 MEMS module. The simulation of the mixer is performed to evaluate mixing by optimizing the dimensions under different inlet flow rates. The isometric and top view of the design simulated in COMSOL with a flow rate of 10µl/min is shown in Figure 8.1(A, B). To have normalized concentrations at the outlet, the water containing solutes with concentrations of C = 0 and C = 1 are used as the fluids to be mixed. An initial study on the effect of element sizes, show that element sizes less than 0.07mm, with a maximum limit of 0.13mm, will not improve the precision of the results but the CPU time. So, the whole volume of 3D model was discretized with a maximum element size of 0.07mm. The diffusion coefficient of the water and the convergence limit for the normalized relative error was set to 2.5 x 10^{-10} m/s^2 and 1 x 10^{-3}, respectively.

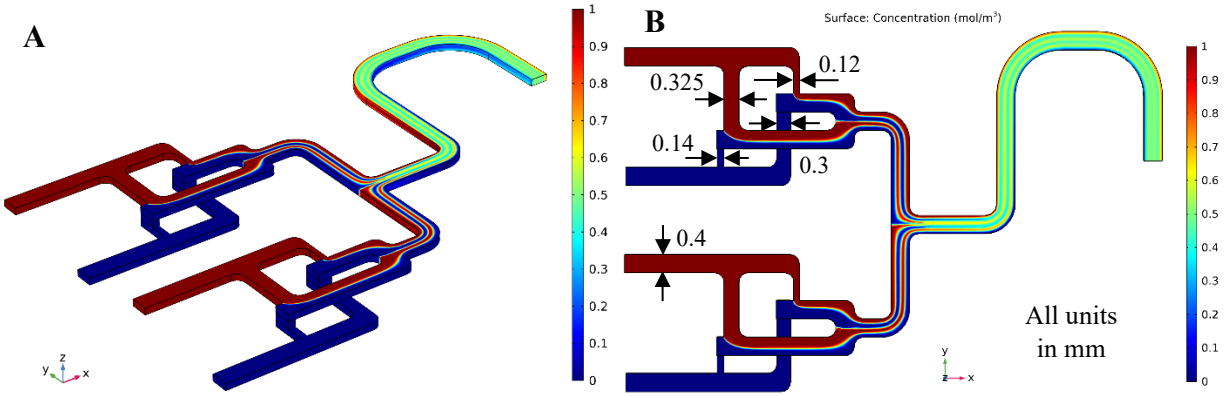

Figure 8.1: COMSOL simulation of split and recombine 3D mixer at a flow rate of 10µl/min; (A) Isometric view; (B) Top view

8.2.2. Mixing performance of the proposed 3D mixer

When the fluids infused into the mixer, the mixing happens at the molar concentration meaning, as the mixing starts by diffusion, the concentration of the solute starts decreasing from 1, while on the other side it starts increases from 0. So, the complete mixing is achieved when the concentration reaches to 0.5. A method, which is mathematically simpler than the conventional methods described in the paper [198] was used to quantitatively assess the simulation results. To assess the mixing, the profile of concentration at various stages of the mixer is obtained through COMSOL by generating the cross-sectional profiles and the corresponding 1-D plot of the mixing ranging between 0 and 1. Figure 8.2(A) shows the performance of mixing with the variation of concentration at various stages of the mixer and the corresponding 1-D plot for a flow rate of

10µl/min. The variation of concentration in the cross-sectional images at various stages clearly shows a clear diffusion of fluids into each other to have better mixing. To assess the mixing efficiency of the mixer for a flow rate of 10µl/min, the 1-D plot corresponding to the last stage of the channel (section D-D) is considered for further analysis as shown in Figure 8.2(B). The real distribution of the concentration in the 1-D plots is presented in pink line and is represented by the function f(x), where x is the normalized width. In a worst-case scenario, when the infused fluids do not mix because of no diffusion between them, the plot looks like the line shown in blue in the figure, which is represented in as $f_1(x)$. And on the other hand, as mentioned before, if there is a perfect mixing, then the concentration corresponds to 0.5 as shown in the figure with a green line and it is represented as $f_2(x)$. The degree of diffusion of one fluid into the other is represented using the hatched area, which is the difference between actual distribution (f(x)) and no mixing ($f_1(x)$) in Figure 8.2(B). So, the mixing efficiency, is therefore defined as the ratio between the hatched area corresponding to actual mixing, and the area between $f_2(x)$ and $f_1(x)$ corresponding to full mixing, as shown in equation (4) below:

$$\eta = \frac{\text{area corresponding to actual mixing}}{\text{area corresponding to full mixing}} = \frac{\int_0^1 |f_1(x) - f(x)| dx}{\int_0^1 |f_2(x) - f_1(x)| dx} = \frac{\int_0^1 |f_1(x) - f(x)| dx}{0.5} \quad (4)$$

The efficiency of the mixer corresponding to 10µl/min is calculated using the formula mentioned above and found to be around 90%. The same technique is applied to find the efficiency corresponding to various other flow rates and shown in Figure 8.2(C). From the plot it can be observed that the diffusion of fluids into the other fluid is higher as the flow rate reduces with a maximum mixing efficiency that could be obtained is around 96% with a flow rate of 1µl/min. As the simulation results shows that the fluids could be well mixed with the design proposed, the liquid biopsy chip was fabricated using soft lithography by integrating a sedimentation unit in the design for the isolation of EVs.

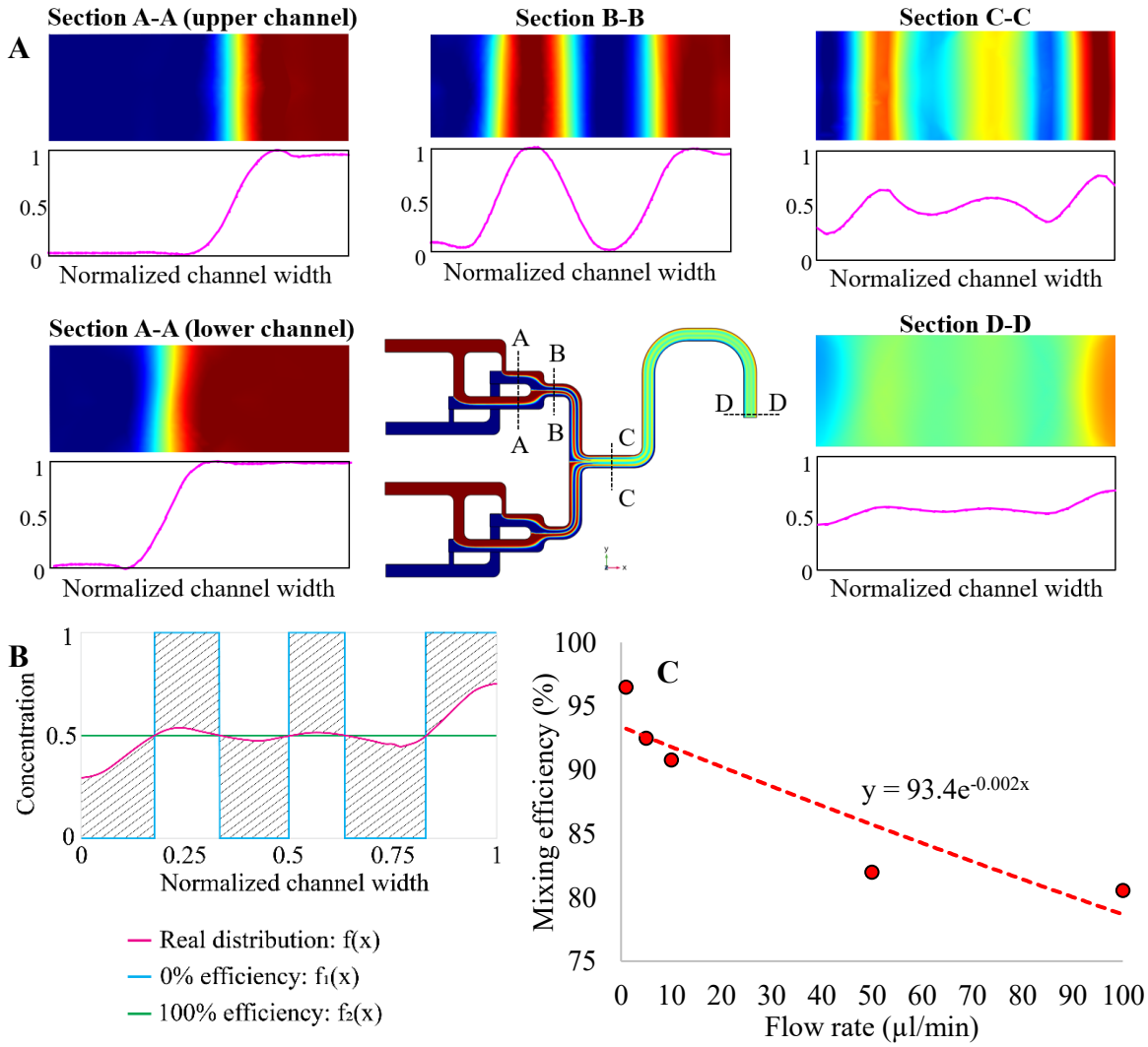

Figure 8.2: COMSOL simulation of 3D mixer at a flow rate of 10µl/min and mixing performance assessment; (A) The performance of mixing at various stages and their corresponding 1-D plot; (B) 1-D data plot of mixing at section D-D in the proposed 3D mixer; (C) Simulated mixing efficiency of the proposed 3D mixer at various flow rates

8.2.3. Fabrication of Liquid biopsy chip

The fabrication of the liquid biopsy chip is based on soft-lithography technique. There are three layers in fabrication of this chip, out of which top and bottom layers are both the standard microchannels on side of a PDMS layer whereas the middle layer or the layer that is connecting the both the top and bottom microchannels. So, it has to be a thin PDMS layer with the connecting points throughout the thickness of the layer. Therefore, there are individual mask for the fabrication of the mold for top/bottom and middle layer. The schematic of the fabrication steps of

the chip is shown in Figure 8.3. The SU-8 molds and their corresponding PDMS layers include top, middle, and bottom layers. Standard patterning of SU-8_{2075} photoresist was used for the fabrication of these molds to obtain a SU-8 thickness of 150µm. All the molds have been silanized for 2 hours after the fabrication to be used for PDMS fabrication.

The chip was fabricated using poly (dimethylsiloxane) (PDMS) from Sylgard® 184 elastomer kit from Dow Corning Corporation. The base polymer (pre-polymer) and the curing agent (crosslinking agent) are mixed in the ratio of 10:1 by weight and the bubbles were removed using the desiccator. As shown in Figure 8.3(A), the proposed chip includes two thick layers (top and bottom) having 150 µm microchannels and a middle layer with a thickness of 150 µm with the connecting points throughout. The fabrication process of the middle layer is schematically shown in Figure 8.3(B). The PDMS was poured onto the mold, and then a large glass slide was placed on PDMS and pushed gently to remove the excess of PDMS from the mold. While maintaining the same pressure on the glass slide with a clamp, the PDMS was cured at 80°C for 2 hours. As the mold was already silanized, the PDMS layer can be easily peeled off from the mold after curing. The exploded view schematic of the liquid biopsy chip is shown in Figure 8.3(C). The fabricated chip shown in Figure 8.3(D) was then considered for the isolation of EVs from the CCM using the magnetic particles.

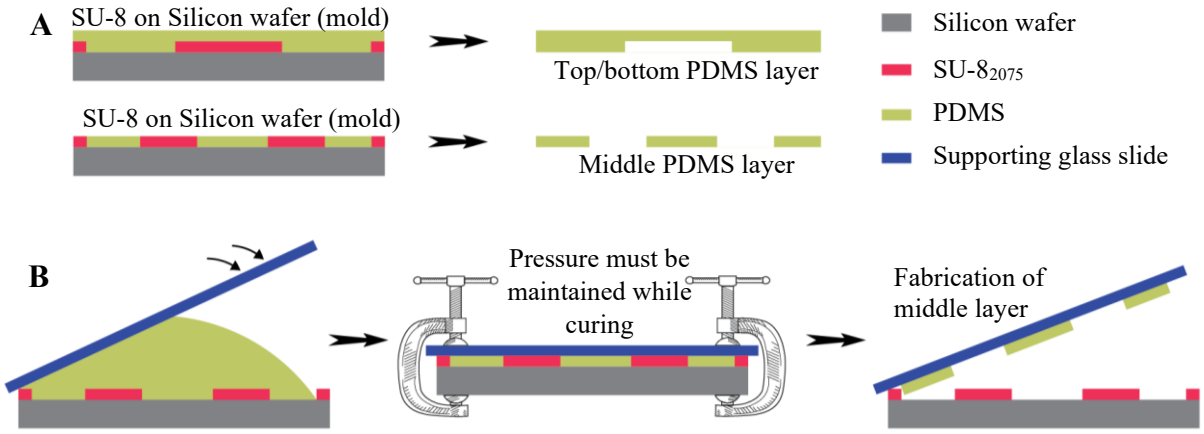

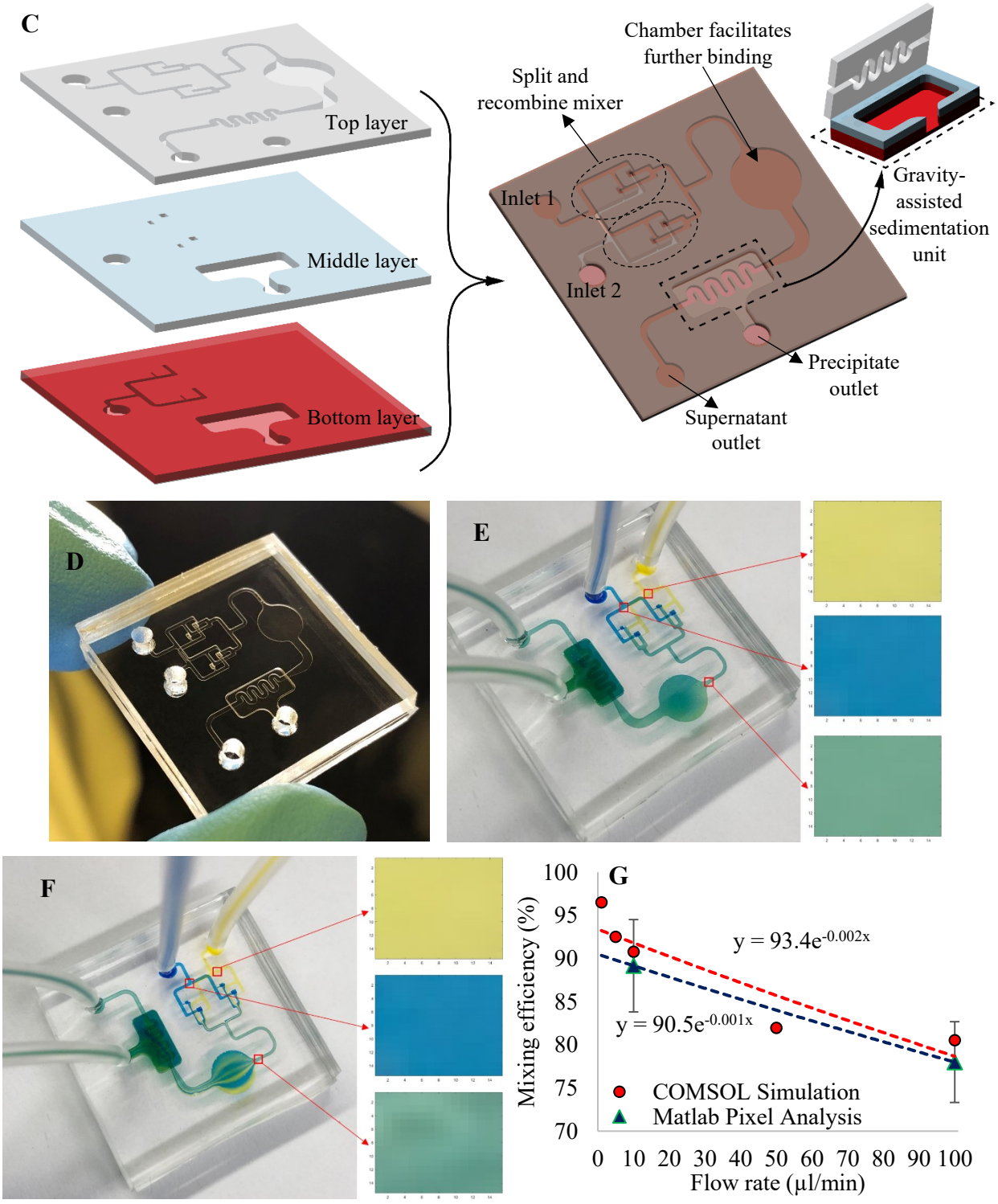

Figure 8.3: Fabrication process of the liquid biopsy chip; (A) SU-8 molds for fabrication of top/bottom and the middle layer; (B) Fabrication process to make the middle layer (C) Schematic of exploded view of the liquid biopsy chip; (D) Fabricated liquid biopsy chip; (E,F) Pictures of

color mixing at a flow rate of 10µl/min and 100µl/min; (G) Comparison of mixing efficiency from simulation and the pixel analysis by MATLAB (n=6).

The fabricated liquid biopsy chip was tested to check the performance of mixing, before using the chip for the isolation of EVs. It is well known that the mixing of blue and yellow colors results in green, same strategy is used in this chip to check the performance mixing, by flowing the blue and yellow colors through the chip at a flow rate of 10µl/min and 100µl/min and the pictures were captured as shown in Figure 8.3(E, F). From the pictures, it can be seen visually that the infused colors have mixed and resulted in green, but to quantify the efficiency of mixing, pixel analysis was performed on the captured pictures. To do this, the picture was cropped for blue and yellow portions at various places of 15x15 pixels each. Then the cropped images were read through MATLAB to obtain individual RGB channels from the pictures and then fused at each pixel to obtain green color, which is a reference green. The reference green is the green color that could be obtained when the mixing efficiency is 100%. Each pixel of the image is normalized to one (0-255 to 0-1) and then transformed to its associated wavelength in the spectra space by convolution, considering the standard wavelengths of RGB. The standard weights (W_r, W_g, W_b) used for RGB are 600nm, 550nm, and 450nm, respectively. The formula used to convert each pixel to its associated wavelength is as shown in equation (5):

$$\lambda_{(i,j)} = \frac{W_r \times R(i,j) + W_g \times G(i,j) + W_b \times B(i,j)}{W_r + W_g + W_b} \quad (5)$$

The same procedure is repeated for all the green sample pictures (15x15 pixels cropped from the device picture as shown in Fig. 8.3(E, F)) and the reference green. Then the wavelengths of reference green and the sample green were compared to find the variation. This variation was used further to calculate the efficiency of mixing in percentage. The efficiency with the pixel analysis was found to be around 89% and 78% for a flow rate of 10µl/min and 100µl/min, respectively as presented in Figure 8.3(G). The efficiency found using pixel analysis is in a good match with that of the simulated mixing performance. Considering these results, further experiments were conducted for the capture and isolation of EVs from the MCF7 CCM using the functionalized magnetic particles at a flow rate of 10µl/min.

8.2.4. Isolation of EVs using magnetic particles

There are two sizes of magnetic particles, 4.0-4.5µm and 8.0-9.9µm that were used for the isolation of EVs from the MCF7 CCM. These particles were purchased from Spherotech Inc. The

magnetic particles are the polystyrene beads polymerized with magnetite and the percentage of magnetite varies based on the size of bead. These particles are stored with 0.02% Sodium Azide (NaN_3) preservative. For better results, as recommended by the manufacturers, the particles should be washed to remove the preservative before using in any experiments. The washing procedure typically includes the centrifugation of particles at 1.5K RPM for 20 minutes, removal of supernatant without touching the pellet and the adding a buffer (PBS) to make the final volume same as before. Then the particles are ready to be used in the experiments.

From the datasheet, mean size of the magnetic particles is known and the number of streptavidin molecules on each particle can be calculated as the particles obtained are already coated with streptavidin on their surface. As per literature, each streptavidin is a tetramer and each subunit can bind to biotin molecules with same affinity, but here in this case there are only two subunits that are available to bind to with the biotin as other two subunits were already bound with the magnetic particle. As the mean size of particles and number of streptavidin molecules available on each particle is known, number of other bio-entities it can accommodate was quantitatively analyzed by calculating the surface of area the particle [181] and presented in Table 8.1. This data is helps in improving the yield as it gives a clear understanding on what concentration of magnetic particles must be used in order to isolate all or maximum of the EVs from the culture media or any other body fluids, for instance.

Table 8.1: Quantification of magnetic particles to find number of bio-entities each particle can capture/accommodate

	4.0 – 4.5 µm	**8.0 – 9.9 µm**
Mean diameter (µm)	4.24	8.92
Mass (g)	51.883×10^{-12}	464.52×10^{-12}
No. of mag. particles/ml	1.93×10^{8}	2.15×10^{7}
Streptavidin/particle	4.92×10^{6}	3.17×10^{7}
Biotin-PEG-Vn96/particle	9.84×10^{6}	6.34×10^{7}
Surface area (μm^2)	59.3	255.8
EVs/particle	6688	29256

In a typical experiment, the streptavidin coated magnetic particles of size 4.0-4.5µm were diluted with PBS to 0.4mg/ml and mixed with biotin-PEG-Vn96 of concentration of 5µg/ml in a

centrifuge tube in the ratio of 1:1 by volume. After 30 minutes of incubation, the Vn96 bound magnetic particles were collected into a syringe and then the Vn96 bound magnetic particles and MCF7 CCM of 0.2ml each were infused into the liquid biopsy chip using a syringe pump at flow rate of 10µl/min simultaneously as shown in Figure 8.4(A). The same procedure was repeated with the particle size 8.0-9.9µm. In another experiment, the volume was increased from 0.2ml to 0.5ml and the same experiment was repeated using 4.0-4.5µm and 8.0-9.9µm particles.

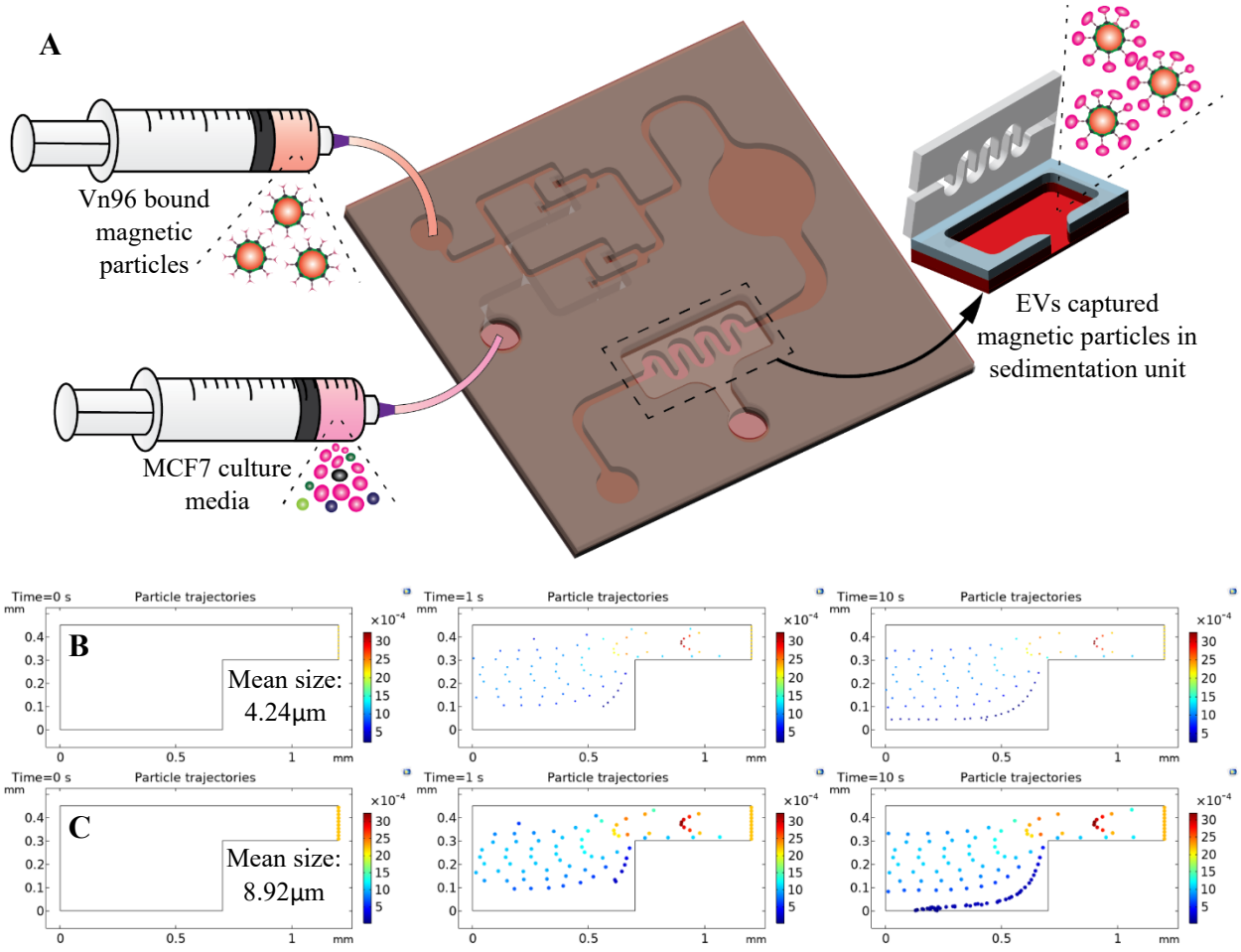

Figure 8.4: Isolation of EVs from the MCF7-CCM; (A) Schematic of the EV-isolation from the CCM when Vn96 bound magnetic particles and CCM were infused into the device; Trajectories of particles flowing in the sedimentation unit with a depth of 0.45mm at 0s, 1s, and 10s (left to right) (B) 4.24µm particles (C) 8.92µm particles

The flow rate of 10µl/min allows magnetic particles and the CCM to mix well in the split and recombine mixture as shown in the color mixing. Meanwhile, the Vn96 bound magnetic particles are expected to capture the EVs from CCM as Vn96, a polypeptide which is specifically

designed to bind to the heat shock proteins (HSPs) present on the surface of EVs. The chamber after the mixing units facilitates further binding of the particles and the EVs. The dimensions of the sedimentation unit after the chamber are 7mm x 3mm (LxW) and has an overall depth of 450µm. The sedimentation unit is simulated for the particle trajectories by considering the mean size of both the particles as shown in Figure 8.4(B, C). The trajectories of particles flown into the chamber clearly shows that the particles start to settle in within 0.5mm from the start of the chamber. As the chamber has a total length of 7mm, all or most of the particles flown will settle due to gravity. As seen in the particle's trajectory simulation, the sedimentation of EVs-captured magnetic particles was seen in the chamber. The precipitate is collected from the chamber for the elution of EVs and their characterization.

8.2.5. Elution and characterization of EVs

The precipitate of the magnetic particles that was settled in the sedimentation unit when MCF7 CCM along with the Vn96 bound magnetic particles was infused into the liquid biopsy chip was collected with a pipette and transferred to a small centrifuge tube. Then the Proteinase K (PK), which is a robust protein/peptide digesting enzyme, with a concentration of 20µg/ml prepared using PBS was used to elute EVs from the magnetic particles. The proteinase K of 15µl and 20µl were added in the centrifuge tube with the precipitate collected where the initial volume of CCM was 0.2ml and 0.5ml, respectively. Then the centrifuge tubes were incubated at 37°C for 1hr and then heat inactivated at 98°C for 15min to avoid further chewing of EVs. Proteinase K was added to digest the protein/peptides bridging EVs and the magnetic particles so that when the magnetic particles are isolated from the tube using a magnet, the liquid remained in the tube consists of the EVs captured and isolated using the magnetic particles. After incubation and heat inactivation, ~15µl and ~20µl of PK was collected from the tube, called eluent after removing the magnetic particles using a magnet. The eluent, containing EVs, was characterized by nanoparticle tracking analysis (NTA), scanning electron microscope (SEM), atomic force microscope (AFM), and by gene copy number amplification using ddPCR.

For the physical characterization of the EVs isolated from the liquid biopsy chip, the size distribution from the eluent was measured by nanoparticle tracking analysis (NTA) using NanoSight LM20 Nanoparticle Analysis System. The scanning electron microscopy (SEM) images of magnetic particles were obtained using Hitachi S-3400N scanning electron microscope

at an accelerating voltage of 15kV. The eluent was characterized for the size of the EVs it contains using Park Systems XE-100 atomic force microscope by scanning in a non-contact mode (f0~300 kHz, Park Systems). Topographic and phase images were recorded simultaneously at a scan rate of 1Hz and then processed using the Park Systems XEI software.

For the absolute quantification of copy numbers of a specific gene present in isolated as quantifiable biomarker, we performed ddPCR. It has been used for absolute copy number quantitation and was shown to be more reliable than conventional PCR methods or any other conventional copy number determination methods. According to manufacturer's instructions, a droplet digital PCR was performed using the QX200™ Droplet Digital™ PCR System (Bio-Rad Laboratories) to determine the number of copies of RPP30 gene which is a subunit of RNAseP present in the EV samples that is eluted from the chip. For the ddPCR reactions 5µl of collected eluent from the chips was used as template. The ddPCR reaction mixture consists of 10µl of 2x QX200TM ddPCR TM supermix for probe (Bio-Rad Laboratories), 0.05µl of 250nM final primer pair solutions (100µM-IDT), 0.025µl of 125nM final probe HEX (100µM-IDT), in the total volume to 20µl reaction mix [216]. Then, this 20µl volume of mixture is loaded in the droplet generator after mixing it with 70µl of droplet generation oil. The PBS buffer used for the negative control, in the measurements. Once the droplets are generated, samples were transferred to a 96-well PCR plate and then, sealed, using the PX1 PCR plate sealer. Then, the PCR amplification was carried out in C1000 Touch™ Thermal Cycler (Bio-Rad laboratories) as per the protocol provided by the manufacturer. After PCR amplification, the QX200™ Droplet Reader (Bio-Rad Laboratories), was used for reading each droplet from the plate for fluorescent signal detection. Then the date was analyzed using Quanta Soft™ analysis software (Bio-Rad Laboratories) to quantify the copy numbers. The background noise was eliminated by setting a threshold signal value based on the resolution of positive and negative droplets.

8.3. Results and discussion

The eluent from the liquid biopsy chips was characterized for bio-physical properties of EVs. The physical characterization by nanoparticle tracking analysis and scanning electron microscopy while the biological characterization by the RPP30 gene copy number amplification using ddPCR.

8.3.1. Characterization of eluent by NTA

The nanoparticle tracking analysis was performed using NanoSight LM20 Nanoparticle Analysis System. The automatic settings were selected for minimum expected particle size, blur, and minimum track length. The particles were tracked for a duration of 60 seconds with the camera shutter set to 450, camera gain to 300, and detection threshold to 3. Sample viscosity was linked to the corresponding viscosity for water at the given temperature. Then, the samples were loaded manually into the sample chamber using a 1 ml syringe. The microscopic field of view was positioned to the area where the particles were most clearly visualized. Samples were analyzed in triplicates and the size distribution of each sample was obtained [217].

The MCF7 CCM was first diluted by 100x using PBS for the measurement purposes and the concentration was found to be 5.65×10^9 particles/ml. Then, the eluent, corresponding to various dilutions of CCM, collected from the chip containing the EVs was measured for their size distribution with the optimized settings. The size distribution of EVs isolated using 4.0-4.5µm and 8.0-9.9µm magnetic particles from 0.2ml infused CCM is shown in Figure 8.5(A) and 8.5(B), respectively. And the total concentration of EVs corresponding to different dilutions of CCM, isolated using the magnetic particles is shown in Figure 8.5(C). From the plot, it is clear that the 8.0-9.9µm magnetic particles have captured a greater number of EVs when compared with the 4.0-4.5µm particles.

As we know the volume and concentration of CCM before infusing it into the chip, and the number EVs in the eluent corresponding to each concentration of CCM were measured using NTA, the efficiency of the isolation ca be defined as the ratio of number of particles present in the CCM before infusion to the number of EVs present in the eluent after isolation as shown in equation (6):

$$\text{Isolation efficiency (\%)} = \frac{\text{No.of EVs in eluent after isolation}}{\text{No.of particles in CCM before isolation}} \times 100 \qquad (6)$$

The efficiency of the isolation using 4.0-4.5µm and 8.0-9.9µm magnetic particles corresponding to various concentrations of CCM is evaluated using the equation above and plotted in Figure 8.5(D). From the plot, it could be observed that the efficiency is higher as the rate of dilution increases, which clearly explains that the undiluted CCM have aggregated EVs which could have prevented its binding with the Vn96 resulting in lower efficiency [197]. As the CCM gets diluted using PBS, the EVs or the particles in the CCM are better distributed which has increased the efficiency of isolation.

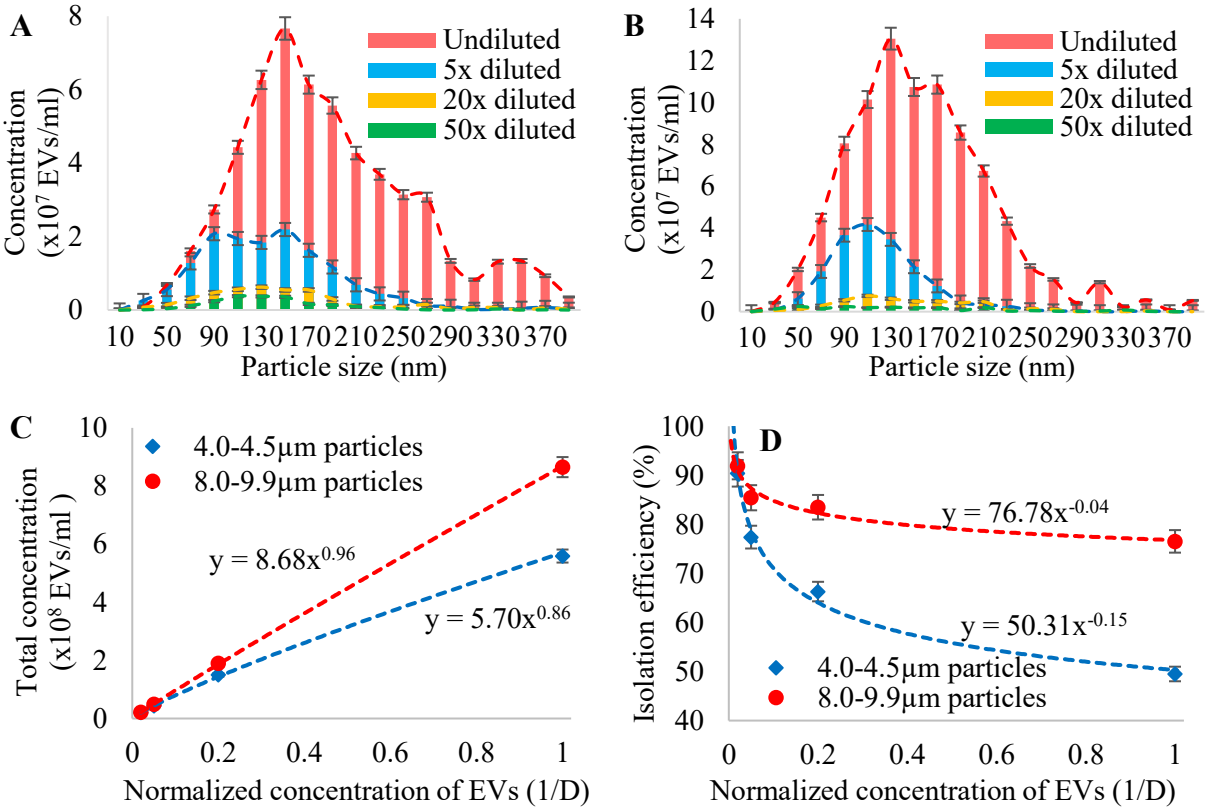

Figure 8.5: Characterization of isolated EVs by NTA when the infused volume of CCM was 0.2ml; (A) Size distribution of EVs isolated by 4.0-4.5µm magnetic particles; (B) Size distribution of EVs isolated by 8.0-9.9µm magnetic particles; (C) Total concentration of EVs isolated using 4.0-4.5µm and 8.0-9.9µm magnetic particles when the different dilutions of MCF7 CCM was infused into the chip (Dilution factor (D): 50x, 20x, 5x, undiluted); (D) Isolation efficiency when various dilutions of EVs isolated using 4.0-4.5µm and 8.0-9.9µm magnetic particles (n=12)

From physical modeling it is proved that the number of EVs/molecules that can be accommodated on a spherical particle is limited by its surface area. So, in another experiment, to understand the effect of volume/increasing the number of EVs, the volume of CCM is increased from 0.2ml to 0.5ml, keeping the number of magnetic particles and all the other experimental conditions same. The eluent from the chips containing EVs corresponding to all the dilutions of CCM was characterized for their size distribution using NTA. The size distribution of EVs isolated using 4.0-4.5µm and 8.0-9.9µm magnetic particles from 0.2ml infused CCM is shown in Figure 8.6(A) and 8.6(B), respectively. And the total concentration of EVs corresponding to different dilutions of CCM and their isolation efficiency is shown in Figure 8.6(C) and Figure 8.6(D),

respectively. When the isolation efficiency plots of 0.5ml CCM is compared with that of 0.2ml, it can be understood that the number of EVs captured by the magnetic particles is reduced when compared to the number EVs that are available, resulting in lower isolation efficiency. These the results confirm and experimentally validates the physical modeling that the number of EVs/molecules that can be captured/accommodated on the surface of a particle are limited by its surface area and the number of such particles available. Therefore, when the volume of CCM is increased, the concentration of magnetic particles must be adjusted based on requirement, in order to isolate all or maximum of EVs that are present in the CCM.

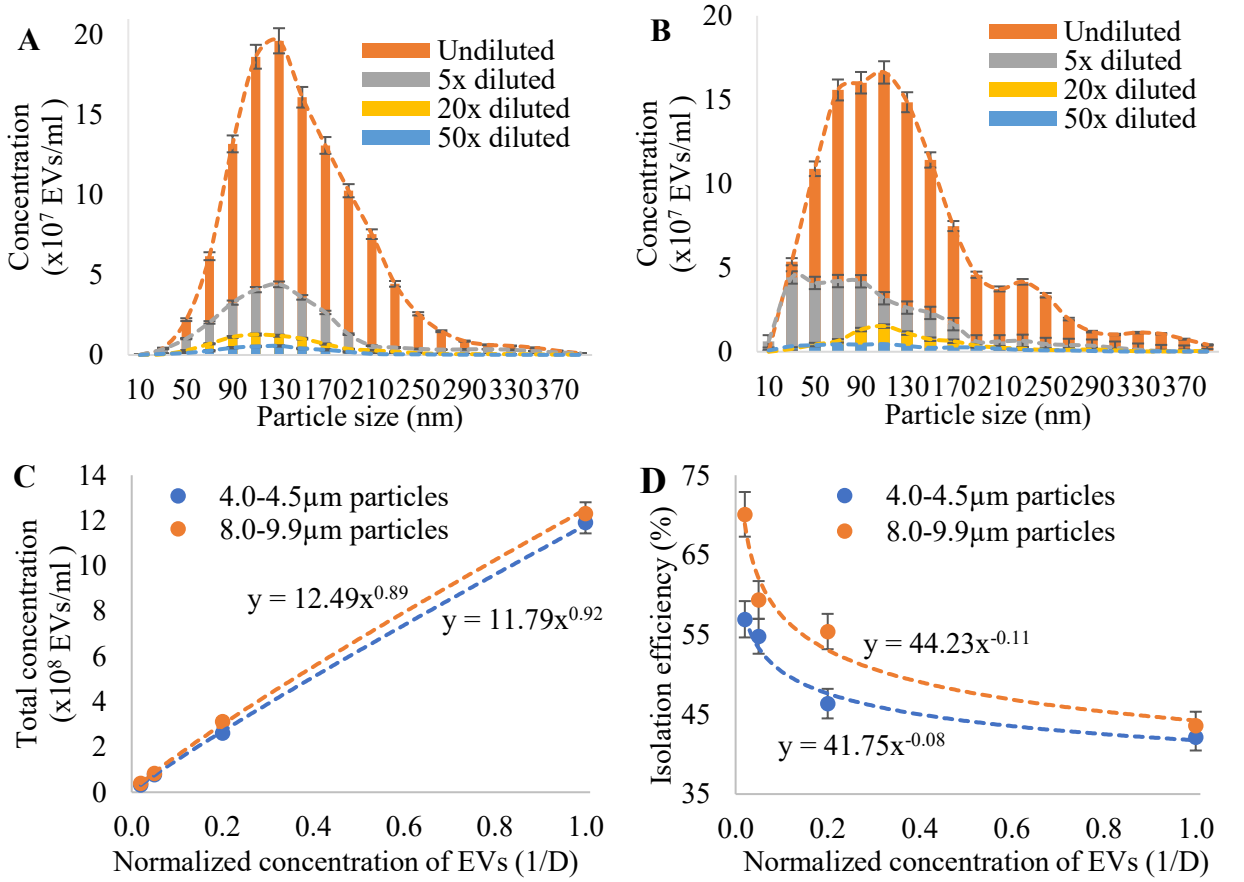

Figure 8.6: Characterization of isolated EVs by NTA when the infused volume of CCM was 0.5ml; (A) Size distribution of EVs isolated by 4.0-4.5µm magnetic particles; (B) Size distribution of EVs isolated by 8.0-9.9µm magnetic particles; (C) Total concentration of EVs isolated using 4.0-4.5µm and 8.0-9.9µm magnetic particles when the different dilutions of MCF7 CCM was infused into the chip (Dilution factor (D): 50x, 20x, 5x, undiluted); (D) Isolation efficiency when various dilutions of EVs isolated using 4.0-4.5µm and 8.0-9.9µm magnetic particles (n=12)

By analyzing the NTA characterization results corresponding to both the volumes, it can be clearly observed that the number of EVs captured by 8.0-9.9µm magnetic particles are relatively higher than that of 4.0-4.5µm particles. This could be due to the smaller size of magnetic particles, which probably is restricting the capture of EVs on their complete surface as they may start to aggregate with each other as the magnetic particles start binding to EVs.

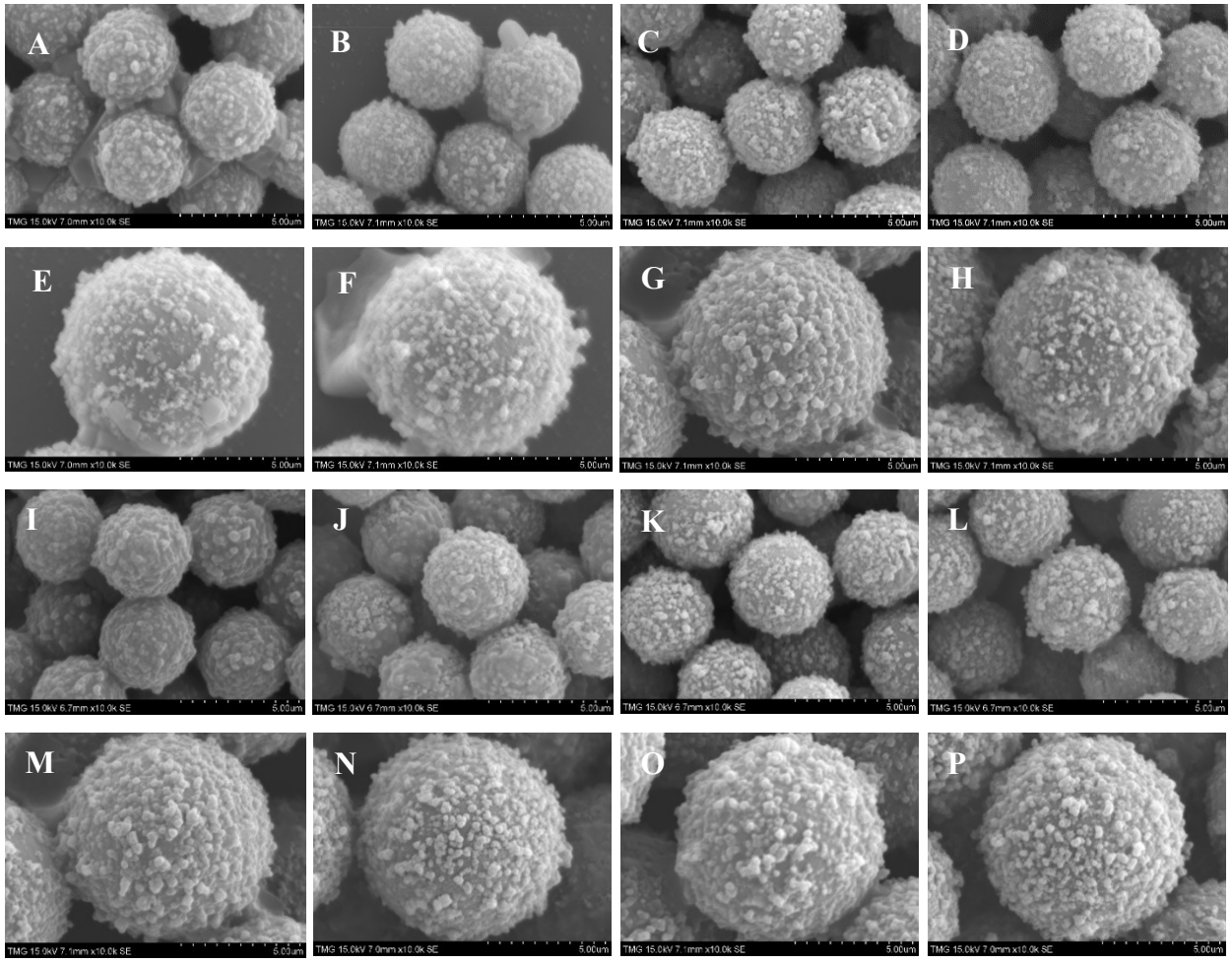

Figure 8.7: SEM images of streptavidin coated magnetic particles, Vn96 bound magnetic particles, EVs captured magnetic particles and the magnetic particles after EVs elution (left to right); (A-D) 4.0-4.5µm particles; (E-H) 8.0-9.9µm particles; SEM images of EVs-captured magnetic particles corresponding to undiluted, 5x diluted, 20x diluted, and 50x diluted CCM; (I-L) 4.0-4.5µm particles; (M-P) 8.0-9.9µm particles.

8.3.2. SEM of the magnetic particles

The images of the EVs-captured magnetic particles collected from the sedimentation unit were obtained by a scanning electron microscope for physical characterization. To understand the developments in the physical appearance of magnetic particles at various stages, the SEM images of streptavidin coated magnetic particles alone were obtained first, then the images of Vn96 bound particles, EVs-captured particles and the magnetic particles collected after EV elution using proteinase K were captured, subsequently. The SEM images of 4.0-4.5µm and 8.0-9.9µm streptavidin coated magnetic particles, Vn96 bound particles, EVs captured particles, and particles after EV elution are shown in Figure 8.7(A-H). Especially, comparing the image of the magnetic particle alone (Fig. 8.7(E)) to that of EV-captured magnetic particle (Fig. 8.7(G)) clearly shows that the number of biomolecules on the surface of magnetic particles have increased after the EVs were captured by Vn96 bound magnetic particles. Then the number of biomolecules on the magnetic particle's surface have reduced after the elution of EVs using proteinase K (Fig. 8.7(H)) compared to EV-captured magnetic particle. Besides, the SEM images shown in Figure 8.7(I-P) clearly shows that the EVs from all the dilutions (undiluted, 5x, 20x, 50x diluted) of CCM were isolated by the 4.0-4.5µm and 8.0-9.9µm magnetic particles. Therefore, from these SEM images, it is evident that the EVs from the CCM were captured by the magnetic particles and the same EVs were isolated by proteinase K elution and were collected in the eluent.

8.3.3. AFM analysis of the eluted EVs

The eluent from the chip was analyzed by AFM to validate the EVs. The samples were adsorbed onto freshly cleaved mica sheets after diluting with de-ionized water to 1:100 to perform AFM scanning. The phase images and line profiles of the EVs from the eluent and the control eluent are shown in Figure 8.8(A, B). The particles from the EVs eluent seem to be spherical as shown in its line profile and are in the height of around 18nm and width of 70 – 80nm. The control eluent, which is from the EV-free media, did not show any spherical particles, but are some irregular shapes around 1-2 nm in height, without any phase contrast. Therefore, as the measured size of EVs from eluent matches with the one reported in the literature [178, 179], AFM measurements confirm the proposed chip has successfully captured and isolated the EVs using magnetic particles by binding to their HSPs using Vn96.

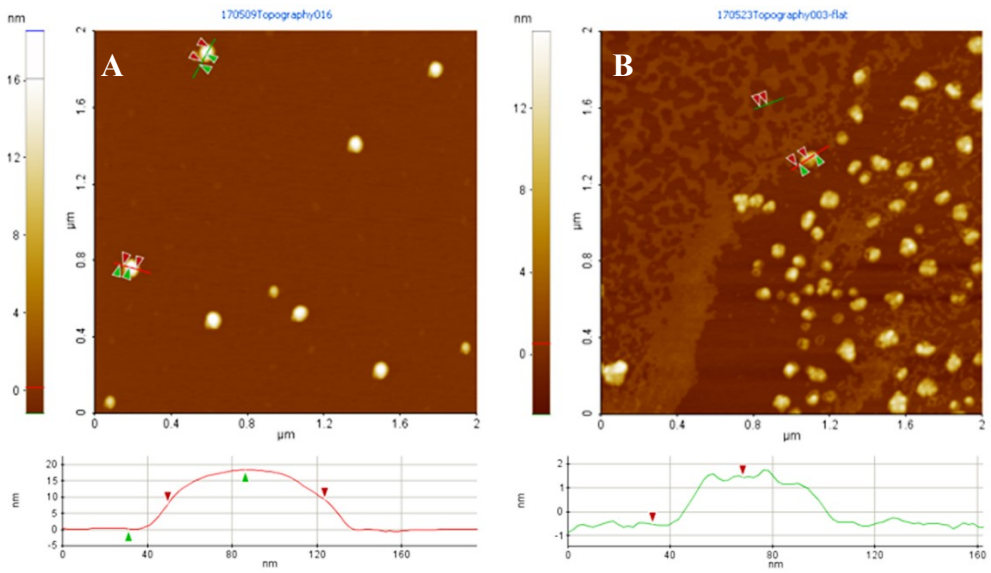

Figure 8.8: AFM measurements of the eluted EVs; (A) Phase image of the EVs (Proteinase K digested) isolated from the chip and its line profile; (B) Phase image of EV-free media as control and its line profile. The spot marked in the image was used to measure the width and thickness

8.3.4. RNase P gene copy number quantification by ddPCR

To further validate the EVs captured and isolated using Vn96 bound magnetic particles, droplet digital PCR (ddPCR) analysis was performed on the fractions of eluent corresponding to various concentrations of CCM, to quantitate the RNAseP DNA as a reference gene by the absolute quantification of its sub-unit, RPP30. It has been shown in the literature that RNase P can be used as a reference gene in ddPCR reactions as the sequence of this DNA is present in the EVs [180]. In this work, various concentrations of MCF7-CCM, namely, undiluted, 5x, 20x, 50x diluted was used to run through the chips to capture EVs on the surface of magnetic particles. The concentration of undiluted EVs was measured by NTA and found to be 5.65×10^9 particles/mL and as per the designed protocol, 0.2ml and 0.5ml was used to run through the chip in different experiments. The RNase P gene copies amplified by ddPCR corresponding to various concentrations of EVs isolated by 4.0-4.5µm and 8.0-9.9µm magnetic particles is represented in Figure 8.9(A-D). The EVs isolated from the CCM using magnetic particles of two different sizes show appreciable number of RNAseP gene copies amplified by ddPCR reactions. As the concentration of EVs decrease, the number of copies of RNAse P DNA segment amplified in both the cases are also decreasing, following the same trend. It is known from other reports that the concentration of EVs present in the body fluids increase tremendously (by many folds) in a cancer

patient, compared to a heathy person. This difference in the concentration was shown as 50x times less EVs in a non-cancerous condition when compared to a cancerous condition [43]. As shown here, the amplification of RNase P DNA can be done in 50x diluted CCM samples, this work clearly shows the potential of the chip and could be considered as a tool in the EV-based early diagnosis of cancer.

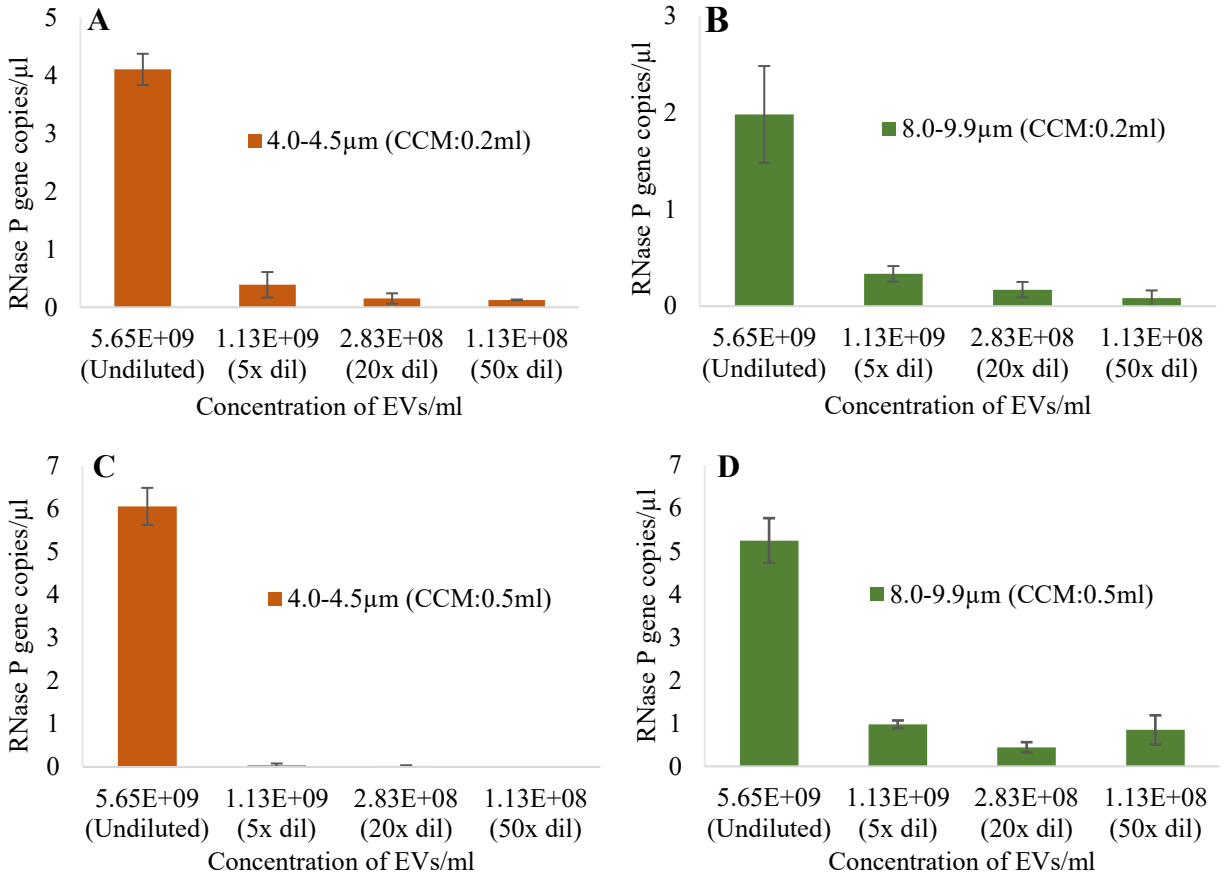

Figure 8.9: RNase P gene amplified from the eluent using ddPCR; (A) Isolation using 4.0-4.5µm particles (CCM:0.2ml); (B) Isolation using 8.0-9.9µm particles (CCM:0.2ml); (C) Isolation using 4.0-4.5µm particles (CCM:0.5ml); (D) Isolation using 8.0-9.9µm particles (CCM:0.5ml) (n=3)

Therefore, the analysis data shows the capability of the liquid biopsy chip for the capture and isolation of extracellular vesicles using magnetic particles from a CCM. In this study, we have demonstrated the capability of magnetic particle based on liquid biopsy chip for the capture and isolation of EVs originating from cancer cells and their morphological characterization by NTA, SEM, AFM, and the absolute quantification of DNA through ddPCR reactions after eluting EVs from the chip.

8.4. Conclusions

In the present study, the ability of the capture and isolation of the developed liquid biopsy chip were examined using the EVs from the breast cancer cell-line (MCF7) conditioned media, grown in a small bioreactor. The performance of the chip was evaluated by infusing various dilutions of MCF7 CCM, namely 50x, 20x, 5x and undiluted, into the chip at a flow rate of 10µl/min and isolation of EVs using magnetic particles. The EVs isolated from the various dilutions of CCM were further validated by NTA, SEM, AFM and ddPCR. The efficiency of isolation was characterized by NTA, morphology of the EVs and the EV-captured magnetic particles by AFM and SEM and then the absolute quantification of RNase P gene copies using ddPCR. The quantification of RNase P gene from the isolated EVs using the chip and the NTA, SEM and AFM data further validate that the developed liquid biopsy chip has the ability to capture and isolate EVs from the CCM, resulting in higher efficiency, without affecting their morphology. The major advantages of this label-free technique using the magnetic particles include faster isolation of EVs from CCM, which is around 20 minutes and easy removal of magnetic particles using a magnet after elution, when compared with the traditional techniques. In addition, one can have better control on the concentration or number magnetic particles required for the isolation of all or majority of the EVs by quantifying the magnetic particles. In EV-based diagnosis and therapeutic applications, isolation and proving the EVs by various analyses are the cornerstones. With the development of the lab-on-a-chip technology, the capture, isolation, and analysis of EVs is enabled. In conclusion, the magnetic particle based liquid biopsy chip, with Vn96 functionalization for the isolation of EVs from CCM or body fluids, can be considered as a potential device in the EV-based diagnosis in a real-life clinical setting.

Chapter 9
Conclusions and Future work

In this thesis, the biosensing protocols and the lab-on-chip devices were developed for the capture, isolation, and detection of extracellular vesicles from MCF7 (breast cancer cell line) culture media. In order to do this, three platforms based on gold nanoparticles, namely, in-situ synthesized gold nanocomposites, gold nano-islands on a substrate, and colloidal platform with suspended gold nanoparticles (AuNPs) were explored. Out of these platforms, based on the refractive index sensitivity, gold nano-island on a substrate and the nanoparticles suspended colloidal platforms were considered for the isolation and detection of EVs are summarized below.

9.1. Summary and Conclusions

The biosensing protocol for the LSPR detection of extracellular vesicles was developed, based on their high affinity to the Vn96 polypeptide. Vn96 is a synthetic polypeptide specifically designed to capture EVs by binding to the heat shock proteins (HSPs) present on their surface. The protocol was optimized experimentally using the gold nano-islands on a glass substrate platform at each stage for the concentration of the entities used. Particle analysis was performed on SEM images of the nano-islands whose morphology was tuned by heat treatment for an hour. The analysis has shown that the density of nano-islands is around 3 nano-islands/μm^2. Then, a simple physical model was developed by the characteristics of nano-islands, calculating their surface area and the number of various biochemical entities that can be successively immobilized on the surface of a nano-island. This modeling has shown that each nano-island can accommodate about 9 EVs per nano-island. By modeling and the surface density, it was found that a total of 27 EVs per μm^2 can be accommodated. It means, compared to the concentration of MCF7 CCM used, the developed Au nano-island platform can capture a much higher number of EVs, providing a very broad detection range covering from early stages to advanced stages.

Further, a simple microfluidic method for the capture, isolation, and detection of EVs has been developed, containing a glass substrate with gold nano-islands, sealed by a PDMS film that contains a microchannel with a collection chamber in between. The detection is based on the sensitivity of the LSPR property of gold nano-islands to any change in the surrounding

environment. The biosensing protocol was carried out in a microfluidic environment and the LSPR measurements were performed at each stage after the incubation. The results have shown that label-free technique is promising for the detection of EVs using the Vn96 polypeptide.

Then, the microchannel was redesigned to have a better distribution of entities flown and the microfluidic device has been fabricated. To evaluate the performance of the device, two concentrations, the undiluted and 5x diluted EVs were flown at a flow rate of 10µl/min through the Vn96 functionalized microfluidic devices. The captured EVs were isolated from the devices using proteinase K elution and were characterized for physical characteristics by AFM and their RNase P gene amplification by ddPCR. The RNase P gene amplified were in the order of 3.66 and 1.08 copies/µl for undiluted and 5x diluted EVs, respectively, validating the capture and isolation of EVs, without affecting their size or shape, from a very low sample volume around 3µl, in less than 30 minutes. As the protocol for the isolation and detection was optimized, the inconsistencies from the procedure can be reduced and the detection reproducibility improved. But, in order to increase the sensitivity of detection, the approach has to be modified. For which, a two-level microfluidic device is developed by incorporating gold nano-islands on both sides of the substrate sealed by PDMS films having microchannels with the collection chambers aligned one above the other. The first deposited gold nanoparticles go through 2-hour heat treatment for morphological tuning resulting in a higher density of gold nano-islands compared to 1-hour treatment. This increase in density increased the number EVs that could be accommodated per μm^2, meaning, the molecular interactions per μm^2 are increased. The results indicate that the detection sensitivity of the two-level device has been increased 1.54 times when compared with the device having a single-sided gold nano-island substrate as a sensing element. Thus, this technique can be used to build a multi-level microfluidic device by integrating the intermediate channel for the isolation and sensitive detection of EVs for point of care applications.

In order to further improve the sensitivity, instead of gold nano-islands, the gold nanoparticles suspended in a colloidal solution could directly be used, by which the entire surface area of the nanoparticles is utilized to capture the biomolecules. In this study, the colloidal solution was used in a cuvette as a multi-functional sensing platform by mixing the biosensing entities for the capture, isolation, and detection of various biomolecules. This platform was presented in three cases by modifying the biosensing protocol depending on the requirement i.e., capture and detection of any biomolecule that is tagged to biotin, detection of bovine growth hormone, and

capture, isolation, and detection of extracellular vesicles. As the nanoparticles are freely suspended in the solution, the binding of EVs on the entire surface area contributes the nanoparticles to sediment at the bottom of the cuvette. Thus, the precipitation method was used to isolate EVs, and the platform was transferred to a microfluidic environment by developing a liquid biopsy chip.

The performance of the liquid biopsy chip was evaluated by isolation of EVs using magnetic particles from various dilutions of MCF7 CCM, i.e., 50x, 20x, 5x and undiluted EVs flown at a rate of 10µl/min. The isolated EVs were eluted from the chip and were further validated by NTA, SEM, AFM and ddPCR. The efficiency of isolation was characterized by NTA, morphology by AFM and SEM, and then the absolute quantification of RNase P gene copies using ddPCR. The major advantages of using the magnetic particles include faster isolation of EVs, around 20 minutes and easy removal of magnetic particles using a magnet after elution, when compared with the traditional techniques. In addition, better control on the concentration of magnetic particles required for the isolation of all or majority of the EVs by quantifying the magnetic particles. Isolation and analysis of EVs are the cornerstones of any technique for EV-based diagnosis and therapeutic applications. In conclusion, with the results obtained, the lab-on-chips presented in the thesis based on the Vn96 functionalized gold nano-island platform and colloidal platform, could be used for the isolation of EVs from CCM or body fluids. Therefore, these devices could be considered as a potential device in the EV-based diagnosis in a real-life clinical setting.

9.2. Future work

The objective of this thesis was to design and develop a cancer intervention chip to be able to isolate EVs from body fluids. Several steps have been accomplished in designing, fabrication and testing of a reliable platform with the liquid biopsy chip. However, as the research never ends, there are some recommendations for future investigations.

- As the cell cultured media was used in the current thesis, future microfluidic designs can consider integration of a unit at the inlet to process the body fluids and a downstream analysis unit which can identify molecular, cellular, and/or biophysical features of the isolated EVs
- Identification and expression levels of the surface proteins on the isolated EVs in the microfluidic platforms by using integrated micro photonics methods.

- Designing and developing of a device or protocols to identify good or bad cargos in the isolated EVs and also finding a way to put back good cargo EVs in the sample.
- This research could be further extended to study the isolated EVs to be able to diagnose cancer at an early stage and purify the blood by removing the cancerous EVs. A system could be designed to diagnose cancer, which is inspired from the dialyzer used for the treatment of hemodialysis, as shown in Figure 9.1.

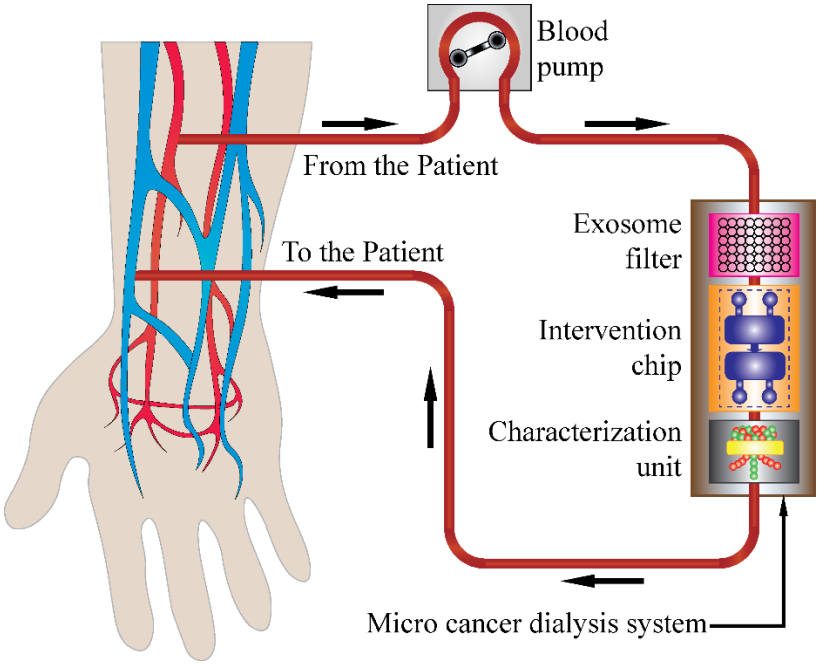

Figure 9.1: Schematic of micro cancer dialysis system (futuristic vision)

- In this futuristic vision of the system, the blood will be drawn from the patient's arm through a hemo-compatible sterile tubing, connected to a blood pump at a controlled flow rate. The drawn blood will be flown through a filter, specifically designed to extract proteins, lipids, EVs (cancerous and non-cancerous) and any other particles that are present in the blood. The filtered media will be routed to the intervention chip, where it reacts with the Vn96 functionalized metal nano or microparticles to capture and isolate the EVs similar to the liquid biopsy chip presented or in a much more sophisticated way. Then the isolated EVs have to be passed to a characterization unit where the cancerous and the non-cancerous EVs will be separated. The non-cancerous EVs should be directed back to the blood, while the cancerous EVs will be removed after separation. Anti-coagulants should be added in the system to prevent blood from clotting.

References

[1] National Cancer Institute, “Understanding Cancer Statistics ” September 2020 < https://www.cancer.gov/about-cancer/understanding/statistics>

[2] Canadian Cancer Society, “Cancer statistics at a glance” September 2020 < https://action.cancer.ca/en/research/cancer-statistics/cancer-statistics-at-a-glance>

[3] Cancer Research UK, “Stages of cancer” July 2020 < https://www.cancerresearchuk.org/about-cancer/what-is-cancer/stages-of-cancer>

[4] Cancer.net, “Stages of Cancer” March 2018 < https://www.cancer.net/navigating-cancer-care/diagnosing-cancer/stages-cancer>

[5] B.Gyorgy, T.G. Szabo, M. Pásztói, Z. Pál, P. Misják, B. Aradi, V. László, É. Pállinger, E. Pap, Á. Kittel, G. Nagy, A. Falus, and E.I. Buzás, “Membrane Vesicles, Current State-of-the-Art: Emerging Role of Extracellular Vesicles,” *Cell Mol Life Sci*., 68, 2667–2688, 2011

[6] J.C. Vancells, E.R. Suarez, N. Embade, D. Gil, R. Matthiesen, M. Valle, F. Elortza, S.C. Lu, J.M. Mato, J.M. Falcon-Perez, “Characterization and comprehensive proteome profiling of exosomes secreted by hepatocytes,” *J Proteome Res.*, 7(12), 5157–5166, 2008

[7] J. Kowal, G. Arras, M. Colombo, M. Jouve, J. P. Morath, B.P. -Bengtson, F. Dingli, D. Loew, M. Tkach, and C. Théry, “Proteomic comparison defines novel markers to characterize heterogeneous populations of extracellular vesicle subtypes,” *Proc. Natl. Acad. Sci. USA*, 113, E968-E77, 2016

[8] M. Simons, and G. Raposo, “Exosomes – vesicular carriers for intercellular communication,” *Curr. Opin. Cell Biol.*, 21(4), 575-581, 2009

[9] R. Nieuwland, and A. Sturk, “Why do cells release vesicles?,” *Thromb. Res.,* 125(1), S49-S51, 2010

[10] E. Chargaff, and R. West, “The Biological significance of the thromoboplastic protein of blood,” *J. Biol. Chem.*, 166(1), 189-197, 1946

[11] P. Wolf, “The nature and significance of platelet products in human plasma,” *Br. J. Haematol.*, 13(3), 269-288, 1967

[12] E.G. Trams, C.J. Lauter, N. Salem Jr, and U. Heine, "Exfoliation of membrane ecto-enzymes in the form of micro-vesicles," *Biochim. Biophys. Acta.*, 645(1), 63-70, 1981

[13] R.M. Johnstone, M. Adam, J.R. Hammond, L. Orr, and C. Turbide, "Vesicle formation during reticulocyte maturation. Association of plasma membrane activities with released vesicles (exosomes)," *J. Biol. Chem.*, 262(19): 9412-9420, 1987

[14] G. Raposo, H.W. Nijman, W. Stoorvogel, R Liejendekker, C.V. Harding, C.J. Melief, and H.J. Geuze, "B lymphocytes secrete antigen-presenting vesicles," *J Exp. Med.*, 183(3), 1161-1172, 1996

[15] L. Zitvogel, A. Regnault, A. Lozier, J. Wolfers, C. Flament, D. Tenza, P. Ricciardi-Castagnoli, G. Raposo, and S. Amigorena, "Eradication of established murine tumors using a novel cell-free vaccine: dendritic cell-derived exosomes," *Nat. Med.*, 4(5), 594-600, 1998

[16] S. Mathivanan, and R. J. Simpson "ExoCarta: A compendium of exosomal proteins and RNA," *Proteomics*, 9(21), 4997-5000, 2009

[17] H. Valadi, K. Ekström, A. Bossios, M. Sjöstrand, J.J. Lee, and J.O. Lötvall, "Exosome-mediated transfer of mRNAs and microRNAs is a novel mechanism of genetic exchange between cells," *Nat Cell Biol.*, 9, 654-659, 2007

[18] http://www.exosome-rna.com/secreted-extracellular-vesicles/

[19] J. Webber, R. Steadman, M. D. Mason, Z. Tabi, and A. Clayton, "Cancer exosomes trigger fibroblast to myofibroblast differentiation," *Cancer Res.*, 70(23), 9621-9630, 2010

[20] S. Rana, K. Malinowska, and M. Zöller, "Exosomal tumor microRNA modulates premetastatic organ cells," *Neoplasia*, 15(3), 281-295, 2013

[21] N. Chaput, and C. Théry, "Exosomes: immune properties and potential clinical implementations," *Semin. Immunopathol.*, 33, 419-440, 2011

[22] E.L. Andaloussi, I. Mäger, X.O. Breakefield, and M.J.A. Wood "Extracellular vesicles: biology and emerging therapeutic opportunities," *Nat. Rev. Drug Discov.*, 12, 347-57, 2013

[23] Z. E. Suntres, M. G. Smith, F. Momen-Heravi, J. Hu, X. Zhang, Y. Wu, H. Zhu, J. Wang, J. Zhou, and W.P. Kuo, "Therapeutic Uses of Exosomes," *J. Circul. Biom*., 1, 2013

[24] A. Delcayre, and J.B. Le "Exosomes as novels therapeutic nanodevices," *Curr. Opin. Mol. Ther.*, 8(1), 31-38, 2006

[25] S. Dai, D. Wei, Z. Wu, X. Zhou, X. Wei, H. Huang, and G. Li, "Phase I clinical trial of autologous ascites-derived exosomes combined with GM-CSF for colorectal cancer," *Mol. Ther.*, 16(4), 782-790, 2008

[26] C. Thery, S. Amigorena, G. Raposo, and A. Clayton "Isolation and characterization of exosomes from cell culture supernatants and biological fluids," *Curr. Protoc. Cell Biol.*, 3, 3.22, 2006

[27] H.G. Lamparski, A. Metha-Damani, J.Y. Yao, S. Patel, D.H. Hsu, C. Ruegg, and J.B.L. Pecq, "Production and characterization of clinical grade exosomes derived from dendritic cells," *J Immunol. Methods*, 270(2), 211-26, 2002

[28] R.V.D. Meel, M. Krawczyk-Durka, W.W.V. Solinge, and R.M. Schiffelers, "Toward routine detection of extracellular vesicles in clinical samples," *Int. J. Lab. Hem.*, 36(3), 244-253, 2014

[29] R. Lacroix, C. Judicone, M. Mooberry, M. Boucekine, N.S. Key, and F. Dignat-George, "Standardization of pre-analytical variables in plasma microparticle determination: results of the International Society on Thrombosis and Haemostasis SSC Collaborative workshop," *J. Thromb. Haemost.*, 11(6), 1190-1193, 2013

[30] K.W. Witwer, E.I. Buzás, L.T. Bemis, A. Bora, C. Lässer, J. Lötvall, E.N. Nolte-'t Hoen, M.G. Piper, S. Sivaraman, J. Skog, C. Théry, M.H. Wauben, and F. Hochberg, "Standardization of sample collection, isolation and analysis methods in extracellular vesicle research," *J Extracellular Vesicles*, 2(1), 2013

[31] B. Gyorgy, K. Pálóczi, A. Kovács, E. Barabás, G. Bekő, K. Várnai, É. Pállinger, K.S.-Taylor, T.G. Szabó, A.A. Kiss, A. Falus, and E.I. Buzás, "Improved circulating microparticle analysis in acid-citrate-dextrose (ACD) anticoagulant tube," *Thromb Res*., 133, 285-92, 2014

[32] R. Lacroix, C. Judicone, P. Poncelet, S. Robert, L. Arnaud, J. Sampol, and F. Dignat-George, "Impact of pre-analytical parameters on the measurement of circulating microparticles: towards standardization of protocol," *J ThrombHaemost*, 10(3), 437-446, 2012

[33] W.L. Chandler, W. Yeung, and J.F. Tait, “A new microparticle size calibration standard for use in measuring smaller microparticles using a new flow cytometer,” *J ThrombHaemost*, 9(6), 1216-1224, 2011

[34] https://www.cancer.org/healthy/find-cancer-early/tests-to-find-and-diagnose-cancer.html

[35] M. He, J. Crow, M. Roth, Y. Zeng, and A. K. Godwin “Integrated Immunoisolation and Protein Analysis of Circulating Exosomes Using Microfluidic Technology,” *Lab Chip*, 14, 3773– 3780, 2014

[36] Ghosh A, M. Davey, I.C. Chute, S.G. Griffiths, S. Lewis, S. Chacko, D. Barnett, N. Crapoulet, S. Fournier, A. Joy, M.C. Caissie, A.D. Ferguson, M. Daigle, M. Vicki Meli, S.M. Lewis, and R.J. Ouellette, “Rapid Isolation of Extracellular Vesicles from Cell Culture and Biological Fluids Using a Synthetic Peptide with Specific Affinity for Heat Shock Proteins,” *PLoS ONE*, 9(10), e110443, 2014

[37] T G. Fuhrmann, I.K. Herrmann, and M. M. Stevensa, “Cell-derived vesicles for drug therapy and diagnostics: Opportunities and challenges,” *Nano Today*, 10, 397- 409, 2015

[38] M.Y.Mo, P.R.M. Siljander, et. al., “Biological properties of extracellular vesicles and their physiological functions,” *J. of Extracellular Vesicles*, 4(1), 27066, 2015

[39] E. Van der Pol, A.N. Böing, P. Harrison, A. Sturk, and R. Nieuwland, “Classification, functions, and clinical relevance of extracellular vesicles”, *Pharmacol. Rev.*, 64(3), 676-705, 2012

[40] C. L. Chaffer, and R. A. Weinberg, “A perspective on cancer cell metastasis,” *Science*, 331, 1559-1564, 2011

[41] F. Diehl, K. Schmidt, M. A. Choti, K. Romans, S. Goodman, M. Li, K. Thornton, N. Agrawal, L. Sokoll, S. A. Szabo, K. W. Kinzler, B. Vogelstein, and L. A. Diaz, “Circulating mutant DNA to assess tumor dynamics,” *Nat. Med.*, 14, 985-990, 2008

[42] T. Sedlackova, G. Repiska, P. Celec, T. Szemes, and G. Minarik, “Fragmentation of DNA affects the accuracy of the DNA quantitation by the commonly used methods,” *Biol. Proced. Online*, 15(1), 5, 2013

[43] C. Chen, J. Skog, C.H. Hsu, R.T. Lessard, L. Balaj, T. Wurdinger, B.S. Carter, S.O. Breakefield, M. Toner, and D. Irimia, “Microfluidic Isolation and Transcriptome Analysis of Serum Microvesicles”, *Lab Chip*, 10, 505-511, 2010

[44] M. He, and Y. Zeng, "Microfluidic Exosome Analysis toward Liquid Biopsy for Cancer," *J Lab Autom.*, 21(4), 599–608, 2016

[45] M. Nawaz, G. Camussi, H. Valadi, I. Nazarenko, K. Ekstrom, X. Wang, S. Principe, N. Shah, N.M. Ashraf, F. Fatima, L. Neder, and T. Kislinger, "The emerging role of extracellular vesicles as biomarkers for urogenital cancers," *Nat. Rev. Urol.*, 11, 688-701, 2014

[46] M.L. Merchant, I.M. Rood, J. K.J. Deegens, and J.B. Klein, "Isolation and characterization of urinary extracellular vesicles: implications for biomarker discovery," *Nat. Rev. Nephrol.*, 13, 731-749, 2017

[47] J. Caradec, G. Kharmate, E. Hosseini-Beheshti, H. Adomat, M. Gleave, and E. Guns, "Reproducibility and efficiency of serum-derived exosome extraction methods," *Clin. Biochem.*, 47(13-14), 1286-1292, 2014

[48] I. Lozano-Ramos, I. Bancu, A. Oliveira-Tercero, M. P. Armengol, A. Menezes-Neto, H. A. Del Portillo, R. Lauzurica-Valdemoros, and F. E. Borras, "Size-exclusion chromatography-based enrichment of extracellular vesicles from urine samples," *J. Extracell. Ves.*, 4, 27369, 2015

[49] E. A. Mol, M. J. Goumans, P. A. Doevendans, J. P. G. Sluijter, and P. Vader, "Higher functionality of extracellular vesicles isolated using size-exclusion chromatography compared to ultracentrifugation," *Nanomedicine*, 13, 2061-2065, 2017

[50] W. Wang, J. Luo, and S. Wang, "Recent Progress in Isolation and Detection of Extracellular Vesicles for Cancer Diagnostics," *Adv Healthc Mater.*, 7(20), e1800484, 2018

[51] K.R. Yamamoto, B.M. Alberts, R. Benzinger, L. Lawhorne, and G. Treiber, "Rapid bacteriophage sedimentation in the presence of polyethylene glycol and its application to large-scale virus purification," *Virology*, 40(3), 734-744, 1970

[52] X. Gallart-Palau, A. Serra, A.S.W. Wong, S. Sandin, M.K.P. Lai, C.P. Chen, O.L. Kon, and S.K. Sze, "Extracellular vesicles are rapidly purified from human plasma by PRotein Organic Solvent PRecipitation (PROSPR)," *Sci. Rep.*, 5, 14664, 2015

[53] C. Chen, B.R. Lin, H.K. Wang, S.T. Fan, M.Y. Hsu, and C.M. Cheng, "Paper-based immunoaffinity devices for accessible isolation and characterization of extracellular vesicles," *Microfluid. Nanofluid.*, 16, 849-856, 2014

[54] S. Wang, L. Zhang, S. Wan, S. Cansiz, C. Cui, Y. Liu, R. Cai, C. Hong, I. T. Teng, M. Shi, Y. Wu, Y. Dong, and W. Tan, "Aptasensor with Expanded Nucleotide Using DNA Nanotetrahedra for Electrochemical Detection of Cancerous Exosomes," *ACS Nano*, 11(4), 3943-3949, 2017

[55] Y. Wan, G. Cheng, X. Liu, S.-J. Hao, M. Nisic, C.-D. Zhu, Y.-Q. Xia, W.-Q. Li, Z.-G. Wang, W.-L. Zhang, S. J. Rice, A. Sebastian, I. Albert, C. P. Belani, and S.-Y. Zheng, "Rapid magnetic isolation of extracellular vesicles via lipid-based nanoprobes," *Nat. Biomed. Eng.*, 1, 0058, 2017

[56] S.S. Kanwar, C.J. Dunlay, D.M. Simeone, and S. Nagrath, "Microfluidic device (ExoChip) for on-chip isolation, quantification and characterization of circulating exosomes," *Lab Chip*, 14(11), 1891-1900, 2014

[57] Z. Zhao, Y. Yang, Y. Zeng, and M. He, "A Microfluidic ExoSearch Chip for Multiplexed Exosome Detection towards Blood- Based Ovarian Cancer Diagnosis," *Lab Chip*, 16(3), 489–496, 2016

[58] J.S. Dudani, D.R. Gossett, H.T. Tse, R.J. Lamm, R.P. Kulkarni, and D.D. Carlo, "Rapid Inertial Solution Exchange for Enrichment and Flow Cytometric Detection of Microvesicles," *Biomicrofluidics*, 9(1), 014112, 2015

[59] Z. Wang, H.J. Wu, D. Fine, J. Schmulen, Y. Hu, B. Godin, J.X.J. Zhang, and X. Liu, "Ciliated Micropillars for the Microfluidic-Based Isolation of Nanoscale Lipid Vesicles," *Lab Chip*, 13(15), 2879–2882, 2013

[60] R.T. Davies, J. Kim, S.C. Jang, E.J. Choi, Y.S. Gho, and J. Park, "Microfluidic Filtration System to Isolate Extracellular Vesicles from Blood", *Lab Chip*, 12(24), 5202–5210, 2012

[61] K. Lee, H. Shao, R. Weissleder, and H. Lee, "Acoustic Purification of Extracellular Microvesicles," *ACS Nano*, 9(3), 2321–2327, 2015

[62] S.M. Santana, M.A. Antonyak, R.A. Cerione, and B.J. Kirby, "Microfluidic Isolation of Cancer-Cell-Derived Microvesicles from Heterogeneous Extracellular Shed Vesicle Populations" *Biomed. Microdevices*, 16(6), 869–877, 2014

[63] A. Bobrie, M. Colombo, S. Krumeich, G. Raposo, and C. Thery, "Diverse Subpopulations of Vesicles Secreted by Different Intracellular Mechanisms Are Present

in Exosome Preparations Obtained by Differential Ultracentrifugation," *J. Extracell. Vesicles*, 1, 18397, 2012

[64] B.J. Tauro, D.W. Greening, R.A. Mathias, H. Ji, S. Mathivanan, A.M. Scott, and R.J. Simpson, "Comparison of Ultracentrifugation, Density Gradient Separation, and Immunoaffinity Capture Methods for Isolating Human Colon Cancer Cell Line LIM1863-Derived Exosomes," *Methods*, 56 (2), 293–304, 2012

[65] H. Im, H. Shao, Y.I. Park, V.M. Peterson, C.M. Castro, R. Weissleder, and H. Lee, "Label-free detection and molecular profiling of exosomes with a nano-plasmonic sensor," *Nat Biotechnol.*, 32(5), 490-495, 2014

[66] Zhang P, He M, and Zeng Y, "Ultrasensitive microfluidic analysis of circulating exosomes using a nanostructured graphene oxide/polydopamine coating," *Lab Chip*, 16(16), 3033-3042, 2016

[67] L. Zhu, K. Wang, J. Cui, H. Liu, X. Bu, H. Ma, W. Wang, H. Gong, C. Lausted, L. Hood, G. Yang, and Z. Hu, "Label-free quantitative detection of tumor-derived exosomes through surface plasmon resonance imaging," *Anal Chem.*, 86(17), 8857-8864, 2014

[68] H. Shao, J. Chung, L. Balaj, A. Charest, D.D. Bigner, B.S. Carter, F.H. Hochberg, X.O. Breakefield, R. Weissleder, and H. Lee, "Protein typing of circulating microvesicles allows real-time monitoring of glioblastoma therapy," *Nat Med.*, 18(12), 1835-1840, 2012

[69] Y. Yoshioka, N. Kosaka, Y. Konishi, H. Ohta, H. Okamoto, H. Sonoda, R. Nonaka, H. Yamamoto, H. Ishii, M. Mori, K. Furuta, T. Nakajima, H. Hayashi, H. Sugisaki, H. Higashimoto, T. Kato, F. Takeshita, and T. Ochiya, "Ultra-sensitive liquid biopsy of circulating extracellular vesicles using ExoScreen," *Nat Commun.*, 5, 3591, 2014

[70] R. Vaidyanathan, M. Naghibosadat, S. Rauf, D. Korbie, L.G. Carrascosa, M.J.A. Shiddiky, and M. Trau, "Detecting Exosomes Specifically: A Multiplexed Device Based on Alternating Current Electrohydrodynamic Induced Nanoshearing," *Anal. Chem.*, 86 (22), 11125-11132, 2014

[71] M. Jørgensen, R. Bæk, S. Pedersen, E.K. Søndergaard, S.R. Kristensen, and K. Varming, "Extracellular Vesicle (EV) Array: microarray capturing of exosomes and other extracellular vesicles for multiplexed phenotyping," *J Extracell Vesicles*, 2, 2013

[72] M.M. Jørgensen, R. Bæk, and K. Varming, "Potentials and capabilities of the Extracellular Vesicle (EV) Array," *J Extracell Vesicles*, 4, 26048, 2015

[73] T. Akagi, N. Hanamura, and T. Ichiki, "Measurement of Individual Nanobioparticles on Microfluidic Chips by Laser Dark-field Imaging," *J. Photopolymer Science and Technology*, 28(5), 727-730, 2015

[74] T. Rojalin, B. Phong, H.J. Koster, and R.P. Carney, "Nanoplasmonic approaches for sensitive detection and molecular characterization of extracellular vesicles," *Front Chem.*, 7, 1-24, 2019

[75] W. Su, H. Li, W. Chen, and J. Qin, "Microfluidic strategies for label-free exosomes isolation and analysis," *Trends in Anal Chem.*, 118, 686-698, 2019

[76] P. Antoine, M. Beishon, et. al., "What can we learn from liquid biopsies?", *Cancerworld*, 68, Sept-Oct 2015

[77] D.A. Haber, and V.E. Velculescu, "Blood-Based Analyses of Cancer: Circulating Tumor Cells and Circulating Tumor DNA," *Cancer Discov.*, 4(6), 650–661, 2014

[78] G. Brock, E. C. Rizaldos, L. Hu, C. Coticchia, and J. Skog, "Liquid biopsy for cancer screening, patient stratification and monitoring," *Transl. Cancer Res*, 4(3): 280-290, 2015

[79] R. Tanos, and A. R. Thierry, "Clinical relevance of liquid biopsy for cancer screening," *Transl. Cancer Res.*, 7, S105-S129, 2018

[80] L. Dykman and N. Khlebtsov, "Chem Soc Rev Gold nanoparticles in biomedical applications: recent advances and perspectives to biological and medical," *Chem Soc Rev*, 41, 2256–2282, 2012

[81] H. Raether, "Surface plasmons on smooth surfaces"; *Springer*, 2, 4−39, 1988

[82] I. Ament, J. Prasad, A. Henkel, S. Schmachtel, and C. Sönnichsen, "Single unlabeled protein detection on individual plasmonic nanoparticles," *Nano Lett.*, 12(2), 1092−1095, 2012

[83] J.A. Ruemmele, W.P. Hall, L.K. Ruvuna, and R.P. Van Duyne, "A Localized Surface Plasmon Resonance Imaging Instrument for Multiplexed Biosensing," *Anal. Chem.*, 85(9), 4560−4566, 2013

[84] T. Chung, S.Y. Lee, E.Y. Song, H. Chun, and B. Lee, "Plasmonic nanostructures for nano-scale bio-sensing," *Sensors*, 11, 10907-10929, 2011

[85] K.S. Lee, and M.A. El-Sayed, "Gold and silver nanoparticles in sensing and imaging: sensitivity of plasmon response to size, shape, and metal composition," *J Phys Chem B*, 110, 19220-19225, 2006

[86] K.A. Willets, and R.P. Van Duyne, "Localized Surface Plasmon Resonance Spectroscopy and Sensing," *AnnuRev Phys Chem*, 58, 267–297, 2007

[87] L.A. Dykman, and N.G. Khlebtsov, "Gold nanoparticles in biology and medicine: recent advances and prospects," *Acta Naturae*, 3(2), 34–55, 2011

[88] Y.C. Yeh, B. Creran, and V.M. Rotello, "Gold nanoparticles: Preparation, properties, and applications in bionanotechnology," *Nanoscale*, 4, 1871-1880, 2012

[89] D.S. Wang, and S.K. Fan, "Microfluidic Surface Plasmon Resonance Sensors: From Principles to Point-of-Care Applications," *Sensors (Basel)*, 16(8), 1175, 2016

[90] J. Ozhikandathil, S. Badilescu, and M. Packirisamy, "A brief review on microfluidic platforms for hormones detection," *J. of Neural Transmission*, 124(1), 47-55, 2016

[91] J.F. Algorri, D. Poudereux, B. García-Cámara, V. Urruchi, J.M. Sánchez-Pena, R. Vergaz, M. Caño-García, X. Quintana, M.A. Geday, and J.M. Otón, "Metal nanoparticles-PDMS nanocomposites for tunable optical filters and sensors," *Opt. Data Process. Storage*, 2,1-6, 2016

[92] L.L. Beecroft, and C.K. Ober, "Nanocomposite materials for optical applications," *Chem Mater*., 9(6), 1302-1317, 1997

[93] F. Faupel, V. Zaporojtchenko, T. Strunkus, and M. Elbahri, "Metal polymer nanocomposites for functional applications," *Adv Eng Mater.*, 12(12), 1177-1190, 2010

[94] W. Caseri, "Nanocomposites of polymers and metals or semiconductors: Historical background and optical properties," *Macromolecular Rapid Comm.*, 21(11), 705–722, 2000

[95] W. Caseri, "Inorganic Nanoparticles as Optically Effective Additives for Polymers," *Chemical Engineering Comm*., 196(5), 549–572, 2009

[96] G. Carotenuto, G. LaPeruta, and L. Nicolais, "Thermo-chromic materials based on polymer-embedded silver clusters," *Sensors and Actuators B: Chemical*, 114(2), 1092-1095, 2006

[97] P.H.C. Camargo, K.G. Satyanarayana, and F. Wypych, "Nanocomposites: Synthesis, Structure, Properties and New Application Opportunities," *Materials Research*, 12(1), 1–39, 2009

[98] H. Althues, J. Henle, and S. Kaskel, "Functional inorganic nanofillers for transparent polymers," *Chem. Soc. Rev*., 36, 1454-1465, 2007

[99] S. Li, M.M. Lin, M.S. Toprak, D.K. Kim, and M. Muhammed, "Nanocomposites of polymer and inorganic nanoparticles for optical and magnetic applications," *Nano Reviews*, 1, 1-19, 2010

[100] H.S. Chuang, and S. Wereley, "Design, fabrication, and characterization of a conducting PDMS for microheaters and temperature sensors," *J Micromech Microeng*., 19(4), 1, 2009

[101] U. Cataldi, P. Cerminara, L. DeSio, R. Caputo, and C.P. Umeton, "Fabrication and characterization of stretchable PDMS structures doped with Au nanoparticles," *Molecular Crystals and Liquid Crystals*, 558(1), 22-27, 2012

[102] D. Li, C. Li, A. Wang, Q. He, and J. Li, "Hierarchical gold/copolymer nanostructures as hydrophobic nanotanks for drug encapsulation," *J. Mat. Chem.*, 20, 7782–7787, 2010

[103] L. Nicolais, and G. Carotenuto, "Preparation and characterization of metal-polymer nanocomposites. In: Nanocomposites: In situ synthesis of polymer-embedded nanostructures," First Edition, *John Wiley & Sons, Inc.*, 73–95, 2014

[104] A. Scott, R. Gupt, and G.U. Kulkarni, "A Simple Water-Based Synthesis of Au Nanoparticle/PDMS Composites for Water Purification and Targeted Drug Release," *Macromol Chem Phys.*, 211, 1640-1647, 2010

[105] M.A. De Jesús, K.S. Giesfeldt, and M.J. Sepaniak, "Improving the analytical figures of merit of SERS for the analysis of model environmental pollutants," *J. Raman Spectroscopy*, 35(10), 895–904, 2004

[106] S.K. Kumar, and R. Krishnamoorti, "Nanocomposites: Structure, Phase Behavior, and Properties," *Annu Rev Chem Biomol Eng.,* 1, 37–58, 2010

[107] A.L. Stepanov, and R.I. Khaibullin, "Optics of metal nanoparticles fabricated in organic matrix by ion implantation," *Rev Adv Master Sci.*, 7, 108-125, 2004

[108] M. Niklaus, and H.R. Shea, "Electrical conductivity and Young's modulus of flexible nanocomposites made by metal-ion implantation of polydimethylsiloxane: The

relationship between nanostructure and macroscopic properties," *Acta Materialia,* 59, 830–840, 2011

[109] G.J. Kovacs, and P.S. Vincett, "Subsurface particle monolayer and film formation in softenable substrates: Techniques and thermodynamic criteria," *Thin Solid Films*, 111(1), 65–81, 1984

[110] G.V. Ramesh, S. Porel, T.P. Radhakrishnan, "Polymer thin films embedded with in situ grown metal nanoparticles," *Chem Soc Rev.,* 38(9), 2646–2656, 2009

[111] K.S. Giesfeldt, R.M. Connatser, M.A. De Jesús, P. Dutta, and M.J. Sepaniak, "Gold-polymer nanocomposites: studies of their optical properties and their potential as SERS substrates," *J. Raman Spectroscopy*, 36(12), 1134–1142, 2005

[112] T. Hasell, L. Lagonigro, A.C. Peacock, S. Yoda, P.D. Brown, P.J.A. Sazio, and S.M. Howdle, "Silver Nanoparticle Impregnated Polycarbonate Substrates for Surface Enhanced Raman Spectroscopy," *Advanced Functional Materials*, 18(8), 1265–1271, 2008

[113] A. Bonyar, Z. Izsold, L. Himics, M. Veres, and I. Csarnovics, "Investigation of PDMS-gold nanoparticle composite films for plasmonic sensors," *2017 IEEE 23rd International Symposium for Design and Technology in Electronic Packaging, SIITME 2017 - Proceedings*, 25–28, 2018

[114] A. Bonyár, Z. Izsold, A. Borók, I. Csarnovics, L. Himics, M. Veres, and G. Harsányi, "PDMS-Au/Ag Nanocomposite Films as Highly Sensitive SERS Substrates," *Proceedings*, 2(13), 1060, 2018

[115] M.A. Firestone, S.C. Hayden, and D.L. Huber, "Greater than the sum: Synergy and emergent properties in nanoparticle–polymer composites," *MRS Bulletin*, 40(9), 760–767, 2015

[116] R.D. Deshmukh, and R.J. Composto, "Surface segregation and formation of silver nanoparticles created in situ in poly(methyl methacrylate) films," *Chemistry of Materials*, 19(4), 745–754, 2007

[117] T.R.E. Simpson, B. Parbhoo, and J.L. Keddie, "The dependence of the rate of crosslinking in poly(dimethyl siloxane) on the thickness of coatings," *Polymer*, 44(17), 4829–4838, 2003

[118] G.L. Batch, C.W. Macosko, and D.N. Kemp, "Reaction kinetics and injection molding

of liquid silicone rubber," *Rubber Chemistry and Technology*, 64(2), 218–233, 1991

[119] T.R.E. Simpson, Z. Tabatabaian, C. Jeynes, B. Parbhoo, and J.L. Keddie, "Influence of interfaces on the rates of crosslinking in PDMS coatings," *J of Poly Sci: Part A: Poly Chem.,* 42(6), 1421–1431, 2004

[120] Q. Zhang, J.J. Xu, Y. Liu, and H.Y. Chen, "In-situ synthesis of poly(dimethylsiloxane)-gold nanoparticles composite films and its application in microfluidic systems," *Lab on a Chip*, 8(2), 352–357, 2008

[121] A. Goyal, A. Kumar, P.K. Patra, S. Mahendra, S. Tabatabaei, P.J.J. Alvarez, G. John, and P.M. Ajayan, "In situ synthesis of metal nanoparticle embedded free standing multifunctional pdms films," *Macromolecular Rapid Comm.*, 30(13), 1116–1122, 2009

[122] K.R. Berry Jr, A.G. Russell, P.A. Blake, and D.K. Roper, "Gold nanoparticles reduced in situ and dispersed in polymer thin films: optical and thermal properties," *Nanotechnology*, 23, 375703, 2012

[123] D. Ryu, K.J. Loh, R. Ireland, M. Karimzada, F. Yaghmaie, and A.M. Gusman, "In situ reduction of gold nanoparticles in PDMS matrices and applications for large strain sensing," *Smart Structures and Systems*, 8(5), 471–486, 2011

[124] A. Massaro, F. Spano, R. Cingolani, and A. Athanassiou, "Experimental optical characterization and polymeric layouts of gold PDMS nanocomposite sensor for liquid detection," *IEEE Sensors Journal*, 11(9), 1780-1786, 2011

[125] H. SadAbadi, S. Badilescu, M. Packirisamy, and R. Wuẗhrich, "PDMS-gold nanocomposite platforms with enhanced sensing properties," *J Biomed Nanotechnol*, 8(4), 539–549, 2012

[126] J. Ozhikandathil, S. Badilescu, and M. Packirisamy, "Gold nanoisland structures integrated in a lab-on-a-chip for plasmonic detection of bovine growth hormone," *J Biomedical Optics*, 17(7), 077001, 2012

[127] S. Badilescu, and M. Packirisamy, "Microfluidics-nano-integration for synthesis and sensing," *Polymers*, 4(2), 1278-1310, 2012

[128] M. Fanous, S. Badilescu, and M. Packirisamy, "Thermal Manipulation of Gold Nanocomposites for Microfluidic Platform Optimization," *Plasmonics*, 13, 305–313, 2018

[129] A. D. Maio, “Extracellular heat shock proteins, cellular export vesicles, and the Stress Observation System: A form of communication during injury, infection, and cell damage,” *Cell Stress Chaperones*, 16, 235–249, 2011

[130] V. L. Vega, M. R. Silva, T. Frey, M. Gehrmann, J.C. Diaz, C. Steinem, G. Multhoff, N. Arispe, and A.D. Maio, “Hsp70 Translocates into the Plasma Membrane after Stress and Is Released into the Extracellular Environment in a Membrane-Associated Form that Activates Macrophages,” *J Immunol.*, 180, 4299-4307, 2008.

[131] G I. Lancaster, and M A. Febbraio, “Exosome-dependent trafficking of HSP70 a novel secretory pathway for cellular stress proteins,” *J. Biol Chem.*, 280, 23349 –23355, 2005.

[132] R. Gastpar, M. Gehrmann, M A. Bausero, A.Asea, C. Gross, J A. Schroeder, and G. Multhoff, “Heat Shock Protein 70 Surface-Positive Tumor ExosomesStimulate Migratory and Cytolytic Activity of Natural Killer Cells,” *Cancer Res.*, 65, 5238–5247, 2005

[133] C. Campanella, F.Bucchieri, A M. Merendino , A. Fucarino , G. Burgio, D F. V. Corona, G. Barbieri , S. David , F.Farina , G. Zummo , E. Conway de Macario , A J. L. Macario, and F.Cappello, “The Odyssey of Hsp60 from Tumor Cells to Other Destinations Includes Plasma Membrane-Associated Stages and Golgi and Exosomal Protein-Trafficking Modalities,” *PLoS ONE*, 7, e42008, 2012

[134] J S. Schorey, and S. Bhatnagar, “Exosome Function: From Tumor Immunology to Pathogen Biology,” *Traffic*, 9(6), 871–881, 2008

[135] C. Théry, M. Ostrowski, and E. Segur, “Membrane vesicles as conveyors of immune responses,” *Nature Reviews Immunology*, 9, 581–593, 2009

[136] C.Campanella, C. C. Bavisotto, A.M. Gammazza, D. Nikolic, F.Rappa, S. David, F.Cappello, F.Bucchieri, and S. Fais, “Exosomal Heat Shock Proteins as New Players in Tumour Cell-to-cell Communication,” *J Circ Biomark*. 3, 1-4, 2014

[137] S. Jeong, J. Park, D. Pathania, C. M. Castro, R. Weissleder, and H. Lee, “Integrated Magneto–Electrochemical Sensor for Exosome Analysis,” *ACS Nano*, 10, 1802-1809, 2016

[138] S. Yadav, K. Boriachek, M. N. Islam, R. Lobb, A. Moller, M. M. Hill, M. S. Al Hossain, N. T. Nguyen, and M.J.A. Shiddiky, “An Electrochemical Method for the Detection of Disease-Specific Exosomes,” *ChemElectroChem.*, 4, 967-971, 2017

[139] X. Doldan, P. Fagundez, A. Cayota, J. Laiz, and J. P. Tosar, "Electrochemical Sandwich Immunosensor for Determination of Exosomes Based on Surface Marker-Mediated Signal Amplification," *Anal. Chem.*, 88, 10466-10473, 2016

[140] Y. G. Zhou, R. M. Mohamadi, M. Poudineh, L. Kermanshah, S. Ahmed, T. S. Safaei, J. Stojcic, R. K. Nam, E. H. Sargent, and S. O. Kelley, "Interrogating Circulating Microsomes and Exosomes Using Metal Nanoparticles," *Small*, 12, 727-732, 2016

[141] K. Boriachek, M.N.Islam, A.Moller, C. Salomon, N.T. Nguyen, M.S.A. Hossain, Y. Yamauchi, and M.J.A. Shiddiky, "Biological functions and current advances in isolation and detection strategies for exosome nanovesicles," *Small*, 14, 1-21, 2018

[142] S G. Griffiths , MT. Cormier, A. Clayton , and A.A. Doucette, "Differential Proteome Analysis of Extracellular Vesicles from Breast Cancer Cell Lines by Chaperone Affinity Enrichment," *Proteomes*, 5, 1-16, 2017

[143] J. Gobbo, G. Marcion, M. Cordonnier, A. M. M. Dias, N.Pernet, A. Hammann, S. Richaud, H. Mjahed, N.Isambert, V.Clausse, C.Rébé, A. Bertaut, V.Goussot, F.Lirussi, F. Ghiringhelli, A.de Thonel, P.Fumoleau, R.eigneuric, and C.Garrido, "Restoring Anticancer Immune Response by Targeting Tumor-Derived Exosomes with a HSP70 Peptide Aptamer," *J Natl Cancer Inst.*, 108,1-11, 2016

[144] X. Zhang, X. Yuan, H. Shi, L. Wu, H. Qian, and Xu W, "Exosomes in cancer: small particle, big player," *J Hematol Oncol.*, 8, 83, 2015

[145] M. He, and Y. Zeng, "Microfluidic Exosome Analysis toward Liquid Biopsy for Cancer," *J Lab Autom.*, 21, 599-608, 2016

[146] E.N.M Noelte'N Hoen, E.J. Van der Vlist, M. Aalberts, H.C. H. Mertens, B.J. Bosch, W. Bartelink, E. Mastrobattista, E.V. B van Gaal, W. Stoorvogel, G.J.A. Arkesteijn, and M.H.M. Wauben, "Quantitative and qualitative flow cytometric analysis of nanosized cell-derived membrane vesicles," *Nanomedicine*, 8, 712-720, 2012

[147] S. Unser, I. Bruzas, J. He, and L. Sagle, "Localized Surface Plasmon Resonance Biosensing: Current Challenges and Approaches," *Sensors*, 15, 15684-15716, 2015

[148] P. Singh, "LSPR Biosensing: Recent Advances and Approaches. Reviews in Plasmonics," *Springer*, 211-238, 2016

[149] J. Ozhikandathil, and M. Packirisamy, "Simulation and implementation of a morphology-tuned gold nano-islands integrated plasmonic sensor," *Sensors*, 14, 10497-10513, 2014

[150] H. Sadbadi, S. Badilescu, M. Packirisamy, and R. Wuthrich, "Integration of gold nanoparticles in PDMS microfluidics for lab-on-a-chip plasmonic biosensing of growth hormones," *Biosensors and Bioelectronics*, 44, 77–84, 2013

[151] D. Raju, S. Bathini, S. Badilescu, R.J. Ouellette, A. Ghosh, and M. Packirisamy, "Exosomes detection by a label-free localized surface plasmonic resonance method," *ECS Trans.*, 75, 11–17, 2016

[152] H. Hinterwirth, S. Kappel, T. Waitz, T. Prohaska, W. Lindner, and M. Lammerhofer, "Quantifying thiol ligand density of self-assembled monolayers on gold nanoparticles by inductively coupled plasma-mass spectrometry," *ACS Nano*, 7, 1129-36, 2013

[153] Y. Li, and H. Zhang, "Binding of streptavidin to surface-attached biotin with different spacer thicknesses", *J. Wuhan University of Tech. (Material Science Edition)*, 30, 1304-1309, 2015

[154] P.C. Weber, D. H. Ohlendorf, J. J. Wendoloski, and F. R Salemme, "Structural Origins of High-affinity Biotin Binding to Streptavidin," *Science*, 243, 85-88, 1989

[155] P. C. Weber, J. J. Wendoloski, M. W. Pantoliano, and F. R. Salemme, "Crystallographic and Thermodynamic Comparison of Natural and Synthetic Ligands Bound to Streptavidin," *J. Am. Chem. Soc.*, 114, 3197-3200, 1992

[156] M. Lösche, C. Erdelen, E. Rump, and H. Ringsdorf, "On the Lipid Head Group Hydration of Floating Surface Monolayers Bound to Self-assembled Molecular Protein Layers," *Thin Solid Films*, 242, 112-117, 1994

[157] E.P. Diamandis, and T.K. Christopoulos, "The biotin-(strept) avidin system: principles and applications in biotechnology," *Clin Chem.*, 37, 625-36, 1991

[158] J. Turkevich, P. C. Stevenson, and J. Hillier, "A Study of the nucleation and growth processes in the synthesis of colloidal gold," *Discussions of the Faraday Society*, 11, 55-75, 1951

[159] N. Nath, and A. Chilkoti, "Label-Free Biosensing by Surface Plasmon Resonance of Nanoparticles on Glass: Optimization of Nanoparticle Size," *Anal. Chem.*, 76(18), 5370–5378, 2004

[160] N. Nath, and A. Chilkoti, "Label Free Colorimetric Biosensing Using Nanoparticles," *J. Fluoresc.*, 14(4), 377–389, 2004

[161] F. Frederix, J. M. Friedt, K. H. Choi, W. Laureyn, A. Campitelli, D. Mondelaers, G. Maes, and G. Borghs, "Biosensing Based on Light Absorption of Nanoscaled Gold and Silver Particles," *Anal. Chem.*, 75 (24), 6894–6900, 2003

[162] J. C. Hulteen, D. A. Treichel, M.T. Smith, M.L. Duval, T.R. Jensen, and R. P. Van Duyne, "Nanosphere Lithography: Size-Tunable Silver Nanoparticle and Surface Cluster Arrays," *J. Phys. Chem. B*, 103 (19), 3854–3863, 1999

[163] M. D. Malinsky, K. L. Kelly, G. C. Schatz, and R. P. Van Duyne, "Chain Length Dependence and Sensing Capabilities of the Localized Surface Plasmon Resonance of Silver Nanoparticles Chemically Modified with Alkanethiol Self-Assembled Monolayers," *J. Am. Chem. Soc*, 123(7), 1471–1482, 2001

[164] B. Sepulveda, P. C. Angelome, L. M.Lechuga, and L. M. Liz-Marzan, "LSPR-based nanobiosensors", *Nano Today*, 4, 244-251, 2009

[165] K. M. Byun, "Development of nanostructured plasmonic substrates for enhanced optical biosensing," *J. Opt. Soc. of Korea*, 14, 65-76, 2010

[166] http://www.cepower.ch/view/userfiles/files/CELLine(3).pdf

[167] J.P. Mitchell, J. Court, M.D. Mason, Z. Tabi, and A. Clayton, "Increased exosome production from tumour cell cultures using the Integra CELLine Culture System", *J. Immunol. Methods*, 335, 98–105, 2008

[168] J. Ozhikandathil, S. Badilescu, and M. Packirisamy, "Technical note: A portable on-chip assay system for absorbance and plasmonic detection of protein hormone in milk", *J Dairy Sci*., 98, 4384-4391, 2015

[169] C. Huang, K. Bonroy, G. Reeckmanns, W. Laureyn, K. Verhaegen, I.D. Vlaminck, L. Lagae, and G. Borghs, "Localized surface plasmon resonance integrated with microfluidic chip," *Biomed Microdevices*, 11(4), 893-901, 2009

[170] Y. Zhang, Y. Liu, H. Liu, and W.H. Tang, "Exosomes: biogenesis, biologic function and clinical potential," *Cell Biosci*, 9(19), 2019

[171] X. Mao, J.R. Waldeisen, B.K. Juluri, and T.J. Huang, "Hydrodynamically tunable optofluidic cylindrical microlens," *Lab Chip*, 7, 1303-1308, 2007

[172] H. Im, H. Shao, R. Weissleder, C.M. Castro, and H. Lee, "Nano-plasmonic exosome diagnostics," *Expert Rev Mol Diagn*, 15, 725-733, 2015

[173] S. Bathini, D. Raju, S. Badilescu, and M. Packirisamy, "Microfluidic Plasmonic Bio-Sensing of Exosomes by Using a Gold Nano-Island Platform," *Intl J of Biomed Biol Engg (WASET)*, 12, 226 – 229, 2018

[174] J. Kimling, M. Maier, B. Okenve, V. Kotaidis, H. Ballot, and A. Plech, "Turkevich method for gold nanoparticle synthesis revisited," *J Phys Chem B*, 110, 15700-15707, 2016

[175] G. Binnig, C.F. Quate, and Ch. Gerber, "Atomic force microscope", *Phys Rev Lett.*, 56(9), 930-933, 1986

[176] Y. Yuana, T.H. Oosterkamp, S. Bahatyrova, B. Ashcroft, P.G. Rodriguez, R.M. Bertina, and S. Osanto, "Atomic force microscopy: a novel approach to detect nanosized blood microparticles," *J ThrombHaemost.*, 8(2), 315-323, 2009

[177] Britannica, T. Editors of Encyclopaedia. Polymerase chain reaction. Encyclopedia Britannica., April 18, 2019

[178] S. Sharma, H. I. Rasool, V. Palanisamy, C. Mathisen, M. Schmidt, D.T. Wong, and J.K. Gimzewski, "Structural-Mechanical Characterization of Nanoparticle Exosomes in Human Saliva, Using Correlative AFM, FESEM, and Force Spectroscopy," *ACS Nano*, 4(4), 1921-1926, 2010

[179] V.S. Chernyshev, R. Rachamadugu, Y.H. Tseng, D.M. Belnap, Y. Jia, K.J. Branch, A.E. Butterfield, L.F. Pease III, P.S. Bernard, and M. Skliar, "Size and shape characterization of hydrated and desiccated exosomes," *Anal Bioanal Chem*, 407, 3285-3301, 2015

[180] T. Vagner, C. Spinelli, V.R. Minciacchi, L. Balaj, M. Zandian, A. Conley, A. Zijlstra, M.R. Freeman, F. Demichelis, S. De, E.M. Posadas, H. Tanaka, and D.D. Vizio, "Large extracellular vesicles carry most of the tumour DNA circulating in prostate cancer patient plasma," *J Extracell Vesicles*, 7(1), 1505403, 2018

[181] S. Bathini, D. Raju, S. Badilescu, A. Kumar, R.J. Ouellette, A. Ghosh, and M. Packirisamy, "Nano-bio interactions of extracellular vesicles with gold nanoislands for early cancer diagnosis," *Research*, 2018, 3917986, 2018

[182] W.C. Tian and E. Finehout, “Microfluidic Diagnostic Systems for the Rapid Detection and Quantification of Pathogens Microfluidics for Biological Applications,” *Springer*, 271–322, 2009

[183] P. N. Nge, C. I. Rogers, and A. T. Woolley, “Advances in Microfluidic Materials, Functions, Integration and Applications,” *Chemical reviews*, 113, 2550-2583, 2013

[184] P. M. Valencia, O. C. Farokhzad, R. Karnik and R. Langer, “Microfluidic technologies for accelerating the clinical translation of nanoparticles,” *Nature nanotechnology*, 7, 623-629, 2012

[185] E. K. Sackmann, A. L. Fulton, and D. J. Beebe, “The present and future role of microfluidics in biomedical research,” *Nature*, 507, 181-189, 2014

[186] N. Gupta, J. R. Liu, B. Patel, D. Solomon, B. Vaidya, and V. Gupta, “Microfluidics-based 3D cell culture models: Utility in novel drug discovery and delivery research,” *Bioengineering & Translational Medicine*, 1(1), 63-81, 2016

[187] I. E. Araci, and P. Brisk, “Recent developments in microfluidic large-scale integration,” *Current Opinion in Biotechnology*, 25, 60-68, 2014

[188] S. Halldorsson, E. Lucumi, R. Gómez-Sjöberg and R. M. Fleming, “Advantages and challenges of microfluidic cell culture in polydimethylsiloxane devices,” *Biosensors and Bioelectronics*, 63, 218-231, 2015

[189] C. Szydzik, B. Niego, G. Dalzell, M. Knoerzer, F. Ball, W.S. Nesbitt, R.L. Medcalf, K. Khoshmanesh, and A. Mitchell, “Fabrication of complex PDMS microfluidic structures and embedded functional substrates by one-step injection moulding,” *RSC Adv.*, 6(91), 87988-87994, 2016

[190] J. Raveendran, and T.G. Satheesh Babu, “Design and fabrication of a three-layered microfluidic device for lab on a chip application,” *Mat. Tod. Proc.*, 5(8), 16286-16292, 2018

[191] Y. Jiang, Z. Yu, X. Huang, R. Chen, W. Chen, Y. Zeng, C. Xu, H. Min, N. Zheng, and X. Cheng “A multilayer lateral-flow microfluidic device for particle separation,” *Microfluid Nanofluid*., 22, 40, 2018

[192] M. Masrie, B.Y. Majlis, and J. Yunas, “Fabrication of multilayer-PDMS based microfluidic device for bio-particles concentration detection,” *Bio-Med. Mat. and Engg,* 24, 1951–1958, 2014

[193] B.H. Jo, L.M. Van Lerberghe, K. M. Motsegood, and D. J. Beebe, "Three-dimensional micro-channel fabrication in polydimethylsiloxane (PDMS) elastomer," *J. MEMS*, 9, 76-81, 2000

[194] M. Zhang, J. Wu, L. Wang, K. Xiao, and W. Wen, "A simple method for fabricating multi-layer PDMS structures for 3D microfluidic chips," *Lab on a Chip*, 10, 1199-1203, 2010

[195] H. N. Chan, Y. Chen, Y. Shu, Y. Chen, Q. Tian, and H. Wu, "Direct, one-step molding of 3D-printed structures for convenient fabrication of truly 3D PDMS microfluidic chips," *Microfluidics and Nanofluidics*, 19, 9-18, 2015

[196] J.R. Anderson, D.T. Chiu, R.J. Jackman, O. Cherniavskaya, J.C. McDonald, H. Wu, S.H. Whitesides, and G.M. Whitesides, "Fabrication of Topologically Complex Three-Dimensional Microfluidic Systems in PDMS by Rapid Prototyping," *Analytical chemistry*, 72, 3158-3164, 2000

[197] S. Bathini, S. Pakkirisami, D. Raju, S. Badilescu, R. J. Ouellette, A. Ghosh, and M. Packirisamy, "Microfluidic Isolation of Extracellular Vesicles and Validation through AFM and DNA Amplification," *Eur. J. Extr. Ves.*, 1, 3-10, 2020

[198] H. SadAbadi, M. Packirisamy, and R. Wuthrich, "High performance cascaded PDMS micromixer based on split-and-recombination flows for lab-on-a-chip applications," *RSC Advances*, 3, 7296-7305, 2013

[199] J. Ozhikandathil, S. Badilescu, and M. Packirisamy, "Detection of fluorophore-tagged recombinant bovine somatotropin (rbST) by using a silica-on-silicon (SOS)-PDMS lab-on-a-chip," *IEEE Sens. J.*, 12(9), 2791–2798, 2012

[200] P. P. Anglim, T. A. Alonzo, and I. A. Laird-Offringa, "DNA methylation-based biomarkers for early detection of nonsmall cell lung cancer: an update," Molecular Cancer, vol. 7, no. 1, p. 81, 2008

[201] L. Altucci, H. G. Stunnenberg, J. Zhu, and X. Yao, "Use of DNA methylation for cancer detection: promises and challenges," *Int. J. Biochem. Cell Biol.*, 41(1), 147–154, 2009

[202] C. L. Bartels and G. J. Tsongalis, "MicroRNAs: novel biomarkers for human cancer," *Clinical Chemistry*, 55(4), 623–631, 2009

[203] S. F. Kingsmore, "Multiplexed protein measurement: technologies and applications of protein and antibody arrays," *Nature Reviews Drug Discovery*, 5(4), 310–321, 2006

[204] J.A. Ludwig and J.N. Weinstein, “Biomarkers in cancer staging, prognosis and treatment selection,” *Nature Reviews Cancer*, 5(11), 845–856, 2005

[205] M. Colombo, G. Raposo, and C. Théry, “Biogenesis, secretion, and intercellular interactions of exosomes and other extracellular vesicles,” *Annu Rev Cell Dev Biol.*, 30, 255–289, 2014

[206] G. Raposo and W. Stoorvogel, “Extracellular vesicles: exosomes, microvesicles, and friends,” *J. Cell Biol.*, 200(4), 373–383, 2013

[207] B.A. Ashcroft, J. De Sonneville, Y. Yuana, S Osanto, R Bertina, M E Kuil, and T H Oosterkamp, “Determination of the size distribution of blood microparticles directly in plasma using atomic force microscopy and microfluidics,” *Biomedical Microdevices*, 14(4), 641–649, 2012

[208] H. Shao, J. Chung, K. Lee, L. Balaj, C. Min, B.S. Carter, F.H. Hochberg, X.O. Breakefield, H. Lee, and R. Weissleder, “Chip-based analysis of exosomal mRNA mediating drug resistance in glioblastoma,” *Nat Commun*., 6, 6999, 2015

[209] M.A.M. Gijs, “Magnetic bead handling on-chip: New opportunities for analytical applications,” *Microfluid. Nanofluid.*, 1, 22–40, 2004

[210] B. Hickstein, and U.A. Peuker, “Characterization of protein capacity of nanocation exchanger particles as filling material for functional magnetic beads for bio-separation purposes,” *Biotechnol. Prog.*, 24, 409–416, 2008

[211] N. Pamme, “Continuous flow separations in microfluidic devices”, *Lab Chip*, 7, 1644–1659, 2007

[212] C. Tekin, and M.A.M. Gijs, “Ultrasensitive protein detection: A case for microfluidic magnetic bead-based assays,” *Lab Chip*, 13, 4711–4759, 2013

[213] A. Clayton, J. Court, H. Navabi, M. Adams, M.D. Mason, J.A. Hobot, G.R. Newman, and B. Jasani, “Analysis of antigen presenting cell derived exosomes, based on immuno-magnetic isolation and flow cytometry,” *J. Immunological Methods*, 247(1-2), 163–174, 2001

[214] M. P. Oksvold, A. Neurauter, and K. W. Pedersen, “Magnetic bead-based isolation of exosomes,” *Methods in Molecular Biology*, 1218, 465–481, 2015

[215] H. Xu, C. Liao, P. Zuo, Z. Liu, and B.C. Ye, "Magnetic-Based Microfluidic Device for On-Chip Isolation and Detection of Tumor-Derived Exosomes," *Anal. Chem.*, 90, 13451−13458, 2018

[216] S. C. Taylora, J. Carbonneaub, D. N. Sheltonc, and G. Boivin, "Optimization of Droplet Digital PCR from RNA and DNA extracts with direct comparison to RT-qPCR: Clinical implications for quantification of Oseltamivir-resistant subpopulations," *J. Viro. Meth.*, 224, 58–66, 2015

[217] M. Mørk, S. Pedersen, J. Botha, S. M. Lund, and S. R. Kristensen, "Preanalytical, analytical, and biological variation of blood plasma submicron particle levels measured with nanoparticle tracking analysis and tunable resistive pulse sensing," *Scan. J. of Clin. Labo. Inve*, 76(5), 349-360, 2016